Friction Stir Spot Welding of 6061 Aluminum-to-Copper

By

Robert J. Heideman

A dissertation submitted in partial fulfillment of

the requirements for the degree of

Doctor of Philosophy

(Materials Engineering)

at the

UNIVERSITY OF WISCONSIN-MADISON

2015

Date of final oral examination: 11/23/2015

The dissertation is approved by the following members of the Final Oral Committee:

Sindo Kou, Professor, Material Science and Engineering
John H. Perepezko, Professor, Materials Science and Engineering
Dane D. Morgan, Professor, Material Science and Engineering
Frank E. Pfefferkorn, Associate Professor, Mechanical Engineering
Kumar Sridharan, Distinguished Research Professor, Engineering Physics

Acknowledgements

I would first and foremost thank my wife, Vicki Heideman, for her patience and encouragement throughout my studies. Without her support, finishing this work would not have been possible.

I would like to thank the late John F. Hinrichs who first introduced me to friction stir welding in 1994 and provided mentoring and encouragement throughout my career and in the pursuit my PhD. In addition to John, I would like to thank Jeff Noruk who continued encouraging me to complete these studies after John's death.

I would also like to thank Professor Sindo Kou for his patience and guidance during my studies. His insight into the friction stir welding process and my research were invaluable in helping me complete this work.

I would also like to thank the A.O. Smith Corporation for its financial support and for this work for numerous employees who provided experimental assistance during my studies. In particular, I am very appreciative of Dr. Chuck Bishop and Ron Massa from A.O. Smith whom first encouraged me to pursue a PhD. In addition, I am very grateful to Matt Critchley for all of his prototype support and for making 1000's of friction stir spot welds. I am also grateful for the administrative support and document proofing provided by Jacky Hansen in preparation of this dissertation.

I would like to thank Dr. Youngki Yang of the University of Wisconsin-Madison for his help on the weld macrographs presented in Chapter 1.

I would like to thank Amber Shrivastava from the University of Wisconsin-Madison for his insight into welding power in Chapter 3 and Jiangwei Liu, also from the University of Wisconsin-Madison, for his help in preparing the figures in Chapter 3.

I would also like to thank John Fournelle and Rie Takagi Fredrickson from the Department of Geoscience at the University of Wisconsin-Madison. John was especially helpful in completing electron microprobe analyses. Rie helped on very short notice complete some necessary x-ray diffraction. Without their dedication and willingness to help students, my work would have been much more difficult.

Lastly, I would like to thank Dan Jones for his final proof reading of this document. Without his work, this document would contain many more annoying typographical errors than it currently does.

Abstract

Friction stir spot welding between a 1.5mm 6061 Al-T6 sheet and a 1.5mm Cu sheet was conducted. The effects of the following parameters on the lap shear weld strength were investigated: FSSW tool pin length, shoulder plunge depth, weld time, and tool rotation speed. With rotation speeds of 2000rpm and a 2.60mm tool pin length, weld strengths just over 2000N were produced. Welds made at 1000rpm with 1.83mm or 2.60mm tool pin lengths produced weak welds, with strengths below 900N. Stronger welds had a Cu ring extruded upward from the lower Cu sheet into the upper 6061 Al-sheet, which promoted bonding and interlocking between the sheets. The interface between this Cu ring and the surrounding aluminum was free of Al/Cu intermetallics. The weld strength appeared driven by the aluminum-rich stir zone layer thickness between the tip of the Cu ring and the weld keyhole, with the strength increasing by 2833N per millimeter of aluminum layer thickness. This aluminum-rich stir zone layer consisted of an Al(Cu) solid solution with numerous small layered particles. These layered particles were identified via electron microprobe analysis and consisted of discrete Al-Cu phases of a Cu(Al) solid solution, γ_2-Cu_9Al_4, and θ-$CuAl_2$.

An issue with weld consistency was identified during the design of experiment work and, to understand weld inconsistency, the flow of material that occurred during friction stir spot welding of a 1.5mm 6061 Al-T6 on the top to a 1.5mm Cu sheet on the bottom was next studied. To study material flow, the welding process was stopped with a non-consumable tool left in the welded sample at various plunge depths. A cause for weld inconsistency was identified, that is, after making just a few welds, the tool threads became filled with large layered Cu/Al-Cu intermetallic structures that appeared to clog

the threads and prevent the material flow necessary for quality welds. Material flow analysis identified that the threads on the tool pin promote a flow of aluminum-rich material downward; ensuring that an Al-rich stir zone needed for quality welds forms. The macro-material flow needed for forming quality welds commences when the tool shoulder touches the 6061 Al sheet and is completed at the end of the weld plunge. Dwell time after the plunge is completed does not affect the weld macrostructure, but does lead to more dissolution of Cu into to the Al-rich stir zone. The likely source of the large layered Cu-rich particles that lead to thread clogging in poor quality welds was also identified while studying material flow. The cause of these particles is Cu-rich material (layered in structure) that adheres to the tool tip during the plunge portion of the welding process. This material first adheres to the non-consumable FSSW tool tip during the plunge process and is present on the tool after it is withdrawn from the weld. This adhered-material fractures and spalls off the tip during the plunging portion of the subsequent weld and then reforms as the plunge progresses. If the size of fractured particles is large enough (approximately the size of the tool threads), thread clogging is possible.

To further improve weld consistency, a study was conducted to understand weld temperatures, torque and vertical force. A wireless temperature measurement device was designed and used to measure temperatures at the outer radii of a friction stir spot weld (FSSW) tool shoulder and pin in 1.5mm thick 6061 Al on the top, to 1.5mm Cu on the bottom FSSW. In addition, a dynamometer was used to measure the torque and vertical force, which were used to estimate the weld plunge energy, while making these welds. Temperature and torque measurements were used to show that plunge rate is a

key parameter that can be used to improve weld strength and consistency, because plunge energy is a key variable in forming high quality 6061 Al to Cu FSSWs. Slowing the plunge rate, thus increasing weld energy, however, did not impact peak temperatures achieved during welding. Peak temperatures were affected by changing the rotation speed, with higher rotation speeds producing higher peak temperatures. Peak temperatures for 2000rpm and less were below the 582°C eutectic temperature for 6061 Al. With a 3000rpm rotation speed, a peak temperature above this eutectic temperature indicated that melting likely took place. The presence of melting was supported by a drop in power (torque x angular velocity) at the 3000rpm rotation speed. Peak temperature, however, was shown to not be indicative of weld quality since quality welds could be produced at different rotation speeds, provided the plunge rate was slow enough to produce the energy needed to form a weld structure with an Al-rich stir zone and an upward extruded Cu ring. Plunge depth directly influenced weld energy; with energy increased with deeper plunge depths. However, the increase energy occurred after the shoulder touched the upper 6061 Al surface, at which point the required macrostructure for quality weld formation was already mostly formed. Temperature was not significantly influenced by the plunge depths tested.

Methods to eliminate tool thread clogging as a result of larger layered Cu-rich particles were investigated to eliminate randomly occurring poor quality welds. Using NaOH to etch the tool clean between each weld improved weld quality and eliminated poor quality welds, but was not practical because it took up to ten minutes to remove the excess material from the tool. Another method explored to clean the non-consumable FSSW tool was with a CNC lathe to machine the tool tip back to its original

surface between each weld. Removing material build up via this machining operation improved weld consistency, proving that the source of particles that lead to thread clogging is the layered Cu-rich material adhered to the tool tip. While the machining step improved weld consistency, it would require an added step and additional time in manufacturing, making it a less-than-optimal solution.

The optimal solution was to prevent material from building up on the tool tip. Physical vapor deposited (PVD) CrN and TiCN tool coatings were evaluated as means to prevent material buildup on the tool tip. Both coatings improved weld consistency, but wore from areas of the tool threads in less than twenty welds. Neither coating completely eliminated material buildup on the tool tip. CrN seemed to reduce the amount of buildup and improve weld strength before it began to wear off the tool. However, since the life of tool coatings was less than twenty welds, CrN and TiCN were deemed to be poor solutions to evaluate further. Densimet 17.7, a tungsten-based tool material, was evaluated as a method to eliminate tool tip material buildup. Densimet 17.7 did not eliminate tool tip material buildup, but increased the average weld strength by 43% over standard H13 steel tool. The increased strength resulted from a wider aluminum-rich stir zone between the upward extruded Cu ring the weld keyhole. Comparing the welding temperature profile for the Densimet 17.7 tool and standard H13 steel tool suggested that material was flowing more easily, indicated by a slower heat rate of the Densimet 17.7 tool, at the end of the plunge portion of welding process. The improved flow resulted in a wider stir zone and stronger weld. No method of eliminating material buildup on the non-consumable FSSW tool tip was identified, but changing

materials to a tungsten based alloys appeared to be a viable approach to improving weld strength and consistency.

Table of Contents

List of Figures

List of Tables

List of Equations

Chapter 1: Friction Stir Spot Welding of Aluminum to Copper

1.1 Introduction

Friction stir welding (FSW) was a process invented in England in 1991 at The Welding Institute (TWI) [1]. The process involves pushing a spinning non-consumable rotating tool through a weld joint. The frictional and viscous heat generated by the tool softens the weld area sufficiently so that the material can be stirred and mixed [2]. An illustration of the process is shown in Figure 1-1. The reduced heat input and relatively flat weld profile associated with FSW improves weld joint performance, particularly when butt joints are used.

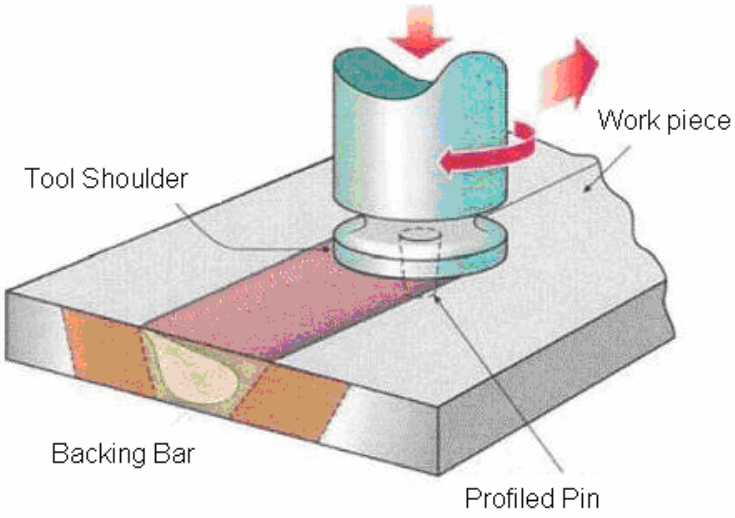

Figure 1-1. Schematic of FSW process [3]

Initial FSW development efforts focused on welding aluminum and magnesium alloys because these alloys are typically more difficult to weld via conventional fusion processes. Today, numerous applications of FSW technology are used in a variety of industries from aerospace to automotive [4, 5]. Since the initial work performed with

aluminum alloys, FSW of other materials such as titanium, stainless steel, carbon steel, brass, and copper have been successfully accomplished [5, 6] and some industrial applications of these materials are appearing [5].

Some of the most recent FSW research involves welding dissimilar materials such as aluminum to steel, titanium to stainless steel, and aluminum to copper [7, 8, 9, 10, 13, 14, 15, 19, 20, 21, 23, 25, and 30]. Most of these combinations cannot be welded with traditional fusion welding methods. Soldering, brazing, or rotary friction welding can be used to join dissimilar metal combinations. However, FSW, if successful, could produce stronger welds faster and with higher levels of reliability when compared to soldering or brazing. Rotary friction welding is similar to FSW, but the rotary welding process is generally limited to circular cross sections and requires the ability to spin one of the parts to be welded. FSW, however, can be used on butt, lap, and t-joint configurations. [11, 12, 13]

A variation of the FSW process, known as friction stir spot welding (FSSW), was also developed. As illustrated in Figure 1-2, in FSSW, the tool is plunged into a lap joint, and after the shoulder touches the work piece, the tool dwells in the work piece for a desired time. After the dwell period, the tool is withdrawn and the weld is completed. In FSSW specifically, the tool does not move linearly (perpendicular to the plunge direction) [14]. An example of a 6061 Al-T6 to 6061 Al-T6 FSSW is shown in Figure 1-3. As with traditional resistance spot welding, the FSSW process is limited to lap joint configurations. The primary advantage of the FSSW process in aluminum alloys is that many welds can be made with a single tool because a non-consumable hardened steel

tool is employed [16]. In conventional resistance spot welding [16], the copper electrode degrades due to reactions between the electrode material and aluminum being welded.

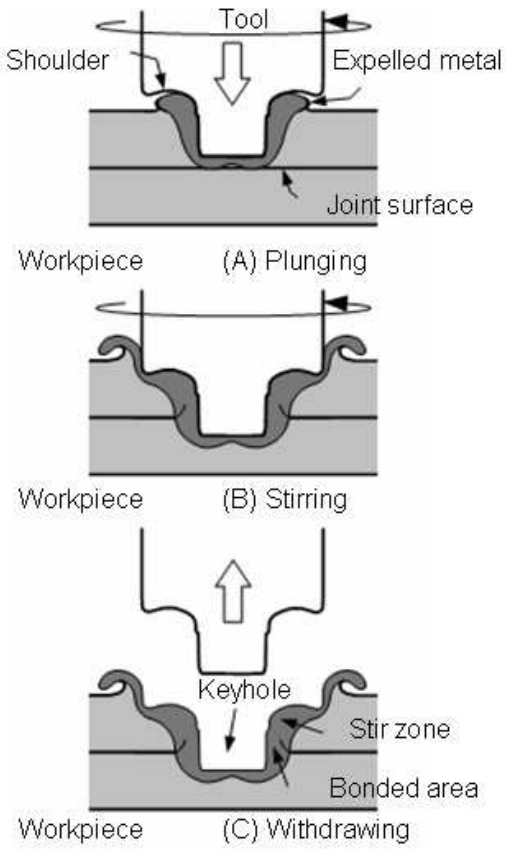

Figure 1-2. Schematic of FSSW Process [22]

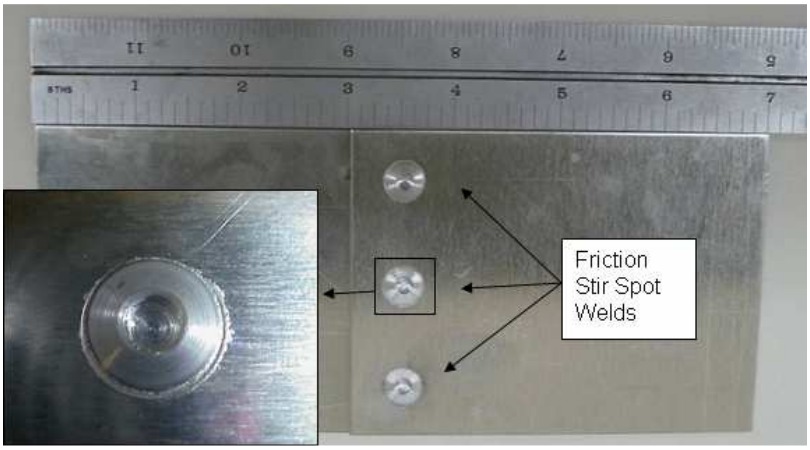

Figure 1-3. Three friction stir spot welds joining 6061-T6 Al to 6061-T6 Al

Most FSSW work has focused on welding aluminum to aluminum alloys and magnesium to magnesium alloys [8, 17, 18, 22, and 32]. Another dissimilar combination, aluminum and its alloys to copper could be useful in making electrical connections and components. Some limited literature exists on making linear welds with both butt and lap penetration joints [13, 19, 20, 21, 24, 25, 26, 27, 29, and 30]. However, only limited success is reported in making quality welds through the linear welding process. In lap penetration welds, intermetallic formation caused poor weld quality; subsequently, to improve weld quality a thin zinc sheet was employed between the copper and aluminum sheets to prevent detrimental intermetallics from forming [13]. In butt joint welding, only limited success was reported, with the most success achieved by having a tool pin almost entirely on the aluminum side of the butt joint, so that the tool pin just barely rubs or kisses the copper side of the joint [30].

Welding aluminum and its alloys to copper via FSW presents a significant challenge given the large 452C difference in melting points between the two materials. The lower melting point of aluminum (660°C) will tend to stir weld much easier and more readily as it approaches its melting point and becomes less viscous. By comparison, copper, with melting point of 1085C, will be highly viscous and difficult to stir even at the melting point of aluminum alloys. FSSW could be a plausible method to join these two materials, because the FSSW of the materials is limited to a single spot where the amount of mixing and weld morphology can be controlled and limited. In comparison, the entire length of a linear weld will likely require extensive mixing.

Literature on aluminum to copper FSSW does not appear to exist; consequently, basic process development and understanding are needed. Initial focus of this research

was to determine the influence of weld parameters on weld quality for 6061 Al-T6 to oxygen-free pure copper (OFC) and to determine the weld morphology that produced welds of reasonable quality.

To gain process and joint strength understanding, a design of experiment (DOE) was used to determine the influence of process parameters on weld strength. Follow-up experimentation and metallurgical analyses were also used to help better understand the findings indicated by the original DOE. The samples generated during this experiment were then evaluated to determine the interface shape and microstructure of strong and weak welds.

1.2 Experimental Design

To develop a basic process understanding and to guide further in-depth investigations of FSSW of 6061 Al-T6 (referred to as 6061 Al in this document) to oxygen-free copper (referred to as Cu in this document) in the H01 condition (i.e. quarter hard), a 2^4 factorial experimental design was used to investigate the factors and interactions that could impact the weld strength. The FSSW samples consisted of 25mm wide, 50mm long, and 1.5mm thick 6061 Al welded to 25mm wide, 50mm long, and 1.5mm thick Cu. A lap weld joint was used with the 6061 Al on top and the Cu on the bottom with a 25mm overlap. The compositions, determined by inductively coupled plasma, of the 6061 Al and Cu are shown in Tables 1-1 and 1-2.

Table 1-1. Composition of 6061 Al as determined by ICP and compared to 6061 Al Specification.

	Si	Fe	Cu	Mn	Mg	Cr	Zn	Ti	Al
Sample Composition	0.69	0.60	0.28	0.006	1.03	0.15	<0.001	0.014	Rem.
Specification	0.4 - 0.8	0.7 Max	0.15 - 0.40	0.15 Max	0.8 - 1.2	0.04 - .35	0.25 Max	0.15 Max	Rem.

Table 1-2. Composition of oxygen-free copper (weight percent) as determined by ICP and compared to oxygen-free copper specification. Other elements combine to 0.017 weight percent with individual elements all less than or equal to 0.001 weight percent.

	Cu	Ag	As	Sb	S	P	Fe	Ni	Mn	Sn	Other*
Sample Composition	99.95	0.001	0.002	0.006	0.002	0.001	0.005	0.002	0.001	0.013	0.017
Specification	99.95	----	----	----	----	----	----	----	----	----	

Table 1-3. Full factorial experimental design (2^4) produced using Minitab software.

Standard Order	Run Order	Pin Length (mm)	Rotation Speed (RPM)	Plunge Depth (mm)	Weld Time (seconds)
1	32	1.83	1000	0.00	3
2	9	2.60	1000	0.00	3
3	11	1.83	2000	0.00	3
4	4	2.60	2000	0.00	3
5	27	1.83	1000	0.13	3
6	7	2.60	1000	0.13	3
7	12	1.83	2000	0.13	3
8	21	2.60	2000	0.13	3
9	6	1.83	1000	0.00	6
10	3	2.60	1000	0.00	6
11	18	1.83	2000	0.00	6
12	1	2.60	2000	0.00	6
13	16	1.83	1000	0.13	6
14	22	2.60	1000	0.13	6
15	31	1.83	2000	0.13	6
16	10	2.60	2000	0.13	6
17	34	1.83	1000	0.00	3
18	5	2.60	1000	0.00	3
19	29	1.83	2000	0.00	3
20	25	2.60	2000	0.00	3
21	26	1.83	1000	0.13	3
22	33	2.60	1000	0.13	3
23	20	1.83	2000	0.13	3
24	8	2.60	2000	0.13	3
25	2	1.83	1000	0.00	6
26	23	2.60	1000	0.00	6
27	17	1.83	2000	0.00	6
28	30	2.60	2000	0.00	6
29	19	1.83	1000	0.13	6
30	13	2.60	1000	0.13	6
31	24	1.83	2000	0.13	6
32	15	2.60	2000	0.13	6
33	14	2.22	1500	0.06	4.5
34	28	2.22	1500	0.06	4.5

The weld strength (shear tension) was targeted to evaluate weld quality since this property is of interest to most users and is a good indicator of weld quality. The following four factors, at two levels each, were included in the initial DOE: (1) tool pin length, (2) plunge depth, (3) weld time, and (4) rotation speed. Table 1-3 shows the experimental design and each experimental run that was used in this initial DOE. The

right-most four columns show the independent variables explored in the DOE. The “standard order” column is a logical order, or grouping, of the experimental runs where the “run order” is in a randomized order to sequence each experimental run, and is done to minimize experimental error. Two replications were used for each run, and a center point with 2 replications was included in the design. Two replications were used because the FSSW process in aluminum alloys tends to be very repeatable, and therefore, two replications should indicate any process variability. The center points were used to determine if any process curvature exists. No blocking was used since all samples were made in a single day, and all testing was completed the following day.

Tool pin length is the length from the pin tip to the point the pin enters the shoulder, and was the only tool feature explored in this study. The tool design used is shown in Figure 1-4. The tool pin lengths tested were 1.83mm, 2.22mm, and 2.60mm. The 1.83mm pin length was selected to ensure only a small level of mixing between the upper and lower sheets. At 1.83mm, the pin only plunged 19% into the lower Cu sheet. The 2.60mm pin length was selected to achieve a much higher level of mixing, as this tool penetrated 68% into the lower Cu sheet. The 2.22mm pin length was selected as a middle point and is considered a good test point in formal design of experiments. The tool material, trade name Viscount 44, was also held constant in the original DOE. Viscount 44 is a pre-hardened H13 tool steel with a hardness of 42-46HRC. One tool for each pin length was used in the experiment, such that only three different tools were used for the entire experiment.

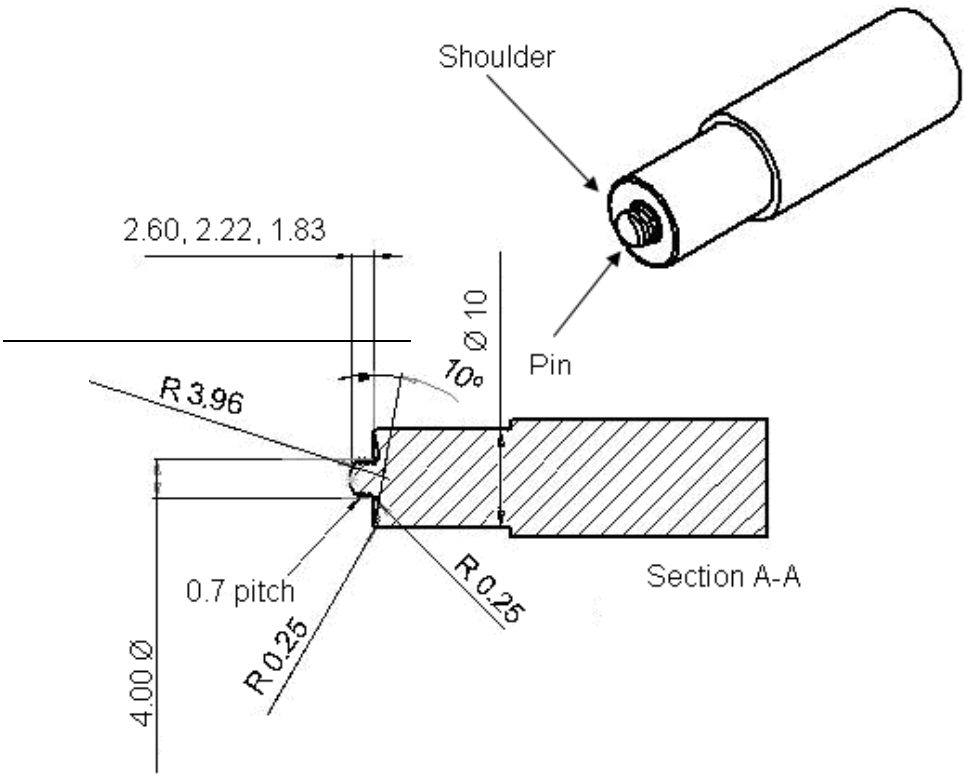

Figure 1-4. Non-consumable welding tool drawing with the dimensions in mm.

The plunge depth is defined as the depth the tool shoulder penetrates into original surface plane of the top plate in the weld joint, in this case a 6061 Al sheet. For example, a 0.00mm plunge depth corresponds to the shoulder just drawing level with the original top surface of the 6061 Al sheet. In comparison, a 0.13mm plunge depth implies that the shoulder was pushed 0.13mm below the original surface of the 6061 Al sheet. The 0.00mm plunge is considered the minimum required plunge depth for a FSSW. At any depth less than this, the tool shoulder would not impact weld quality. The 0.13mm plunge depth was 8% of the total 6061 Al sheet thickness and was expected to be sufficient to determine if plunge depth was statistically significant to weld quality.

Weld time is defined as the time the tool was held at the desired plunge depth. The time it takes to plunge to the desired depth and the retraction time are not included

in the weld time. Two different weld times (3s and 6s) were used for this investigation and are typical of those used in FSSW of aluminum alloys.

The rotation speed is the speed at which the tool spins and is reported in rotations per minute (rpm). The rotation speed used for the DOE varied between 1000rpm, 1500rpm, and 2000rpm. In addition, follow-up testing evaluated a rotation speed of 3000rpm. These speeds were selected because they are commonly used to weld aluminum alloys of similar sheet thicknesses.

The variables not explored in the original DOE study were plunge rate, which was held constant at 2.54mm/s and the other features associated with the non-consumable welding tool geometry.

The FSSWs in this study were made using 1991 Hurco BMC 40 CNC milling machine (15 horsepower with a maximum spindle speed of 4000rpm) and a specially designed fixture (see Figures 1-5 and 1-6). For each experimental run, four welds were made with each of the weld conditions for the run. Between each weld, the tool was plunged into a piece of 6061-T6 material in an attempt to clean the tool of any copper and/or aluminum-copper intermetallics that may have stuck to the tool from the previous weld.

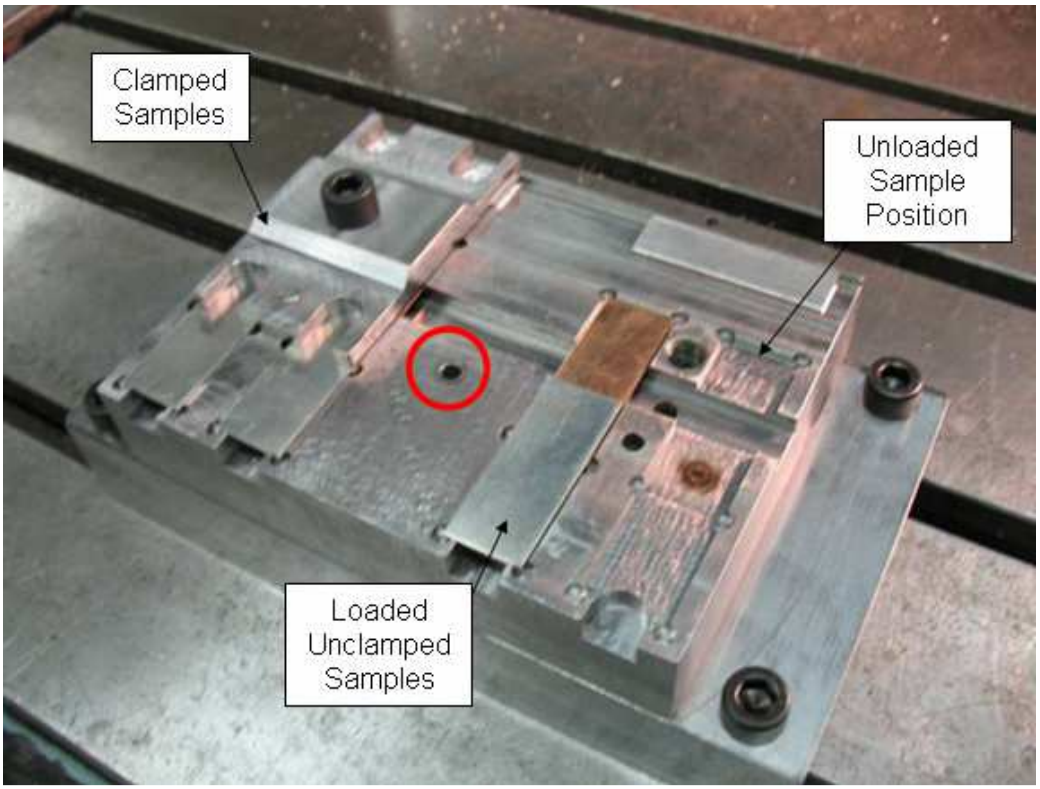

Figure 1-5. Four sample weld fixtures were used for the original DOE. The left two samples are clamped and ready to be welded; the second from the right sample (aluminum and copper are both visible) is loaded but not clamped; and right-most sample area is empty. The hole circled in red was the area used to locate the zero-point for the tool shoulder.

(a)

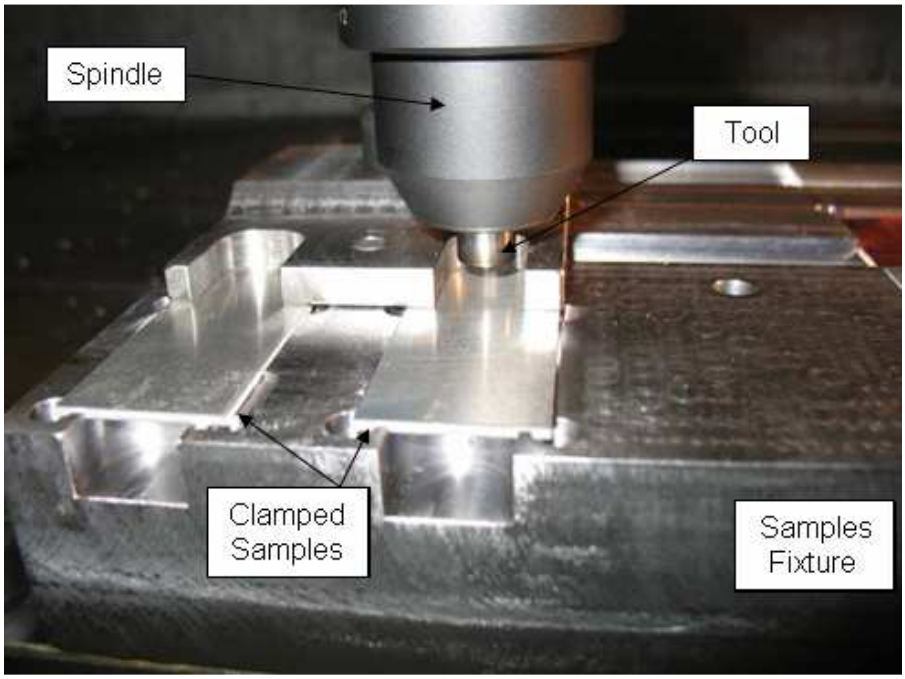

(b)

Figure 1-6. (a) CNC machining center used for this experiment and (b) a close-up of the tool contacting the sample in the weld fixture.

During the first two experimental runs some inconsistencies were noted in the sample surfaces. Testing of these samples yielded very inconsistent shear strengths.

This observation made it necessary, before conducting the experiment, to determine the variability responsible for the inconsistent results. To improve consistency, sources of variability were found in the fixtures and in the material to be welded:

1) **Aluminum thickness**: Sample thickness varied by up to 0.003” depending on the samples’ original sheets.
2) **Fixture flatness:** The weld fixture was out-of-flatness by 0.002.
3) **Welding tool z-position:** The tool was slipping in the holder and moving in the vertical direction.
4) **Fixture flexure:** The weld fixture was secured in a vise on the CNC machining table and the middle of the fixture was flexing several thousands of an inch during welding.
5) **Part cleanliness:** The aluminum parts contained an oil substance.
6) **Lap shear test grips:** Twisting of the sample was possible during lap shear testing.
7) **Zero position:** Buildup of aluminum on the tool tip was causing the zero position to vary.

Each source of identified variability was resolved by:

1) **Aluminum thickness:** The sample thicknesses were verified and sorted using a caliper such that each sample was less than 0.001” from one another.
2) **Fixture flatness:** The fixture was re-machined to flat within 0.0015”.
3) **Welding tool z-position:** A back up rod was placed in the tool holder such that no vertical motion of the tool was possible.

4) **Fixture flexure:** The fixture was bolted directly to the CNC machining table, eliminating all flexing associated with using a vise.
5) **Part cleanliness:** All parts were cleaned with acetone before welding.
6) **Lap shear test grips:** Twisting was eliminated by purchasing new grips for the tension test instrument.
7) **Zero position:** The zero position turned out to be the most problematic, but was resolved by drilling a hole in the fixture such that the zero point was the tool shoulder just touching the sample surface. The hole used for zero-point determination is identified with a red circle in Figure 1-5. The average offset between the top fixture surface and the aluminum sample surface was accounted for in the zero-point determination. This eliminated any variability in material buildup and any potential variability in tool length.

Following welding, two of the four welds made were tensile tested. Lap shear tensile testing, with a spacer added to each end of the sample to minimize bending (see Figure 1-7), was conducted using an Instron tension test instrument with a cross-head speed of 2.11mm/s. The maximum load measured at failure for each sample was recorded; this maximum load will be referred to as the weld strength.

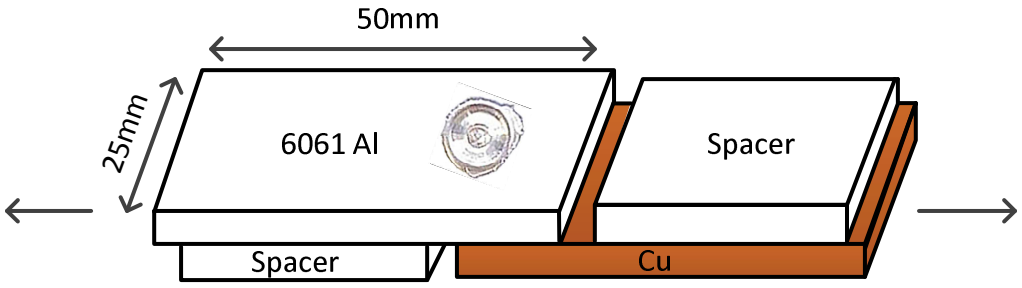

Figure 1-7. Shear sample used to measure FSSW joint strength (note that spacers were added to the sample during testing to minimize sample bending).

Statistical analysis of independent variables along with the dependent weld strength variable was done using Minitab software [28]. After statistical analysis, the fracture surfaces from the tensile testing were analyzed using stereomicroscope and a scanning electron microscope (SEM) with energy dispersion spectroscopy (EDS). Using the stereomicroscope and image analysis software, the fracture surface area was plotted against weld strength. SEM analyses were used to determine the fracture mode and to estimate the chemical composition of fracture surfaces.

After completing these analyses, selected failed samples, along with samples that were not tested, were cross-sectioned and metallographically prepared. Metallographic preparation used standard techniques with a final polishing step of 0.04 μm SiC suspension in 100ml water, 100ml ethanol, and 10g iron III nitrate added to the suspension solution, which helped remove copper scratches. A 0.5% HF etchant solution for 10 seconds was used on selected samples. These samples were analyzed using light microscopy, SEM, and electron microprobe analysis (EMPA). EMPA was used to determine the chemical composition of various features of the weld cross sections. The advantage of this approach is that accurate chemical composition determination is possible, because standards are used to calibrate the microprobe prior to running any analysis. For EMPA analysis, a known 6061 Al and pure Cu standards were used for calibration.

1.3 Results and Discussion

An example of a weld produced during the DOE is shown in Figure 1-8, and the welds strengths obtained from the DOE are shown Table 1-4. The green highlighted

data points were identified as outliers and were not included in the statistical analysis discussed. This data was removed since it was inconsistent with other results with similar weld parameters. However, the inconsistencies remained a concern, and the reasons for these inconsistencies were investigated; the reason for these inconsistencies will be discussed in later chapters.

A graphical representation of the raw data is shown in a multi-variant chart in Figure 1-9. This chart shows the experimental data in a series of four graphs. Each graph shows the shear strength on the y-axis and the rotation speed on the x-axis with the data within each graph sorted by pin length. The other two independent variables are listed at the top of each graph. It is important to realize that the x-axis is a category axis (i.e. not linear) such that data group around each rotation speed is for that particular speed. The red square in the center of each rotation speed corresponds to the average weld strength for the data shown to the immediate right and left of the square. The data to the left of each square corresponds to a pin length of 1.83mm and the data to right corresponds to a 2.60mm pin length. The multi-variant graph shows that the rotation speed significantly impacts weld strength; the red squares for the rotation speed of 1000rpm are lower than those for 2000PM.

Further statistical analysis was used to validate this observation as well as evaluate other independent variables. One important feature of the multi-variant chart is a scatter in the data; ideally, there would be one circle to the right and left of each red square indicating that the weld strength for all four samples were exactly the same (all four circles would have been overlaid on each other giving the appearance of a single

circle). This scatter, similar to the data that was excluded from the statistical analysis required more research and is discussed later.

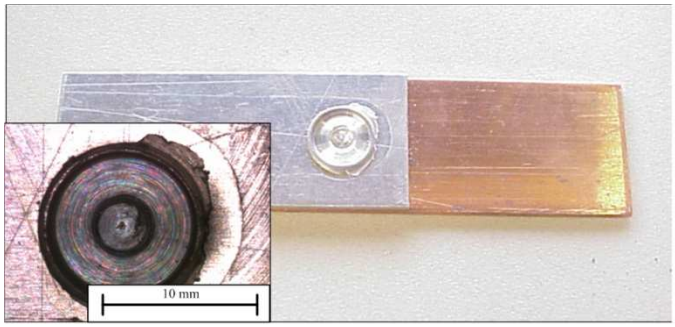

Figure 1-8. Top-view of a sample of weld made by FSSW.

Table 1-4. Experimental Raw Data

Standard Order	Run Order	Pin Length (mm)	Rotation Speed (RPM)	Plunge Depth (mm)	Weld Time (seconds)	Shear Strength (Newtons)	Shear Strength (Newtons)
1	32	1.83	1000	0.00	3	520	233
2	9	2.60	1000	0.00	3	654	549
3	11	1.83	2000	0.00	3	644	789
4	4	2.60	2000	0.00	3	2394	1807
5	27	1.83	1000	0.13	3	414	759
6	7	2.60	1000	0.13	3	686	879
7	12	1.83	2000	0.13	3	1504	2025
8	21	2.60	2000	0.13	3	2275	876
9	6	1.83	1000	0.00	6	532	58
10	3	2.60	1000	0.00	6	1105	1367
11	18	1.83	2000	0.00	6	769	668
12	1	2.60	2000	0.00	6	1888	2039
13	16	1.83	1000	0.13	6	244	748
14	22	2.60	1000	0.13	6	402	352
15	31	1.83	2000	0.13	6	1999	1745
16	10	2.60	2000	0.13	6	1972	1359
17	34	1.83	1000	0.00	3	276	13
18	5	2.60	1000	0.00	3	6	452
19	29	1.83	2000	0.00	3	675	534
20	25	2.60	2000	0.00	3	1120	2054
21	26	1.83	1000	0.13	3	415	535
22	33	2.60	1000	0.13	3	0	0
23	20	1.83	2000	0.13	3	754	1203
24	8	2.60	2000	0.13	3	2045	1919
25	2	1.83	1000	0.00	6	436	637
26	23	2.60	1000	0.00	6	621	547
27	17	1.83	2000	0.00	6	649	883
28	30	2.60	2000	0.00	6	534	480
29	19	1.83	1000	0.13	6	1141	915
30	13	2.60	1000	0.13	6	712	256
31	24	1.83	2000	0.13	6	1599	1434
32	15	2.60	2000	0.13	6	1539	2064
33	14	2.22	1500	0.06	4.5	1323	1130
34	28	2.22	1500	0.06	4.5	924	879

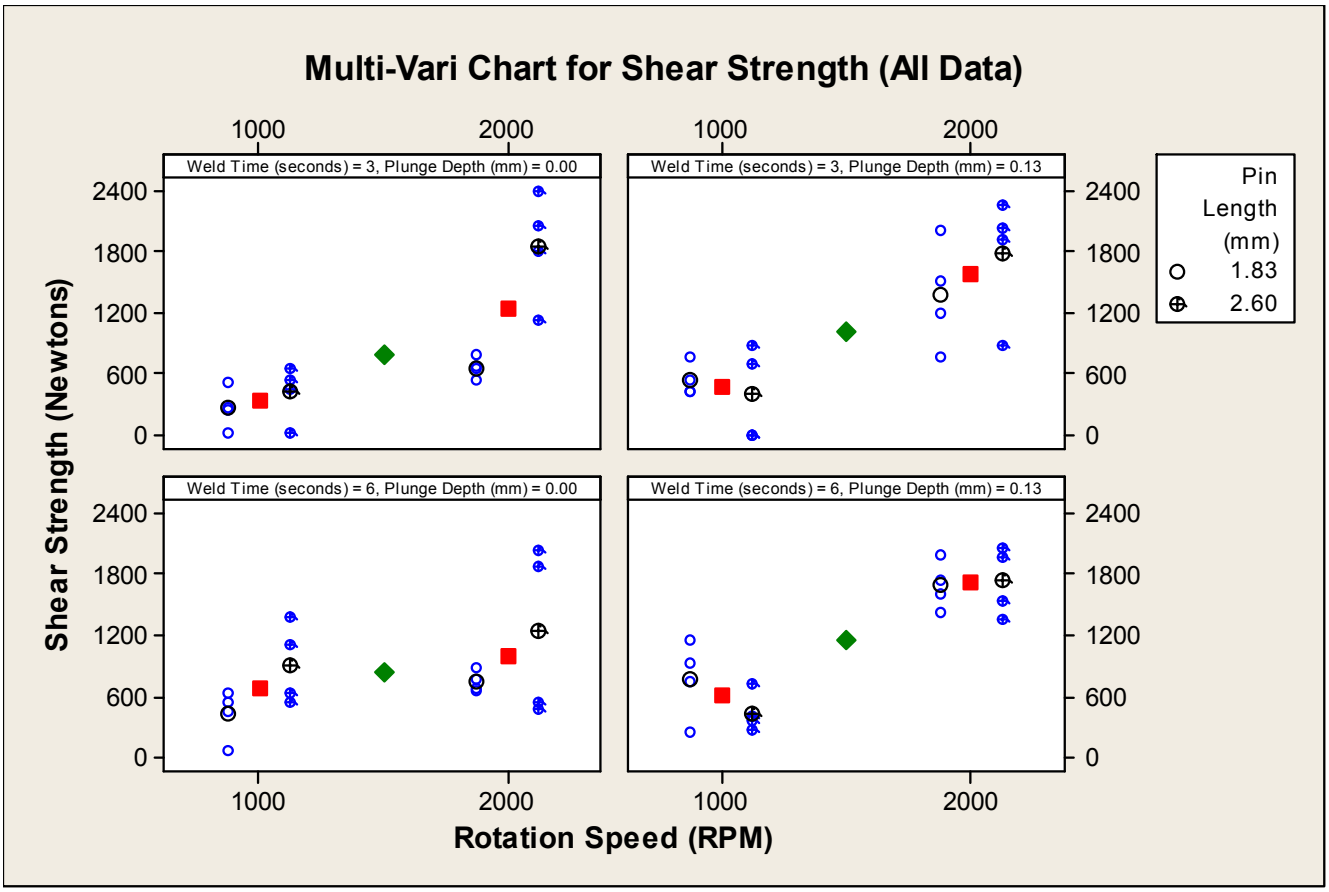

Figure 1-9. Multi-variant charts containing all data points.

After reviewing the multi-variant graphs, a standard statistical analysis was completed. The results from this analysis are shown in Table 1-5. This analysis looked at the statistical significance of the main effects as well as the significance of all possible interactions (two, three, and four-way) between the independent variables. The key data in Table 1-5 is the farthest right column (p-values) with other data columns being used to calculate the p-values shown. The p-values for each independent variable and the interactions are the probabilities that the weld strengths are the same for each level tested. For example, a p-value of 1.0, which it is not, for the rotation speed would mean the weld strength produced with a rotation speed of 1000rpm and 2000rpm are exactly the same. Conversely, the p-value of 0.001 for the rotation speed variable, as

shown in Table 1-5, indicates that the weld strengths from 1000rpm weld are different than the weld strengths produced with a rotation speed of 2000rpm.

Table 1-5. Summary of the Analysis of Average Shear Strength

Term	Effect	Coef	SE Coef	T	P
Constant		1037.2	49.93	20.78	0.000
Pin Length	418.4	209.2	49.93	4.19	0.001
Rotation Speed	873.3	436.7	49.93	8.75	0.000
Plunge Depth	197.1	98.5	49.93	1.97	0.067
Weld Time	118.6	59.3	49.93	1.19	0.254
Pin Length*Rotation Speed	294.3	147.2	49.93	2.95	0.010
Pin Length*Plunge Depth	-326.7	-163.3	49.93	-3.27	0.005
Pin Length*Weld Time	-92.2	-46.1	49.93	-0.92	0.370
Rotation Speed*Plunge Depth	144.9	72.5	49.93	1.45	0.167
Rotation Speed*Weld Time	1.2	0.6	49.93	0.01	0.991
Plunge Depth*Weld Time	-79.6	-39.8	49.93	-0.80	0.438
Pin Length*Rotation Speed* Plunge Depth	-162.8	-81.4	49.93	-1.63	0.124
Pin Length*Rotation Speed*Weld Time	9.9	5.0	49.93	0.10	0.922
Pin Length*Plunge Depth*Weld Time	-145.6	-72.8	49.93	-1.46	0.166
Rotation Speed*Plunge Depth* Weld Time	98.6	49.3	49.93	0.99	0.339
Pin Length*Rotation Speed* Plunge Depth*Weld Time	44.1	22.0	49.93	0.44	0.665
Ct Pt		62.3	194.79	0.32	0.754

Statistical significance is usually identified by a maximum allowable p-value. Typically, the maximum allowable p-value falls in the 0.050 to 0.100 range, meaning any variable or interaction with a p-value less than these values is considered to significantly impact the dependent variable, which in the case of this work is the weld strength. For this investigation, a p-value less than 0.100 was used to determine statistical significance.

With this background information and the data in Table 1-5, the p-values indicated that (1) pin length, (2) rotation speed, (3) plunge depth, (4) pin length*plunge depth interaction, and (5) pin length*rotation speed interaction are statistically significant. Neither the weld time, as tested in the three to six second range, nor any

other interactions were statistically significant. Similarly, the center point was statistically insignificant, indicating that statistical curvature was not present.

After reviewing the statistical analysis results in Table 1-5, the main-effects graphs shown in Figure 1-10 were evaluated to further explore the directional influence of the independent variables tested in DOE. These graphs show the overall average weld strength for each independent variable. For example, the overall average weld strength for each run that was done at 1000rpm is compared to the average weld strength for each run done at 2000rpm. The red square represents the center-point experiment that was included in the DOE. So, in the rotation speed graph, the red square represents the average weld strength of those welds made at 1500rpm. The key with the main-effects graphs is to look for a line with a significant slope indicating that a particular independent variable affects the weld strength (the dependent variable).

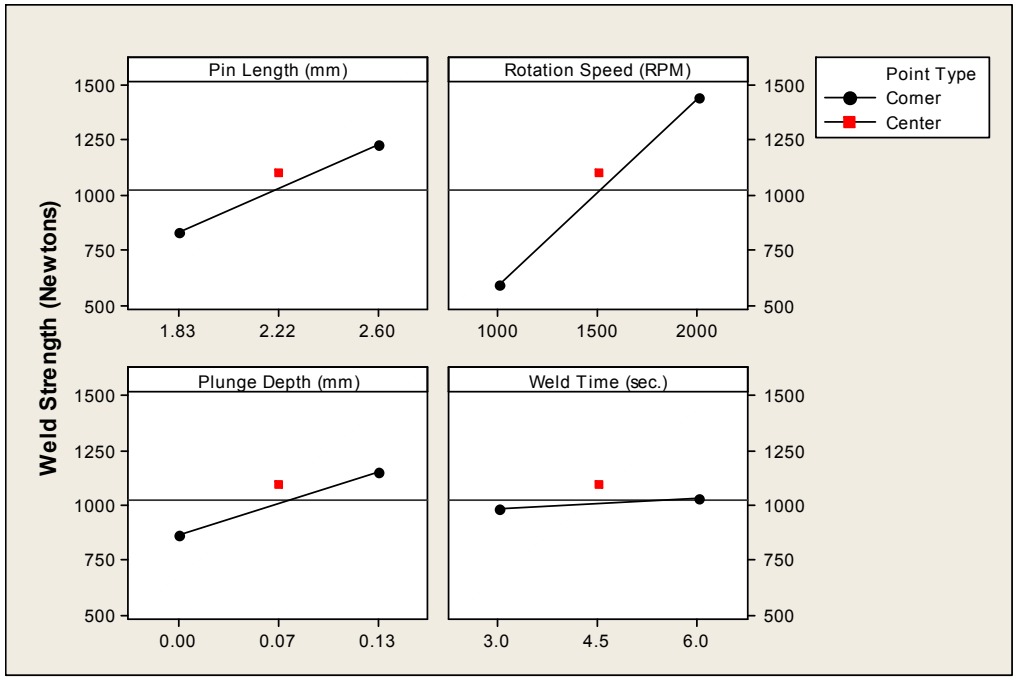

Figure 1-10. Main-effect graphs for average shear strength.

Looking at the main-effect graphs, the conclusions from the earlier statistical analysis can be further supported and additional information learned. Three of the four independent variables tested in the DOE impacted weld strength: (1) rotation speed (faster rotation leads to higher weld strengths), (2) pin length (longer pin length leads to stronger weld strengths), and (3) plunge depth (deeper plunges leads to higher weld strengths). Once again, from these graphs the dwell time does not appear to impact the weld strength. The other key feature of these graphs is the center point data; if these points are significantly off the line, a linear relationship is unlikely. In the case of this data, the center points are sufficiently close to the lines that one cannot conclude a non-linear relationship.

Sound statistical analysis requires the exploration of any statistically significant interactions before drawing final conclusions on the significance of any single independent variable involved in the specific interaction. Therefore, based on the statistical analysis in Table 1-5 and the selected definition of statistical significance (p-value is ≤ 0.100), the pin-length*plunge-depth ($p = 0.005$) and pin-length*rotation-speed interactions ($p = 0.010$) were explored further (before drawing conclusions on the pin length, plunge depth, and rotation speed variables alone) using the interaction graphs shown in Figure 1-11. The interaction graphs are the average weld strength for a particular independent variable. For example, the upper-left-most graph shows the relationship between pin length and rotation speed. The green diamond at a rotation speed of 1000rpm is the average weld strength for all welds made with a 2.60mm pin length at 1000rpm regardless of the other welding conditions. When using interaction graphs, the more the two lines diverge from parallel, the more significant the interaction.

Parallel, or nearly parallel lines, indicate that the interaction is not particularly strong. For example, in the center graph in the top row in Figure 1-11, the slopes of the 2.60mm pin length line are nearly zero while a substantial positive slope can be seen for the 1.83mm pin length; the difference in slopes indicates a potentially strong interaction.

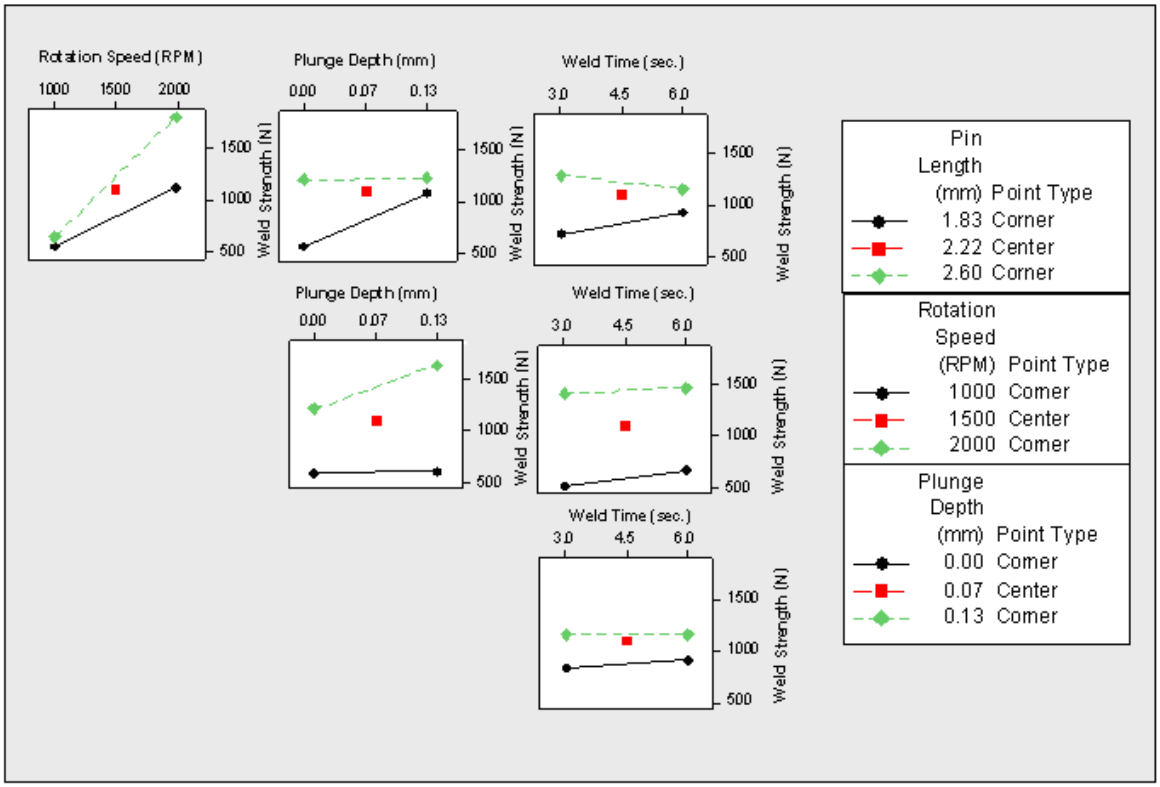

Figure 1-11. Interaction graphs for average shear strength (produced using Minitab).

The rotation-speed*pin-length interaction (upper-left most graph in Figure 1-11) shows that at 1000rpm, the weld strength was consistently low (i.e. less than 800N) and independent of pin length. In comparison, at 2000rpm, the weld strength was influenced by pin length (i.e. the longer 2.60mm pin length produced weld strengths over 1500N, whereas the 1.83mm pin produced weld strengths just over 1000N). This observation supports the main-effect graphs (Figure 1-10) that indicated the longer pin lengths and

higher rotation speeds impacted the weld strength. Follow-up experimentation was conducted to determine if higher rotation speeds (2500rpm and 3000rpm) could produce even stronger welds. However, these higher rotation speeds produced no appreciable increase in weld strength compared to welds made at 2000rpm. This finding is not particularly surprising given that the findings by Gerlich et al. [32] show that maximum temperature reached in FSSW approached (i.e. 94-99% of) the minimum eutectic temperature in Al 2024, Al 5754, Al 6111, Al 6061, Al 7075 aluminum alloys FSSW and AZ31, AZ91 and AM50 magnesium alloy FSSW. When the maximum temperature was reached, Gerlich et al. [32] indicated limited melting takes place and tool slippage occurs. Once this maximum process temperature was reached, no significant increase in weld strength was observed.

The pin length*plunge depth interaction graph (Figure 1-11) also showed a significant interaction (i.e. the two pin length lines diverge from parallelism). The impact of plunge depth was particularly evident in the shorter 1.83mm pin length at rotation speed of 2000rpm, where increasing the plunge depth from 0.00mm to 0.13mm increased the average weld strength from 702N to 1533N, respectively. Conversely, the plunge depth did not appear significant with the longer pin length. With the 2.60mm pin length and a rotation speed of 2000rpm, the average weld strength changed from 1904N with a 0.00mm plunge depth to 1908N with the 0.13mm plunge depth. Consequently, if a tool with a longer pin length is used, the plunge depth may not be particularly important. Additional follow-up experimentation showed that increasing the plunge depth to 0.25mm resulted in no significant improvement in weld strength with average weld strengths of 1855N achieved at this deeper plunge depth.

The pin length was also determined to be significant with the longer (2.60mm) pin length yielding stronger and more consistent welds. Weld strengths greater than 1500N were possible with the shorter (1.83mm) pin length, but in general the shorter pin length yielded more inconsistent results. More specifically, at a rotation speed of 2000rpm, the 2.60mm pin length produced average weld strengths of 1905N whereas the 1.83mm pin length produced average weld strength of only 1117N.

The results from the DOE and follow-up experiments suggest that the most robust method to achieve strong welds is to use the 2.60mm pin length tool at higher rotation speeds and a plunge depth greater than 0.00mm. Strong welds are possible at the shorter pin lengths, but results were more inconsistent and a deeper plunge depth was needed to make welds of adequate strength.

1.4 Metallurgical Analysis

Before discussing the weld microstructure, a brief review of the Cu-Al phase diagram (see Figure 1-12) and previous Al to Cu joining studies may be useful. The Al-Cu system is complex with six equilibrium intermetallic phases possible at temperatures below 500^{o}C. Along with these equilibrium phases, several meta-stable intermetallic phases are also possible [34]. Fortunately, only two or three intermetallic phases (γ_2-Cu_9Al_4, η_2-CuAl, and θ-$CuAl_2$) typically show up in rotary friction welding [35, 37, and 44], linear FSW [13, 15, 17, and 45], diffusion welds [29], and diffusion couples [42] of the Al-Cu system. In 6061 Al to Cu FSW joining studies, Ouyang et al. [19] and Elrefaey et al. [13] reported that intermetallics led to poor weld quality and, in the case of Ouyang et al. [19], cracks in the weld zone. Okamura et al. [24] observes reasonable weld

strengths when two contiguous intermetallic layers (γ_2-Cu_9Al_4 on the Cu side and η_2-CuAl on the Al side) were present. In rotary friction welding, the presence of a contiguous intermetallic layer reduces the weld strength and is the region where weld fractures tend to occur [33 and 44]. In the rotary friction weld studies, the contiguous intermetallic layers were minimized to improve weld quality.

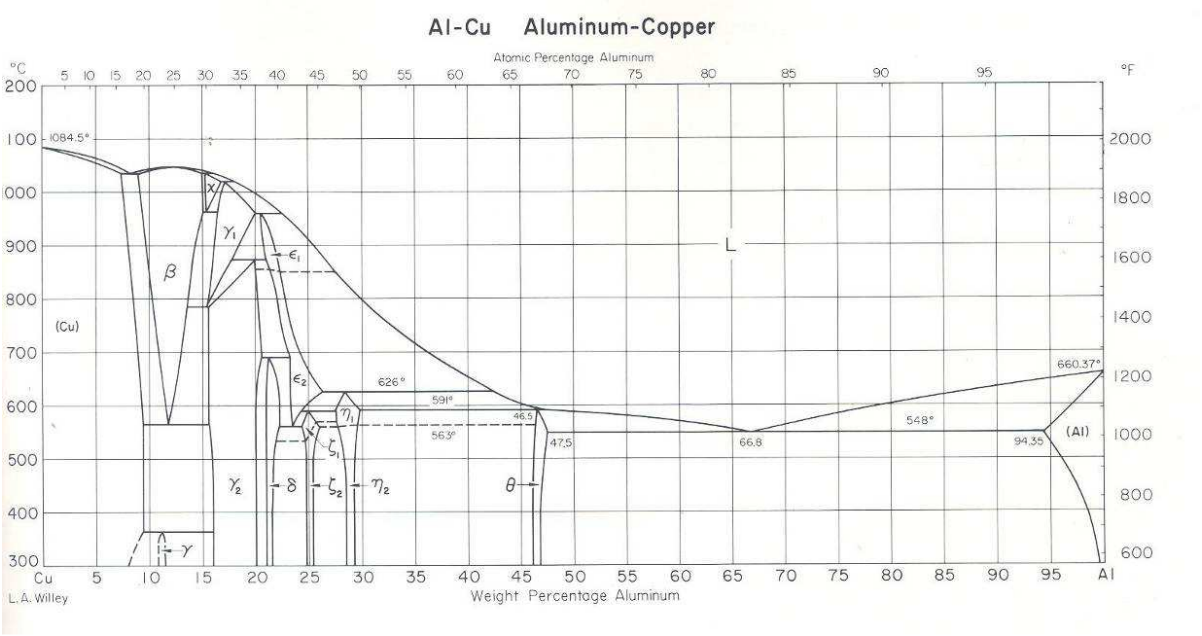

Figure 1-12. Aluminum-Copper Equilibrium Phase Diagram [38]

Understanding the weld morphology of good and bad welds is essential in consistently making acceptable quality welds in a manufacturing environment. The first step in understanding weld quality was the analyses of the fracture surface from a strong weld. Figure 1-13 shows fracture surfaces from a weld with strength of nearly 2000N. Both halves of the fracture had similar dimpled appearances indicating a ductile-type fracture. EDS analysis of both surfaces indicated the presence of mostly aluminum

with less than 3.5 weight percent copper present indicating the fracture surface was likely a Al(Cu) solid solution.

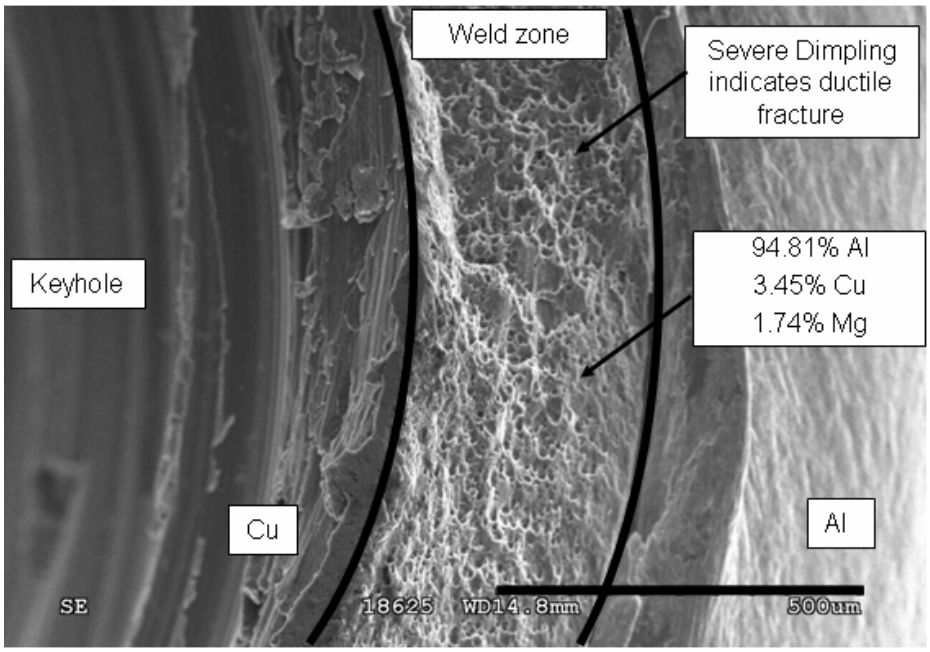

(a)

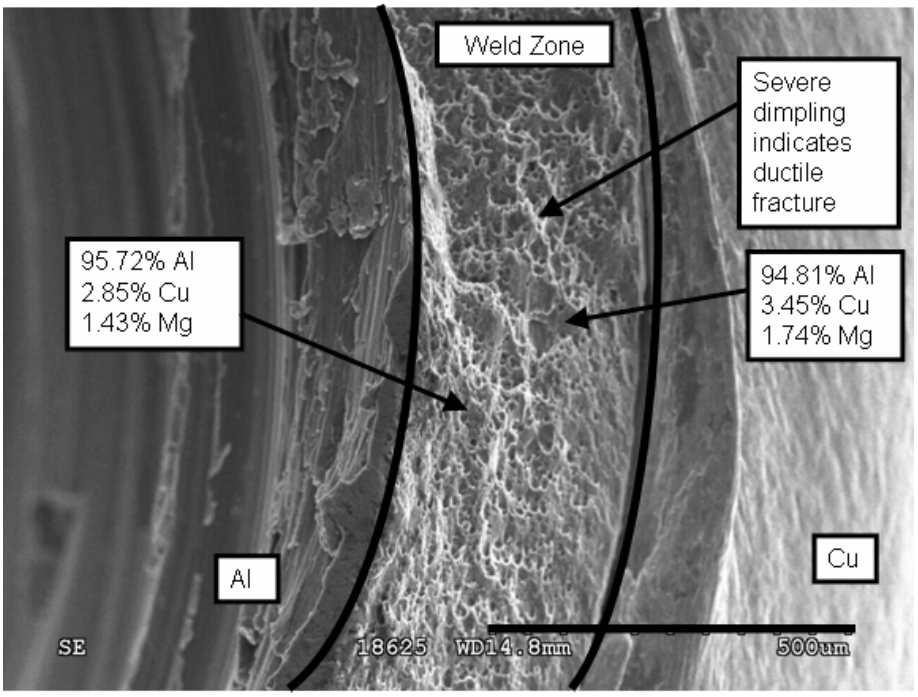

(b)

Figure 1-13. SEM secondary electron images of the fracture surfaces from (a) bottom-side of the upper 6061 Al sheet and (b) top-side of lower Cu sheet. Sample was from Run Order #8 and had weld strength ~ 1900 N. Weld was made with pin length of 2.60mm, rotation speed of 2000rpm, plunge depth of 0.13mm, and weld time of 3.0s.

Figure 1-14 is a cross section of the same specimen shown in Figure 1-13. The cross-sectional image confirms that the weld failed through a layer of aluminum between a Cu ring, which is extruded upward from the lower Cu sheet into the upper 6061 Al sheet (see Figure 1-14) and the weld keyhole. An untested sample using the same weld parameters was cross-sectioned and is shown in Figure 1-15. This image also shows the presence of Cu ring and that this Cu ring was not an anomaly that resulted from the tensile testing process. The Cu ring appeared to interlock the 6061 Al and Cu sheets, and help the dissimilar materials adhere to each other during tensile testing and to achieve high weld strengths before failure. As Figure 1-14 shows, the weld failed through the layer of aluminum between the top of the Cu ring and the weld keyhole. Because Cu is stronger than aluminum, the fracture had to bypass the Cu ring by going over it and then through the Al layer.

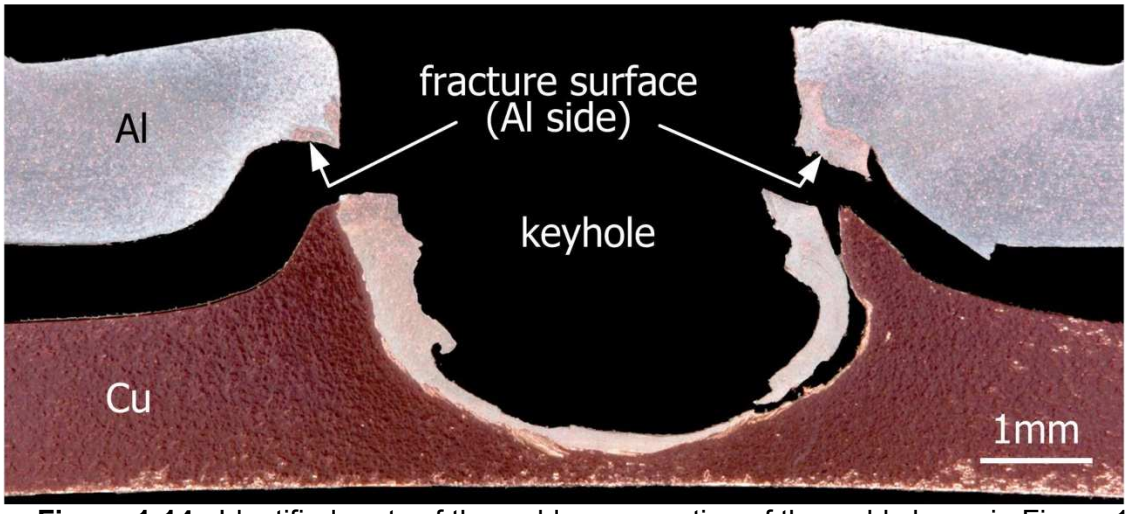

Figure 1-14. Identified parts of the weld cross section of the weld shown in Figure 1-18a.

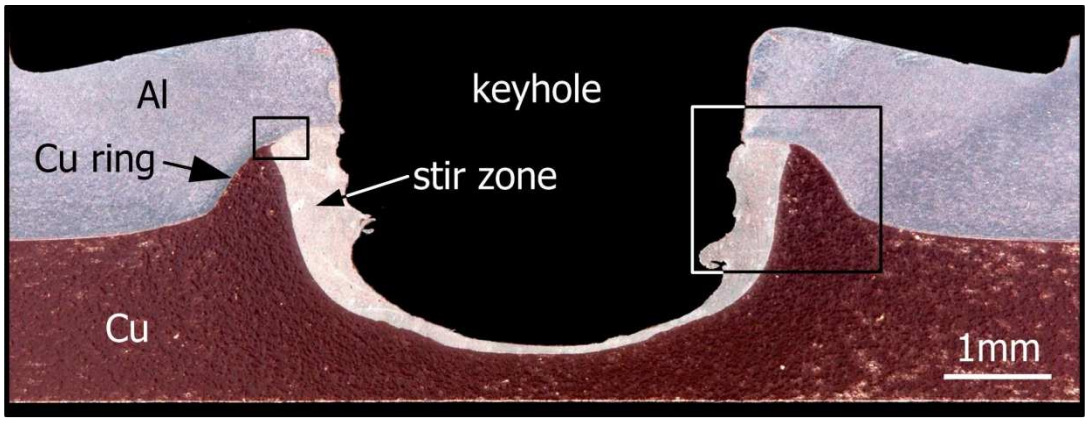

Figure 1-15. A cross section micrograph of an untested sample from Run Order #8. Tested samples in same run had a weld strength of 1900 N. Weld was made with pin length of 2.60mm, rotation speed of 2000rpm, plunge depth of 0.13mm, and weld time of 3.0s.

The presence of Al-Cu intermetallics at the Al/Cu interface was not observed in the strong weld shown in Figure 1-15. As shown in Figures 1-16 and 1-17, intermetallics were only observed in the form of small particles in the Al-rich stir zone; therefore, these particles would likely not be detrimental to the weld quality. In Figures 1-15, 1-16, and 1-17 no significant intermetallics are present along the interface between the Cu ring and the Al stir zone; contiguous intermetallics in this region would likely have been detrimental to weld quality. The absence of intermetallics along the bond line was not entirely surprising for two reasons. First, there is a steep temperature gradient in FSSW with the highest temperature at the tool/weld interface [47]. Second, the tip of the Cu ring is 300-400μm from the weld keyhole. The distance from the weld tool, the steep temperature gradient, and the relatively short weld times could combine to make the time and temperature insufficient to form intermetallics along the interface between the extruded Cu ring and the surrounding Al stir zone. Another factor related to, intermetallic formation is the residence time (distinguished from the actual weld time) of the Al at the Cu-Al interface. The residence time for the illustrated welds would be

substantially shorter than the weld time due to the constant flow of Al in the FSSW stir zone (i.e., the area between the keyhole and Cu ring in Figure 1-12).

The small intermetallic particles shown in Figure 1-17 have a complex layered structure. To better understand this structure, EMPA was conducted; the phases in a selected particle are identified in Figure 1-17(c). As shown, the γ_2-Cu_9Al_4 and θ-$CuAl_2$ phases were identified, but a third phase could not positively be identified because the width (the brightest contrast layer) was smaller than 1μm (the approximate size of the electron microprobe beam). The width being smaller than the beam size made determination of the exact phase not possible. From the EMPA this thin bright contrast phase was likely Cu or ɣ. More than likely, the phase was Cu because the ɣ phase has not been observed in other Al-Cu FSW studies as reported earlier. An attempt to confirm the exact phases present in the stir zone via x-ray diffraction was attempted in this investigation. Some researchers reported using x-ray diffraction to determine the exact phases present in dissimilar weld joint combinations [29, 42, and 43], but in this work the quantities of intermetallics were relatively small compared to Cu and 6061 Al. Therefore, it was not possible to discern any intermetallic phases in the diffraction patterns. The peaks from the Al and Cu overwhelm peaks associated with the low-quantity of intermetallics. In the end, the layered structures are metallurgically interesting, but did not appear to affect weld quality. Nevertheless, the reason for this layered structure will be discussed in Chapter 2.

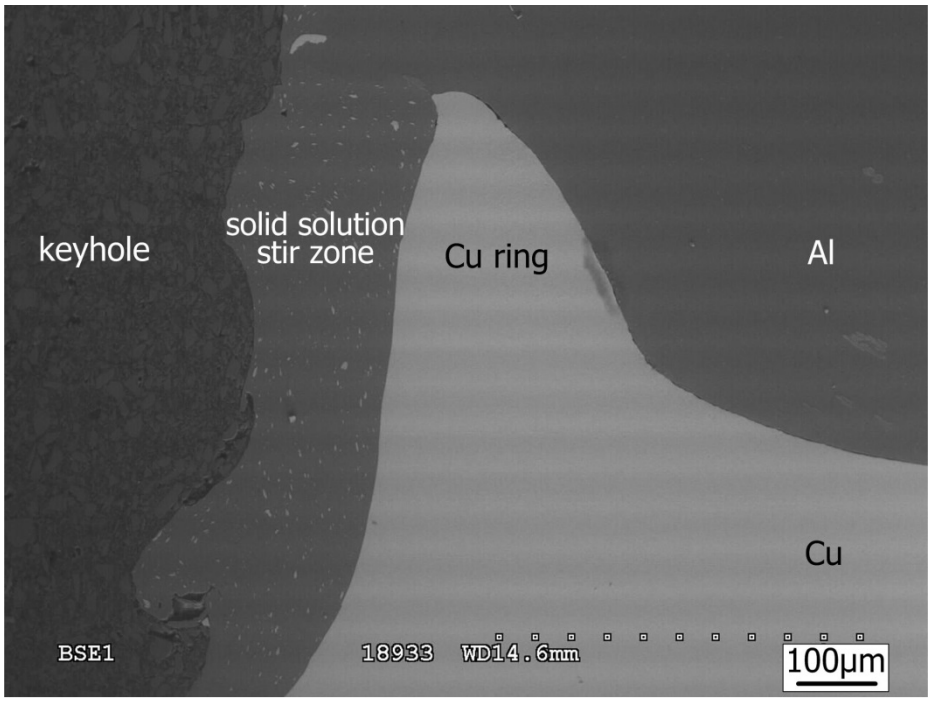

Figure 1-16. SEM backscattered electron micrograph of copper ring portion of untested sample from Run Order #8. Tested samples in same run had a weld strength of 1900 N. Weld was made with pin length of 2.60mm, rotation speed of 2000rpm, plunge depth of 0.13mm, and weld time of 3.0s.

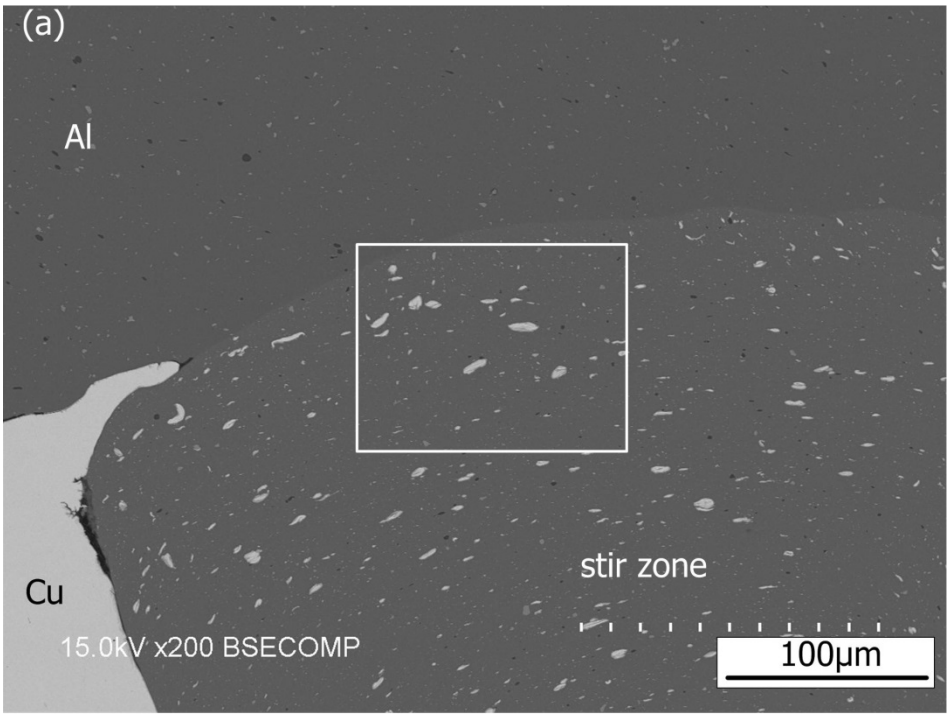

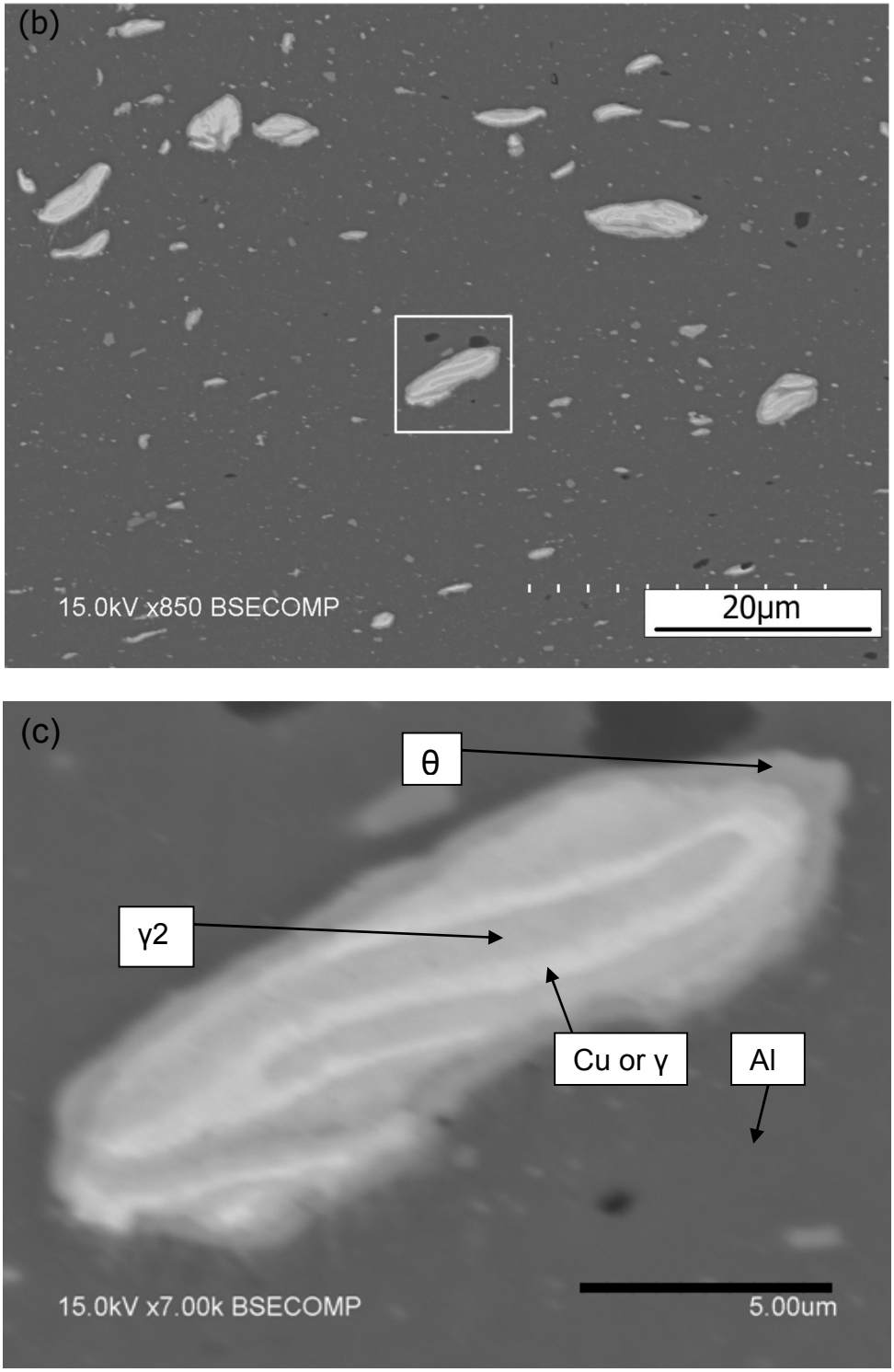

Figure 1-17. Three SEM images of left boxed area in Figure 1-13: (a) overview, (b) numerous layered intermetallic particles, and (c) higher magnification on one particle showing multiple phases present in particles.

To support the need for the formation of an Al(Cu) solid solution stir zone and an upward extruded Cu ring, a cross section of a weld with reasonable strength made with a 1.83mm pin length is shown in Figure 1-18. This weld shows both of these weld features and provides evidence that the width of the Al(Cu) solid solution zone promotes welds of reasonable strength. This sample included numerous small layered intermetallic particles and did no evidence of any intermetallic layer at the Al(Cu) solid solution stir zone and Cu ring interface, which is consistent with the samples made with a longer pin length.

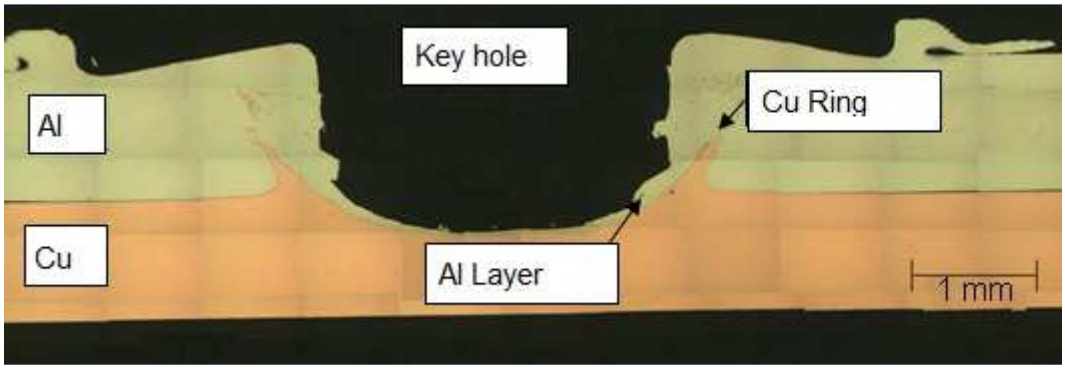

Figure 1-18. A cross section micrograph of an untested sample from Run Order #12. Tested samples in same run had a weld strength of 1900 N. Weld was made with pin length of 1.83mm, rotation speed of 2000rpm, plunge depth of 0.13mm, and weld time of 6.0s.

To validate the importance of the Cu ring, Al(Cu) stir zone, and lack of a contiguous intermetallic layer in the fracture region, an analysis of weak welds was conducted. Weak welds are defined as welds made at 1000rpm with the appropriate plunge depth. An example of the fracture surfaces from a low strength weld is shown in Figure 1-19. This shows a delaminated fracture surface which indicates a brittle failure mode. EDS analysis of the top surface of this sample (i.e. the 6061 Al sheet side of the weld) indicated mostly aluminum with low levels of copper present (less than 3 weight

percent) suggesting an Al(Cu) solid solution. The lower portion of the weld (i.e. the Cu sheet side of the weld) contained high levels of both Al and Cu suggesting the possible presence of a intermetallic on the Cu sheet half, and furthermore, that the sample failed between the Al(Cu) solid solution on the bottom of the 6061 Al sheet and an Al-Cu intermetallic on the lower Cu sheet.

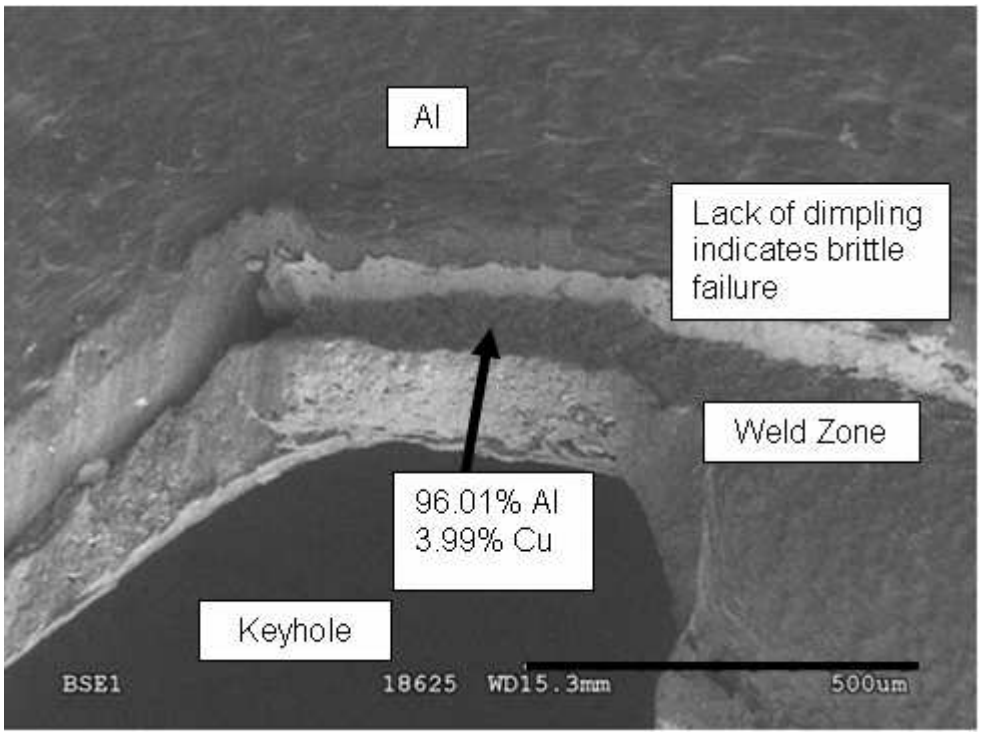

(a)

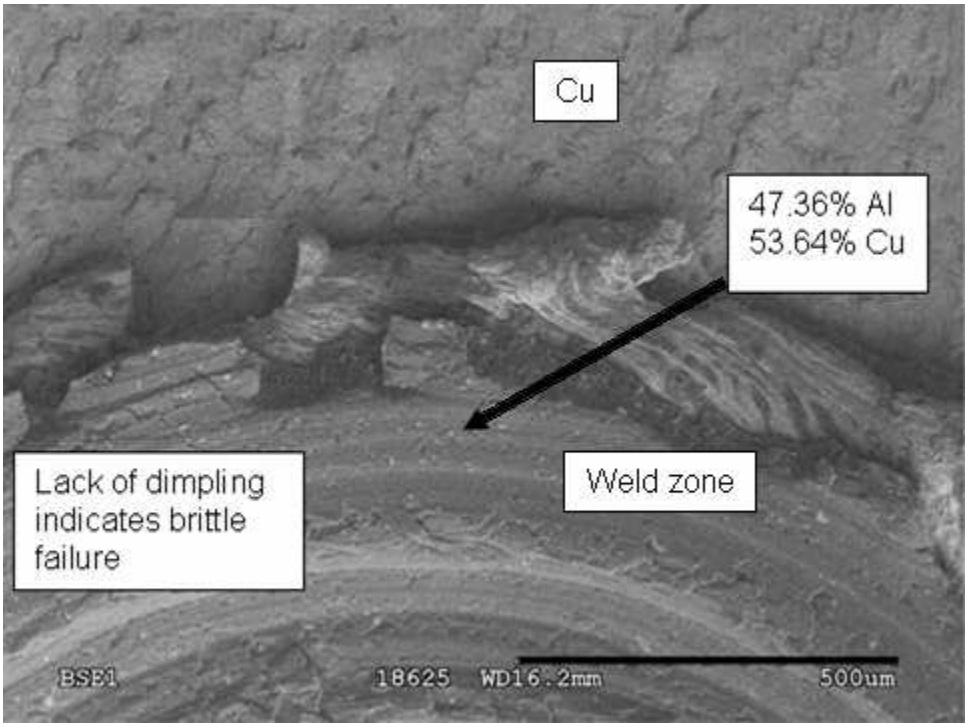

(b)

Figure 1-19. SEM backscattered electron micrographs of the fracture surfaces from (a) bottom-side of the upper 6061 Al sheet and (b) top-side of lower Cu sheet. Sample was from Run Order #27 and had weld strength ~ 400-500 N. Weld was made with pin length of 1.83mm, rotation speed of 1000rpm, plunge depth of 0.13mm, and weld time of 3.0s.

A cross section of the same weld in Figure 1-19 is shown in Figure 1-20. This cross section revealed only a thin Al(Cu) solution layer to carry the load. Failure occurred at the Al-Cu interface where intermetallic formation was likely. Neither a significantly wide aluminum stir zone nor an extruded copper ring, both of which were very apparent in strong welds, developed in this sample. To further understand this region, a sample, that was made with the same weld parameters as the sample in Figures 1-20, but was not tensile tested, was cross-sectioned and is shown in Figure 1-21. This cross section was also analyzed using EMPA. As in Figure 1-20, there is no evidence of a Cu ring to promote interlocking and bonding between the two sheets; instead, there is only a thin Al layer to carry the load. The SEM photomicrographs in Figure 1-22 of a weak weld show, as was the case in strong welds, a layered intermetallic structure existing in particles in the stir zone (Figure 1-22(c)). In addition, weak welds also exhibited a layered structure at the stir zone-Cu interface as shown in Figure 1-22(d). The layered structure was too fine for phase identification via EMPA. The structure observed in Figure 1-22(d) explains the fracture surface that contained both an Al(Cu) solid solution on one half and a intermetallic layer of the other half.

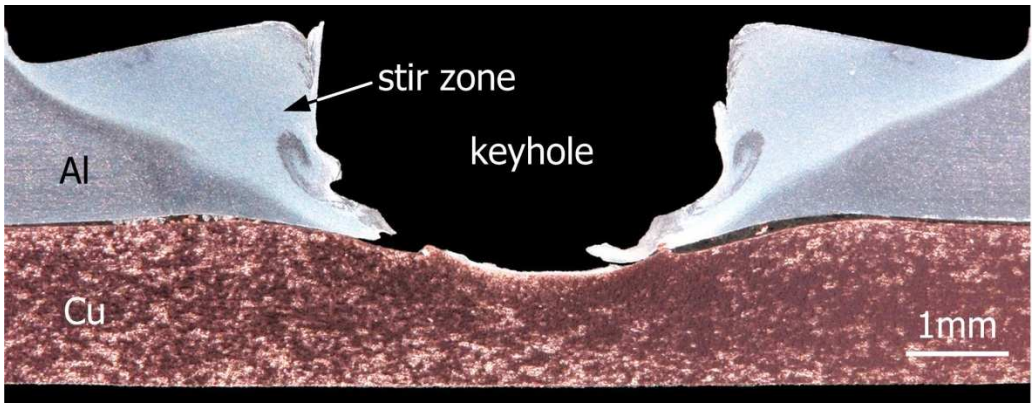

Figure 1-20. Cross section of same weld after shear tension testing as shown in Figure 1-19.

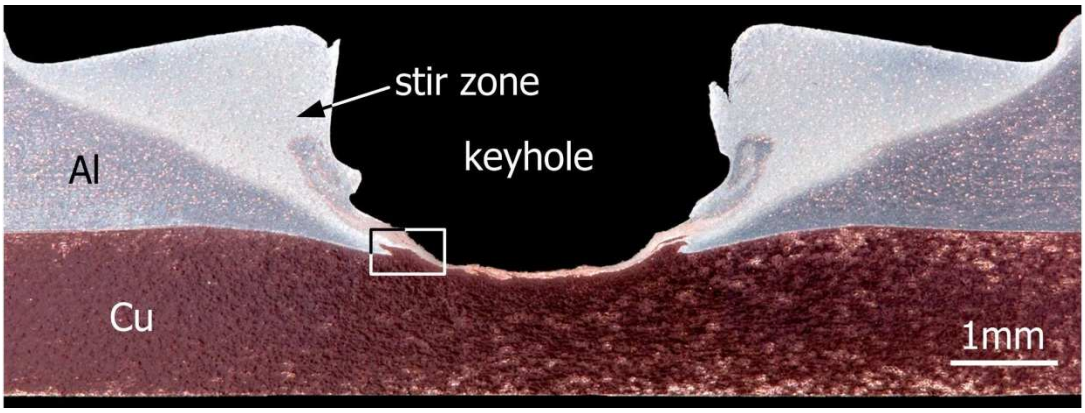

Figure 1-21. A cross section micrograph of an untested sample from Run Order #26. Tested samples in same run had weld strength of ~400-500 N. Weld was made with pin length of 1.83mm, rotation speed of 1000rpm, plunge depth of 0.13mm, and weld time of 3.0s.

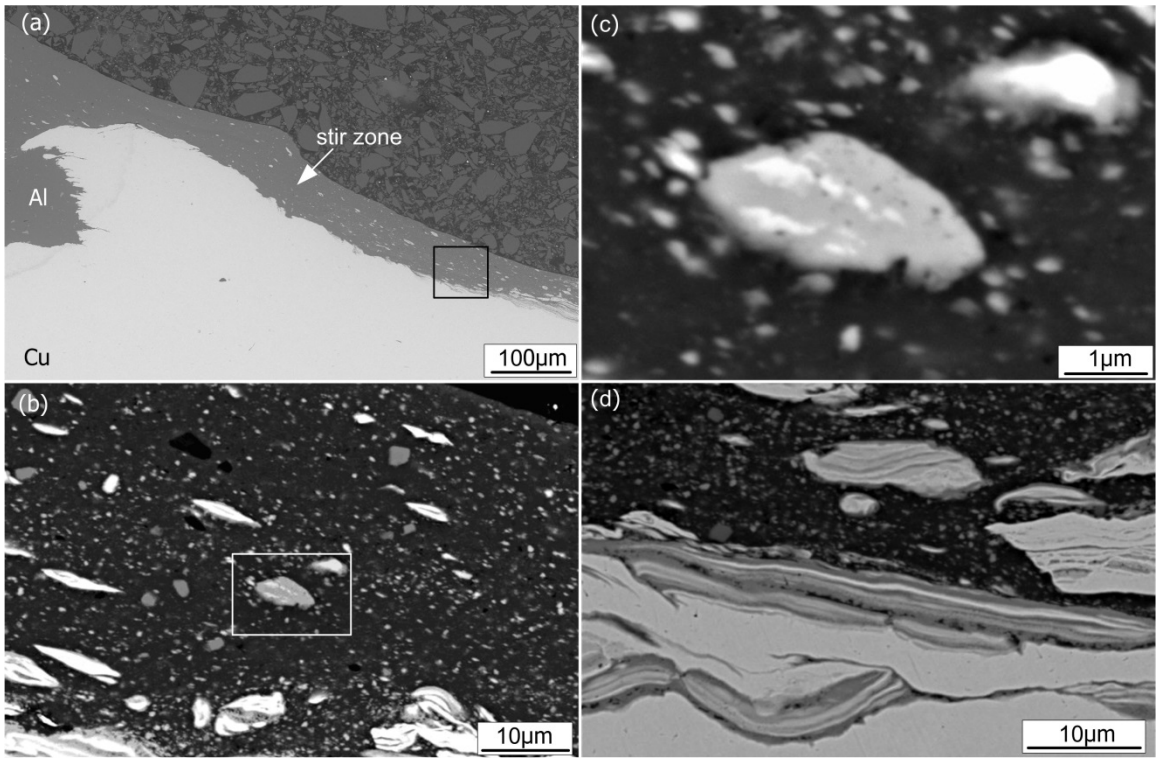

Figure 1-22. SEM images of boxed area in Figure 1-20: (a) overview; (b) boxed area in (a) enlarged; (c) particles in (b) enlarged; (d) stir zone-Cu interface region in the boxed region in (a).

Also noted in this sample and shown in Figure 1-22(b) and 1-22(c) were numerous, very small (<1 μm) higher-content copper particles (the brighter contrast

particles). These particles were so numerous and closely spaced that it was not possible to obtain a true chemical analysis via EMPA of the aluminum solid solution stir zone; any 1 μm circle (approximate size of the electron beam) that was hit with the electron beam contained at least one of these particles. The presence of these small particles in a weld made at 1000rpm and the lack of these particles in strong welds made at 2000rpm suggests that at the higher rotation speeds, copper is dissolving/diffusing more quickly into the Al(Cu) solid solution stir zone. This is not entirely surprising since increasing the rotation speed likely significantly increases the weld heat input, and consequently the weld temperature. Increasing weld temperature would increase the diffusion rate of copper into the Al stir zone.

To further confirm the hypothesis that a strong weld needs both an Al(Cu) stir zone of adequate width in combination with a Cu ring that promotes interlocking of the two sheets, a cross section from a weld with low weld strength that was made using the longer 2.60mm pin length and with a speed of 1000rpm is shown in Figure 1-23. This sample shows that neither a significant Al(Cu) solid solution stir zone nor a Cu ring formed at this lower rotation speed. The lack of a solid solution stir zone forced the weld to fail in the bottom of the keyhole where brittle Al-Cu intermetallics form and led to lower weld strength. This further supports the need for higher rotation speeds that permit, what would appear to be, appropriate material flow that allowed the formation of a reasonably wide Al(Cu) solid solution stir zone which in turn leads to higher strength welds.

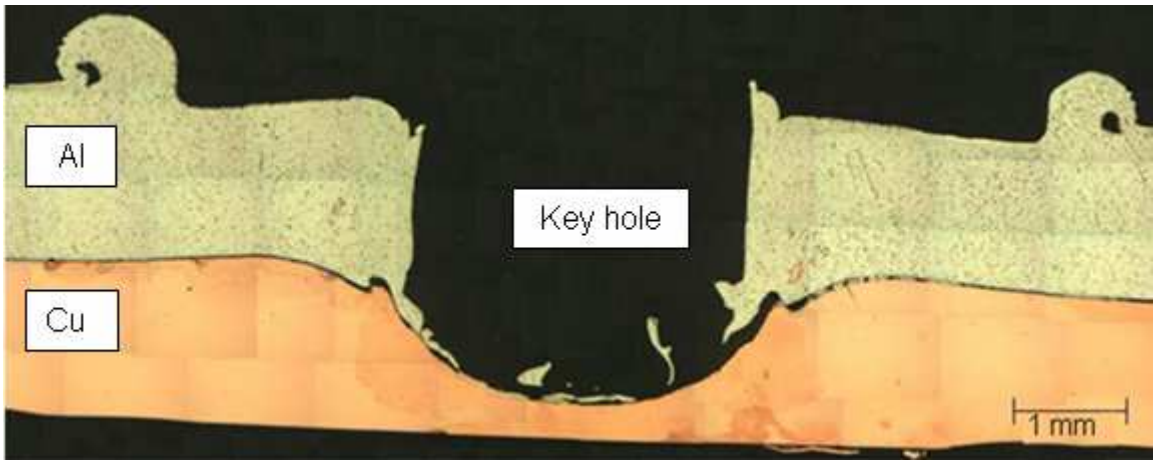

Figure 1-23. A cross section of weld made from Run Order #6 and had weld strength of ~880N. Weld was made with pin length of 2.60mm, rotation speed of 1000rpm, plunge depth of 0.13mm, and weld time of 3.0s.

Figure 1-24 schematically shows the comparison between a strong weld and a weak one, based on the welds shown in Figures 1-15 and 1-21, respectively. As mentioned previously and shown in Table 1-4, a longer pin with a length of 2.60mm and a higher rotation speed of 2000rpm or greater are more likely to produce a stronger weld, with strengths to just over 2000N possible. A strong weld tends to have a clear Cu ring extruded from the lower Cu sheet into the upper Al sheet to promote interlocking and bonding between the sheets, which is shown in Figure 1-24(a). Furthermore, the interface between the Cu ring and the surrounding Al is free of the contiguous intermetallics that are brittle and detrimental to the weld strength. As mentioned earlier, intermetallics are less likely to form along the interface, which is away from the rotating tool and thus relatively low in temperature in view of the high temperature gradients at the pin/Al interface during FSSW. On the other hand, a shorter pin with a 1.83mm length and a lower rotation speed of 1000rpm is more likely to produce a weaker weld with strengths typically less than 900N, as noted in Table 1-4. As presented in Figure 1-24(b), a weak weld tends to have no clear Cu ring to strengthen the weld, and the

layered contiguous intermetallic structure tends to be present along the interface to weaken the weld. The particles with layered intermetallics are likely fragments from the contiguous intermetallics along the interface. Predictably, with a longer pin at a higher rotation speed, the contiguous intermetallics near the pin tip continue to be broken and stirred into the Al around the pin as the pin plunges deeper during FSSW. This may explain the presence in a stronger weld of numerous layered particles in the Al layer between the Cu ring and the keyhole (Figure 1-17).

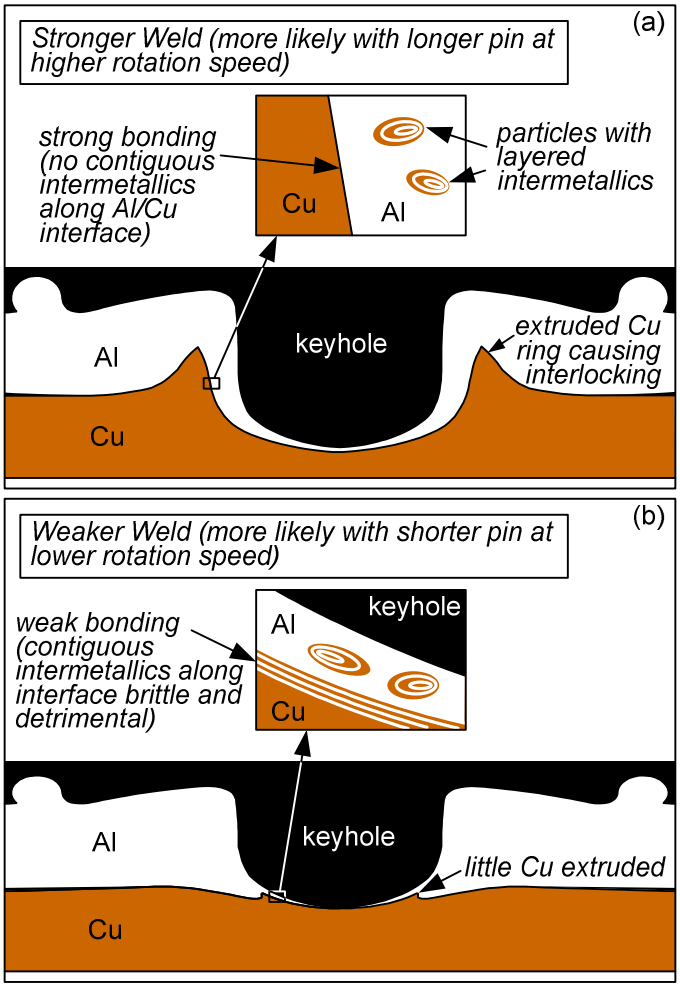

Figure 1-24. Comparison between welds: (a) strong weld with a Cu ring extruded upward from lower Cu sheet into upper Al sheet promoting bonding and interlocking between Al and Cu sheets; (b) weak weld with little Cu extrusion.

It was observed that the higher the Cu ring is, the more likely a thicker aluminum layer exists between the top of Cu ring and the keyhole. In Figure 1-25, the thickness of the Al(Cu) stir zone layer is plotted against the weld strength. A correlation seems to exist between the two, the weld strength increases by 2833N per millimeter increase in Al layer thickness. The resulting linear regression equation where "s" is the weld strength in kN and "t" is the aluminum layer thickness in millimeters is:

$$\mathbf{s = 2833t + 33} \qquad \textbf{(1-1)}$$

However, the non-dimensional linear correlation parameter (R^2) was not particularly high at 0.78 (closer to 1.0 is better, as 1.0 indicates perfect correlation); consequently, this equation should only be used for preliminary estimates. As an approximation, these measurements assumed the aluminum thickness was consistent (i.e. axisymmetric) around the entire weld circumference. The less-than-ideal correlation likely stems from two sources of error. First, the location of the measurement in a given cross section may not have been in the true mid-plane. While care was taken to cut, grind, and polish through weld mid-plane (done by visually trying to polish to the deepest part of the keyhole or the mid-plane of the weld), the exact mid-plane was not known. Consequently, some measurements were likely made slightly off center which would cause the aluminum layer to be thicker that it actually was. Secondly, the measurements were made after the samples were tensile pulled, so some distortion or elongation of the aluminum layer was possible.

One last note regarding the weld strengths measured in this study is that the average peak strength measured for 6061 Al-Cu FSSW in this investigation was 2080N. In comparison, Al-Al FSSWs made using a 2.60mm pin length, at 2000rpm rotation

speed, with a 6s dwell time, a 0.13mm plunge depth, and a 2.5mm/s plunge rate yielded average weld strengths of 2903N, or about 38% stronger than the strongest 6061 Al-Cu FSSWs. Since, the FSSW welds fail through the aluminum layer, having weld strengths much greater than the Al-Al would not be expected. Furthermore, the average strengths achieved in this study show that further improvements in strength may be possible by understanding the formation of, and then optimizing, the copper ring and aluminum layer thickness.

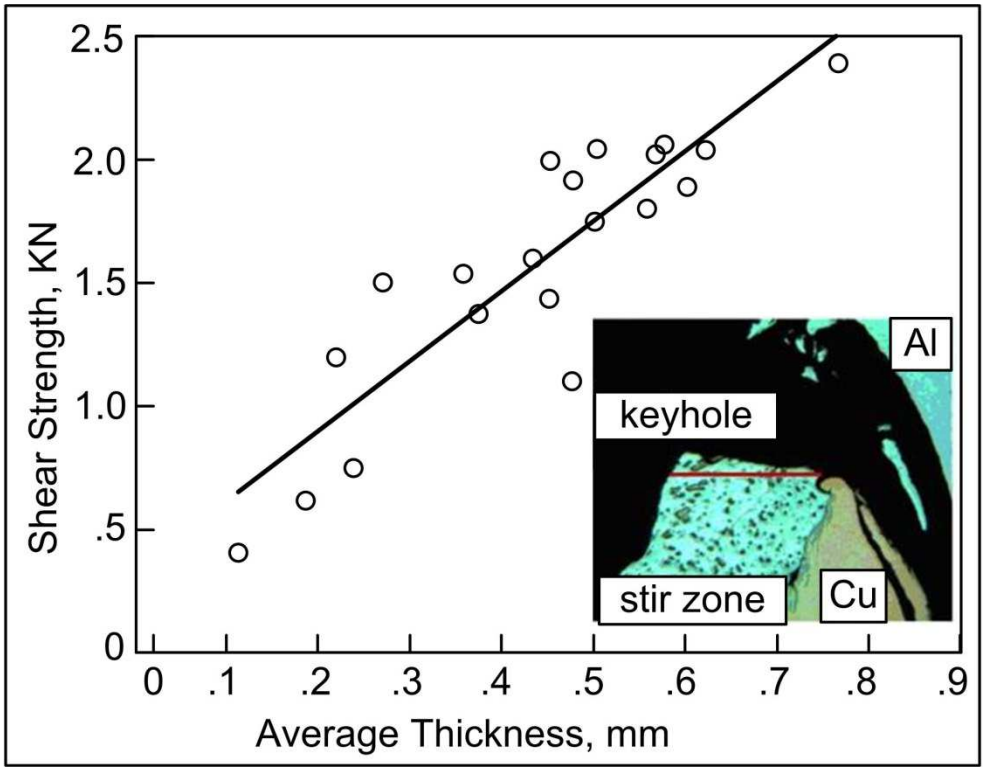

Figure 1-25. The weld strength vs. thickness of aluminum between top of the Cu ring and keyhole, with inset showing vertical cross-section near top of Cu ring.

1.5 Conclusions

FSSW between 1.5mm 6061 Al and 1.5mm oxygen-free Cu was conducted using a pre-hardened H13 tool steel with a 10mm shoulder diameter under the following welding conditions: tool pin length from 1.83mm to 2.60mm, shoulder plunge depth from 0mm

to 0.13mm, weld time from 3s to 6s, and tool rotation speed from 1000rpm to 3000rpm. Within these ranges of welding parameters, the following conclusions can be reached:

1. The rotation speed had the most significant effect on the weld strength, which augments with increasing rotation speed. The average weld strength improved by 150% when the rotation speed was increased from 1000rpm to 2000rpm. However, further increasing the rotation speeds from 2000rpm to 3000rpm did not produce an increase in the weld strength.
2. The average weld strength also increases with a longer pin length. A 2.60mm pin length at 2000rpm produced an average weld strength that was 70% stronger than those made with a 1.83mm pin length at 2000rpm.
3. Strong welds tend to have a Cu ring extruded upward from the Cu sheet into the upper Al sheet. The Cu ring promotes interlocking and bonding between the two sheets. The interface between the Cu ring and the surrounding Al was free from contiguous intermetallics in strong welds.
4. The thickness of the aluminum layer between the tip of the Cu ring and the key hole was correlated to the weld strength, with the average weld strength increasing approximately 2833N per each millimeter of aluminum layer thickness.

Chapter 2: Material Flow in Friction Stir Spot Welds of Aluminum to Copper

2.1 Introduction

Friction stir welding (FSW) is a process that was invented in England in 1991 by The Welding Institute (TWI) [1]. The process consists of pushing a non-consumable rotating tool into a weld joint. The frictional and viscous heating generated by the tool softens the weld area sufficiently so that the material can be stirred and mixed to cause bonding. Because no melting is needed to form an acceptable weld, some of the issues associated with fusion processes, such as solidification cracking and cold fusion, can be avoided. Initial FSW research focused on welding aluminum alloys, but there has also been interest in using FSW to join dissimilar materials such as aluminum to steel, aluminum to stainless steel, aluminum to magnesium, and steel to copper [6-9]. These combinations are of interest because these material combinations cannot be welded with traditional fusion welding methods.

A variation of the FSW process, known as friction stir spot welding (FSSW,) was also developed. As shown in Figure 1-1, In FSSW, the rotating tool is plunged into a lap joint and withdrawn after the shoulder touches the work piece and dwells for a desired time; the tool does not move forward in FSSW [8 and 22]. As with traditional resistance spot welding, FSSW is limited to lap joint configurations. A primary advantage of FSSW with aluminum alloys is that many welds can be made with a single tool because a hardened tool-steel is employed; Hinrichs et al. [16] reported that a single tool, which was heat treated to the optimal hardness made 100,000 welds, which was equivalent to 6 days of production. At the end of their study, weld quality was still acceptable. This

fact, combined with the relatively low tool hardness (<50HRC), led the researchers to speculate that tool life could be 100,000's of welds.

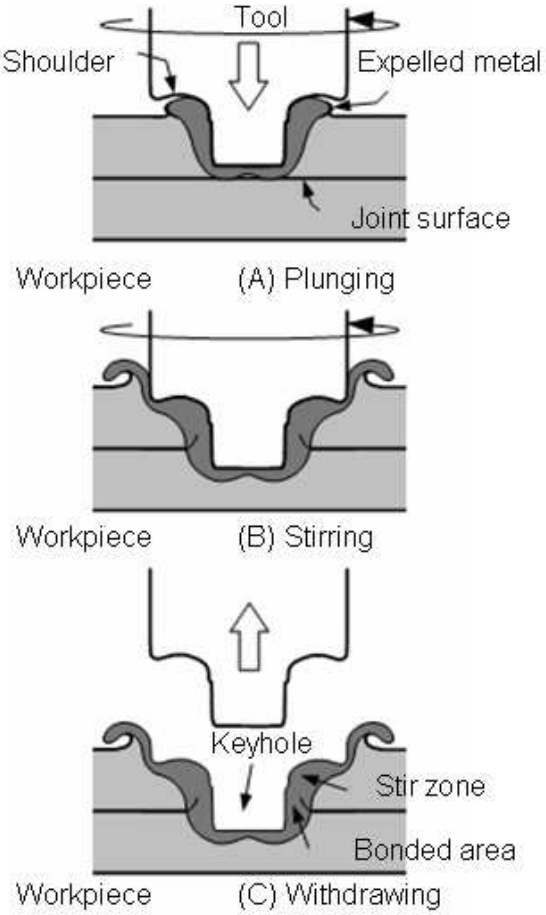

Figure 2-1. Schematic of the FSSW Process [22]

Most FSSW work has focused on welding aluminum to aluminum alloys and magnesium to magnesium alloys [8, 16, 17, 18, and 22]. A dissimilar combination of aluminum to copper could be useful in making electrical connections and components. Although literature on aluminum-to-copper FSW is available [13, 15, 19, 20, 23, 24, 25, 38, and 45], only limited work has been reported on aluminum to copper FSSW [61]. Heideman et al. [61] reported the weld parameters and weld macrostructure needed for quality FSSW welds with a 1.5mm 6061 Al top sheet and a 1.5mm oxygen-free copper bottom sheet. The macrostructure leading to welds of reasonable strength consists of a

combination of a copper ring that is extruded upward into 6061 Al sheet and the widest possible Al-rich stir zone between the weld keyhole and the upward extruded Cu-ring (see Figure 2-2). Heideman et al. [61] further identified that this macrostructure was best formed by using longer tool pins (up to 2.60mm) and rotation speeds of at least 1500rpm. While Heideman et al. [61] noted that 6061 Al to Cu FSSWs of reasonable strength could be produced, it also was observed that unexplainable inconsistency in weld strength namely, both strong and weak welds under the exact same welding parameters.

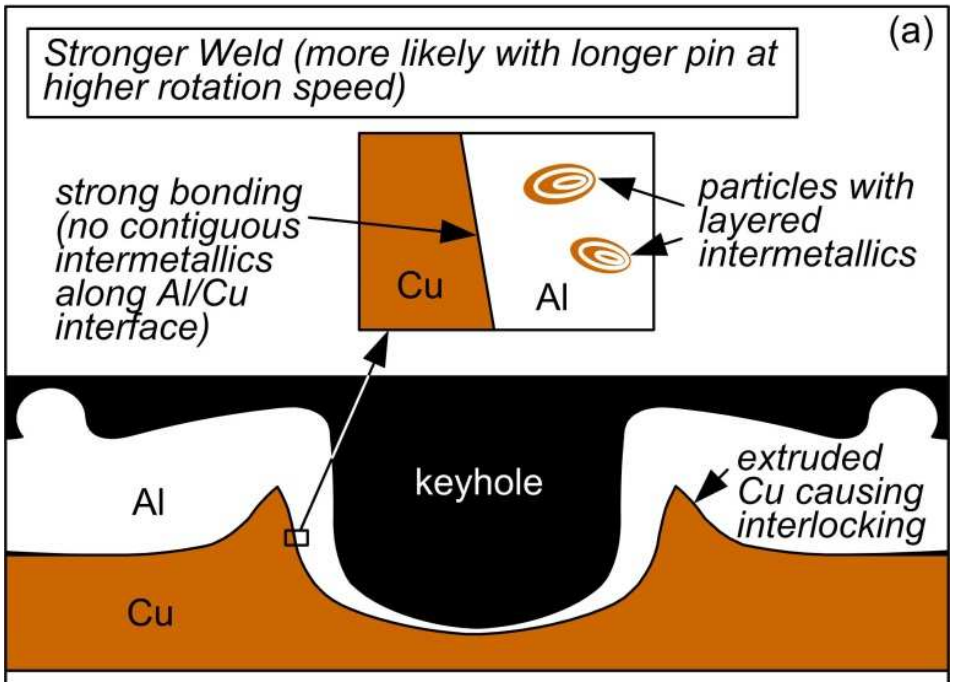

Figure 2-2. Schematic of the weld macrostructure necessary for strong weld [20]

The focus of this part of the 6061 Al to Cu FSSW investigation is to (1) identify the cause of weld inconsistency and (2) understand the material flow that leads to higher strength FSSW between 6061 Al and oxygen-free pure Cu. By understanding the material flow that leads to higher strength welds, the FSSW process may be further

optimized to ensure high quality welds can be consistently made. To understand material flow, welds were made where the non-consumable tool was not extracted from the weld. This approach permitted a better understanding of (1) the function of the threads on the tool pin; (2) the macro material flow that leads to acceptable strength welds; (3) the microstructure of the Al-rich stir zone between the weld keyhole and the upward extruded Cu ring; and (4) the potential sources of residual material that lead to weld inconsistencies.

2.2 Experimental Procedure

The materials used consisted of 1.5mm thick 6061-T6 aluminum (referred to as 6061 Al) with an average hardness of 58HRB and 1.5mm oxygen-free pure copper (referred to as Cu) in the H01 condition (i.e. quarter hard) with an average hardness of 73HRF. The 6061 Al and Cu compositions are shown in Tables 2-1 and 2-2. The FSSW samples consisted of a 6061 Al top sheet and Cu sheet on the bottom with a 25mm overlap between sheets. The tool design used for all but two experiments, as shown in Figure 2-3, consisted of a 10.00mm diameter concave shoulder, a threaded 4.00mm diameter pin with a convex tip, and a 2.34mm pin length. The tool material for all tools was pre-hardened H13 (42-46HRC) tool steel. The only difference in the other tool design, which was used two experiments, was that the other tool design featured a smooth threadless pin. This design was used to understand the functions of the tool threads.

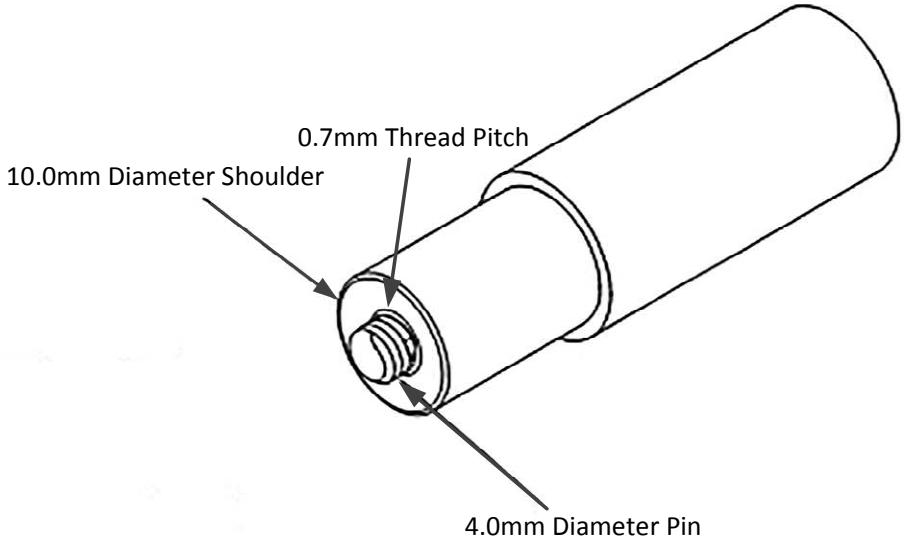

Figure 2-3. Tool used for weld strength variation of 100 welds made at the same welding conditions: 2000rpm, 2.34mm plunge depth, 2.54mm/s plunge rate, 6.00s dwell time.

Table 2-1. Composition of 6061 Al as determined by ICP and compared to 6061 Al Specification.

	Si	Fe	Cu	Mn	Mg	Cr	Zn	Ti	Al
Sample Comp.	0.69	0.60	0.28	0.006	1.03	0.15	<0.001	0.014	Rem.
Specification	0.4 - 0.8	0.7 Max	0.15 - 0.40	0.15 Max	0.8 - 1.2	0.04 - .35	0.25 Max	0.15 Max	Rem.

Table 2-2. Composition of oxygen-free copper (weight percent) as determined by ICP and compared to oxygen-free copper specification. Other elements combine to 0.017 weight percent with individual elements all less than or equal to 0.001 weight percent.

	Cu	Ag	As	Sb	S	P	Fe	Ni	Mn	Sn	Other*
Sample Comp.	99.95	0.001	0.002	0.006	0.002	0.001	0.005	0.002	0.001	0.013	0.017
Specification	99.95	----	----	----	----	----	----	----	----	----	

To determine welding consistency, 100 consecutive welds were made using a single tool as described above and shown in Figure 2-3. The welding conditions were held constant for all 100 welds and consisted of the following: 2000rpm rotation speed,

2.34mm plunge depth, 2.54mm/s plunge rate, and 6.00s dwell time. After welding, weld strength, used to indicate weld quality, was measured via lap shear tensile testing. This testing employed the use of a spacer on each end of the sample to minimize bending as shown in Figure 2-4. Lap shear testing was conducted using an Instron tension test instrument with a cross-head speed of 2.11mm/s. The maximum load measured at failure for each sample was recorded; this maximum load will be referred to as the weld strength. After measuring weld strength, low strength (poor quality) and high strength (acceptable quality) welds were cross-sectioned and metallographically prepared. Metallographic preparation used standard techniques with a final polishing step consisting of 0.04 μm SiC suspension in 100ml water, 100ml ethanol, and 10g iron III nitrate added suspension solution to help remove copper scratches. After metallographic preparation, the samples were viewed using light microscopy. The weld zone of these samples was distorted during weld strength testing making welding features somewhat difficult to observe. This distortion makes it difficult to understand much of what happened during welding.

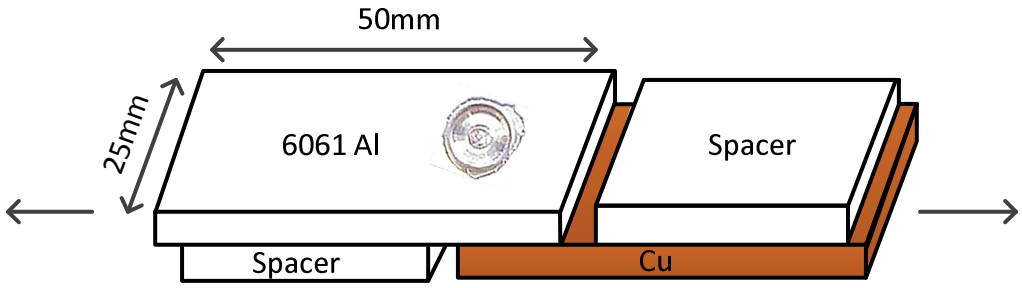

Figure 2-4. Shear sample used to measure FSSW joint strength (note that spacers were added to the sample during testing to minimize sample bending).

To understand material flow, the tool needed to remain in the sample at the end of each prescribed weld. The CNC mill used for this work was abruptly stopped at the end of the weld sequence such that the tool remained in the weld sample, as shown in

Figure 2-5. Since the tool was left in the welded sample, for most experiments a new tool was used for each weld sample. The only exception was that during early flow experiments, tools that had previously made FSSW 6061 Al to Cu welds were used. Following welding, each sample was cross-sectioned and metallographically prepared as described earlier. These samples were analyzed via light microscopy and scanning electron microscopy.

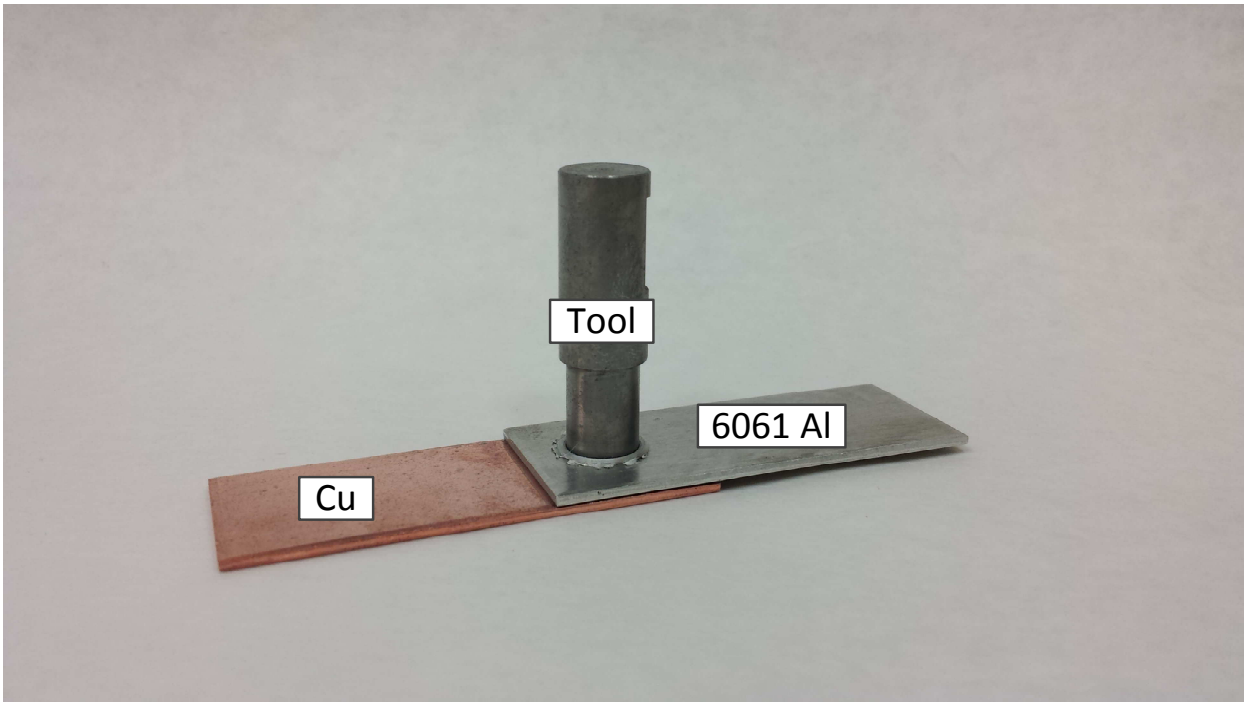

Figure 2-5. Sample of FSSW where the tool was left in the sample after the desired weld time.

Early flow experiments used weld rotation speeds of 2000rpm and 3000rpm, with the plunge rate and plunge depth held constant at 2.54mm and 2.34mm respectively. Here, plunge depth is defined as the depth the pin tip is plunged into the work piece. A 0.00mm plunge depth would imply the tool tip is level with the top surface of the upper 6061 Al sheet, and a plunge depth of 2.34mm would imply (for a tool with a 2.34mm pin length) the tool shoulder is just touching the top surface of the 6061 Al sheet. Dwell

time, the time from the end of plunge to the time the tool rotation was stopped, varied from 6.0s to 10.0s. These weld parameters were selected based on early work by Heideman et al. [61] that showed welds of reasonable strength were possible under these conditions.

These early experiments yielded limited information about material flow and weld macrostructure development. To gain better material flow understanding, seven samples were made with tool plunge depths of 1.65mm, 1.74mm, 1.78mm, 1.86mm, 1.95mm, 2.34mm and 2.59mm. The 1.65mm plunge depth was selected as the starting point because it was believed that the tool should be plunging into the lower Cu sheet by 0.15mm (the upper Al sheet was 1.50mm thick). The 2.59mm plunge depth was selected as the endpoint because at this depth the shoulder would be plunged 0.25mm into the top 6061 Al sheet and based on the earlier work by Heideman et al. [61], this depth is more than sufficient to produce welds of reasonable strength. The plunge rate for this phase of experimentation was fixed at 0.21mm/s and the dwell time was 0.0s with the CNC mill stopped exactly when it reached the desired plunge depth. The samples appeared similar to Figure 2-5 with the only exception being that the shoulder would not have engaged the upper 6061 Al surface until a plunge depth reached 2.34mm. Following welding, the sample was removed from the CNC and metallographically prepared as outlined earlier.

2.3 Results and Discussion

This section will be split into four sections. First, the issue of 6061 Al to Cu FSSW weld inconsistency will be addressed (Section 2.3.1) followed by three sections on

material flow in a 6061 Al to Cu FSSW. In Section 2.3.2, the early work with the tool left in the weld will be discussed. Next, the role of the tool threads will be explored by comparing tool pins with threaded and threadless features (Section 2.3.3). Lastly, with the role of tool pin threads understood, material flow will be discussed through a series of seven different plunge depths beginning at 1.65mm and ending 2.59mm (Section 2.3.4).

2.3.1 Weld Inconsistency

The results from 100 consecutive weld experiments are shown in Figure 2-6. In this figure, the weld strength varied from approximately 500N to 2500N.

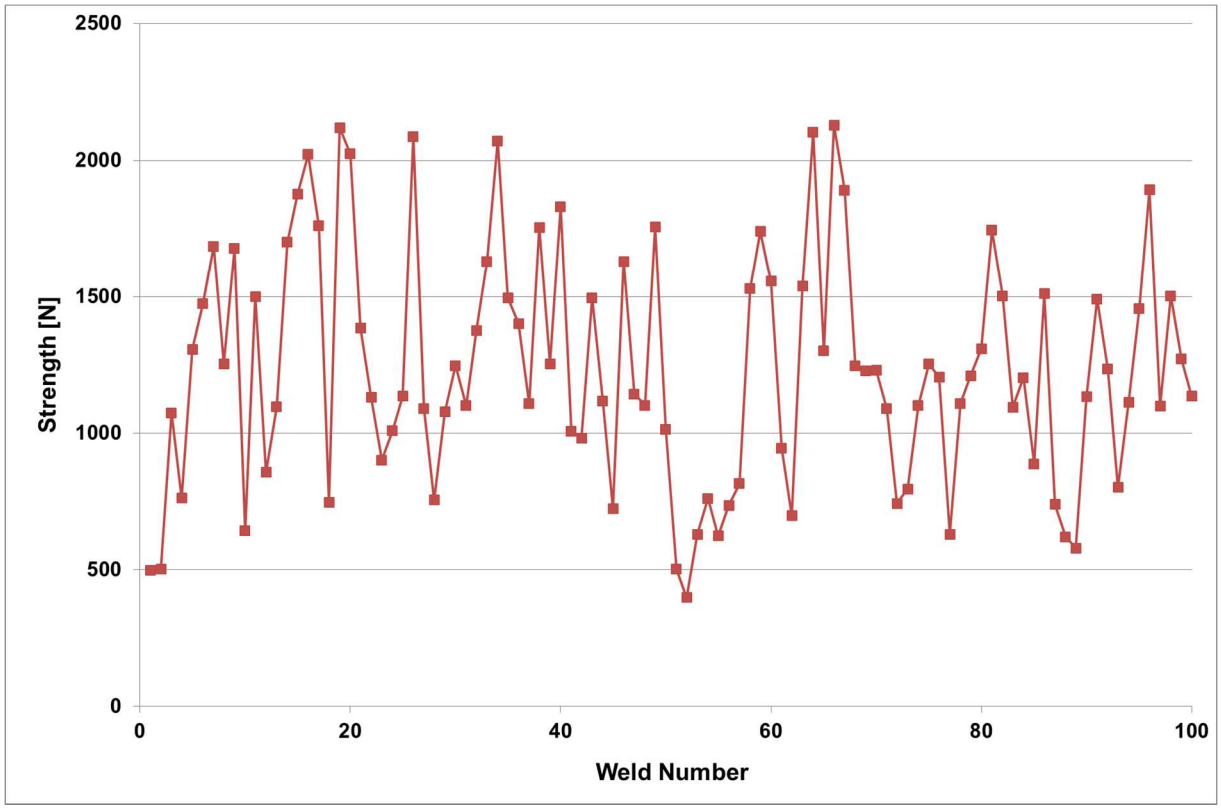

Figure 2-6. Weld strength variation of 100 welds made at the same welding conditions: 2000rpm, 2.34mm plunge depth. 2.54mm/s plunge rate, 6.0s dwell time.

To understand the reason for the inconsistency, the structure of welds with strengths 876N and 2,275N were evaluated. Figure 2-7 shows the cross-sectional structure of these welds after measuring their strength. The cross sections were aligned as close as possible when mounted for metallurgical sample preparation. However, they could not be aligned perfectly and therefore horizontal cracks (where the samples failed during strength testing) are visible in the cross-sections. Additionally, the structure observed should not be taken as the structure immediately after welding. During testing the structure of the weld changes due to material flow and the weld elongates during strength testing. The important difference between these two welds, even though welding conditions were exactly the same, is the lack of a contiguous Al layer along the vertical wall of the Cu ring on the lower strength weld (see Figure 2-7(a)). By comparison, the stronger welds show a noticeable Al stir zone between the upward extruded Cu ring and the weld keyhole (see Figure 2-7(a)). Also, the structure of lower strength weld shows that some Al-Cu intermetallics formed in the bottom of the weld indicating that some Al moved during the welding process, but there must have been insufficient material flow to form the contiguous Al layer required to achieve welds of reasonable strength. The reason for the inconsistency in the Al layer presence was unclear. To determine the reason for this inconsistency, samples were made to understand material flow with the tool remaining in the sample at the end of the welding cycle.

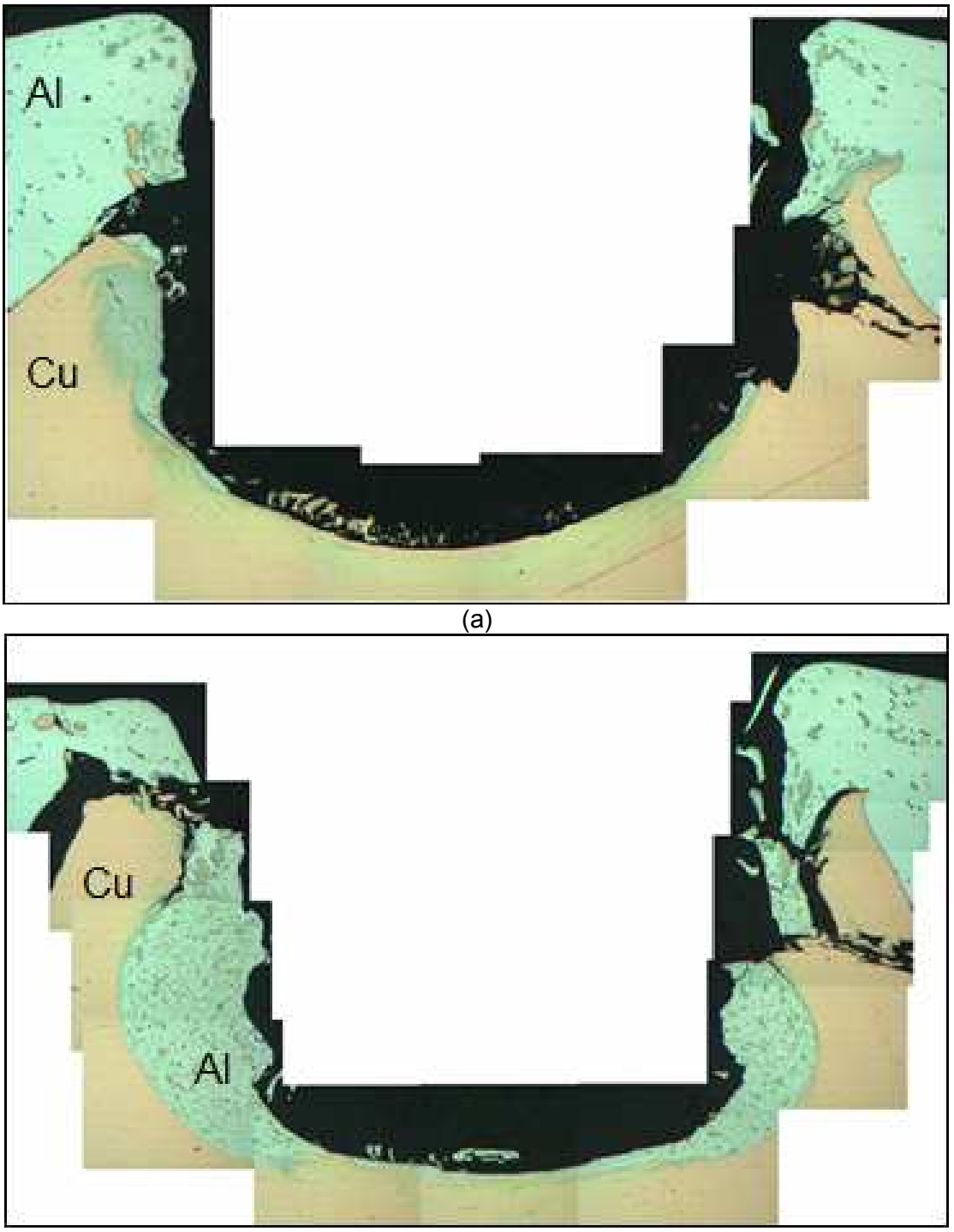

Figure 2-7. Photomicrographs of a weld with strengths of (a)876N and (b) 2275N.

2.3.2 Early Flow Experimentation

In the first material flow experiments, the tool rotation was stopped at the end of the prescribed dwell period; with two weld cross sections are shown in Figures 2-8 and 2-9. These first experiments provided little information on material flow because the required Cu ring was formed and may have changed shape with dwell time, which is in agreement with earlier work by Heideman et al. [61]. The notable issue observed in Figure 2-9 was the lack of an Al-rich stir zone region between the upward-extruded Cu ring. Based on work reported by Heideman et al. [61], the weld in Figure 2-9 would be expected to be of low strength because it lacks the Al-rich stir zone region between welding tool and the Cu ring. By comparison, the weld macrostructure in Figure 2-8 shows both the upward extruded Cu ring and the Al-rich stir zone between the Cu ring and welding tool. With the presence of both of these features, this weld would be expected to be of reasonable strength (likely in excess of 2000N). (Weld strength cannot be tested when tools are left in the weld at the end of the process; strength determination is estimated based on Heideman et al. [61].)

In comparing the two macrostructures in Figures 2-8 and 2-9, the tool threads in Figure 2-9 are filled with a complex layered structure. In these layered structures, the light (nearly white) regions are Al-rich regions, whereas the yellowish-orange regions are copper-rich regions made up of various Al-Cu intermetallics. These layered copper-rich and intermetallic structures are expected to be harder and less capable of flow compared to the Al-rich material in the stir zone in Figure 2-8. While the exact phases may be metallurgically interesting, two important questions can be raised. First, do the tool threads promote the formation of the macrostructure in Figure 2-9? The answer is

yes, based on a comparison of material flow associated with a tool with a smooth (unthreaded) pin and that associated with a traditional threaded pin tool; this explanation will be presented below.

The second question is what is the source of the large complex layered structures? The second query cannot yet be fully answered, but through the seven step plunge depth flow experiment, a potential source for large layered particles will be identified. Another important note is that the tools used to make the samples in Figures 2-8 and 2-9, had previously made welds so there was material adhered to them from previous welds.

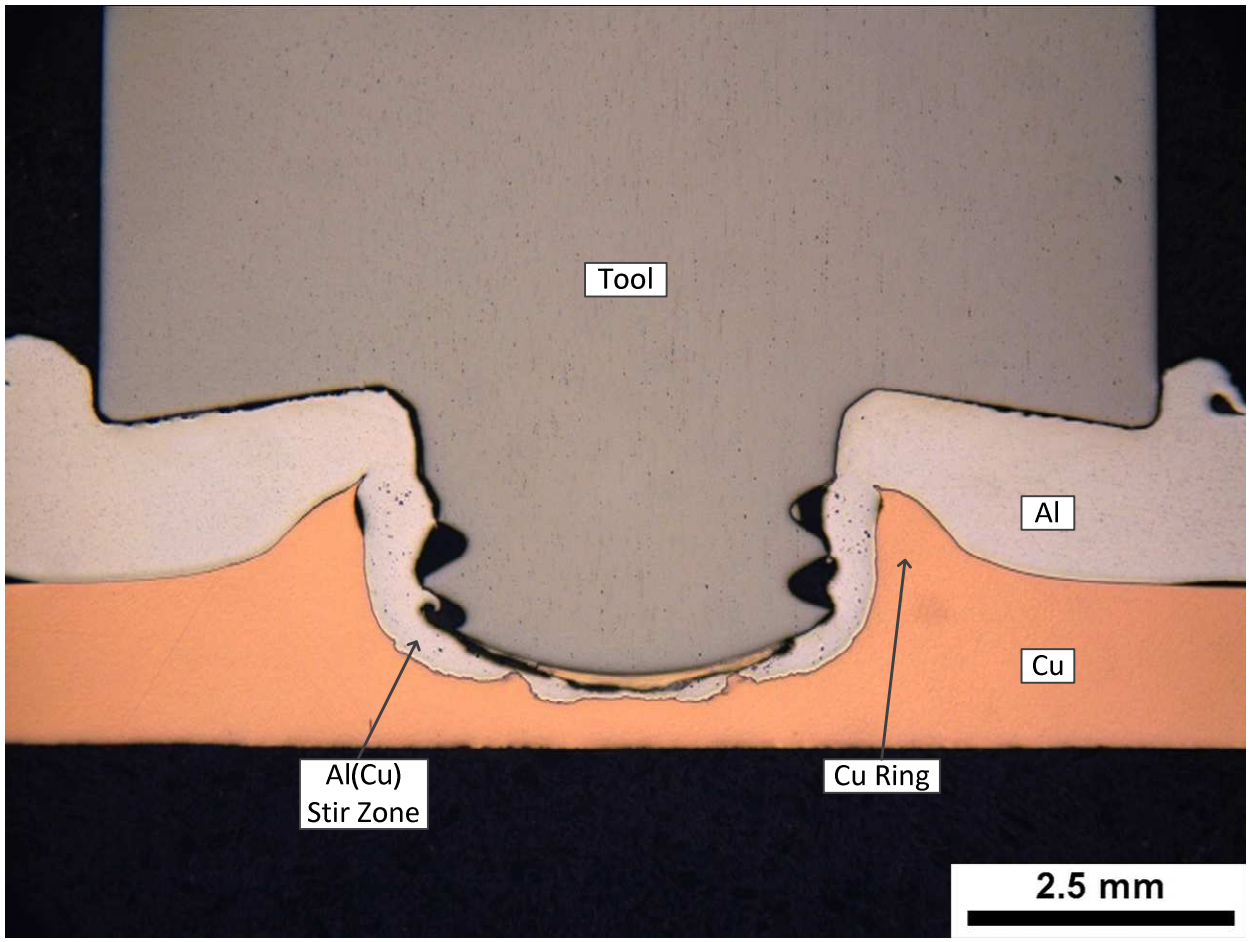

Figure 2-8. A FSSW with the tool remaining in the weld after the dwell time was reached. Welding conditions: 2000rpm, 2.34mm plunge depth, 2.54mm/s plunge rate, 15.0s dwell time.

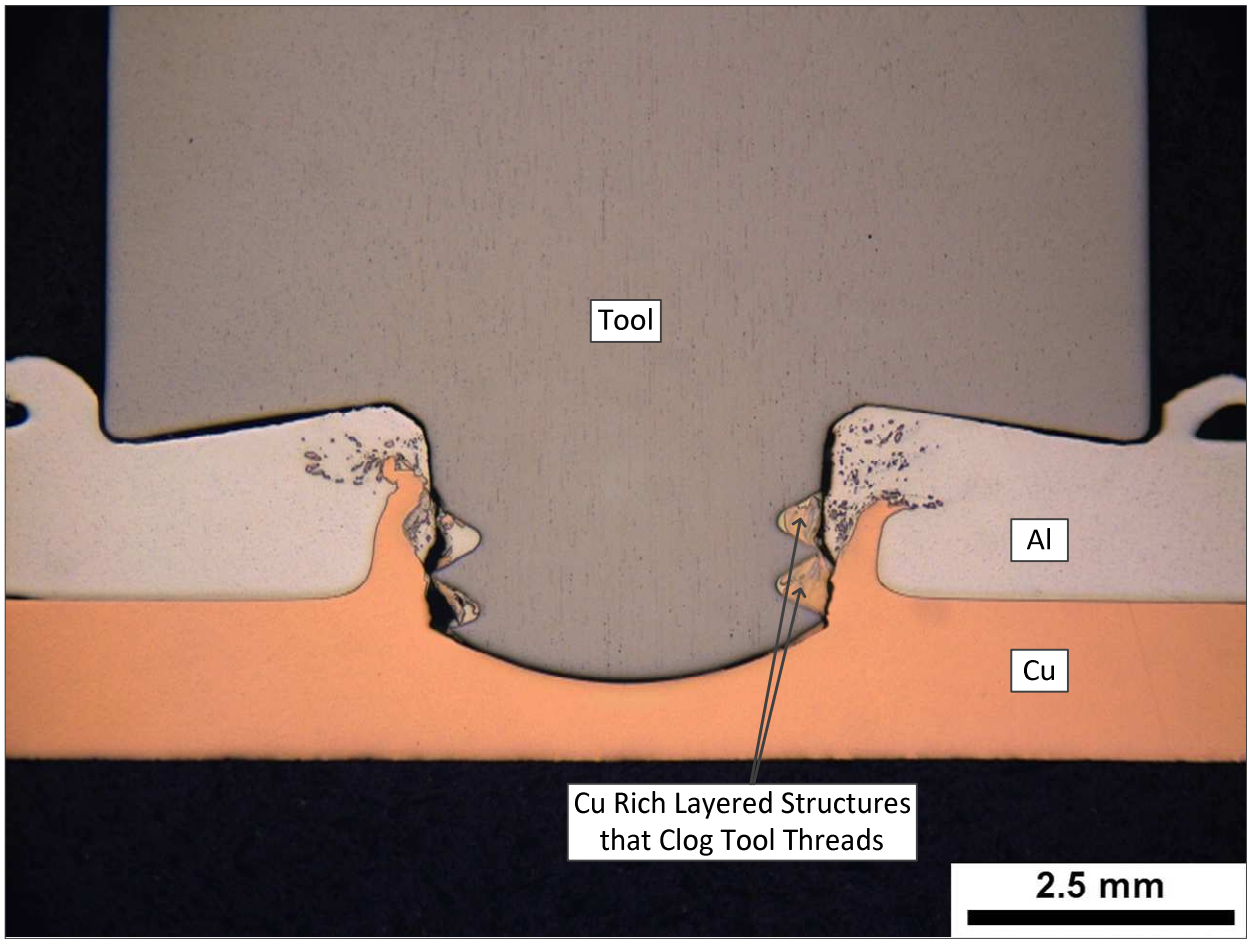

Figure 2-9. A FSSW with the tool remaining in the weld after the dwell time was reached. Welding conditions: 3000rpm, 2.34mm plunge depth, 2.54mm/s plunge rate, 6.0s dwell time.

The observation that the tool threads could become clogged during welding was an important finding because in earlier work weld strength apparently randomly dropping below 1000N was observed. For example, twenty consecutive welds were made using the same tool and welding parameters, 75% of weld strengths were in excess of 1500N and 10% of the welds were less than 1000N. The only explicable reason for the low strength was that the Al-rich stir zone layer was not present between required upward extruded Cu ring and the weld keyhole. However, the reason for the lack of an Al-rich layer could not be explained. Figure 2-9 shows that the likely reason

for the absence of Al-rich stir zone is that the threads became clogged. Additionally, in all of the experimentation done, the first weld made with a new tool was always of reasonable strength (nearly 2000N or more), provided the correct weld parameters are used. Consequently, material adhered to the weld tool is potentially a cause of random low-strength welds.

It should be noted that both welds in Figures 2-8 and 2-9 have black areas that would appear to be voids present in the cross sections. It is highly unlikely that these black areas would be present during welding since voids like these would impede material flow. More than likely, the abrupt stop of the welding process (going from 2000rpm or 3000rpm to 0rpm in an instant) leads to damage in the cross-section, and thus, these voids are present. The tool was abruptly stopped at the end of the welding cycle to capture the material flow at a precise period in time; permitting the slow ramp down of tool rotation could have altered material flow, so it was not attempted. Additional damage leading to the appearance of a void could be done while removing the tool from the welding spindle, the sample from the fixture, or during sample preparation. An argument could be made that the reason there is a difference in thread appearances in Figures 2-8 and 2-9, is the change in rotation speed and dwell time. While possible, Heideman et al. [61] reported acceptable welds were made using both sets of weld parameters. Finding the clogged thread in Figure 2-9 was fortunate since low welds strengths have appeared randomly throughout the FSSW research.

2.3.3 Function of Tool Threads

From the early days of linear FSW, the function of the tool threads was to push material from the tool shoulder downward along the threads toward the pin tip. This type

of material flow was important to prevent voids in linear welds [1]. This same material movement will remain important in 6061 Al/Cu FSSW but for different reasons. Figure 2-10 shows the cross sections of welds made using FSSW tools with threadless pin tools. Ideally, the tool would be visible in the Figure 2-10(b) micrograph, but the tool fell out of the sample during metallographic preparation. Figure 2-10(a) shows that a strand of Cu is extruded upward along the edge of the tool pin as the pin plunges into the work piece (at the plunge depth in Figure 2-10(a), the tool shoulder is not impacting material flow). Figure 2-10(b) shows that when the tool shoulder plunges into 6061 Al surface, an upward extruded Cu ring is formed. However, the Al-rich stir zone between the tool and Cu ring is nonexistent. Some limited intermetallic formation appears as evident by the darker gray striation on the vertical wall of the Cu ring. These intermetallics were likely the results of some residual 6061 Al being attached to the tool from plunging through upper 6061 Al sheet. Without the formation of an Al-rich stir zone, the sample would be expected to be very low strength, as was the case with Figure 2-10(b). This sample nearly fell apart while handling for metallographic preparation. Aside from the tool not being present in the cross section in Figure 2-10(b), the weld macrostructure appears very similar to Figure 2-9. This observation suggests that if the tool threads become clogged with the complex layered intermetallics, as was the case in Figure 2-9, the tool can behave like a smooth pin tool.

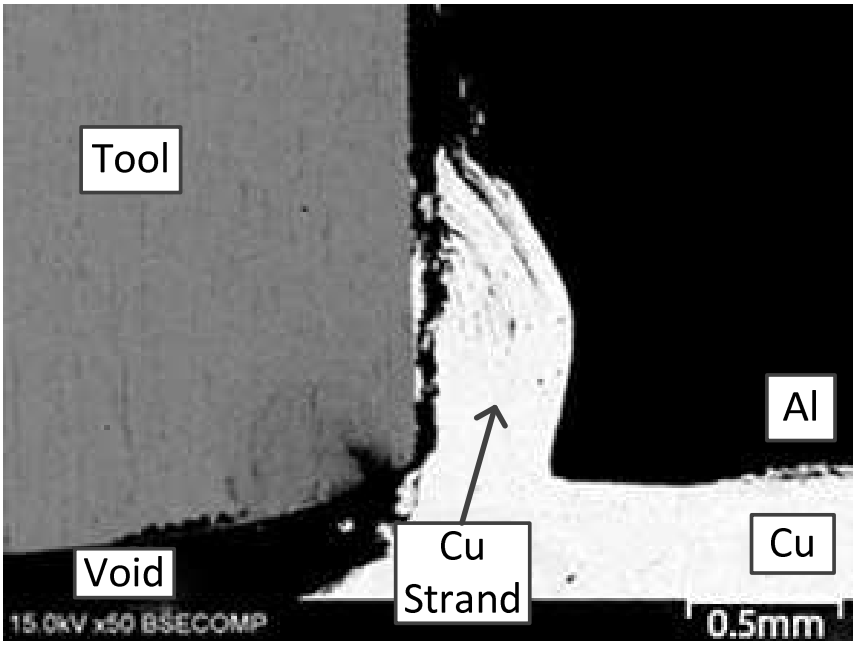

(a)

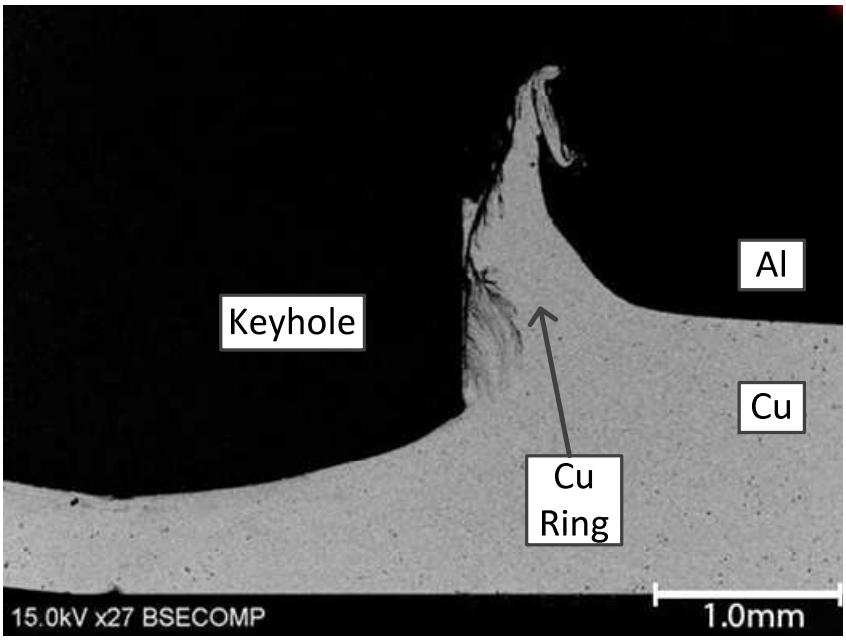

(b)

Figure 2-10. Backscattered electron mode SEM images of FSSW cross sections made with tools with threadless pins and using a rotation speed of 2000rpm, a plunge of 0.21mm/s, a 0.0s dwell time, and a plunge depth of (a) 1.96mm and (b) 2.59mm.

Figure 2-11 shows the weld structures that form when a threaded tool is used. In Figure 2-11(a) a strand of Cu is extruded upward when the tool is partially penetrated

(tool shoulder is not yet impacting material flow), but the difference, as compared to the threadless pin, is the presence of an Al-rich region between the Cu strand and the tool pin and that extends partially under the tool tip. This Al-rich region in Figure 2-11(a) must be material movement associated with the tool threads. The extension of the material under the tool tip suggests that threads are pushing a small volume of material downward prior to the shoulder engaging the workpiece. When the plunge depth was increased, such that the shoulder is plunged 0.25mm into the 6061 Al surface, the Cu ring increased in height and the Al(Cu) stir zone increased in width. Comparing Figures 2-10 and 2-11, the tool threads created the material movement necessary to form an Al-rich stir zone region and pushed the Cu ring outward producing a weld macrostructure necessary for a reasonably strong weld. Heideman et al. [61] demonstrated that increasing the width of the Al-rich stir zone, defined by the horizontal distance between the tip of the Cu ring and the weld keyhole, increases weld strength. The width of the stir zone is substantially wider in Figure 2-11 than in the weld in Figure 2-10, suggesting that the tool threads are necessary to form the Al-rich stir zone needed for quality weld formation.

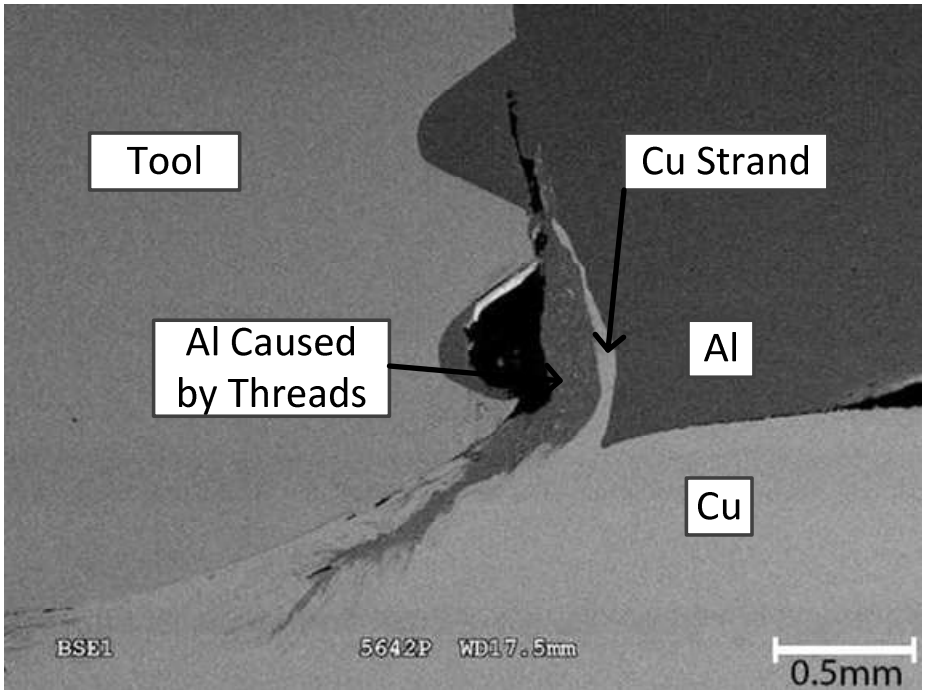

(a)

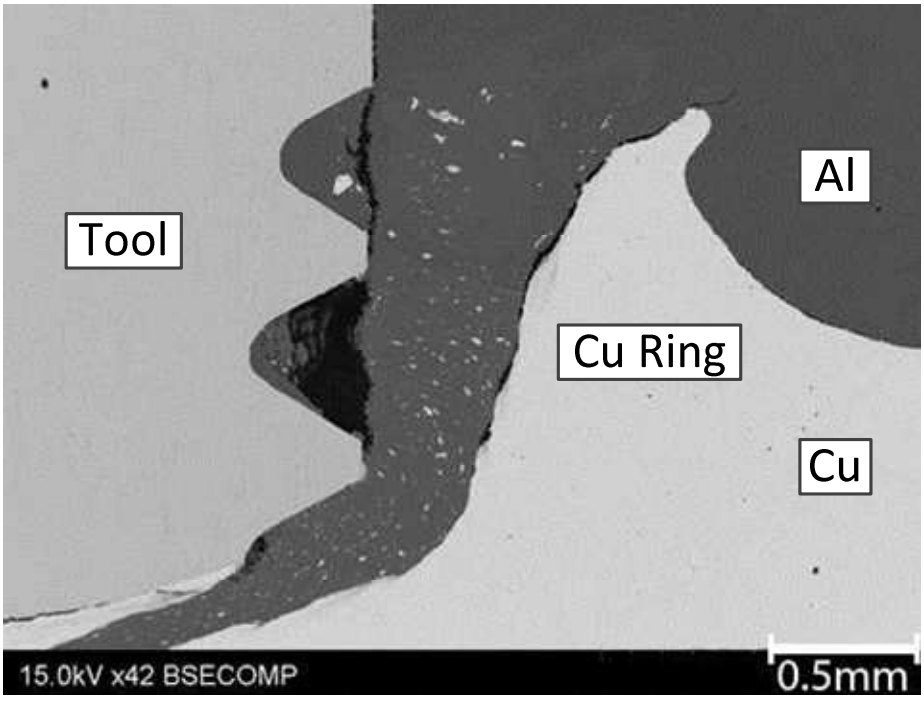

(b)

Figure 2-11. Backscattered electron mode SEM images of FSSW cross sections made with tools with standard threaded pins using a conventional counter-clockwise rotation with a speed of 2000rpm, a plunge rate of 0.21mm/s, a 0.0s dwell time, and a plunge depth of (a) 1.96mm and (b) 2.59mm.

2.3.4 Material Flow in a 6061 Al to Cu FSSW

The first step in explaining material flow was to identify what happens when the FSSW tool begins to mix the upper 6061 Al sheet with lower Cu sheet. Using a four step plunge depth progression from 1.65mm to 1.74mm to 1.78mm to 1.86mm, the first evidence of mixing between the 6061 Al and Cu sheets was observed at a tool plunge depth of 1.74mm. This can be seen in Figure 2-12. This implies that the tool caused interactions between the two materials when the tool reached a plunge depth greater than 1.65mm and less than or equal to 1.74mm. As shown in Figure 2-12(b), the first interaction appears as thin ribbon-like structures of Cu protruding or being pulled upward from the lower Cu sheet into the upper 6061 Al sheet. Clearly, the FSSW tool is not in contact with the lower Cu sheet region, suggesting that a volume of material is rotating under the tool tip. At the 1.74mm plunge depth, the material rotating under the tool tip would be mostly 6061 Al with small amounts of Cu that appears as small bright particles in the Al region between the tool tip and the lower Cu sheet in Figure 2-12. These particles very likely could separate from the ribbon like structures that are apparent at the 6061 Al sheet and lower Cu sheet interface in Figure 2-12. These small Cu-rich particles were present in small numbers and only in the region between the tool tip (i.e. convex region of the tool) and Cu sheet at a plunge depth of 1.74mm. The Cu rich particles were not observed along the vertical walls of the tool. These small particles, as will be shown shortly, became more apparent and numerous as the tool plunge depth increased. These initial small particles, along with more like them, are likely dissolved into the Al as the plunging process continues and will lead to the

formation of an Al-rich stir zone, which is an Al(Cu) solid solution, as discussed by Heideman et al. [61].

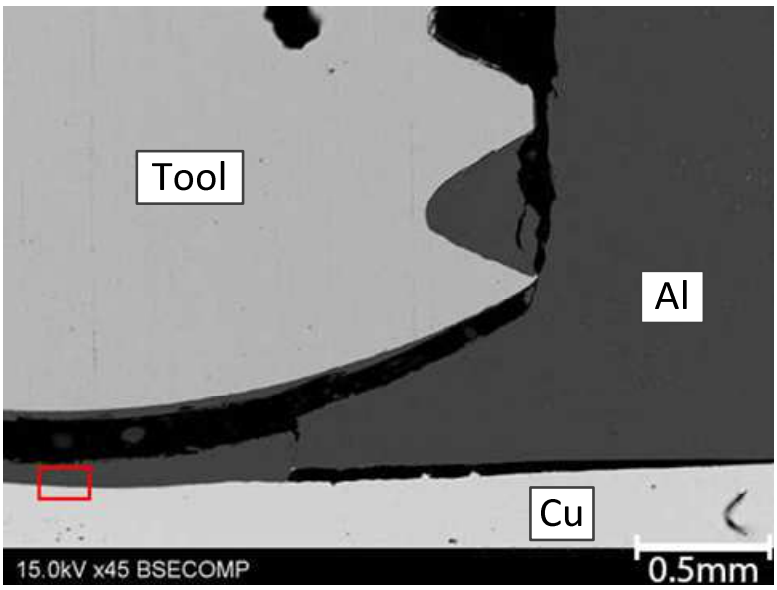

(a)

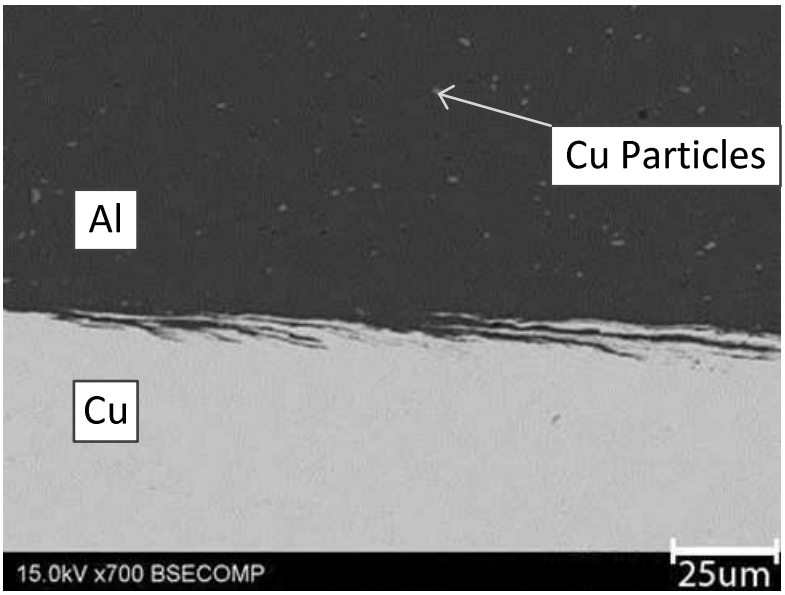

(b)

Figure 2-12. Backscattered electron mode SEM micrographs showing the appearance of the Al-Cu interfaced using welding conditions of 2000rpm, 0.21mm/s plunge rate, 1.74mm plunge depth and 0.0s dwell time; (b) is a higher magnification of the boxed region in (a).

Seeing the first sign of mixing at the 1.74mm plunge depth was surprising because interaction was expected to begin when the tool penetration depth reached the thickness of the upper 6061 Al sheet, or 1.50mm. However, during plunging the Al-Cu interface was deformed and pushed away from the tool tip which was evident by a noticeable depression of the 6061 Al-Cu interface immediately under the tool tip. Consequently, additional plunge depth (beyond 1.50mm) was needed before interactions between the 6061 Al and Cu became noticeable. While the first sign of interaction was observed at 1.74mm, a potential error exists in the reported plunge depth. The CNC mill used to make the welds has a c-frame structure. With the high loads associated with the plunging process, the possibility exists that the c-frame opened slightly, and the actual plunge depth could have been over-reported. Still, the Al-Cu interface was noticeably moved downward during the plunging process, and consequently, the need for additional plunge depth (more than the 1.50mm thickness of the 6061 Al sheet) is likely needed to produce noticeable interactions between the 6061 Al and Cu sheets.

Interactions between the 6061 Al and Cu sheets are more noticeable when the plunge depth was increased to 1.86mm (see Figure 2-13). At the 1.86mm plunge depth, the ribbon-like structures first visible at the 1.74mm plunge depth became more numerous and more pronounced, as shown in Figure 2-13. Also, as seen in Figure 2-13, the presence of Al-Cu intermetallics is more prominent, as evident by the lighter gray striated regions under the tool tip. Additionally, some of the Cu-rich ribbon-like structures in the light gray (Al-rich) region between the tool tip and lower Cu sheet appear as broken ribbons, suggesting that these are being dissolved into the Al-rich

region leading to the further development of an Al(Cu) solid solution stir zone. For clarity, the brightest regions (i.e. highest molecular weight phase) in Figure 2-13 are Cu or Cu(Al) solid solution, the darkest gray regions (lowest molecular weight phase) are Al or Al(Cu) solid solution. The other shades of gray indicated a phase with a molecular weight between pure Al and pure Cu and, hence Al-Cu, intermetallics. Figure 2-13 also shows that a significant volume of material under the tool is being mixed, as evident by the volume of material under the tool pin tip with the ribbon-like/layered structures. Lastly, Figure 2-13 shows that the presence of the Cu or Al-Cu intermetallics particles in the Al-rich layer is increasing, but these particles are still only apparent underneath the tool pin at this depth in the plunging process.

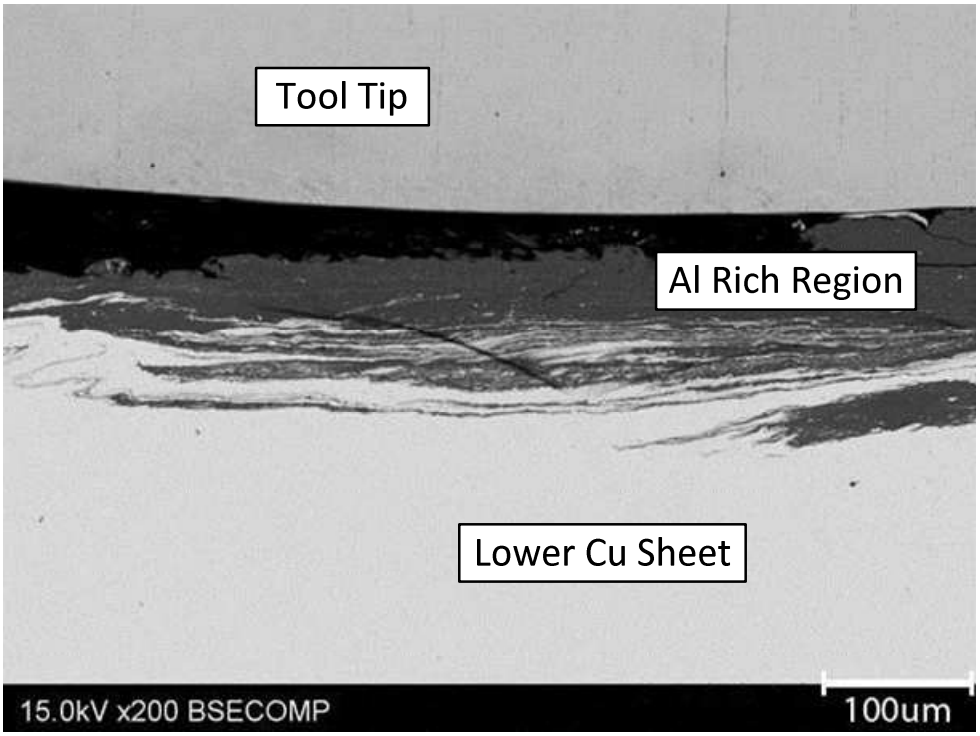

Figure 2-13. Backscattered electron mode SEM micrographs showing the appearance of the Al-Cu interfaced using welding conditions of 2000rpm, 0.21mm/s plunge rate, 1.86mm plunge depth, and 0.0s dwell time.

Figure 2-14 shows the macrostructure around the tool when the plunge depth was increased to 1.95mm, which is 83% of the total pin length and 0.45mm into the lower Cu sheet. In these two SEM images, Cu is being pushed upward into the upper 6061 Al sheet a short distance from the tool's vertical border with an Al-rich region. The Al-rich region contains Cu and Cu-Al intermetallic particles. Pushing the Cu upward is logical, because as the tool is plunged downward into the two sheets, the volume of the tool has to be displaced because metal is largely incompressible. Pushing the Cu downward would be difficult because the rigid steel fixture used to hold the weld specimen prevents downward movement. Consequently, the path of least resistance for the Cu is upward into the 6061 Al sheet and toward the unrestrained upper 6061 Al sheet surface. The Al-rich region between upward-extruded Cu and FSSW tool is being pushed downward as a result of the tool threads as previously discussed. The images in Figure 2-14 are from the right and left side of a single cross section. In these images, a contiguous Al-rich 6061 has not yet formed under the tool tip. Rather the Al-rich region only extends partially under the tool tip with the center of the tool tip being a Cu-rich region. The lower magnification of Figure 2-14(b) makes this observation very evident. At the 1.95mm plunge depth, Al being pushed downward and Cu being pushed upward combined with the mixing of material under the tool pin makes for a very complex flow phenomenon. The weld macrostructure shown in Figure 2-14 remained mostly unchanged regardless of additional plunge depth until the tool shoulder contacted the upper 6061 Al sheet surface. The unchanging macrostructure was explored by plunging a shoulder-less tool (i.e. threaded pin of the same dimensions as the tool pin in Figure 2-14) 2.34mm and seeing a weld macrostructure that was very similar to Figure 2-14.

The 2.34mm plunge depth was chosen for this experiment because this would be the plunge depth at which the shoulder would initially contact the upper 6061 Al surface.

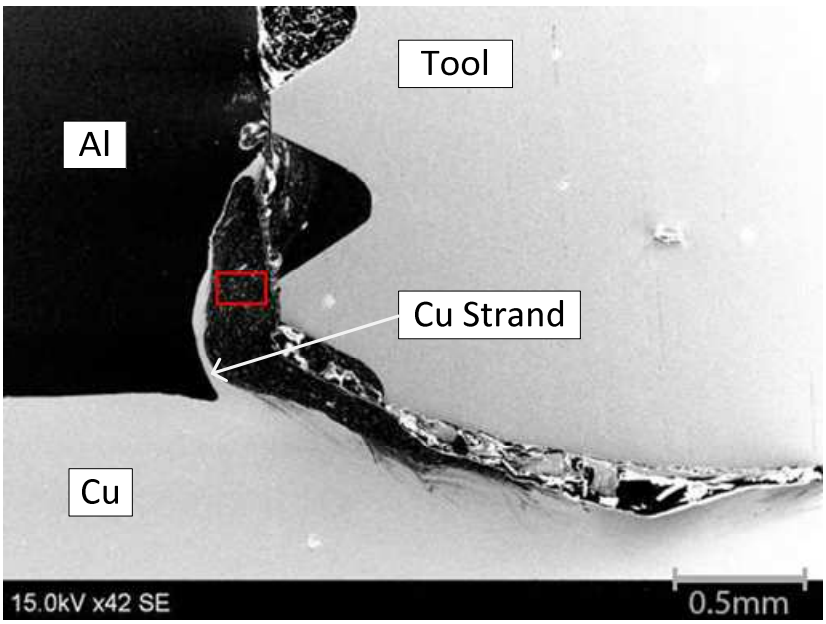

(a)

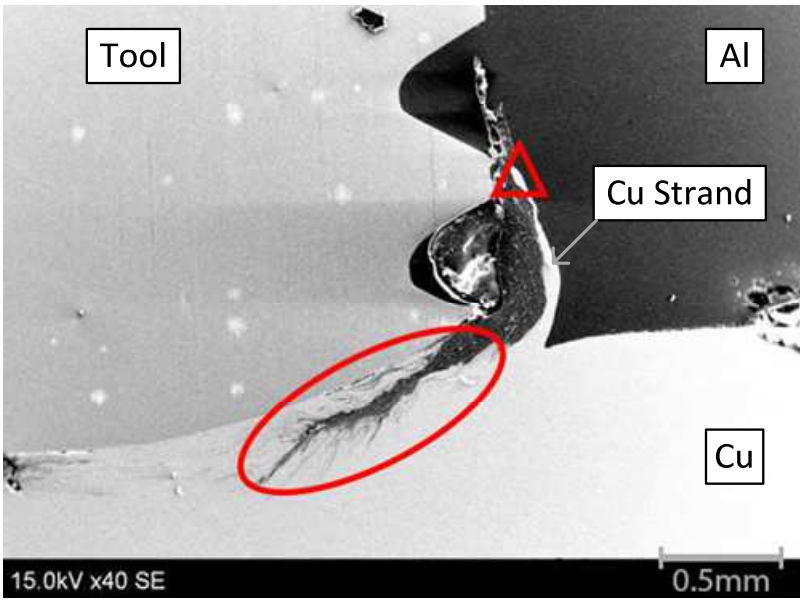

(b)

Figure 2-14. Secondary electron SEM images of (a) the left side of the weld and (b) the right side of the same weld where the tool was plunged a depth of 1.95mm and stopped (0s dwell time). The other welding conditions were 2000rpm and 0.21mm/s plunge rate.

Figure 2-15 is a higher magnification image of the Al-rich region in Figure 2-14(a) and shows numerous small particles. These particles are lighter in contrast compared to the Al-rich material that surrounds them, indicating these particles contain higher levels of Cu. Given the small size, it is difficult with SEM chemical analysis techniques to determine their exact composition, but it would be expected to be Cu or a Cu(Al) solid solution, and /or Al-Cu intermetallics.

The source of the Cu-rich and Al-Cu intermetallic particles in the Al-rich region between the upward-extruded Cu region and the welding tool could be twofold. First, some of the layered particles likely stem from the ribbon-like structure formed at the bottom of the tool as shown in Figure 2-16(a). The circled region in Figure 2-16(b) shows a long particle that is in the Al-rich region of the weld. It would appear this particle is one of the ribbon structures that broke free from the lower Cu sheet. Given time, through the deformation associated with the spinning action of the material and some of the ribbon structure being dissolved into the Al-rich region, it becomes a likely source of small Cu-rich layered particles.

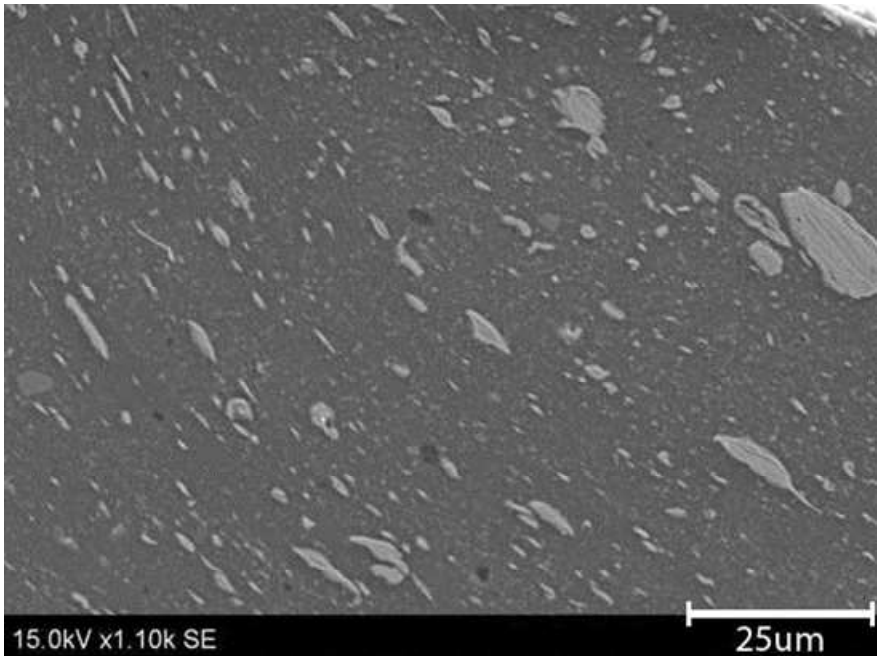

Figure 2-15. Secondary electron SEM image of boxed-region on Figure 2-14(a).

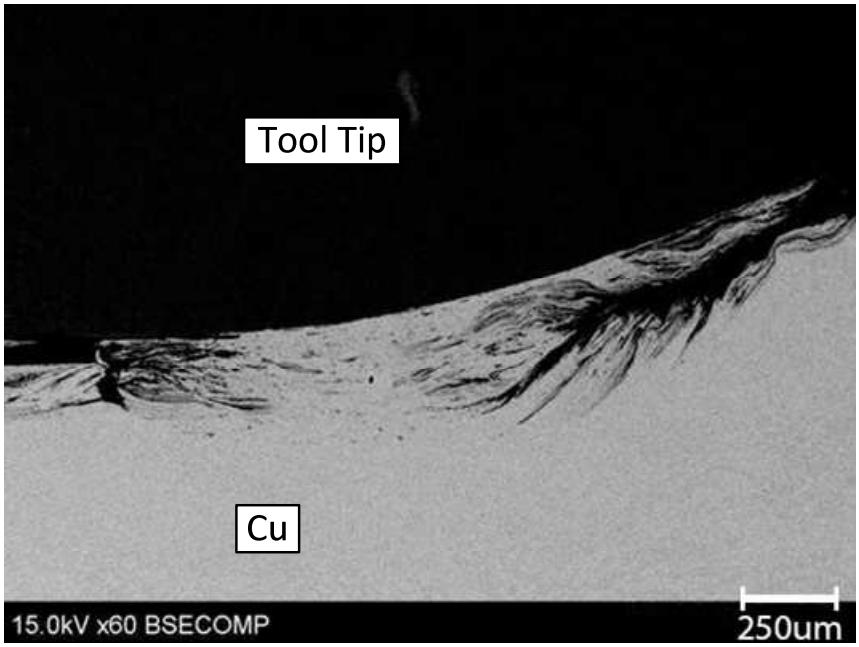

(a)

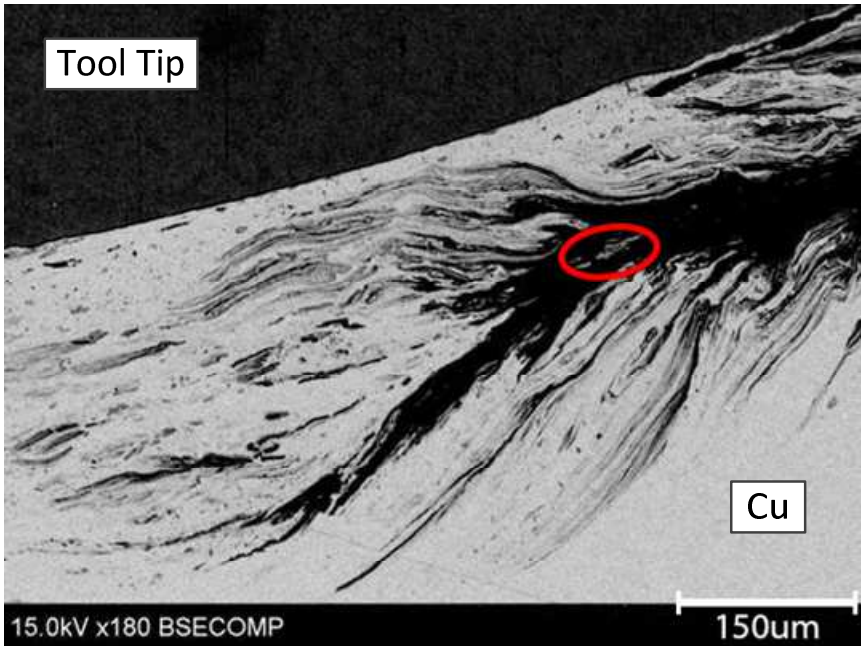

(b)

Figure 2-16. Backscattered electron SEM images of (a) the circled-region in Figure 2-13(b) and (b) higher magnification of (a).

The second likely source of the layered particles in Figure 2-14 is the Cu strand that is extruded upward into the upper 6061 Al sheet. From Figure 2-14, the Cu strand

appears to get pulled into tool threads higher up on the tool, as indicated by the triangular region in Figure 2-14. As a Cu strand is pulled into the tool thread, the strand breaks up and once in the tool thread becomes deformed by essentially folding onto itself. In the deformation process, Al-rich material is likely trapped in the folds leading to a complex layered structure, yielding another source for layered particles. The purpose of identifying sources of the layered structures is that weld inconsistency was associated the tool threads becoming clogged with a Cu-rich layered structure. However, these particles are likely not the cause of thread clogging because all are much smaller than those observed in Figure 2-9.

Figure 2-17 shows the weld structure as the tool penetration depth was increased to 2.34mm. At this plunge depth, the tool shoulder just contacted the surface of the upper 6061 Al sheet and is now influencing material flow. The tool shoulder appears to cause a downward flow of the Al-rich material and an upward flow of Cu. This flow will be explained in detail below.

Figure 2-17(a) shows how once the shoulder contacted the work piece the Cu ring needed for a quality high strength weld begins to form (see boxed region). The formation of the Cu ring is the result of the Cu being pushed upward into upper 6061 Al sheet. This Cu ring in Figure 2-17(a) has much more Cu volume (i.e. thicker from a cross-sectional view) than the Cu strand shown in Figure 2-14. The sizable volume/thickness increase is important in forming a strong interlocking structure observed in high strength welds as illustrated in Figure 2-2. The thin Cu strand in Figure 2-14(a), by comparison, could be easily sheared during weld strength testing and would likely contribute only minimally to weld strength.

The tool shoulder contacting the upper 6061 Al sheet also caused the Al-rich region between the Cu ring and the tool threads to substantially increase in thickness, as shown in Figure 2-17(a), compared to the 1.95mm plunge depth where the tool shoulder had not yet affected flow (see Figure 2-10(a)). In addition, as shown in Figure 2-17(b), the Al-rich region under the tool tip appears to have thickened and grown in length compared to the weld in Figure 2-14. Figure 2-17(b) also shows the presence of a void (or separation between the left and right sides of the Al-rich region) between a Cu-rich layer immediately adjacent to the tool tip (outlined in red) and the lower Cu sheet. Before the tool shoulder contacted the upper 6061 Al surface in Figure 2-14, the center part of the tool tip was in contact with the lower Cu sheet and there was only a thin Al-rich region on the outer diameter of the tool tip separating a Cu-rich region immediately adjacent to the outer edge of the tool tip and the lower Cu sheet (the circled region in Figure 2-13(b)). The increase in thickness of the Al-rich region under the tool tip and the extension of this region further under the tool tip suggests that the 6061 Al material is being pushed downward when the shoulder begins influencing material flow. This downward movement will be further supported when the plunge depth was increased further, and the void identified in Figure 2-17(b) disappears.

Additionally, the downward movement of Al-rich material appears to follow the path under the tool tip that was present prior to the tool shoulder affecting material flow (circled region in Figure 2-9(b)) explaining why in Figure 2-13(b), the Al-rich region is present between Cu-rich region (outlined in red in Figure 2-13(b)) immediately adjacent to the tool tip and the lower Cu sheet.

The Cu-rich layer outlined in red in Figure 2-17(b) immediately adjacent to the tool tip does not appear to be in contact with the tool tip. However, this separation is likely the result from the abrupt stop of the tool during welding or may have occurred during sample preparation. More than likely, the Cu-rich region was adhered to the tool tip during the welding process. If the Cu-rich material was not adhered to the tool tip, it would have remained in the weld, and the bottom of the weld would have a copper-colored appearance. However, this is not the case in Figure 2-17(b); the bottom of 6061 Al to Cu FSSWs are white in appearance (i.e. covered with an Al-rich material). Additionally, this adherence of the material to the tool tip is supported by a noticeable appearance of material buildup on the tool tip after making just one weld with a new tool. The reason to refer to this Cu-rich tool tip buildup is that it is of significant volume and could be a source for Cu-rich material. If dislodged during subsequent welds, the Cu-rich material could lead to the thread clogging as observed in Figure 2-9.

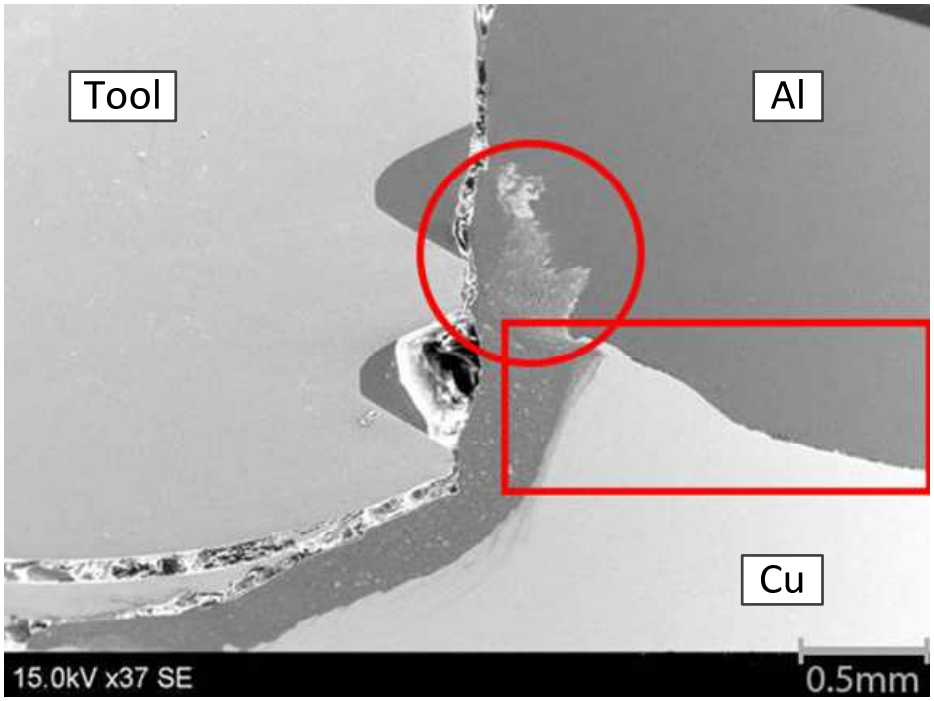

(a)

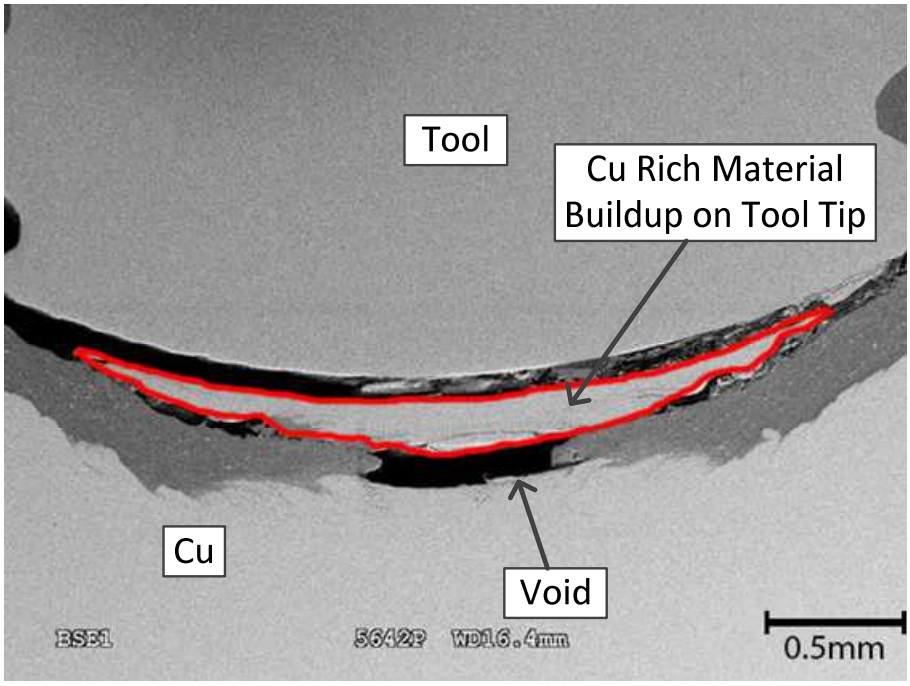

(b)

Figure 2-17. Secondary electron SEM images of (a) right side region of a FSSW tool and (b) the region on the tool tip of weld that was made plunging to a depth of 2.34mm and stopped (0s dwell time). The other welding conditions were 2000rpm and 0.21mm/s plunge rate.

The extruded upward strand of Cu seen in Figure 2-14 is not immediately visible in Figure 2-17(a), but there is a circled region in Figure 2-17(a) that by its brighter contrast contains more Cu than the Al just immediately to its left. This region is likely the same Cu strand present in Figure 2-14 but the strand is being pulled into the stir zone region by tool threads as a result of the tool shoulder impacting material. As the strand makes this movement, some of the strand is dissolving into the Al region, transforming the 6061 Al to an Al(Cu) solid solution. The dissolution of Cu into the Al is evident by the lighter-gray-speckled region running mostly vertical in Figure 2-18. Other portions of the Cu strand (brightest region in the top-center of the Figure 2-18) are being deformed and folded onto themselves, thus forming a layered structure as a result of Al being trapped between the folds. However, this layered structure is also unlikely to lead to tool clogging because the particle sizes are relatively small in comparison to the thread size and particle sizes that clogged the threads in Figure 2-9.

As can be seen, material in the circled portion of Figure 2-17(a) is being pulled upward toward the highest tool thread. This upward movement suggests material away from the tool surface is being pulled upward. Once the material is into the thread portion of the tool, these particles will likely be carried to the bottom of weld by the bulk Al-rich material flow around it. This would be expected based on the discussion of the role of the tool threads discussed earlier. As the material moves through the thread structure, more of it will be dissolved into the Al leading to an even smaller particle.

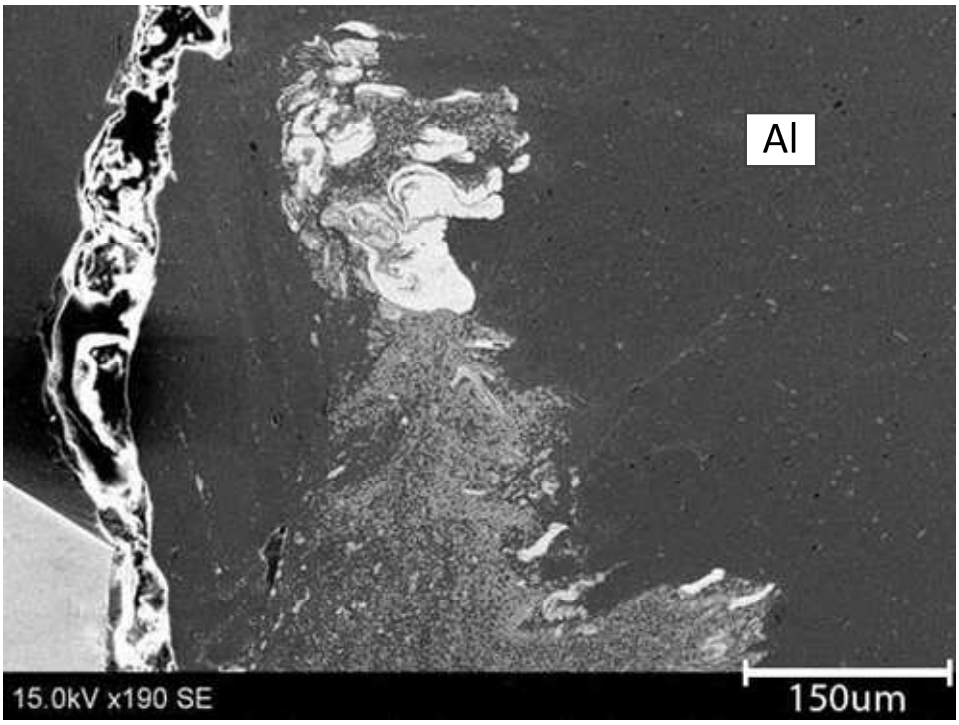

Figure 2-18. Secondary electron SEM images of a higher magnification of the circled region in Figure 2-17(a)

The next step in analyzing material flow was to increase the plunge depth to 2.59mm such that the tool shoulder was pushed 0.25mm into the upper 6061 Al sheet. This was a plunge depth that produced welds of reasonable strength in previous work [61]. Figure 2-19 shows portions of the weld produced with the 2.59mm plunge depth. The void observed in the region under the tool tip in Figure 2-17(b) is no longer present indicating that as the shoulder plunged beyond the surface of the Al sheet, more Al-rich material is pushed to the bottom of weld, forming a contiguous Al-rich layer between the tool tip and the lower Cu sheet. Having more Al-rich material being pushed downward is reasonable since the volume of 6061 Al displaced by the tool shoulder as it plunged into 6061 sheet has to go somewhere (i.e. volume conservation). The path of least resistance would be to fill the void seen in Figure 2-17(b) thus forming the contiguous Al-rich layer under the tool tip in in Figure 2-19(b).

The region outlined in red in Figure 2-19(b) also shows that tool buildup seen in Figure 2-17(b) is present at the increased plunge depth. For reasons explained earlier, it is believed that this material would have remained adhered to the tool after it was retracted from the weld as would be done in a normal welding cycle. This material could be a source of material that clogged the threads in Figure 2-9.

Increasing the plunge depth to 2.59mm also caused an increase in the Cu ring height compared the 2.34mm plunge depth. In Figure 2-17(a), the Cu ring height is below the first full thread on the tool (from the bottom of the tool). In Figure 2-19(a), the Cu ring height extends beyond the highest thread from the tool tip. Intuitively, the Cu-ring height increasing with additional plunge depth is reasonable because the shoulder displaces significant volume over even a short distance; the shoulder radius is 2x the radius of the pin, hence it displaced 8x the volume over the same distance. The increasing volume of material being pushed downward results in more of the Cu being pushed upward to compensate for the volume change taking place. Thus, the Cu ring increases in height which in turn helps promote a feature needed for welds of reasonable strength.

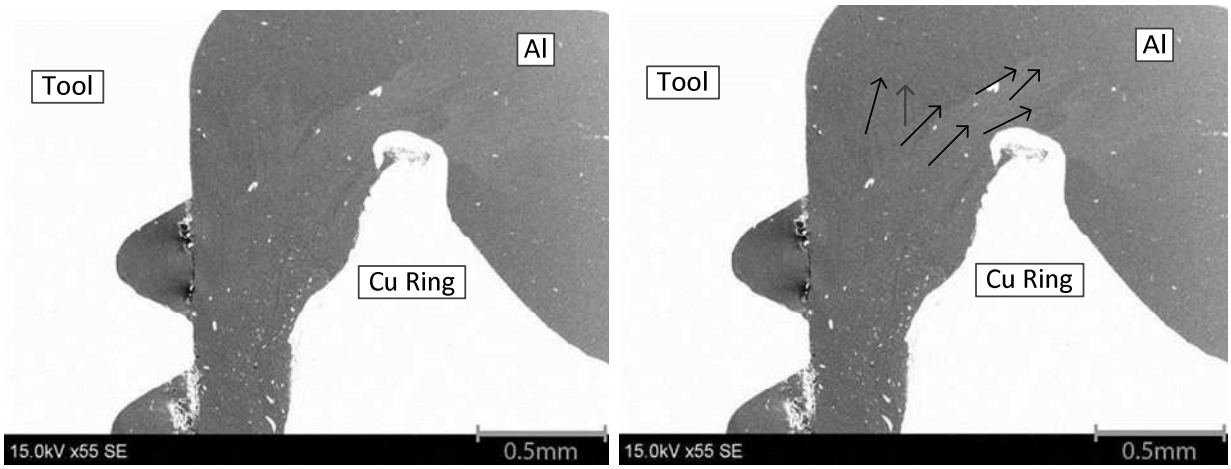

(a)

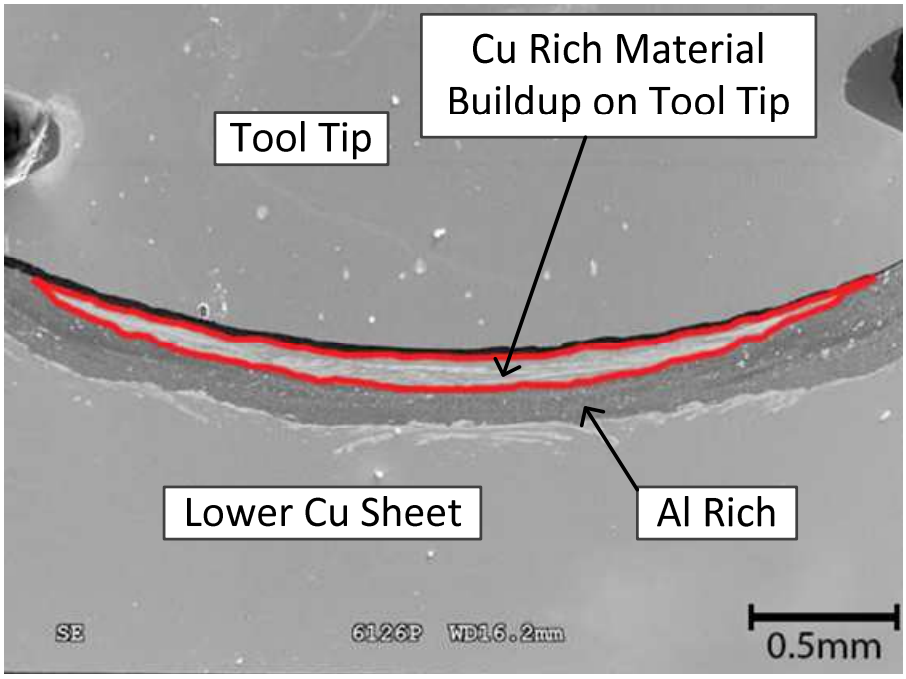

(b)

Figure 2-19. Secondary electron SEM images of (a) region to the right of FSSW tool with a second identical image showing the material flow of Al(Cu) in the stir zone and (b) the region on the tool tip of weld that was made plunging to a depth of 2.59mm and stopped (0s dwell time). The other welding conditions were 2000rpm and 0.21mm/s plunge rate. Note, the poor contrast (pure white) of the Cu sheet and the tool was necessary to show the region indicated by the arrows in Figure 14(a).

As pointed out by arrows in Figure 2-19(a), the Al-rich stir zone region has a region of brighter contrast, compared to the Al region nearby. This brighter contrast region indicates a slightly higher Cu concentration than the Al-rich region immediately

above it. The jagged shape of the Al-rich region as pointed out by the arrows in Figure 2-19(a) is a region of higher Cu concentration. This regions has the appearance that it extends over the top of the Cu ring suggests that some of the material in the Al-rich stir zone region moves upward. This observation combined with the observation that additional material was pushed downward under the tool tip when the plunge depth was increased from 2.34mm to 2.59mm suggests that a complex counterflow phenomena takes place in the stir zone. Based on the function of the threads which, as discussed previously, is to push material downward toward the tool tip, the material closest to the tool is likely be pushed down. In opposition, the material further away from the tool surfaces, while closer to the Cu ring is moves upward. The demarcation between downward and upward flow in the Al- rich stir zone was not evident in this analysis.

All flow analyses to this point were completed using new tools so the possibility that the large particles seen clogging the threads in Figure 2-9 were being released from material adhered to the tool tip is speculative. To explore this hypothesis further, a tool that was already used to make 6061 Al to Cu FSSWs was plunged to depth of 1.82mm and immediately stopped to determine what happens to the tool material buildup in the early stage of interacting with the lower Cu sheet. The process used for this experiment was identical to process followed for the samples already discussed. The only changes were the plunge depth and that the tool had been previously used and had material from the previous weld adhered to it. Figure 2-20(a) is a photograph of the tool used for this experiment when it was new. The tool has a pin with clean threads and smooth rounded tool tip. Figure 2-20(b) is photograph of the same tool after making five welds and just prior to plunging it to the 1.82mm depth. The used tool shows the

thread covered, and nearly filled with a material that on the surface would appear, based on the color, to be Al-rich. The tool tip in Figure 2-20(b) has some sort of material buildup based the tip's different shape as compared to Figure 2-19(a).

Figure 2-21 shows SEM, in the backscatter electron mode, micrographs of the 1.82mm plunge sample. This sample shows, based on the darker contrast, that the threads were filled with primarily Al-rich material. The tool tip, even though it had an aluminum appearance on the surface, has Cu-rich material adhered to it that is Cu-rich as evident by its brighter contrast in Figure 2-21(a). The-Cu rich observation was confirmed by EDS analysis. The adhered material is a complex layered structure which, based on previous work [13, 15, 19, 20, 23, 24, 25, 38, 45, and 61], consists of multiple phases (likely Al(Cu), Cu(Al), CuAl and Cu9Al4). The right side of the tool tip (boxed region in Figure 2-21(a)) shows a fracture in the adhered material. A fracture of this material is not unexpected due to the brittleness of Al-Cu intermetallics; the force on the tool tip increases as it gets closer to the lower Cu sheet, which is substantially harder than the 6061 Al upper sheet. At a higher magnification, as shown in Figure 2-21(b), the fracture is complex and somewhat spider-webbed in appearance and would produce particles of many different sizes particles. A reasonable expectation is that as the plunging process continues, these particles will get pushed into the stir zone. If any of these particles became lodged in a thread, and were large enough to fill the thread, clogging of the tool pin threads, similar to what is shown Figure 2-9, is possible. From this work, the material adhered to the tool tip is the only source identified with particles large enough to lead the thread clogging, as seen in Figure 2-9.

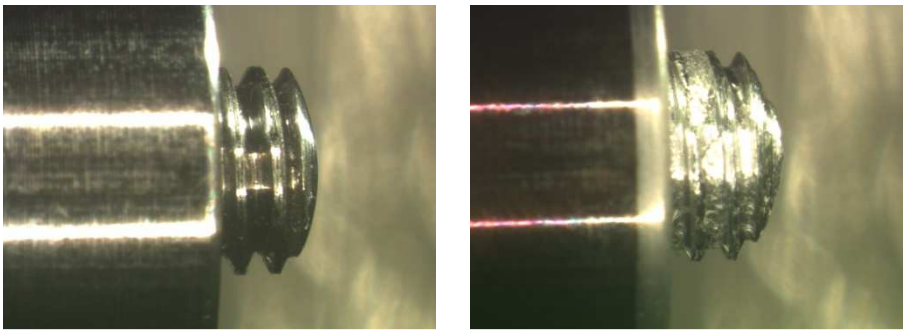

(a) (b)

Figure 2-20. Photographs of (a) a new FSW tool and (b) a tool after making five 6061 Al to Cu FSSWs

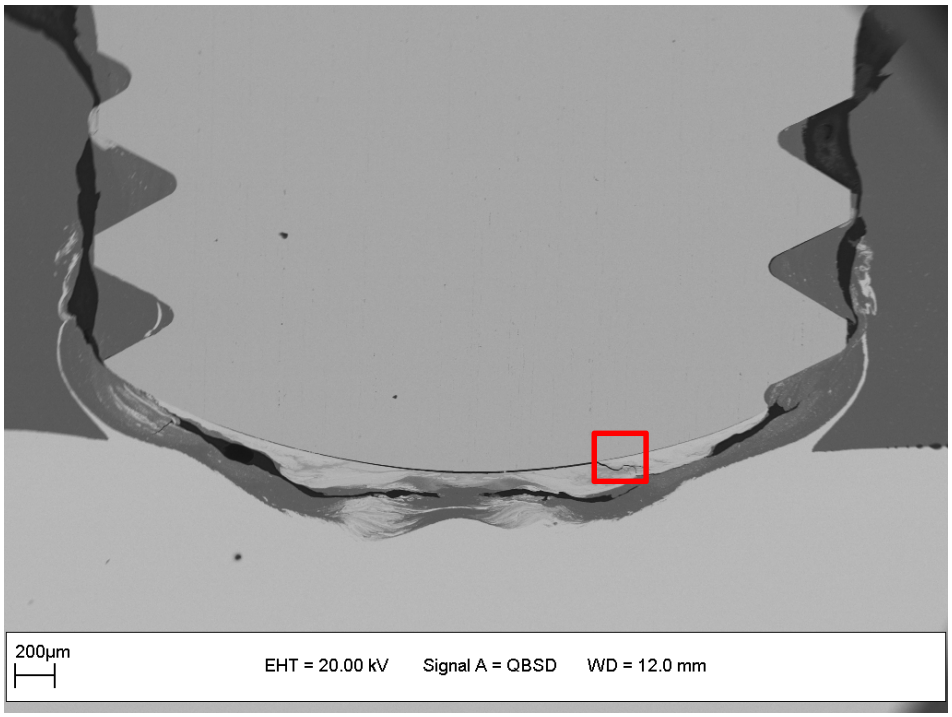

(a)

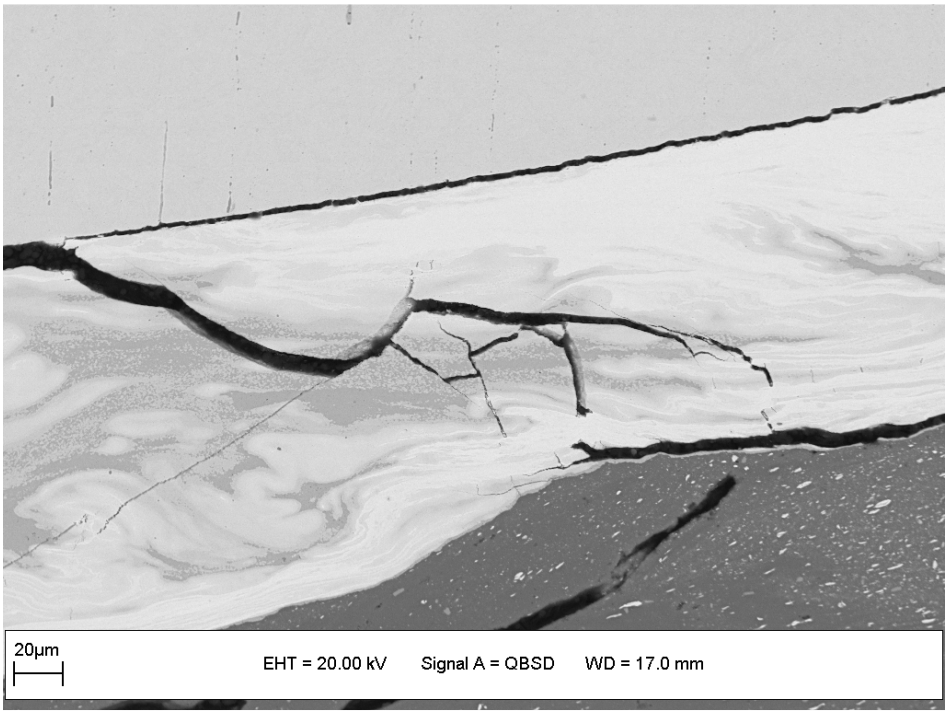

(b)

Figure 2-21. Backscattered electron SEM images of (a) cross section from the sample made with a 1.82mm plunge depth using a tool that had been used to make five welds previously, and (b) a higher magnification of the red- boxed region in (a). The welding conditions were 2000rpm, 0.21mm/s plunge rate, 1.82mm plunge depth, and a 0s dwell time (tool was stopped as soon as it reached the 1.82 plunge depth).

The final step in evaluating material flow was the investigation of the effect of dwell time. The weld macrostructure remained unchanged from a zero second dwell time shown in Figure 2-22(a) to a 6s dwell time shown in Figure 2-22(c) suggesting the basic weld macrostructure, as illustrated in Figure 2-1 (Cu ring plus and Al-rich stir zone between the tool and the Cu), is formed at the end of the plunging process. As the dwell time is increased from 1s to 3s to 6s (Figures 2-22(a), 2-22(b) and 2-22(c)), the number of visible Cu-rich particles (smaller bright contrast particle) in the Al-rich stir zone decreases. This decrease in the number of bright Cu-rich particles in the Al-rich stir zone is because the added time at the elevated temperatures permits the Cu to dissolve into the Al-rich stir zone region, forming a higher copper content Al(Cu) solid solution in the stir zone. The observation that dwell time does not change the overall weld macrostructure but only leads to more Cu-rich particles dissolving into the Al-rich stir zone region explains why Heideman et al. [61] found weld strength to be independent of dwell time.

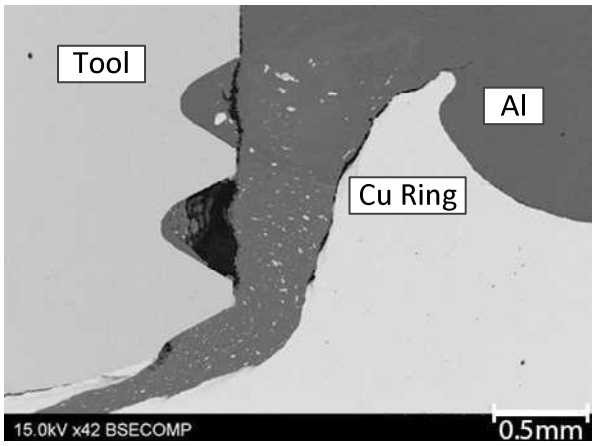

(a)

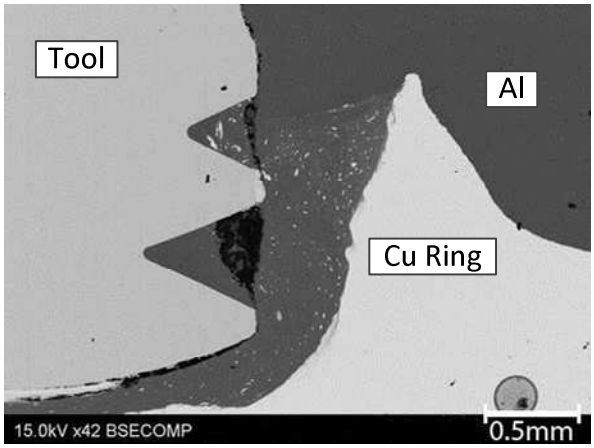

(b)

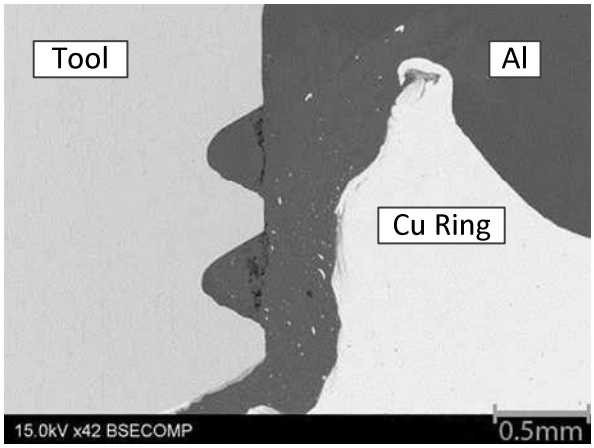

(c)

Figure 2-22. Secondary electron SEM images of welds made with a 2.59mm plunge depth, 2000rpm rotation speed, a plunge rate of 0.21mm/s and (a) a 1s dwell time, (b) a 3s dwell time, and (c) a 6s dwell time.

2.4 Conclusions

1. One source of weld strength inconsistency is the result of threads on the FSSW tool becoming clogged with a complex Cu-rich layered structure. When the threads clog, the tool produces a weld structure similar to a tool with a threadless pin.

2. The function of the threads during the plunging process is to push the 6061 Al toward the bottom of the weld, such that the Al-rich stir zone exists between the upward extruded Cu ring and the FSSW tool.
3. The first interactions between the 6061 Al sheet and Cu sheet begin as a ribbon-like structure before the tool pin actually contacts the Cu sheet surface. These ribbon-like structures are a source of layered Al/Cu intermetallic particles in the Al-rich stir zone region.
4. The Cu ring substantially forms when the tool shoulder contacts the surface of the 6061 Al sheet. The Cu ring formation is the result of a larger volume of Al material being pushed toward the bottom of the weld, while at the same time the Cu interface is extruded upwards.
5. Plunging the shoulder deeper into the work piece results in an increased height of the Cu ring and some dissolution of Cu-rich particles into the Al-rich stir zone. Increasing the plunge depth also pushed more Al-rich material under the tool tip forming a contiguous Al-rich layer at the bottom of the weld.
6. The structure necessary to form welds of reasonable strength (Cu ring + Al-rich stir zone) is complete at the end of the plunging process. Dwell time does not change the basic weld structure, but does impact the weld microstructure by allowing more time for Cu-rich particles to dissolve into the Al-rich stir zone. Consequently, setting the appropriate plunge parameters are essential to quality weld formation.
7. The likely source of large particles that can lead to thread clogging was identified. The buildup of brittle Al-Cu intermetallics on the tool tip which forms during

previous welds, fractures when the tool first begins interacting with the lower Cu sheet. This fractured material is then expelled into the stir zone and if the fractured material remains large in size, this material will clog the thread and lead to a poor quality weld.

Chapter 3: Use of Wireless Temperature Measurement Device and Torque Measurements to Identify Key Weld Parameters in 6061 Al to Cu Friction Stir Spot

3.1 Introduction

Friction stir welding (FSW) was a process invented in England in 1991 by The Welding Institute (TWI) [1]. The process involves pushing a spinning non-consumable rotating tool through a weld joint. The frictional and viscous heating generated by the tool softens the weld area sufficiently so that the material can be stirred and mixed [2]. The reduced heat input and relatively flat weld profile associated with FSW improves weld joint performance, particularly when butt joints are used.

Initial FSW development efforts focused on welding aluminum and magnesium alloys because these alloys are typically more difficult to weld via conventional fusion processes. Today, numerous applications of FSW technology are use in a variety of industries from aerospace to automotive [4, 5]. Since the initial work performed with aluminum alloys, FSW of other materials such as titanium, stainless steel, carbon steel, brass, and copper have been successfully accomplished [5, 6] and some industrial applications of these materials are appearing [5].

Some of the more recent FSW research involves welding dissimilar materials such as aluminum to steel, titanium to stainless steel, and aluminum to copper [7, 8, 9, 10, 13, 14, 15, 19, 20, 21, 23, 25, 30, 62, 63, 64, and 65]. Most of these combinations are of interest because these materials cannot be welded with traditional fusion welding methods. Soldering, brazing, or rotary friction welding can be used to join dissimilar metal combinations. However, FSW, if successful, could produce stronger welds faster

and with higher levels of reliability when compared to soldering or brazing. Rotary friction welding is similar to FSW, but the rotary welding process is generally limited to circular cross sections and requires the ability to spin one of the parts to be welded. FSW, however, can use butt, lap, and t-joint configurations. [11, 12, 13]

Along with the standard FSW process, a variation of the process was also developed. This variation is known as friction stir spot welding (FSSW). As illustrated in Figure 3-1, in FSSW, the tool is plunged into a lap joint and withdrawn after the shoulder touches the workpiece and dwelled for a desired time; the tool does not move forward [14]. As with traditional resistance spot welding, the FSSW process is limited to lap joint configurations. The primary advantage of FSSW process in aluminum alloys is that many welds can be made with a single tool because a hardened steel tool is employed [16]. In this regard, FSSW is superior to conventional resistance spot welding [16] in which the copper electrode degrades due to reactions between the electrode material and aluminum being welded.

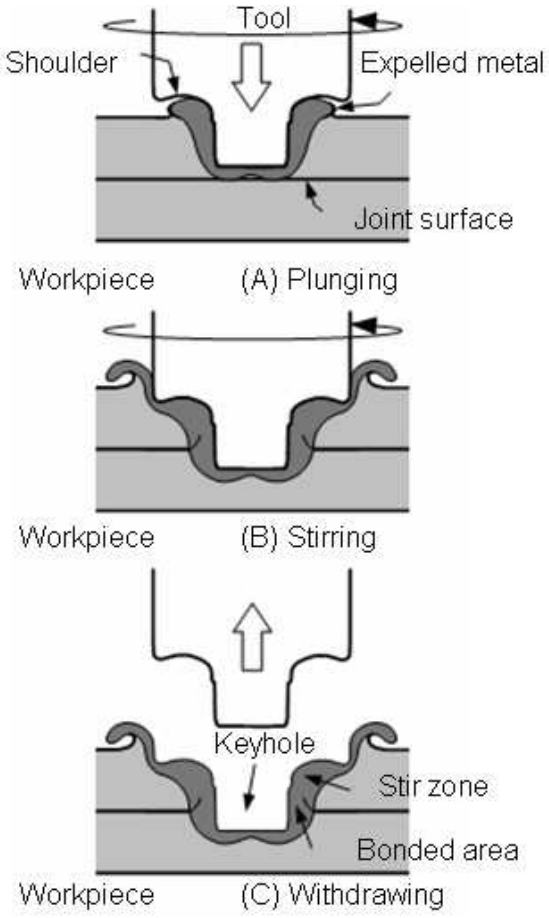

Figure 3-1. Schematic of FSSW Process [22]

Most FSSW work has focused on welding aluminum to aluminum alloys and magnesium to magnesium alloys [8, 17, 18, 22, and 32]. Another dissimilar combination, aluminum, and its alloys, to copper, could be useful in making electrical connections and components. Some limited literature exists on making linear welds with both butt and lap penetration joints [13, 19, 20, 21, 24, 25, 26, 27, 29, 30, 62, 63, 64, 65, and 67]. However, only limited success is reported in making quality welds through the linear welding process. In lap penetration welds, intermetallic formation caused poor weld quality; subsequently, to improve weld quality, a thin zinc sheet was employed between the copper and aluminum sheets to prevent detrimental intermetallics from forming [13]. Akabari et al. [62] also showed success by using an anodized copper

sheet between the aluminum alloy and pure copper to improve weld strength. In butt joint welding, only limited success was reported, with the most success achieved by having a tool pin almost entirely on the aluminum side of the butt joint, so that the tool pin just barely touches, or kisses, the copper side of the joint [30].

Welding aluminum and its alloys to copper via FSW presents a significant challenge given the large 452°C difference in melting points between the two materials. The lower melting point of aluminum (660^{o}C) will tend to stir weld much easier and more readily as it approaches its melting point and becomes less viscous. By comparison, copper, with melting point of 1085^{o}C, will be highly viscous and difficult to stir even at the melting point of aluminum. FSSW could be a useful method to join these two materials because the FSSW of the materials is limited to a single spot where the amount of mixing can be limited and the weld morphology controlled.

Heideman et al. [61] demonstrated 6061 Al to oxygen-free pure copper FSSWs with strengths in excess of 2000N. To generate welds of this strength, a weld morphology consisting of both an upward extruded copper ring and a contiguous aluminum layer on the inside diameter of the copper ring were needed (See Figure 3-2). Without these two features, weld strength was less than 1000N. To determine the proper combination of weld parameters, a design of experiments was completed investigating rotation speed, plunge depth, weld dwell time, and non-consumable pin length. From initial work of Heideman et al. [61], the rotation speed and the tool pin length were identified to be significant independent variables, and the dwell time and the plunge depth were found to be statistically insignificant in affecting weld strength. The plunge depth is defined as the depth the pin tip is plunged into the workpiece. The dwell

time is defined as the time from the end of the plunge to the time the tool begins to be retracted from the work piece. While welds of reasonable strength were observed, Heideman et al. [61] also reported inconsistencies (weld strengths <1000N) using welding condition that produced weld strength greater than 2000N).

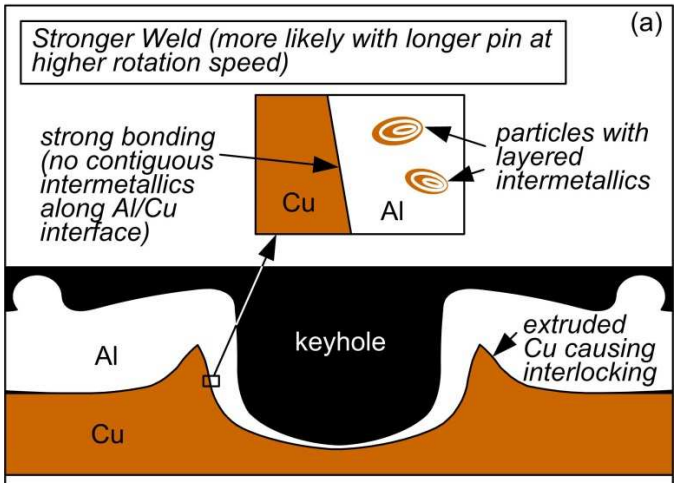

Figure 3-2. Schematic of the weld macrostructure necessary for strong weld [61]

To further understand FSSW of aluminum to copper, the plunge rate, which was not explored in the initial work of Heideman et al. [61] will be explored as a possible welding parameter to improve weld strength and consistency. In addition, tool temperatures (from the start to the end of the FSSW process) at the outside edges of the tool tip and shoulder will be measured and analyzed to understand how welding parameters (rotation speed, plunge rate, weld dwell time, and plunge depth) affect temperature profiles. Temperature measurements will be obtained through a specially designed tool holder equipped with a Bluetooth® data transmitter so that data can be collected from the rotating tool, which is similar to an approach that Fehrenbacher et al. [71] used to study 6061 Al linear FSWs. The measured FSSW temperatures will then be

related back to the initial work of Heideman et al. [61] to determine if temperature can be correlated to the weld quality. In addition, the method of measuring these temperatures along with the process to help ensure accuracy will be presented. Lastly, weld torque and vertical force measurements will be made for various welding conditions and used to calculate the energy generated during the FSSW process. The temperature measurements and energy calculations along with the work done by Heideman et al. [66] will be used to show that having sufficient plunge energy is necessary to form quality 6061 Al to Cu FSSWs.

3.2 Experimental Procedure

The FSSW samples in this study consisted of 25mm wide, 50mm long, and 1.5mm thick 6061 Al-T6 (referred to as 6061 Al in this document) with an average hardness of 58HRB; and 25mm wide, 50mm long, and 1.5mm thick oxygen-free copper (referred to as Cu in this document) in the H01 condition (i.e. quarter hard) with an average hardness of 73HRF. A lap weld joint with the 6061 Al sheet on top and the Cu sheet at the bottom with a 25mm overlap was used for all welding trials. The compositions, determined by inductively coupled plasma, of the 6061 Al and Cu are shown in Tables 3-1 and 3-2.

Table 3-1. Composition of 6061 Al as determined by ICP and compared to 6061 Al Specification.

	Si	Fe	Cu	Mn	Mg	Cr	Zn	Ti	Al
Sample Comp.	0.69	0.60	0.28	0.006	1.03	0.15	<0.001	0.014	Rem.
Specifi-cation	0.4 - 0.8	0.7 Max	0.15 - 0.40	0.15 Max	0.8 - 1.2	0.04 - .35	0.25 Max	0.15 Max	Rem.

Table 3-2. Composition of oxygen-free copper (weight percent) as determined by ICP and compared to oxygen-free copper specification. Other elements combine to 0.017 weight percent with individual elements all less than or equal to 0.001 weight percent.

	Cu	Ag	As	Sb	S	P	Fe	Ni	Mn	Sn	Other*
Sample Comp.	99.95	0.001	0.002	0.006	0.002	0.001	0.005	0.002	0.001	0.013	0.017
Specification	99.95	----	----	----	----	----	----	----	----	----	

FSSWs were made using a 1991 Hurco BMC 40 CNC milling machine (15 horsepower with a maximum spindle speed of 4000rpm), and is shown Figure 3-3. The tool design for all welds was a standard threaded pin design using a pre-hardened H13 tool steel (42-46HRC) with a trade name of Viscount 44. The shoulder diameter, pin diameter, thread pitch, and pin length were held constant at 10.00mm, 4.00mm, 0.70mm and 2.34mm respectively. The shoulder geometry was concave-shaped and the pin tip shape was a convex shape with a 3.96mm radius.

Figure 3-3. 15hp Hurco BMC 40 CNC machining center used for this experiment

Heideman et al. [61] reported the strongest welds were made using a rotation speed of 2000rpm, but as already mentioned, reported some weld inconsistency concerns. Since the plunge rate was not initially explored by Heideman et al. [61], then consecutive welds were made at six different plunge rates (0.21mm/s, 1.27mm/s, 2.54mm/s, 4.23mm/s, and 6.35mm/s, and 8.47mm/s). For these welds, the rotation speed, dwell time, and plunge depth were held constant at 2000rpm, 6.0s, and 2.34mm respectively, and a new tool was used for each plunge rate. The dwell time is defined as the time the tool was held at the desired plunge depth . The plunge depth is defined as the total distance that the welding tool tip is plunged into the sample. A 2.34mm plunge depth implies the shoulder of the tool is just contacting the original top surface plane of the 6061 Al sheet since the pin length was 2.34mm. These weld parameters were selected based on the work already done by Heideman et al. [61]. After welding, each sample was lap shear tensile tested, with a 1.5mm thick spacer added to each end of

the sample to minimize bending (see Figure 3-4), using an Instron tension test instrument with a cross-head speed of 2.11mm/s. The maximum load measured at failure for each sample was recorded; this maximum load will be referred to as the weld strength.

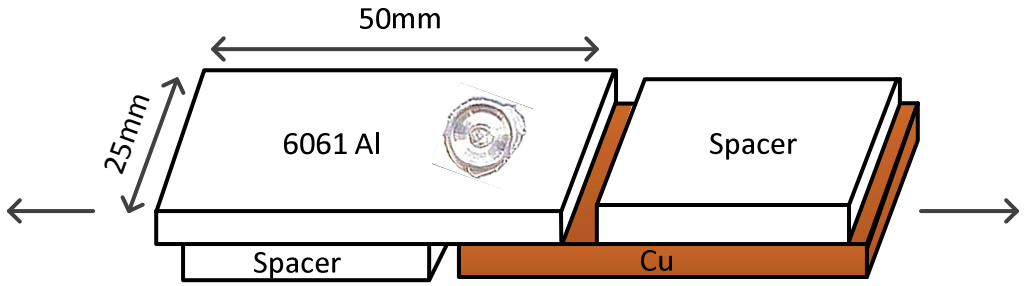

Figure 3-4. Shear sample used to measure FSSW joint strength (note that spacers were added to the sample during testing to minimize sample bending).

For temperature measurements, one thermocouple was placed on the outer radius of the pin tip, and the other was placed on the outer radius of the shoulder (see Figure 3-5). These locations were selected because temperatures should be the highest where surface velocities are the highest (i.e. outer radii of the pin and shoulder). The angle of installation of the thermocouple proved important to minimize noise in the temperature data and prevent the thermocouple from moving during the welding process. In early testing, the pin thermocouple was installed at a 40° angle from the tool centerline, while the shoulder thermocouple was installed 7° from the centerline. These angles were chosen to facilitate easy installation of the thermocouple into the tool. However, during experimentation, on occasion the temperature of the shoulder thermocouple suddenly dropped, indicating that the thermocouple was pushed up into the tool. This sudden and unexpected temperature drop issue was not seen on the tip thermocouple. It was determined that inserting the shoulder thermocouple at a less

vertical angle (40^{o} with respect to the tool centerline instead of the original 7^{o}) alleviated the sudden temperature drop issue.

The thermocouples consisted of Omega K-type, ungrounded, 0.25mm diameter, 150.24mm long thermocouples (Omega part number: KMTSS-010U-6). While calibrated thermocouples were purchased, standard thermocouple accuracy as reported by Omega was ±2% which translated to ±10°C at 500°C. To improve accuracy, prior to use, all thermocouples were calibrated using a Fluke 9141 thermocouple calibration device. Using the Fluke device to calibrate thermocouples from ambient to 600°C yielded an accuracy of ±1.7% (±10°C at 600°C), which was only slightly better than the as-received thermocouple. To improve accuracy, calibration was limited from 400°C to 600°C. Limiting the calibration range improved accuracy to ±0.7% (±4°C). Limiting calibration seemed plausible because the peak temperature was of most interest and was expected to be in the 400°C to 600°C range based on work done by Gerlich et al. [32].

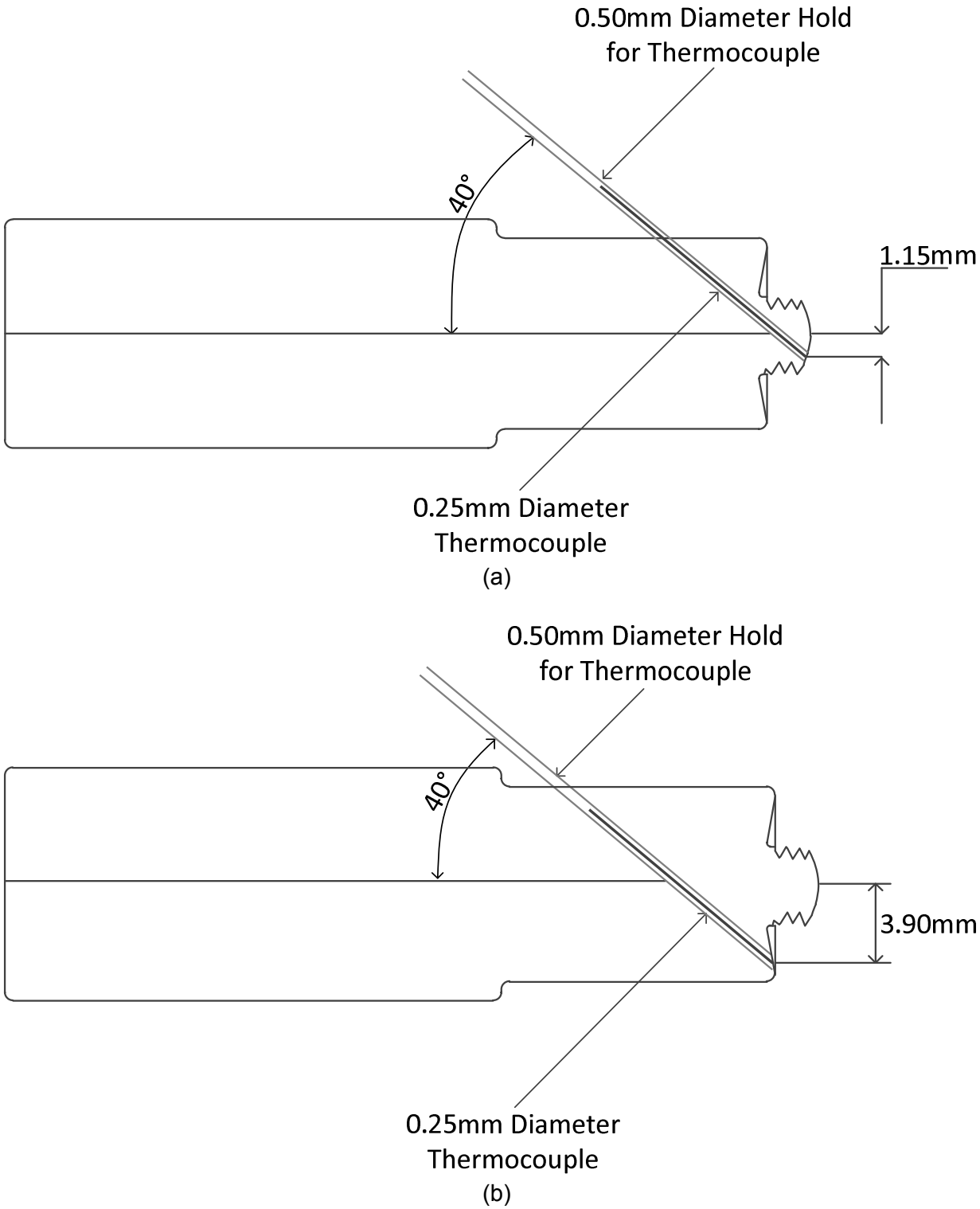

Figure 3-5. Drawing showing location of installed thermocouples in tool (a) pin tip and (b) shoulder.

To install thermocouples into the tool, 0.50mm diameter holes were drilled on a 40° angle through the tool to the desired location. A thermocouple was inserted into the hole and placed flush to the outer surface of the tool. The thermocouples were bonded into place using a high temperature ceramic paste adhesive with a maximum service temperature of 1649ºC; the trade name of this adhesive was Sauereisen Aluseal Adhesive Cement No 2.

The tool containing the two thermocouples was installed in a specially designed tool holder as shown in Figure 3-6. This tool holder contained three custom-machined inserts which were used to contain two printed circuit boards and a 9Vdc battery. One printed circuit board was used to use to collect thermocouple data; thermocouples were directly connected to this printed circuit board. The second printed circuit board was a Bluetooth® data transmitter which transmitted the thermocouple data from the rotating tool to a remote data acquisition computer. The key components of the temperature measurement system are highlighted in Figure 3-7.

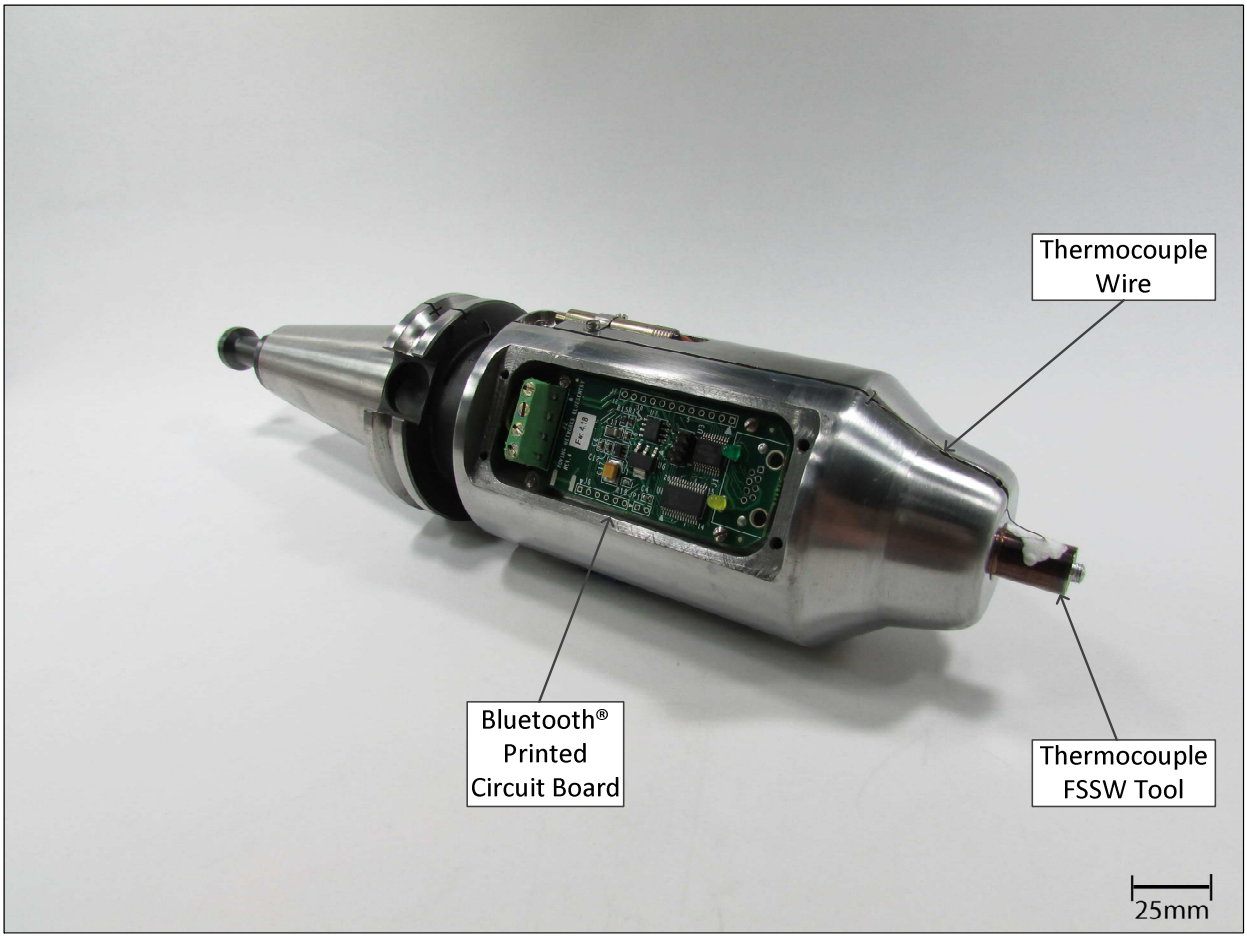

Figure 3-6. CNC tool holder with built-in Bluetooth® communication and thermocouple reader printed circuit boards.

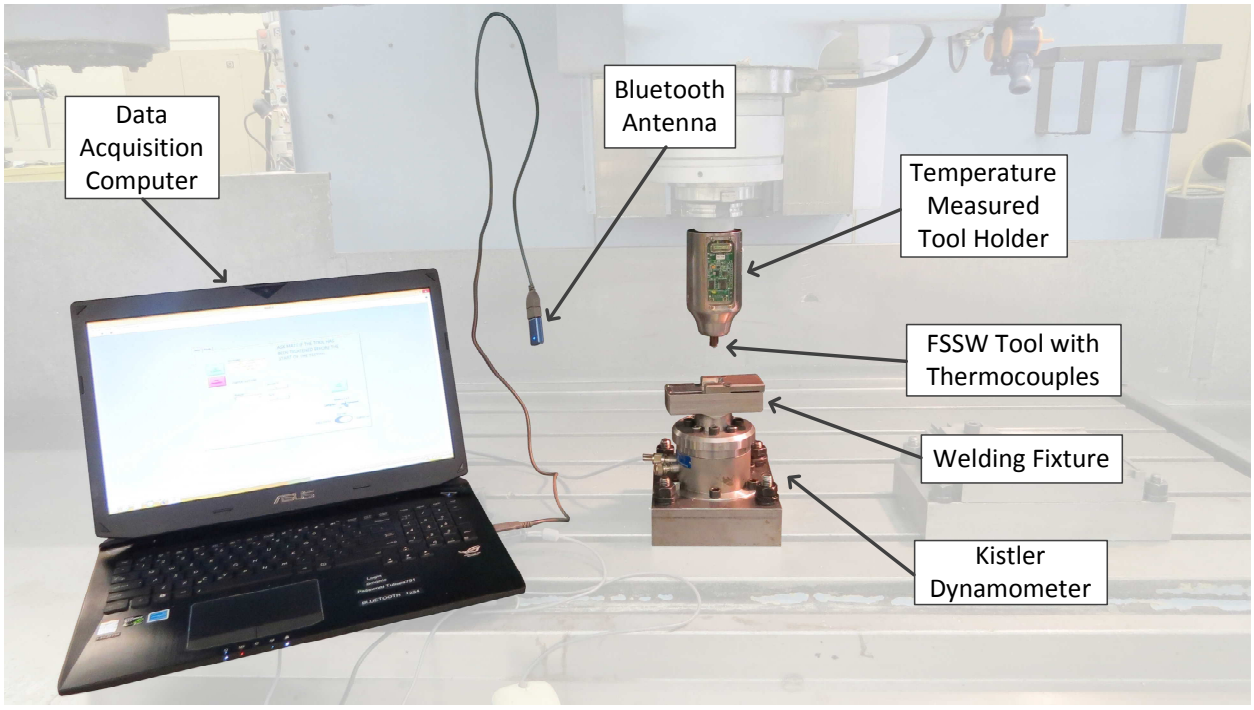

Figure 3-7. Key components needed to wirelessly transmit temperature data from FSSW tool to the data acquisition computer.

The printed circuit board for wireless thermocouple data collection contained three distinct circuits. The first circuit was the thermocouple signal conditioning circuit for the two K-type thermocouples used on the tip and shoulder of the FSSW tool. This circuit employed two Analog Devices AD595 Monolithic Thermocouple Amplifiers, which had the advantage of being a combined instrumentation amplifier with built-in cold junction compensation that was pre-calibrated for Type K thermocouples. These instrumentation amplifiers were useful for the low-noise differential input and precision gain characteristics which help improve precision and repeatability of the temperature measurements. The built-in cold junction compensation was more accurate than discrete cold junction compensation circuits and is more compact, which was a requirement of the unique packaging of this measurement circuit onto the tool holder.

These amplifiers also used a RC low-pass filter on each thermocouple output to reduce high frequency noise and improve accuracy.

The second circuit was an electromagnetic interference (EMI) and electrostatic (ESD) protection circuit that limited the output voltage of the thermocouple amplifiers to a range of ~0Vdc-5Vdc to protect the Bluetooth data transmitter. The EMI/ESD protection circuit used a Texas Instruments TLC2272A rail-to-rail dual op-amp in conjunction with a pair of back-to-back diodes connected directly to the output of the instrumentation amplifier circuits discussed above. The rail-to-rail operation was important to ensure the full range of voltage from power supply circuit could be utilized.

The final circuit on the printed circuit board was the power supply circuit. It utilized a common 9V alkaline battery and a Panasonic AN77L07 Low-Dropout 7V Linear Voltage Regulator. The AN77L07 provided a stable nominal output voltage of 7Vdc for the battery from full charge 9Vdc down to ~7.5Vdc (approximately 60% of full charge). This circuit contained an On/Off switch to disconnect the battery when not in use.

The thermocouple printed circuit board described above was connected via hard wiring to a Roving Networks Bluesentry Revision 4.18 Bluetooth® data transmitter. To help ensure proper communication was taking place during experimentation, the Bluetooth data transmitter printed circuit board contained a green LED and a yellow LED. The green LED flashed once per second when the system was idle. When the Bluetooth device made communication with the data acquisition computer, the yellow LED flashed rapidly until the connection was verified, which took about one to two seconds, and then the yellow LED turned off. Once communication was established, the

green LED flashed three times per second indicating that data was transmitted from the Bluetooth device to the computer. At the start of the welding process, a start icon on the user interface of the LabView program was clicked and voltage data, in hexadecimal format, was acquired by the computer from the Bluetooth device every 0.015s. A data acquisition rate of 0.015s was selected because this was the maximum possible data speed at which erroneous data (i.e. voltage readings out of a normal range) were not observed. The hexadecimal voltage values were then converted to normal decimal numbers using a virtual instrument subroutine that was created in the LabView data acquisition program. These voltage values were then converted to temperature values per the calibrations curve established for each thermocouple.

During initial temperature experimentation, two potential issues were observed. First, in some experimental runs, the peak temperatures were observed to fluctuate rapidly by more than 20^{o}C. In other cases, the peak temperatures were lower than expected by more than 50^{o}C. It was unclear if peak temperature fluctuations or peak temperatures variations were real phenomena or if thermocouples were damaged, or moved from the tool surface during installation into the tool or during the test run. To determine thermocouple integrity, tools that had measurement concerns and tools that were thought to yield reasonable data were placed into an oven at 260°C. The 260°C oven temperature was chosen because the maximum rated temperature for the thermocouple wire insulation is just over 260°C. After a 30 minute oven soak, the temperature of the oven was measured using the FSSW tools that contained the thermocouples. Tools that had rapidly fluctuating temperatures or temperatures were 50°C or more lower than expected indicated the oven temperature was rapidly

fluctuating or measured an erroneous oven temperature. Tools that measured welding temperatures consistently without significant variation measured the oven temperature ±5°C of the oven's digital readout, which was connected to a calibrated thermocouple. These results were an indication that in some instances, thermocouples were damaged or had moved within the tool during installation or during welding. Since running tests and analyzing data is quite laborious, to ensure thermocouple integrity, this oven procedure was implemented before and after each welding run.

In addition to measuring the temperature during this phase of experimentation, welding torque and vertical force measurements were measured. To make these measurements, the same CNC mill used in all previous experiments along with a Kistler 9271A quartz two-component dynamometer with two charge amplifiers. This type of dynamometer is used to measure drilling torques and forces. A fixture was designed to securely hold the two sheets to be welded and this fixture was mounted to the dynamometer (see Figure 3-8). This dynamometer and the charge amplifiers were calibrated by an outside firm prior to making any measurements. The dynamometer has a torque range of -100 to +100 Nm. Data from the dynamometer was collected via a LabView program similar to the one used to collect temperature data. The data acquisition speed for these measurements was 0.03s. The primary difference in the acquisition setup for these measurements, as compared to the temperature measurements, was that the dynamometer was in a fixed position, and therefore data could be collected through a hard connection to the dynamometer's charge amplifiers. A hard wire connection eliminated the complexity associated with wireless communication. Prior to collecting data in a welding trial, a torque wrench was used to

apply a known torque to verify that the data being collected by the LabView program matched the known applied torque.

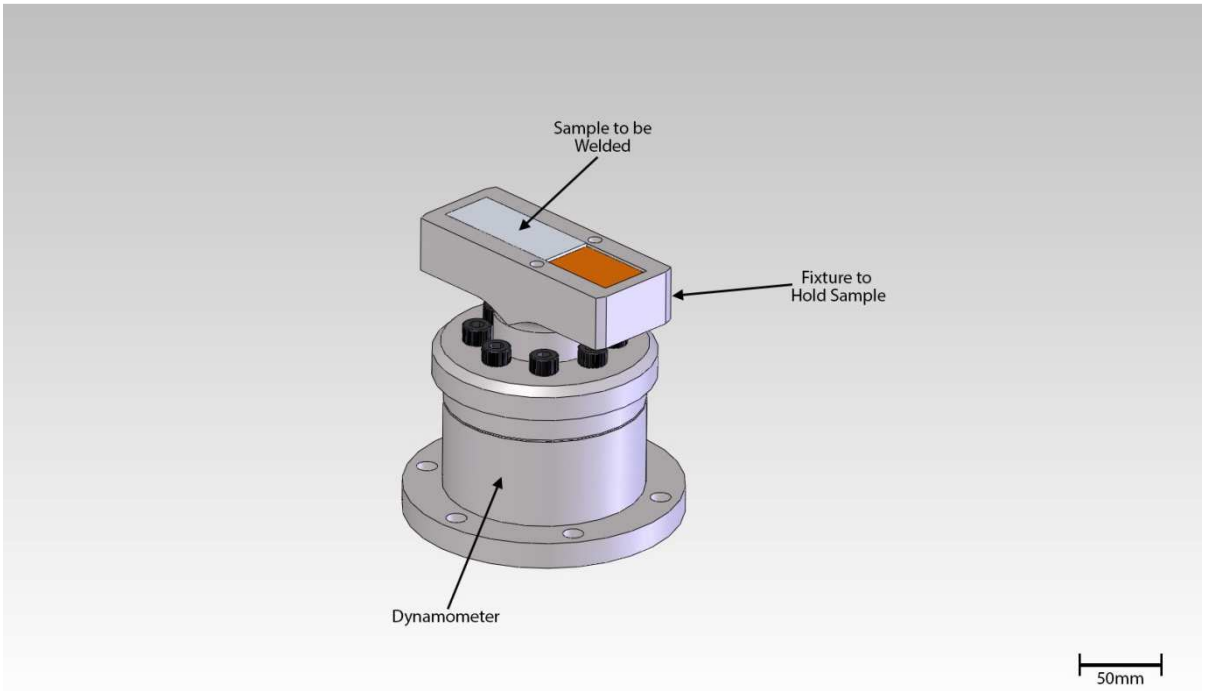

Figure 3-8. Schematic of the Kistler 9271A quartz two-component dynamometer with the welding fixture installed.

All data collected from the LabView programs (temperature, torque, and vertical force) were transferred into an MS Excel file. Because the wireless communication used for temperature measurements was not 100% perfect, the data after each temperature run was reviewed for dropped data (a data point where the voltage reading collected was zero due to an undetermined communication issue). The number of dropped data points was less than 1% and all dropped data points were deleted from the data set.

The welding trials to understand welding temperatures, torques, and vertical force were conducted according to the test matrix shown in Table 3-3. The dwell time

was 6.0s, and in all cases it was long enough to ensure the process had reached equilibrium (i.e. temperature, torque, and vertical forces were mostly stabilized). To eliminate changes to the tool, arising from weld material (6061 Al, Cu, and Al-Cu intermetallics) adhering to the tool from a previous weld a new tool was used for each temperature and torque/force run; 24 new tools were used for the experimental design shown in Table 3-3.

Table 3-3. Experimental Design for Evaluation of Temperature, Torque, and Force Measurements

Run	Rotation Speed (rpm)	Plunge Rate (mm/s)	Plunge Depth (mm)	Weld Time (s)
1	2000	0.21	2.03	6
2	2000	0.21	2.34	6
3	2000	0.21	2.59	6
4	2000	1.27	2.59	6
5	2000	2.54	2.03	6
6	2000	2.54	2.34	6
7	2000	2.54	2.59	6
8	2000	4.23	2.59	6
9	1000	0.21	2.59	6
10	1000	2.54	2.59	6
11	3000	0.21	2.59	6
12	3000	2.54	2.59	6

3.3 Results and Discussion

3.3.1 Plunge Rate's Effect on Weld Strength

The influence of plunge rate on weld strength is shown in Figure 3-9. Clearly, as the plunge rate slowed from 8.47mm/s to 2.54mm/s, the weld strength increased noticeably. At plunge rates greater than 2.54mm/s, the upward-extruded Cu ring did not adequately form. The upward-extruded Cu ring is needed for welds of reasonable strength, as reported by Heideman et al. [61]. Additionally, this experiment showed that further reducing the plunge rate to 0.21mm/s produced even stronger and more consistent welds as both an upward-extruded Cu ring and an Al-rich stir zone formed. From this experiment it was clear that plunge rate is a key independent variable. The measurement of weld temperatures, torques, and vertical forces will be used to better understand of why plunge rate, along with rotation speed and depth, can impact weld strength. Before discussing these results, it would be helpful to summarize a FSSW temperature profile and the repeatability of the temperature measurements.

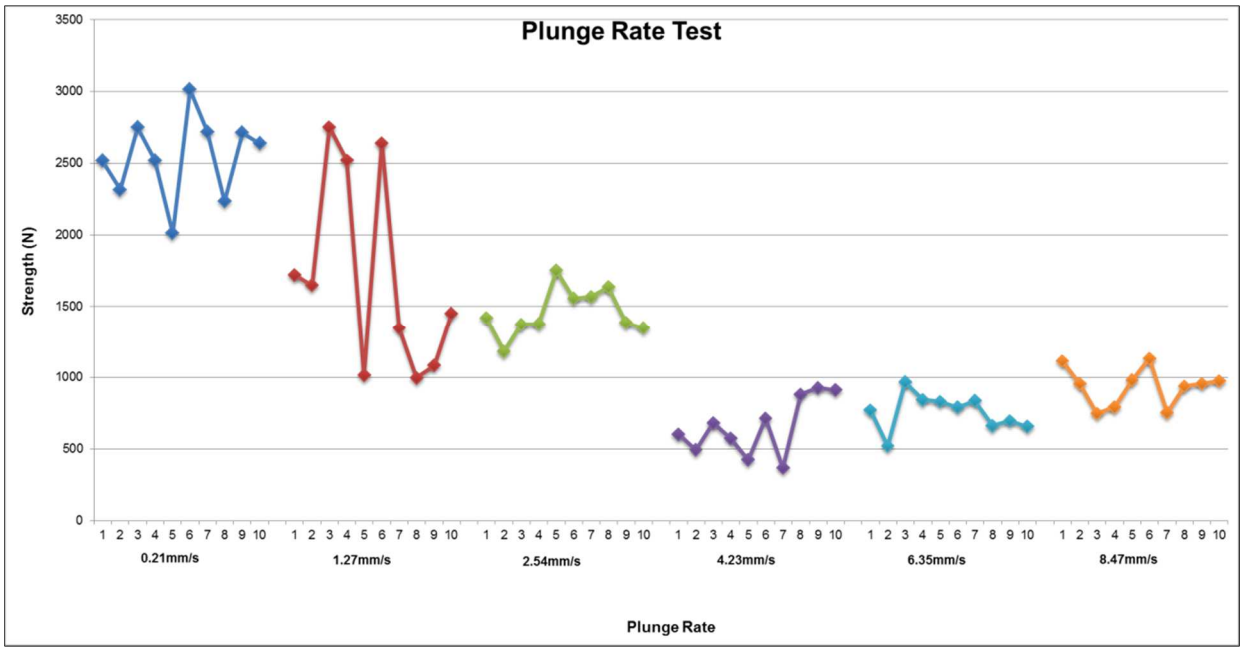

Figure 3-9. The influence of plunge rate on weld strength with a rotation speeds of 2000rpm, a plunge depth of 0.00mm, and a dwell time of 6.0s.

3.3.2 FSSW Temperature Curves and Measurement Repeatability

A 6061 Al to 6061 Al FSSW temperature profile is shown in Figure 3-10. Starting from t=0, there is a constant temperature to a point shortly before t=5s. The temperature in this region is constant because data acquistion was started, but the tool is still moving in air toward the workpiece and has not yet contacted the 6061 Al surface. In future data, this portion of the graph was deleted as it adds no useful information. The rapid increase in pin temperature just before t=5s is the point at which the tool pin contacted the workpiece and is beginning to plunge into the upper 6061 Al sheet at a rate of 0.21mm/s. The heating rate of the pin slows down shortly after the start of the weld but continues to increase until the plunge stops. When the weld plunge stops and the dwell period of the weld begins (as shown in Figure 3-10), the temperature of the outer pin diameter becomes reasonably constant (around 520°C). The heating rate of the

shoulder is less than the tool tip because the shoulder remains in air until just before the plunge ends. The increased shoulder temperature during the plunge is from heat conduction from the pin until the shoulder contacts the upper 6061 Al sheet. When the shoulder contacts the upper 6061 Al sheet, the heating rate of the shoulder increases rapidly until the temperature stablizes near 560°C.

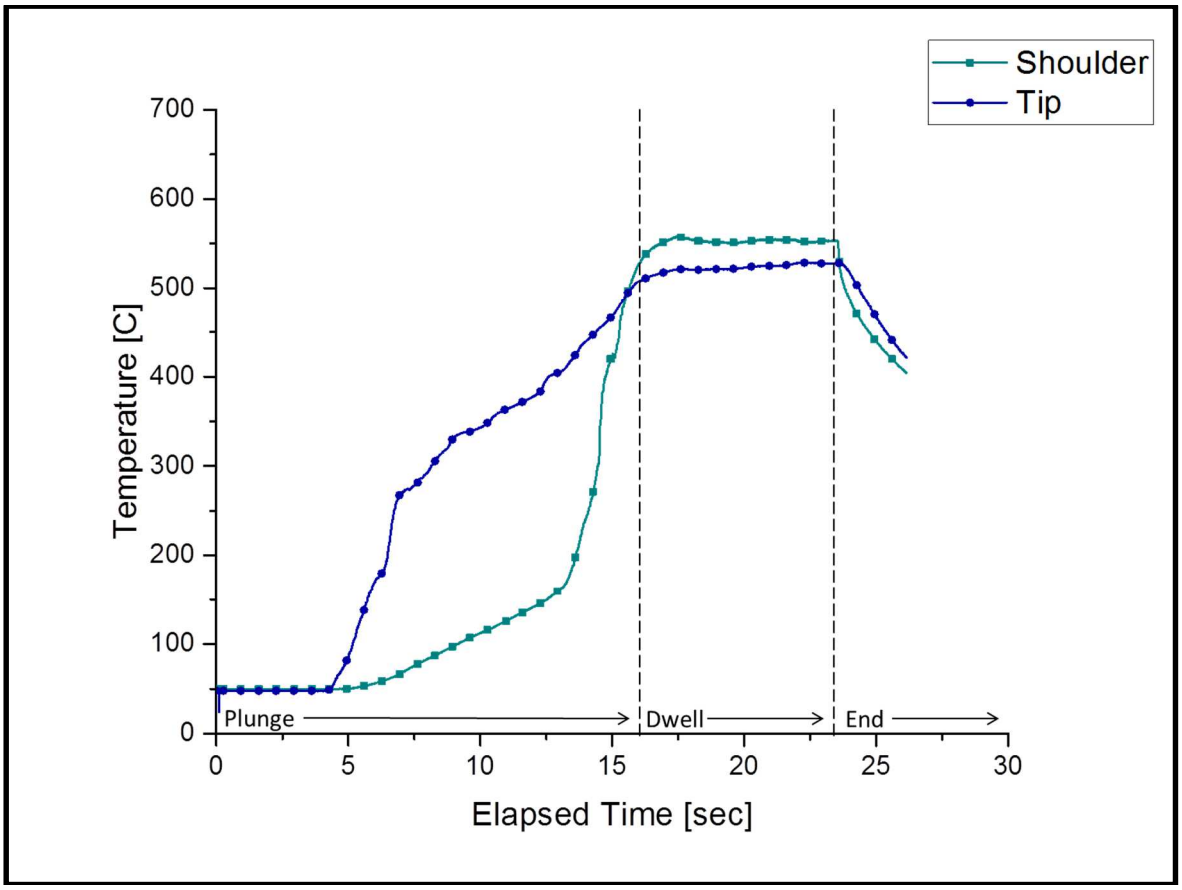

Figure 3-10. FSSW temperature profile for a 6061 Al to 6061 Al weld with welding parameters of a 2000rpm rotation speed, a 2.59mm plunge depth, a 0.21mm/s plunge rate, and a 6s weld dwell time.

To ensure repeatability of the temperature measurements, repeated runs were made in 6061 Al to 6061 Al welds using a different tool for each run. The 6061 Al to 6061 Al welds were used because the thermocouples were less likely to be damaged during these welds than with Al-Cu welds. The 6061 Al alloy softens and flows at lower

temperatures than copper and therefore, the thermocouples are less likely to be damaged.

Figure 3-11 shows the result of repeatability testing in the 6061 Al FSSW. The shoulder temperatures, as shown in Figure 3-11(a) were repeatable and within 10°C of each other. The tip measurements, as shown in Figure 3-11(b) showed a little more variability but were still within 20°C of each other. The observed deviation has multiple sources. First, the deviation could be a result of calibration differences which could account for up to 8°C (±4°C) of the total deviation. Second, the deviation could be a result of variation of the thermocouple position within the tool. Great care was taken to ensure the thermocouple was installed flush to the tool surface, but small variations could impact measurements since the temperature gradients in the region immediately adjacent to the tool are large [47]. Another source of positional error could have occurred due to the size of the drilled hole for the thermocouple, which was approximately twice as large as the thermocouple itself. Having an oversized hole would permit some level of radial positional error, which could also impact the accuracy of the temperature measurement.

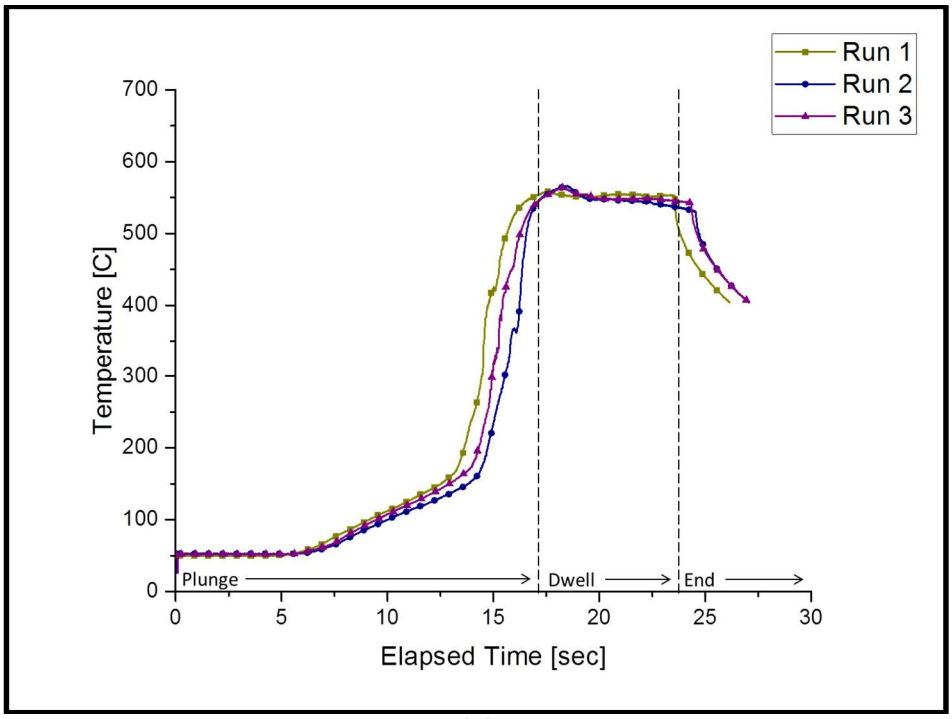

(a)

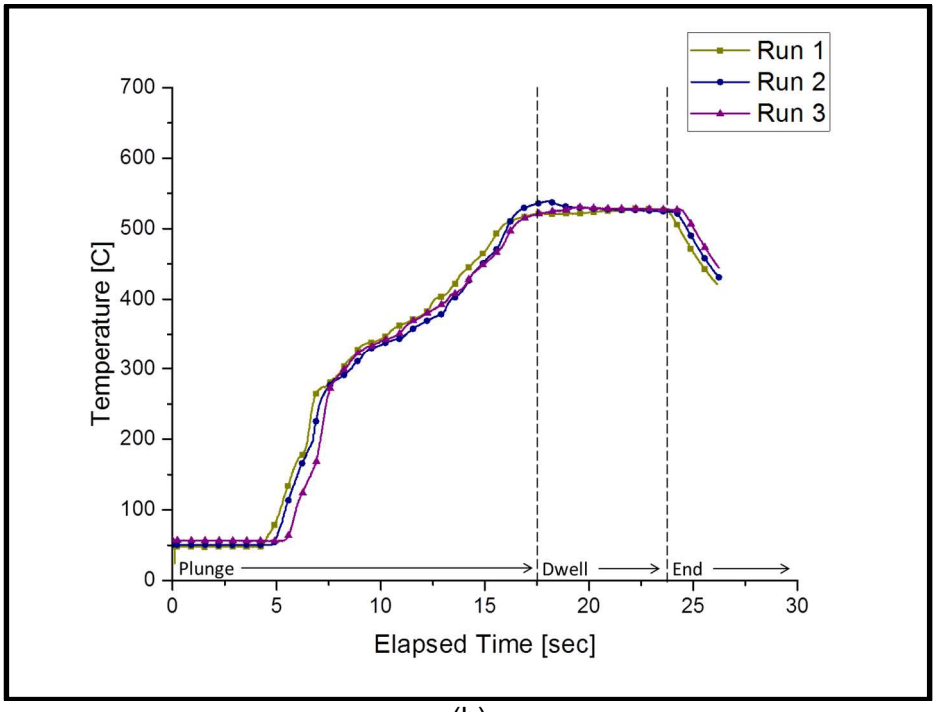

(b)

Figure 3-11. Temperature measurement repeatability testing using 6061 Al to 6061 Al FSSW with (a) being the shoulder temperature and (b) being the pin tip temperature. Each run used a new tool of the same design with welding parameters of a 2000rpm rotation speed, a 2.59mm plunge depth, a 0.21mm/s plunge rate, and a 6s weld dwell time.

The next step was to measure the repeatability of the Al-Cu FSSW temperature measurements (see Figure 3-12). The shoulder graph (Figure 3-12(a)) shows good repeatability through the plunge, but the peak temperatures achieved after the plunge show some variability. Two of the runs have a minor variability of less than 10°C but the third run had a peak temperature that varied by just over 20°C. The larger variance of the third run was likely due to calibration or thermocouple position issues, as discussed earlier.

The variability of the peak pin temperatures in Figure 3-12(b) was less than 10°C during the plunge and dwell portions of the weld. This variation is similar to the 6061 Al to 6061 Al FSSW and seems reasonable.

The Al-Cu FSSW temperature profiles have a shape similar to the 6061 Al to 6061 Al FSSW profiles with the primary difference being an additional tool pin heating rate change during the plunging process. This additional heating rate change takes place about the time the pin makes contact with the lower copper sheet and produces a higher heating rate than when the tool pin is plunging through the upper 6061 Al sheet.

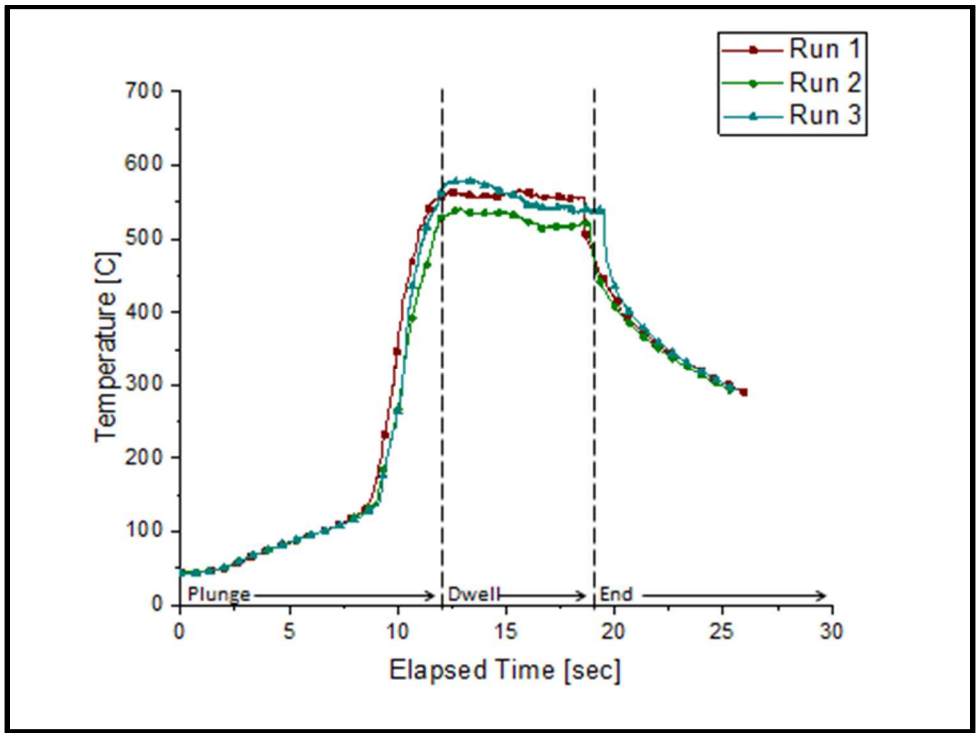

(a)

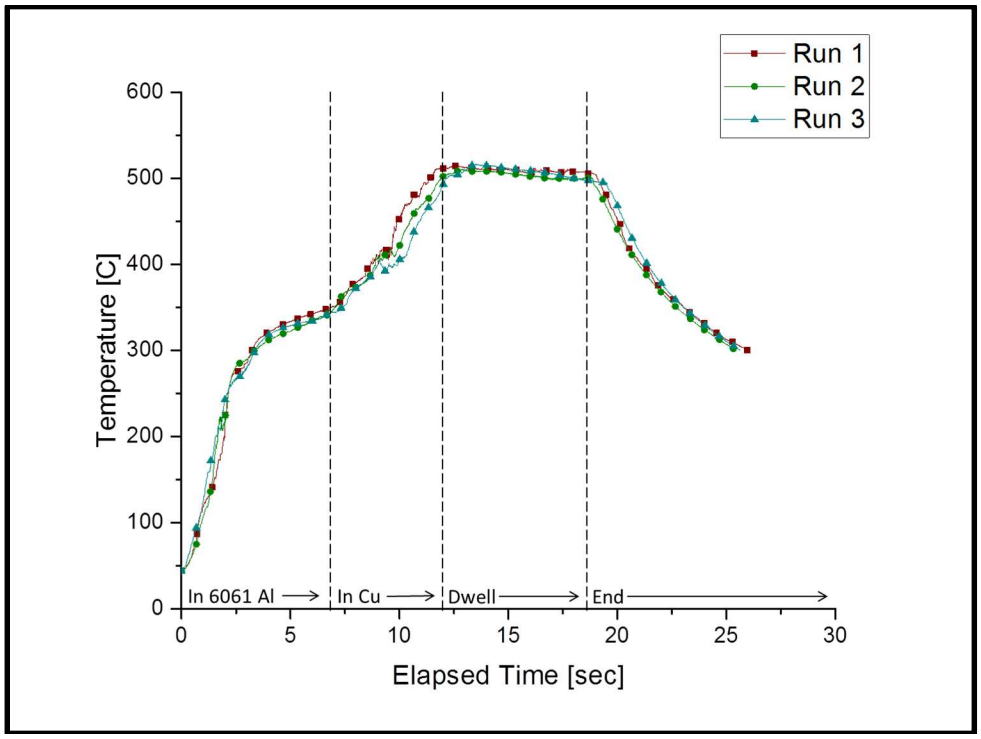

(b)

Figure 3-12. Temperature measurement repeatability testing using 6061 Al to Cu FSSW with (a) being the shoulder temperature and (b) being the pin tip temperature. Each run used a new tool of the same design with welding parameters of 2000rpm rotation speed, 2.59mm plunge depth, 0.21mm/s plunge rate, and 6s weld dwell time.

The conclusions from the repeatability work are:

- Temperature measurements cannot be viewed as completely absolute values. Variations of up 20°C under the same welding conditions are possible.
- Temperature measurements must differ by more than 20°C to be viewed as significant.

3.3.3 Rotation Speed

The influence of rotation speed was first evaluated by Heideman et al. [61] as part of a design-of-experiments, showing that rotation speed, when increased from 1000rpm to 2000rpm, had a significant impact on weld strength. In Figure 3-13, the temperature profiles (tool tip and shoulder) are compared when the rotation speed was varied from 1000rpm to 3000rpm. Clearly, as the rotation speed increased from 1000rpm to 2000rpm, the temperatures of the pin and shoulder amplified with increasing rotation speed. There is also nearly a 100°C pin temperature difference during the plunging process as indicated by the circled regions in Figure 3-13(b). Additionally, the peak temperatures for both the pin and shoulder for the 1000rpm weld were just over 50°C lower than those for the 2000rpm welds. The difference in temperatures between 1000rpm and 2000rpm rotation speeds likely results from less energy being generated when a 1000rpm rotation speed was used. When the rotation speed was increased from 2000rpm to 3000rpm, the shoulder temperatures initially showed a significant difference. The peak temperature at a 2000rpm rotation speed was 575°C compared to 607°C for the 3000rpm rotation speed. The 607°C peak shoulder temperature for the 3000rpm rotation speed was 25°C higher than the 6061 Al eutectic temperature of 582°C [74]. Consequently some level of melting would be expected in

the shoulder region immediately at the end of the plunge process and during the dwell portion of the weld when using a 3000rpm rotation speed. Melting can cause tool slippage and, hence, less frictional heating and a drop in temperature; which is evident at the top of the 3000rpm curve. Comparatively, no melting would be expected for a 2000rpm weld since the peak temperature is less than the 6061 Al eutectic temperature. The shoulder temperature difference between the 2000rpm and 3000rpm welds disappears once the plunge is over and the peak temperature is reached.

The pin temperatures for the 2000rpm and 3000rpm welds varied during the plunge portion of the weld by approximately 60^{o}C, with the 3000rpm weld, as expected, having the higher temperature. This difference can be seen comparing the circled regions in Figure 3-13. Also evident in the circled region is that a heating rate represented by a slight slope in the time vs. temperature curve exists for the 2000rpm and 3000rpm curves. However, the 1000rpm curve is relatively flat in the circled region until the shoulder engages the upper 6061 Al sheet. This minimal heating rate during 1000rpm plunging suggests that heat is being extracted from the welds as fast as heat is being generated. This is not entirely surprising since the lower Cu sheet is a better heatsink than to 6061 Al. The peak pin temperatures for the 2000rpm and 3000rpm welds are nearly identical, 524°C and 521°C, respectively. The higher pin temperatures during plunging for the increased rotation speeds result from the higher strain at increased rotation speeds. As the strain rate increases, more plastic deformation takes place and the energy associated with the deformation is dissipated in the form of heat. Thus, plunge temperatures, as shown in Figure 3-13, are higher for the increased rotation speed. These temperatures can be further understood by looking at the energy

generated during FSSW. This energy can be estimated by using measured welding torque and vertical force data.

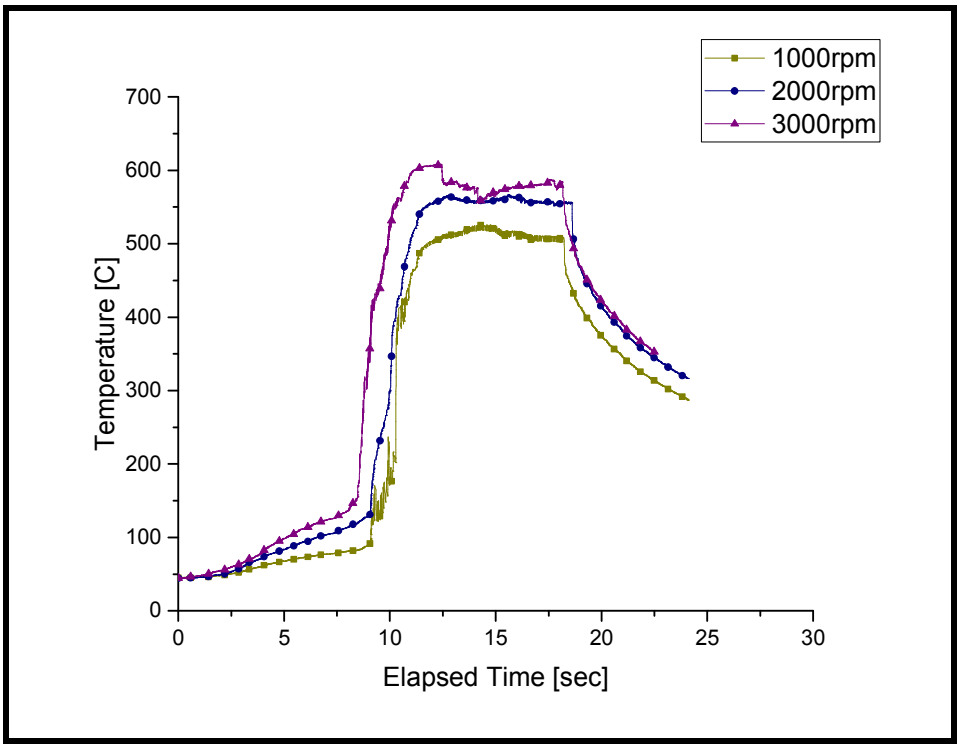

(a)

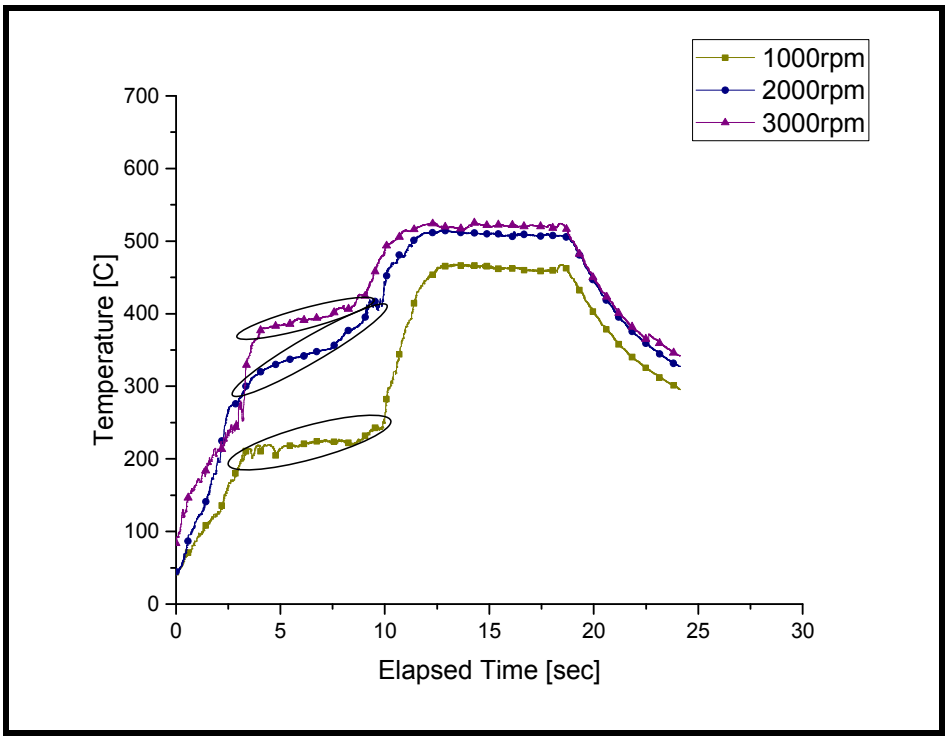

(b)

Figure 3-13. A comparison of temperature profiles for (a) the tool shoulder and (b) the tip at different rotation speeds: 1000rpm, 2000rpm, and 3000rpm. Other welding parameters were a 2.59mm plunge depth, a 0.21mm/s plunge rate, and a 6.0s weld dwell time.

The influence of rotation speed on torque can be seen in Figure 3-14. To understand the torque curve, the estimated power vs. time curve, shown in Figure 3-15 is useful as well, where power = (torque) x (rotation speed). As mentioned earlier, increasing rotation speed results in higher strain rates in the stir zone. Achieving these higher strain rates requires more power. This statement is supported by the 1000rpm power curve in Figure 3-15, which is lowest of the three curves. It would have been expected that the estimated power for the 2000rpm weld would have been substantially lower than the 3000rpm weld but this was not the case. The 2000rpm and 3000rpm power curves in Figure 3-15 are very close to one another during the plunge portion of the process with a 3000rpm curve being just slightly higher (i.e. consuming slightly more power) than the 2000rpm curve. The small difference in the 3000rpm and 2000rpm estimated power curves can be understood by looking at the measured temperatures in Figure 3-13(b). The difference in pin temperatures during the plunge portion of the FSSW process is much greater for the 1000rpm and 2000rpm welds than is the difference between the 2000rpm and 3000rpm welds. The small difference between the two higher rotation speed welds supports the notion that the viscosity difference between these two materials would be small, and hence, the power required to achieve the higher strain rates are similar.

It is interesting to note that at the end of the plunging process, Figure 3-15 shows the power for the 3000rpm and 2000rpm welds are nearly the same even though the peak shoulder temperature of the 3000rpm (607°C) weld was 32°C higher than the 2000rpm weld (575°C) (see Figure 3-13(a)). The unchanging power consumption

accompanied by a peak temperature for the 3000rpm weld being above the 6061 Al eutectic temperature of 582°C likely indicates that some level of melting took place. Once the material melts, tool slippage could occur, as discussed by Gerlich et al. [32], resulting in less power consumption. The evidence of tool slippage is further supported in Figure 3-15; after the plunge is complete, the 3000rpm has consumed the lowest amount of power.

The vertical force of the welds made at different rotation speeds is shown in Figure 3-16. The vertical force curve appears less influenced by rotation speed with the peak forces for 1000rpm and 2000rpm being similar and the 3000rpm peak force being 1000N to 1500N lower than the two slower rotational speeds. The lower peak force of the 3000rpm would be expected since the peak force and peak temperature likely occur at nearly the same time (end of the plunging portion of the weld). The observation that the 2000rpm curve has a peak force approximately 400N higher than that of the 1000rpm curve was surprising and cannot be explained. However, the vertical forces during the plunge portion of the weld (prior to reaching the peak force) are in line with expectations. The 1000rpm curve exhibits the highest vertical force (Figure 3-16) during plunging and also had the lowest plunge temperature (circled region in Figure 3-13). The lower the temperature, the more viscous the material is and consequently the more difficult it would be to plunge the weld tool through the material. Similarly, the 2000rpm and 3000rpm welds had the second highest vertical forces and the lowest vertical forces respectively during the weld plunge.

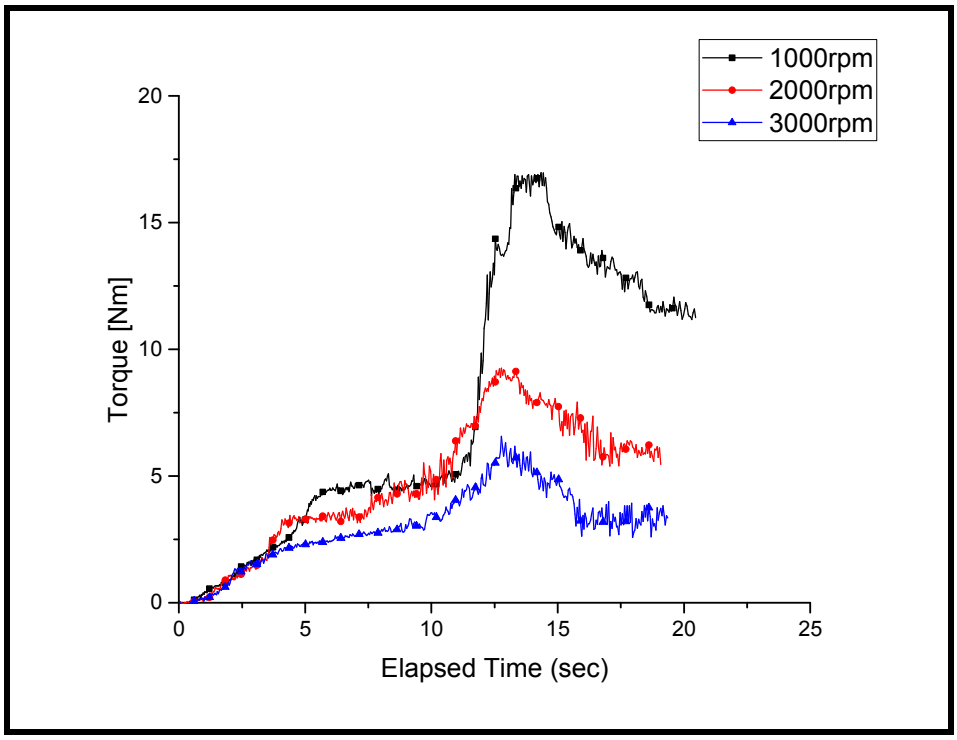

Figure 3-14. Graph showing torque vs. time for three rotation speeds. Other welding parameters were a 2.59mm plunge depth, a 0.21mm/s plunge rate, and a 6.0s weld dwell time.

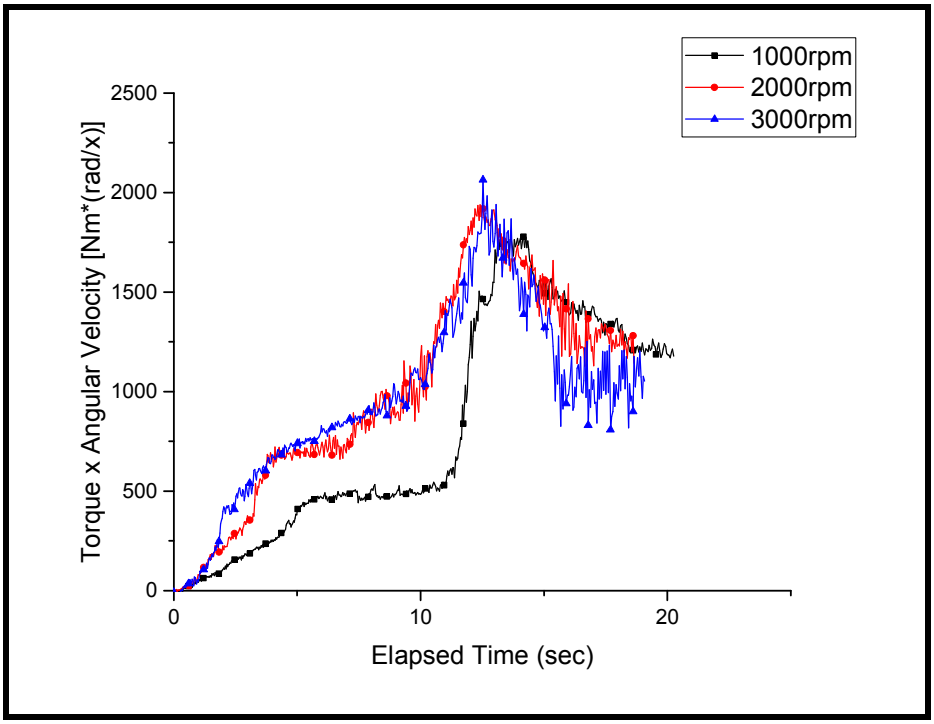

Figure 3-15. Graph showing power (torque x angular velocity) vs. time for three rotation speeds. Other welding parameters were a 2.59mm plunge depth, a 0.21mm/s plunge rate, and a 6.0s weld dwell time.

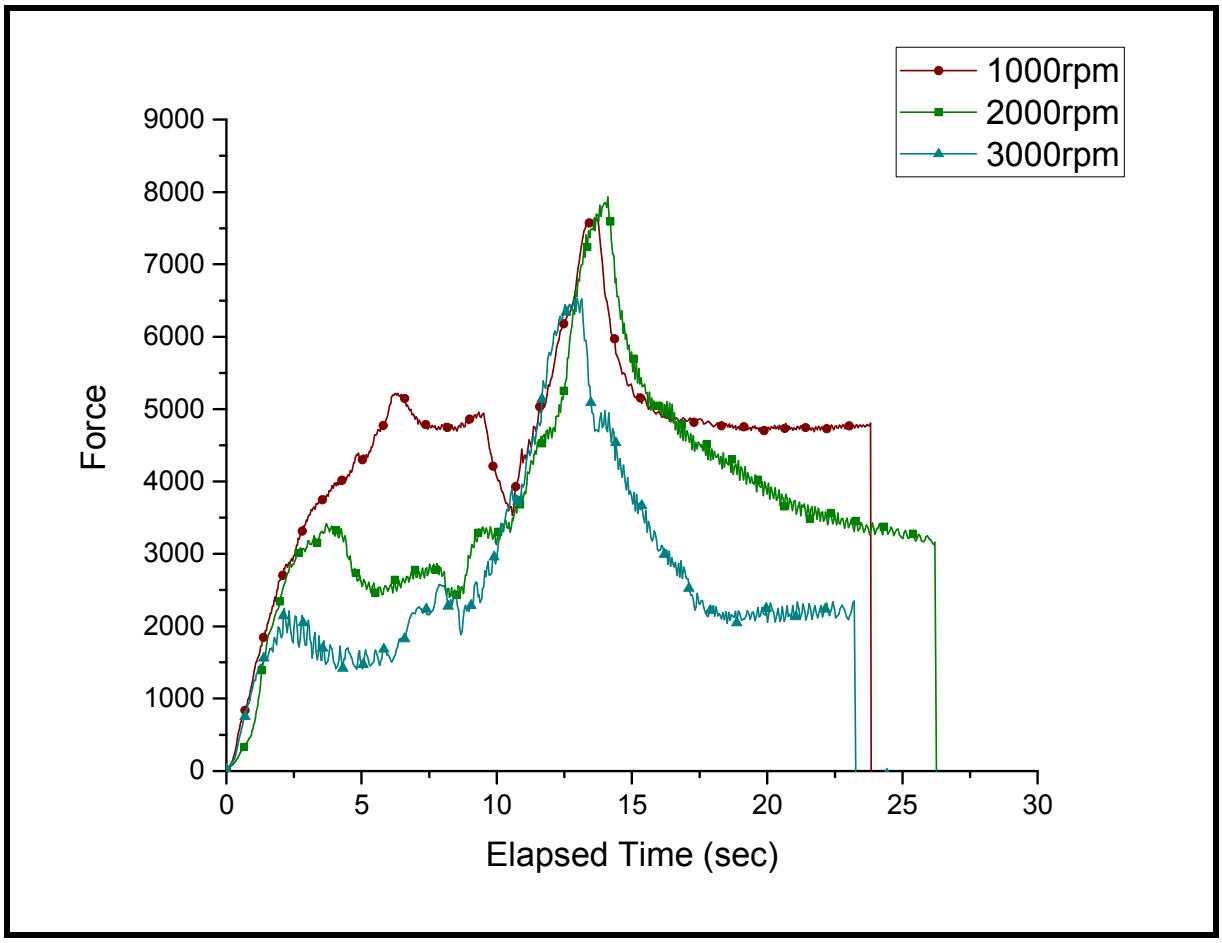

Figure 3-16. Graph showing vertical force vs. time for three rotation speeds. Other welding parameters were a 2.59mm plunge depth, a 0.21mm/s plunge rate, and a 6.0s weld dwell time.

An important observation from the vertical force graph was that the peak forces for these rotational speeds did not occur at the same time even though the plunge times and welding times were assumed to be identical. However, the assumption of identical plunge and welding times (plunge plus dwell time) is apparently incorrect and requires further explanation.

Data acquisition begins when the CNC starts plunging toward the workpiece, but the force remains zero until the tool makes contact with the upper 6061 Al sheet. To further explain, in the raw data that was collected, t=0 is when the tool starts plunging

toward the workpiece, which is not the same point at which t=0 for the actual weld; t=0 for weld occurs when the tool makes first contact with the upper 6061 Al sheet. Consequently, there is an unknown Δt between when the data collection begins and the weld actually starts. Fortunately, the welding starting point is easy to identify in the force data because the force increases dramatically when the tool contacts the workpiece. In addition, the end weld time is easy to identify because the force quickly drops to zero the instant the tool is retracted. Using torque data to determine weld time was more difficult because the torque measurement shows a slower increase during plunging. Since torque and force data were collected simultaneously, the weld start time and end times derived from force data were also used for torque measurements. Determining the weld start and end times are important because these will be needed for welding energy calculations that will be discussed later.

The measured weld time can be easily calculated from the raw time data of force measurements:

$$\boldsymbol{t_w^m = t_e^o - t_s^o} \qquad \textbf{(3-1)}$$

Where t_w^m is the total measured weld time in seconds, t_e^o is the observed end weld time in seconds in raw time data when the force went to zero and the time at which the tool is retracted from the workpiece, and t_s^o is the observed weld starting time in seconds in the raw data when the force increased quickly indicating the tip of the tool had just engaged the upper 6061 Al sheet. Using this calculation (equation 3-1), it was observed that the measured weld times (t_w^m) were always greater than the theoretical weld time, that is:

$$\boldsymbol{t_w = t_d + t_p} \qquad \textbf{(3-2)}$$

Where t_w is the theoretical weld, t_d is the weld dwell time in seconds after the plunge is complete and t_p is theoretical plunge time in seconds. In theory, the t_p can be calculated by:

$$\boldsymbol{t_p = p_r \times d_p} \quad \textbf{(3-3)}$$

Where p_r is the plunge rate set point of the CNC and d_p is plunge depth in mm.

To determine the source of error, analysis began by working backward in time from the end of the weld (in the raw data). The dwell time (t_d) was subtracted from the observed weld end time (t_e^o), and it was noticed that peak force occurred at this time. This was expected since the peak force should be the demarcation between the end of plunge period and the start of dwell period. The constant dwell time also indicated that the dwell time set point in the CNC program was accurate. In the raw data, the time of the peak force is defined as observed plunge time $\left(t_p^o\right)$ that is:

$$\boldsymbol{t_p^o = t_e^o - t_d} \quad \textbf{(3-4)}$$

Working backward in time further, the measured plunge time (t_p^m) was calculated:

$$\boldsymbol{t_p^m = t_p^o - t_s^0} \quad \textbf{(3-5)}$$

Comparing the theoretical plunge time (t_p) to the measures plunge time (t_p^m), $t_p^m$was always greater than t_p indicating that the plunge period was taking longer than expected. The reason for this appears to be an issue with CNC control. As the CNC plunges through air, it can maintain a constant plunge rate (p_r) because there is not a significant load on the spindle. When the tool hits the workpiece, the plunge rate (p_r) will naturally slow, due the resistance associated with the tool tip hitting the upper 6061 Al sheet, until the CNC's control senses the reduced speed and compensates and begins

adjusting its plunge rate until the setpoint is again achieved. Unfortunately, the time required for compensation and the accuracy of this compensation are unknown. To make this more difficult, when the tool hits the copper sheet, the plunge rate would again slow because copper is harder than the aluminum and requires more force to push through it. Using that data analysis technique discussed above, plunge rates were 6.26% to 15.77% slower than the set point, and no identifiable pattern to this error could be observed. The errors associated with various welding conditions are shown in Tables 3-4, 3-5, and 3-6. This error explains why force, torque, and temperature comparison curves can have shifts in measured weld time (t_w^m) of 1s-2s even though the theoretical weld times (t_w) were the same. This also suggests that variations in the force data, particularly during plunging, as observed in Figure 3-15, will be difficult to explain other than that the CNC was varying the plunge rate (p_r) in an effort to achieve the plunge rate (p_r) set-point. Some of the "noise" observed in the plunge region temperature measurements could also be explained from this issue. For future reference, the theoretical plunge rate (p_r) will be identified in torque and temperature data graphs knowing the actual plunge rates were likely 6%-15% slower than the reported theoretical.

As reported by Heideman et al. [61], weld strengths made using 1000rpm rotation speed are weaker than those made with 2000rpm speeds. The lower strength stems from the poor formation of the extruded copper ring needed for good quality welds (see Figure 3-2). Using the force and torque curves to estimate the energy generated during plunge portion of the welding process can help explain this observation. Focusing on plunge energy, as opposed to the total weld energy (i.e.

plunge energy plus dwell energy), is done because Heideman et al. [66] observed that the macrostructure of the weld is formed during the plunging process and the required macrostructure does not show any changes with added weld dwell time. Additionally, evaluating the total weld energy is not of much interest because increasing the dwell time is an easy path to increasing weld energy dramatically but, as shown by Heideman et al. [66], is insignificant in producing quality welds.

Total energy Q in a FSSW is determined by the relation:

$$\boldsymbol{Q = \int Force(z)dz + \int Torque(t)\omega dt} \quad \textbf{(3-6)}$$

Where z is the penetration depth, ω is the angular velocity (rad/s) and dt is the sampling time(s). ω (in radians/s) is directly proportional to the rotation speed through the following relationship:

$$\boldsymbol{\omega = 2\pi R_s} \quad \textbf{(3-7)}$$

Where R_s is the rotation speed in revolutions/s. Equation (3-6) can be used to calculate the weld energy up to any point in the FSSW process. Since the weld macrostructure required to produce quality welds is formed during the plunge portion of the welding process, the relevant energy for FSSW of 6061 Al to Cu would be determined by integrating Equation (3-6) from t=0s to the end of the actual plunge. However, the first term in Equation (3-6), the linear displacement energy, contributes less 0.5% (an insignificant amount) of the energy generated during the plunge portion of the process. Therefore, this term will be ignored when discussing weld energy and no additional force vs. time graphs will be shown and discussed. The second term in Equation (3-6) is the energy required to rotate tool and consequently the energy input to the weld; this is the primary energy source for FSSW. Since the discussion will focus on the plunge

portion of the process, this term will be referred to as the “rotational plunge weld energy”.

Table 3-4. Rotational Plunge Weld Energy Calculations Comparing Rotation Speeds

Speed (rpm)	Plunge Rate (mm/s)	Plunge Depth (mm)	Rotational Plunge Weld Energy (j)
1000	0.21	2.59	12,501
2000	0.21	2.59	17,336
3000	0.21	2.59	19,826

Table 3-4 shows that the rotational plunge weld energy increased 39% when rotation speed was increased from 1000rpm to 2000rpm. The increase was expected since the measured plunge and peak temperatures in Figure 3-13 were substantially lower for the 1000rpm weld. Similarly, Table 3-4 shows that the rotational plunge weld energy further increased when the rotational speed was increased from 2000rpm to 3000rpm, but the increase was only 14%. Furthermore, an undeterminable amount of the 14% increase resulted from a slightly longer plunge time which can be seen the slight shift to the right of the 3000rpm curve at t≈12s in Figure 3-15. The increase in plunge time is an uncontrollable error associated with the CNC control system attempting to maintain the 0.5mm/s plunge rate. The similar rotational plunge rotational plunge weld energy generated at 2000rpm and 3000rpm is a indication that there is a limit to the amount of energy that can generated by just increasing rotation speed.

3.3.4 Plunge Rate

From the prior discussion, rotation speed was shown to be an important parameter in forming Al-Cu FSSWs of reasonable quality. However, rotation speed alone does not determine weld quality, and the plunge rate can be used to improve weld strength and consistency, as shown in Figure 3-9. Additionally, as presented by Heideman et al. [66], the weld macrostructure was shown to be completely developed after the plunge was complete. These observations showed the importance of plunge rate and the plunging process. Temperature and torque measurements can help explain for these observations.

A temperature comparison for four welds with plunge rates varying from a slow rate of 0.21mm/s to relatively high rate of 4.23mm/s are shown in Figure 3-17. As discussed earlier, plunge rates greater than 2.54mm/s produced poor quality FSSWs (i.e. weld strengths consistently under 1000N). As shown in Figure 3-18(a), the required Cu ring (as an interlocking structure) did not form at the 4.23mm/s plunge rate. In comparison, as shown in Figure 3-18(b), the necessary interlocking structure formed in welds was made with the 0.21mm/s plunge rate. Interestingly, the peak temperatures for the four plunge rates vary minimally, indicating that simply using peak temperature to determine weld quality is not plausible.

The most noticeable difference in the temperature profiles is in the slope of the pin temperature profile. With a 0.21mm/s plunge rate, this slope flattens around 300°C at t=4s and lasts until about t=9s. t=9s is the approximate time the shoulder begins to influence the weld and the heating rate is substantially increases. As the plunge rate is increased to 1.27mm/s, the duration of the slope flattening was reduced to

approximately 1s. When the plunge rate was further increased to 2.54mm/s and higher, the slope of the pin temperature does not appear to flatten. The flattening of the temperature curve suggests heat is extracted from the stir zone nearly as fast as it is generated, and the rapid heat extraction is likely due to the superior thermal conductivity of the bottom Cu sheet. As the Cu sheet extracts the heat, its temperature increases. The increased temperature makes the lower Cu sheet easier to extrude which makes the formation of the required macrostructure more likely (see Figure 3-2). Consequently, better welds are achieved at reduced plunge rates exhibiting a pin temperature slope having a flat section during which the Cu sheet is heated.

Interestingly, the pin temperature profiles are similar during the plunge process for each different plunge rate in Figure 3-17. The pin temperatures increase rapidly and then the curves all show a slope shape near 300°C (at slower plunge rates, the curves flatten and level off at approximately 300ºC). Once the shoulder begins to generate heat, as evident by the high heating rate of the shoulders' temperature curves (i.e. the steep slope), the pin and shoulder temperatures quickly rise to peak temperatures, which again are all similar at approximately 510°C and 575°C, respectively. These curves support the hypothesis that weld formation takes place during the plunge. If dwell time and peak temperature were important to formation of quality welds, all welds made at 2000rpm, regardless of plunge rate, should be of reasonable quality because dwell times (as reflected by the time the weld remained at or near peak temperatures) and peak temperatures are similar for all 2000rpm welds regardless of the plunge rate. Also, plunge rate temperature comparisons further support the observation that rotation speed is a key variable in determining peak weld temperatures since the peak

temperatures for the pin and shoulder were similar for all plunge rates when rotation speed was held constant. Further information regarding the importance of plunge rate can be observed by looking at the torque curves and using the torque data to calculate the rotational plunge weld energy.

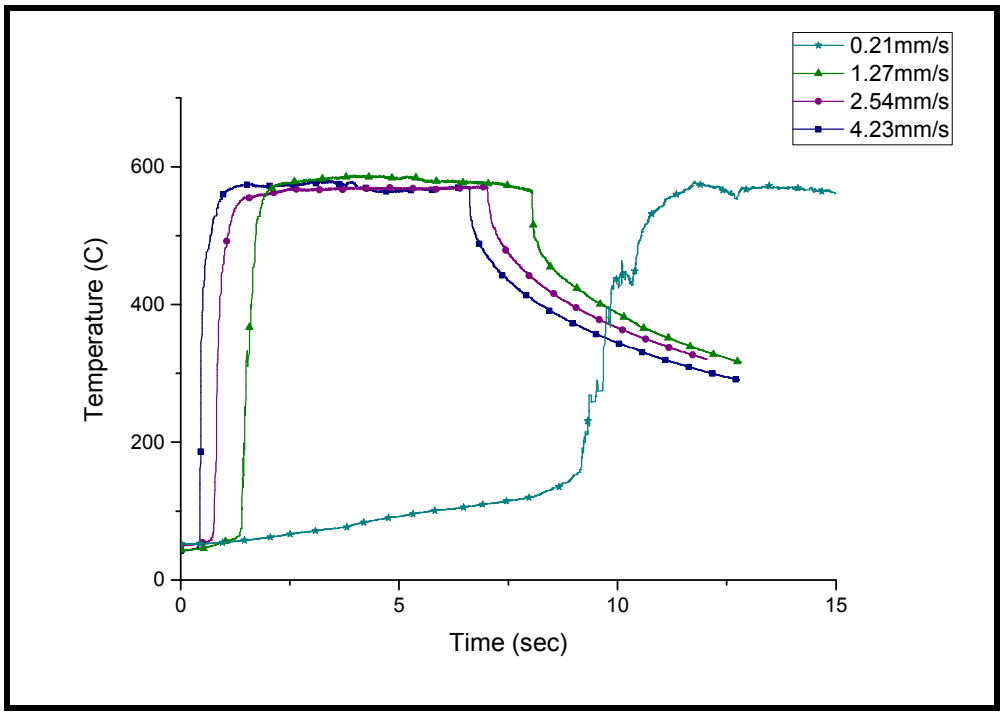

(a)

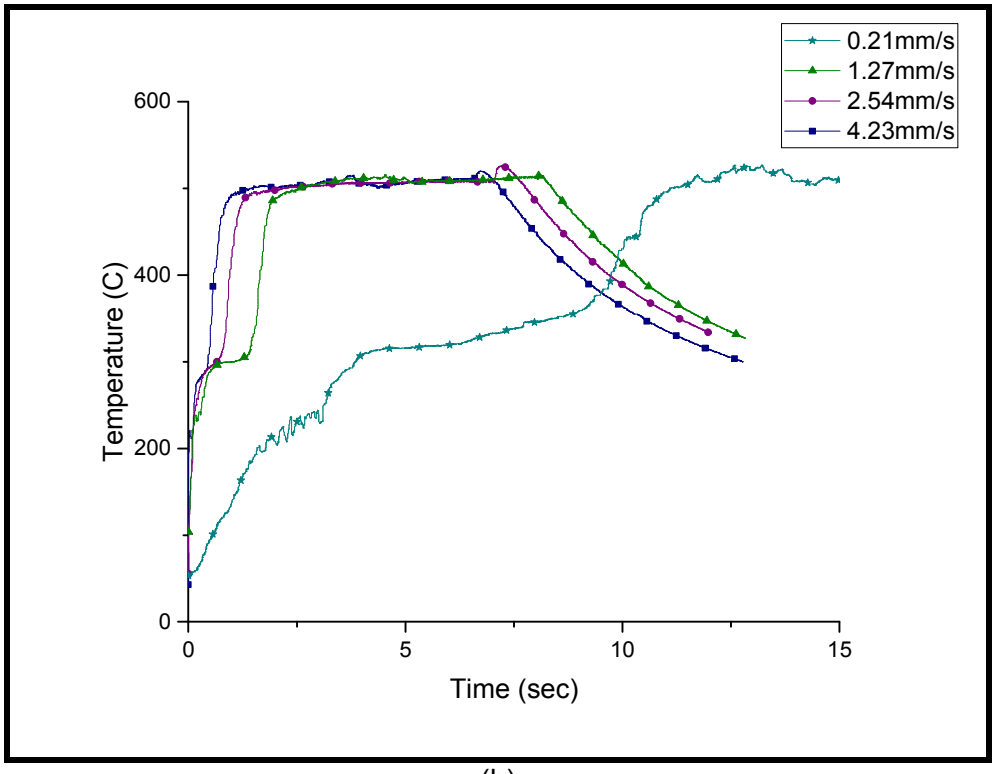

(b)

Figure 3-17. A comparison of temperature profiles for (a) the tool shoulder and (b) the tip temperatures at plunge rates of 0.21mm/s, 1.27mm/s, 2.54mm/s, and 4.23mm/s. Other welding parameters were a 2000rpm rotation speed, a 2.59mm plunge depth, and a 6s weld dwell time.

A comparison of the torque produced during different plunge rates is shown in Figure 3-18. From a FSSW perspective, the important feature to notice is the area under the curves to the first significant slope change (i.e. the point at which the shoulder makes contact with the workpiece). As discussed earlier, at a given point, the rotational plunge weld energy is directly proportional to the area under the curve of torque vs. time. The calculated rotational plunge weld energy is shown in Table 3-5. Clearly the slower plunge rates produce substantially more rotational plunge weld energy to heat and plasticize the material around the pin to help form the upward extruded Cu ring, as shown in Figure 3-19(a), needed for good quality welds. With the higher plunge rates, as shown in Figure 3-19(b), there is insufficient energy generated to form the Cu ring and hence, a low quality weld is formed.

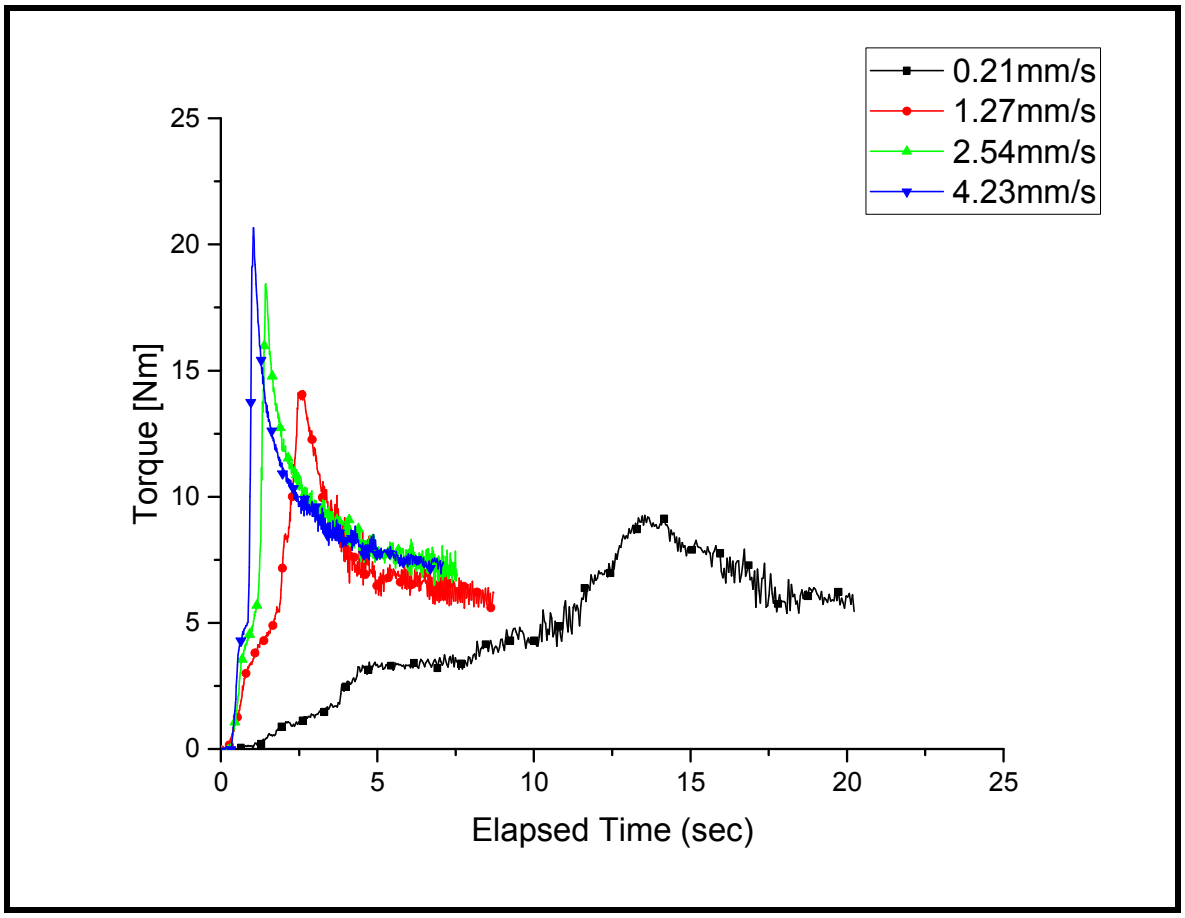

Figure 3-18. Torque vs. time graph for plunge rates. Other welding parameters were a 2000rpm rotation speed, a 2.59mm plunge depth, and a 6.0s weld dwell time.

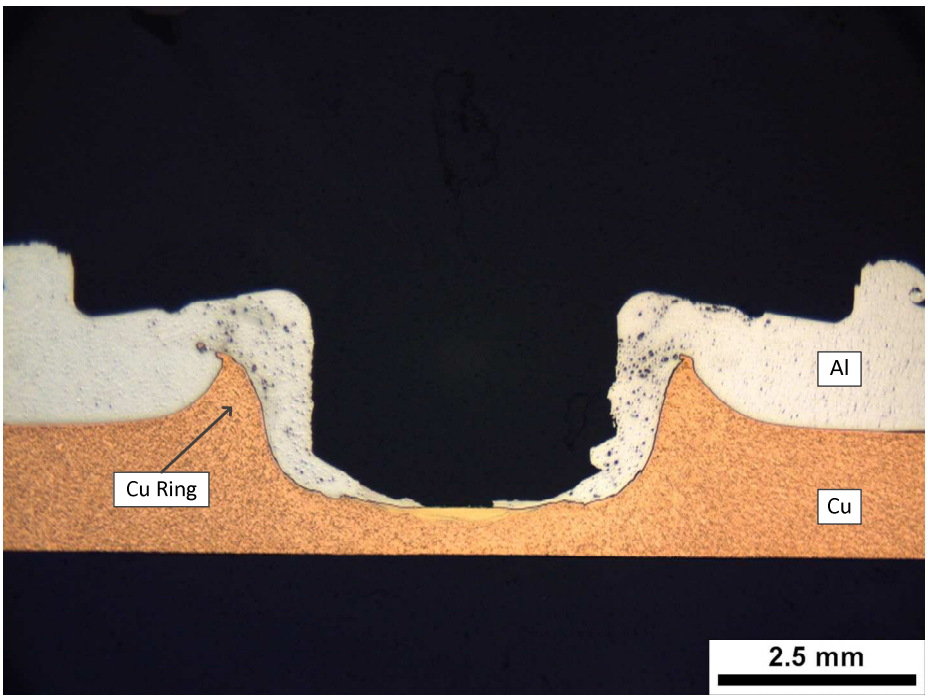

(a)

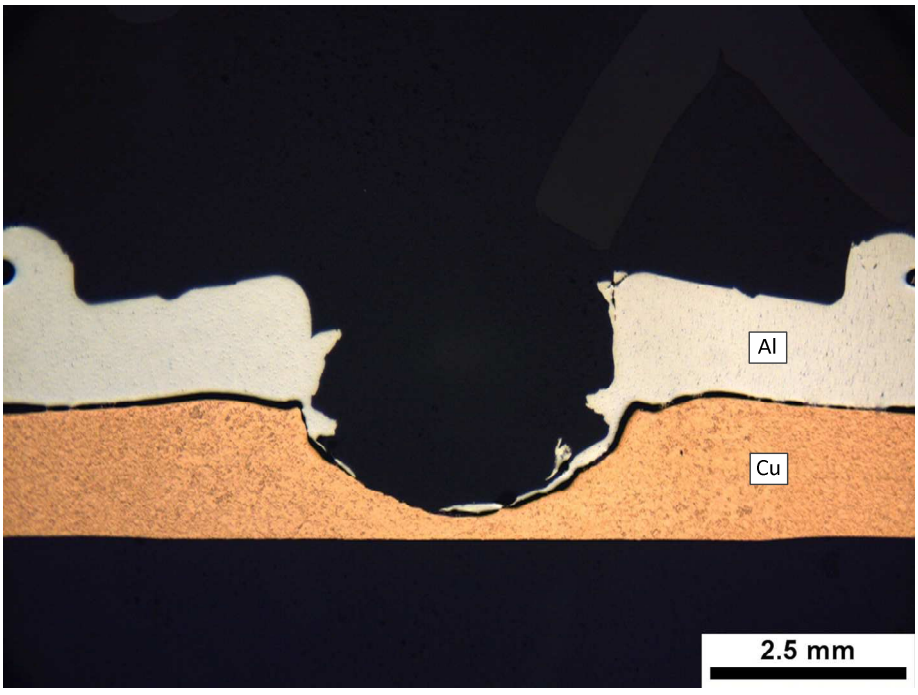

(b)

Figure 3-19. The weld macrostructure after tensile testing for welds made using (a) a plunge rate of 0.21mm/s which shows the presence of an the an Al-rich stir zone but no upward extruded Cu ring and (b) a plunge rate of 4.23mm/s which shows the presence both an Al(Cu) stir zone and upward extruded Cu ring. Other welding parameters were held constant at a 2000rpm rotation speed, a 2.59mm plunge depth, and a 6s weld dwell time.

Table 3-5. Rotational Plunge Weld Energy Calculations Comparing Plunge Rates

Speed (rpm)	Plunge Rate (mm/s)	Plunge Depth (mm)	Rotational Plunge Weld Energy (j)
2000	0.21	2.59	17,336
2000	1.27	2.59	4,858
2000	2.54	2.59	2,707
2000	4.23	2.59	2,134

Looking back to Table 3-4, the rotational plunge weld energy (12,501j) with a 1000rpm rotational speed and 0.21mm/s plunge rate is substantially higher than the rotational plunge weld energy (4,848j) produced using plunge rates of 1.27mm/s and higher. Since good quality welds were possible at 1.27mm/s plunge rates (as shown in Figure 3-9) , the hypothesis that rotational plunge weld energy is the key to forming quality Al-Cu FSSW can be tested by evaluating welds with a 1000rpm rotation speed, a plunge rate of 0.21mm/s and plunge depth of 2.59mm. If the hypothesis is true then, welds of reasonable strength should be produced with these weld conditions, and this was the case.

Fifteen consecutive welds were made using a rotation speed of 1000rpm, a plunge rate of 0.21mm/s, a plunge depth of 2.59mm, and a dwell time of 6.0s. The average weld strength from this trial was 2318N which is in-line with quality welds made at higher rotation speeds. The necessary Cu ring formed and the stir zone between the weld key hole and extruded copper ring were present (see Figure 3-20). This work also suggests there is a minimum energy required to form Al-Cu FSSW and that this energy can be controlled by adjusting the plunge rate.

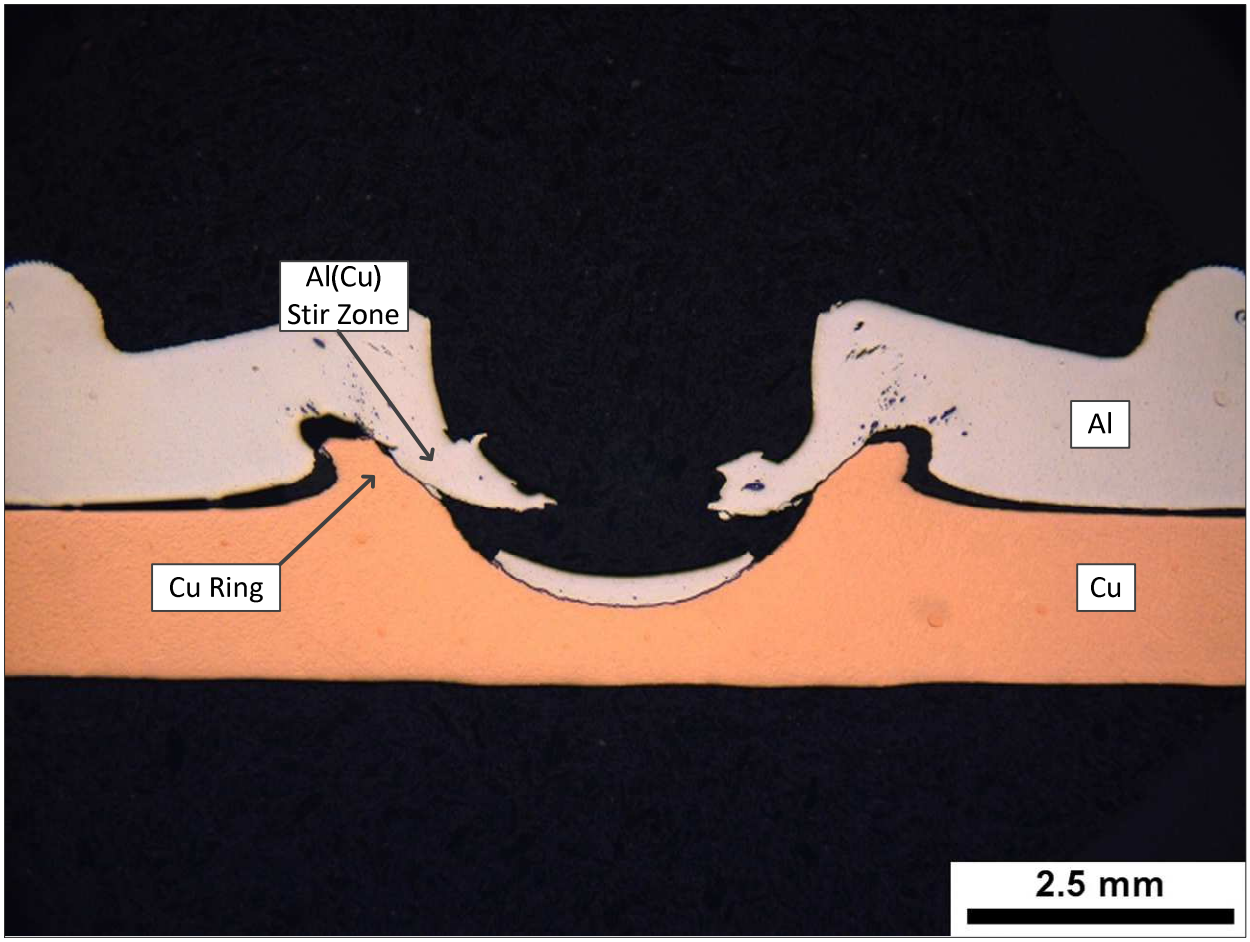

Figure 3-20. A weld macrostructure after tensile testing showing the formation of both an Al-rich stir zone and an upward extruded Cu ring needed for quality weld formation using a 1000rpm rotation speed, a 0.21mm/s plunge rate, a 2.59mm plunge depth, and a 6s weld dwell time. The weld strength of this sample was 2134N. Note that the weld features were elongated and comprised during tensile testing.

The plunge rate sensitivity found in Al-Cu FSSW was not apparent in 6061 Al to 6061 Al FSSWs even though the basic weld macrostructure of an Al-Al, as reported by Gerlich et al. [32], is similar to Al-Cu welds reported here. Su et al. [51] tested plunge rates from 0.1mm/s to 10mm/s and saw no substantial change in weld quality as measured via the width of the stir zone. Lathabai et al. [52] reported that plunge rate ranging from 1-7mm/s and using a smooth pin tool had no effect on the tensile shear strength of 6050-T5 Al to 6050-T5 Al FSSW. The most likely reason for the sensitivity of

plunge rate in Al-Cu FSSW and not in Al-Al welds is that it takes substantially more energy to extrude Cu than 6061 Al.

In conventional extrusion processing, 6061 Al is extruded at temperatures of 400°C to 450°C which is approximately half of the temperature typically used to extrude Cu, which is typically extruded in the 800-950^{o}C[75]. The Cu extrusion temperature is higher because it has a higher melting temperature, and a material must approach its melting point to be sufficiently soft for extruding. In the case of 6061 Al, melting begins at 581°C whereas Cu first melts at 1085°C. The higher extrusion temperature for Cu supports the observation that more energy would be needed to extrude the lower copper sheet to properly form the Cu ring important to weld quality. In addition, more energy is likely needed in Al-Cu because density of Cu is 3.3 times the density of 6061 Al (8.9g/cm^3 for Cu vs. 2.7g/cm^3 for 6061 Al). More energy is also required because the thermal conductivity of Cu, which is more than 2.3 times higher than 6061 Al. 6061 Al has thermal conductivity of 167 W/m-C (at 20°C) compared to Cu's 391W/m-C (at 20°C). In the formation of the Cu ring, the heat generated from rotational energy would ideally be concentrated in the region where the Cu ring forms, but Cu's high conductivity conducts the heat quickly away from this zone when compared to 6061 Al, thus requiring more energy to maintain temperatures sufficient to extrude the lower Cu sheet upward. The higher extrusion temperatures, combined with a higher density and thermal conductivity are the most likely explanations of the increase in energy required to form Al-Cu FSSW when compared to Al-Al FSSW.

3.3.5 Plunge Depth

The last variable to explore is plunge depth. Heideman et al. [66] showed that plunge depth should be set sufficiently deep to ensure the material properly flows into the bottom of the weld. The effect on temperature and torque can be seen in Figures 3-21 and 3-22.

The temperature shows no differences as a result of plunge depth. While an argument could be made from Figure 3-21 that the peak temperature of the shoulder increased slightly (11^{o}C) when the plunge depth was increased from 2.34mm to 2.59mm it would be difficult to prove given the temperature repeatability limitations already discussed.

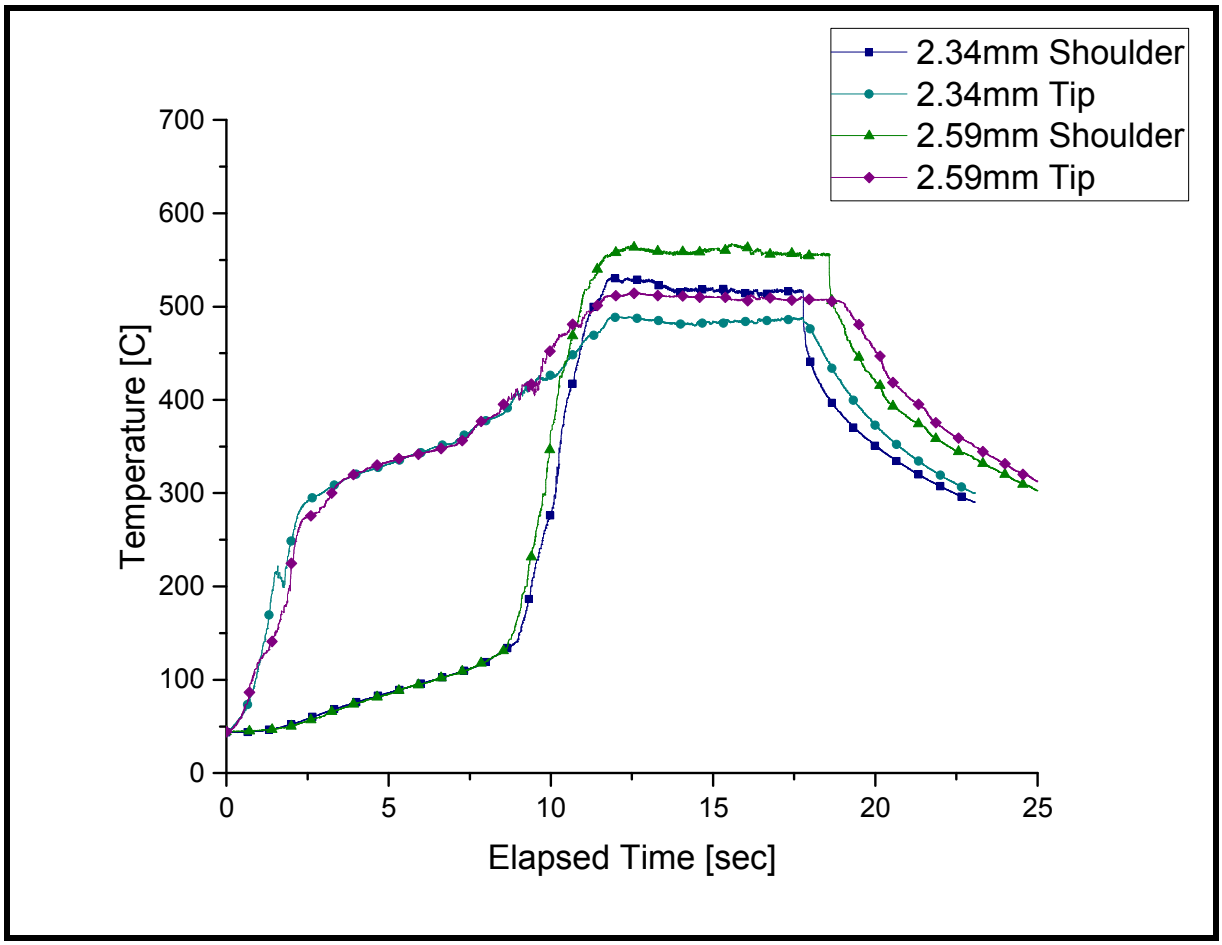

Figure 3-21. A comparison of temperature profiles for the tool shoulder and tip temperatures at two different plunge depths of 2.34mm and 2.59mm. Other welding parameters were a 2000rpm rotation speed, a 0.21mm/s plunge rate, and a 6s weld dwell time.

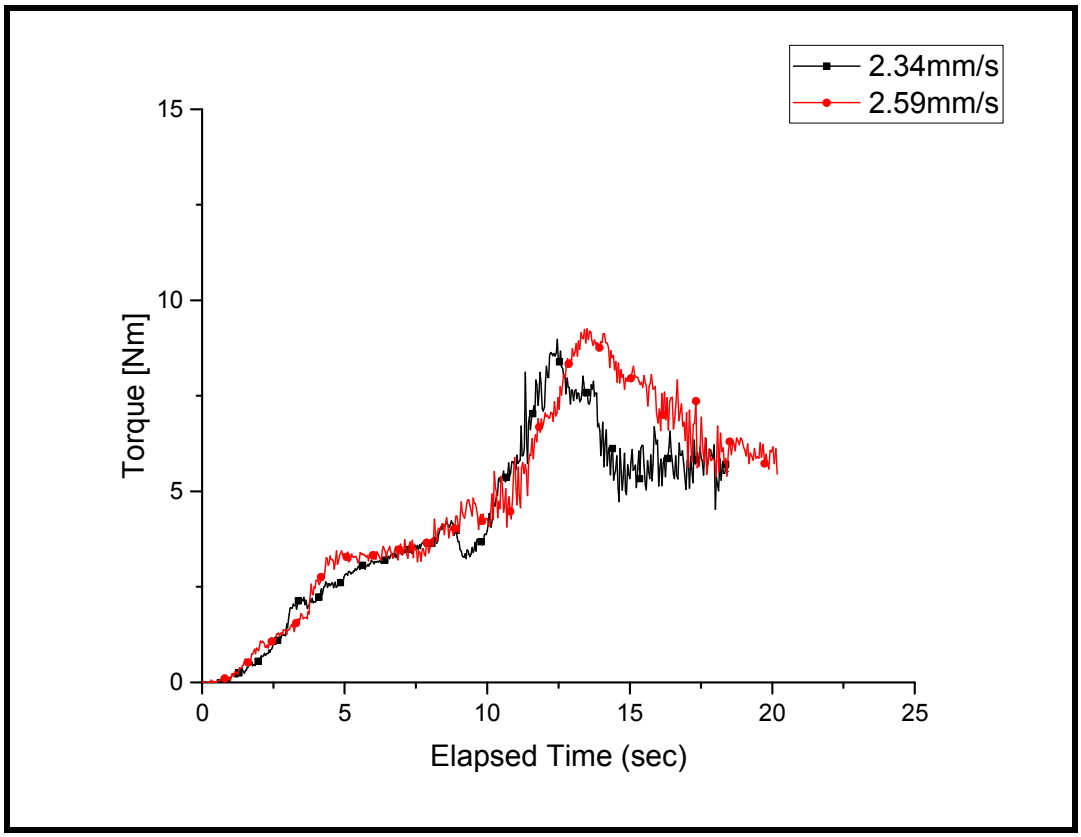

Figure 3-22. Torque vs. time graph for varying plunge depths and plunge rates. Other welding parameters were 2000rpm rotation speed and 6.0s weld dwell time.

Table 3-6. Rotational Plunge Weld Energy Comparing Plunge Depths and Plunge Rates

Speed (rpm)	Plunge Rate (mm/s)	Plunge Depth (mm)	Rotational Plunge Weld Energy (j)
2000	0.21	2.34	17,336
2000	0.21	2.59	13,207

The torque curves and energy calculations in Table 3-6 would give some credence to a slight peak in shoulder temperature increased with a deeper plunge depth. The rotational plunge weld energy increased by 31% (see Table 3-6) when the plunge depths were increased from 2.34mm to 2.59mm with a plunge rate of 0.21mm/s. However, this energy increase takes place near the end of the plunge when the shoulder is in contact with the workpiece. The torque curves in Figure 3-22 are nearly

identical for each plunge rate until the shoulder touches the workpiece. When the plunge is stopped, the torque slowly decreases during the dwell time. However, when the tool is plunged deeper to the 2.59mm plunge depth, the torque increases further, resulting in the increased energy shown in Table 3-6 and shows a similar decrease once the plunge process is stopped. The increased energy resulting from the added plunge depth could result in an increase in peak shoulder temperature. However, the 30+% energy increase only translates to a very small increase in shoulder temperature and no significant increase in pin temperature. The energy increase would be expected because the shoulder, which is 2.5 times greater in diameter than the pin, would require more energy to plunge it, than the smaller diameter pin. From Table 3-6, the slower plunge rate (0.21mm/s) with the 2.34mm plunge depth (i.e. the shoulder just touching the surface of the upper Al sheet) would appear to have more than sufficient rotational plunge weld energy (13,207j) to produce a quality weld. Recall, quality welds were produced with a plunge rate of 1.27mm/s which yielded a weld plunge energy of a 4,858j (see Table 3-5). However, Heideman et al. [66] showed proper material flow is necessary for a quality weld. Increasing the plunge depth beyond 2.34mm (pushing the shoulder of the tool beyond the upper 6061 Al sheet surface) permitted the formation of a contiguous stir zone under the FSSW tool. This contiguous layer would intuitively yield a more consistent process. Therefore, the FSSW process is complicated, requiring a minimum energy level (controlled primarily by plunge rate and rotational speed) to produce proper material flow. But, energy alone will not determine proper material flow. Material flow is also controlled by tool design and plunge depth plus any other factors that occur during the process that could enhance or impede material flow.

3.4 Conclusions

1. Weld energy generated during the plunge portion of the weld is a key variable in determining weld quality in dissimilar 6061 Al and Cu FSSW. The higher the rotational plunge weld energy the more likely a strong weld will consistently be produced.
2. Plunge energy, which can be determined by measuring welding torque, is best controlled by the plunge rate with slower plunge rates producing more plunge energy. This was demonstrated by producing quality welds using a 0.21mm/s plunge rate and a 1000rpm rotation speed and poor quality welds at 2.54mm/s plunge rate at the same rotation speed.
3. Peak temperatures of the pin and shoulder can be increased by increasing rotation speed from 1000rpm to 2000rpm. However, peak temperature is of minimal value in assessing quality welds. Quality welds were made at both 1000rpm and 2000rpm rotation speeds with peak temperatures that were approximately 50°C higher for the faster rotation speed. Additionally, the peak temperatures were nearly the same for all measured plunge rates even though increasing plunge rate beyond 2.59mm/s yields poor quality welds.
4. Increasing rotation speed from 2000rpm to 3000rpm had a negligible effect on peak pin temperature, but did show a temperature increase for the tool shoulder. The tool shoulder temperature was more than 600°C which was above the 582°C eutectic temperature for 6061 Al, suggesting melting likely took place near the tool shoulder using a 3000rpm rotation speed.

5. The increased shoulder temperature for the 3000rpm weld produced less energy than the 2000rpm weld. The likely sources for less rotational plunge weld energy production at the faster 3000rpm rotation speed was the reduced viscosity possibly to the point of melting near the tool shoulder, which in turn required less power to maintain the 3000rpm rotation speed.
6. The plunge rate set point on CNC must be carefully evaluated because actual plunge rate was found to be 6%-15% slower than the setpoint on the CNC machine. This source of error is related to the inability of the CNC's control to respond and react fast enough to account for the changes in load associated with the plunging process.

Chapter 4: Improving Consistency in Dissimilar 6061 Al to Cu Friction Stir Spot Welds

4.1 Introduction

In the first three chapters, influences of weld parameters on weld strength were explored, material flow during FSSW was identified, and influence of weld parameters on weld temperatures, torque, and energy were assessed. From the material flow analysis in Chapter 2, the macrostructure needed to form welds of reasonable strength was found to form during the plunge, and this structure was not affected by changing the weld dwell time. Increasing the dwell time only seems to increase the dissolution of Cu into the Al stir zone region. This result correlated with results found in Chapter 1 indicating that weld strength was not affected by dwell time. Additionally, rotation speed and plunge rate were identified as key variables in the formation of high quality welds. Increasing rotation speed and reducing plunge rate resulted in an increase in the energy generated during the plunging process, with reducing the plunge rate having the most dramatic effect on increasing weld energy and weld strength. Lastly, peak weld temperatures, as measured on the tool tip and weld shoulder, were not a good indication of weld quality and appeared to be mostly influenced by weld rotation speeds. However, peak weld temperatures did not increase significantly with rotation speeds over 2000rpm.

While the influence of weld parameters on weld quality is now understood reasonably well, weld strength consistency, and hence weld quality, remains a significant concern. Throughout this work, weld consistency was observed to vary. The

primary cause of weld inconsistency, provided the other welding parameters were favorable, was determined to be caused by an inability to form an Al(Cu) solid solution stir zone during the plunge process. The lack of an Al(Cu) solid solution stir zone resulted from the threads on the tool pin not functioning as intended, making the threaded tool behave like a smooth pin tool. The root cause of the thread malfunction was clogging with layer structures as shown in Figure 4-1. In Figure 4-1, the tool pin thread was filled with a layered Cu/Al-Cu intermetallic structure, as opposed to an Al(Cu) solid solution with small Al-Cu particles in the threads, as is the case in Figure 4-2. A Cu ring structure was formed in both Figures 4-1 and 4-2, but in Figure 4-1, the Al(Cu) solid solution stir zone is not present. An argument could be made that the reason for the thread clogging in Figure 4-1 and the lack of clogging in Figure 4-2 are a result of the different welding parameters used for the two welds. The thread clogging shown in Figure 4-1 was created with a rotation speed of 3000rpm and a 6s dwell time whereas the good weld, shown in Figure 4-2, was produced with a 2000rpm rotation speed and 15s dwell time. However, good quality welds were formed with a 3000rpm rotation speed and 6s dwell time as reported in Chapter 1. Furthermore, good quality welds were also produced, as reported in Chapter 1, with 2000rpm rotation speed and a 6s dwell time. Obtaining the thread clogging macrostructure as shown in Figure 4-1 was fortunate since low quality welds appeared randomly throughout this research; therefore, knowingly creating this condition has proved problematic.

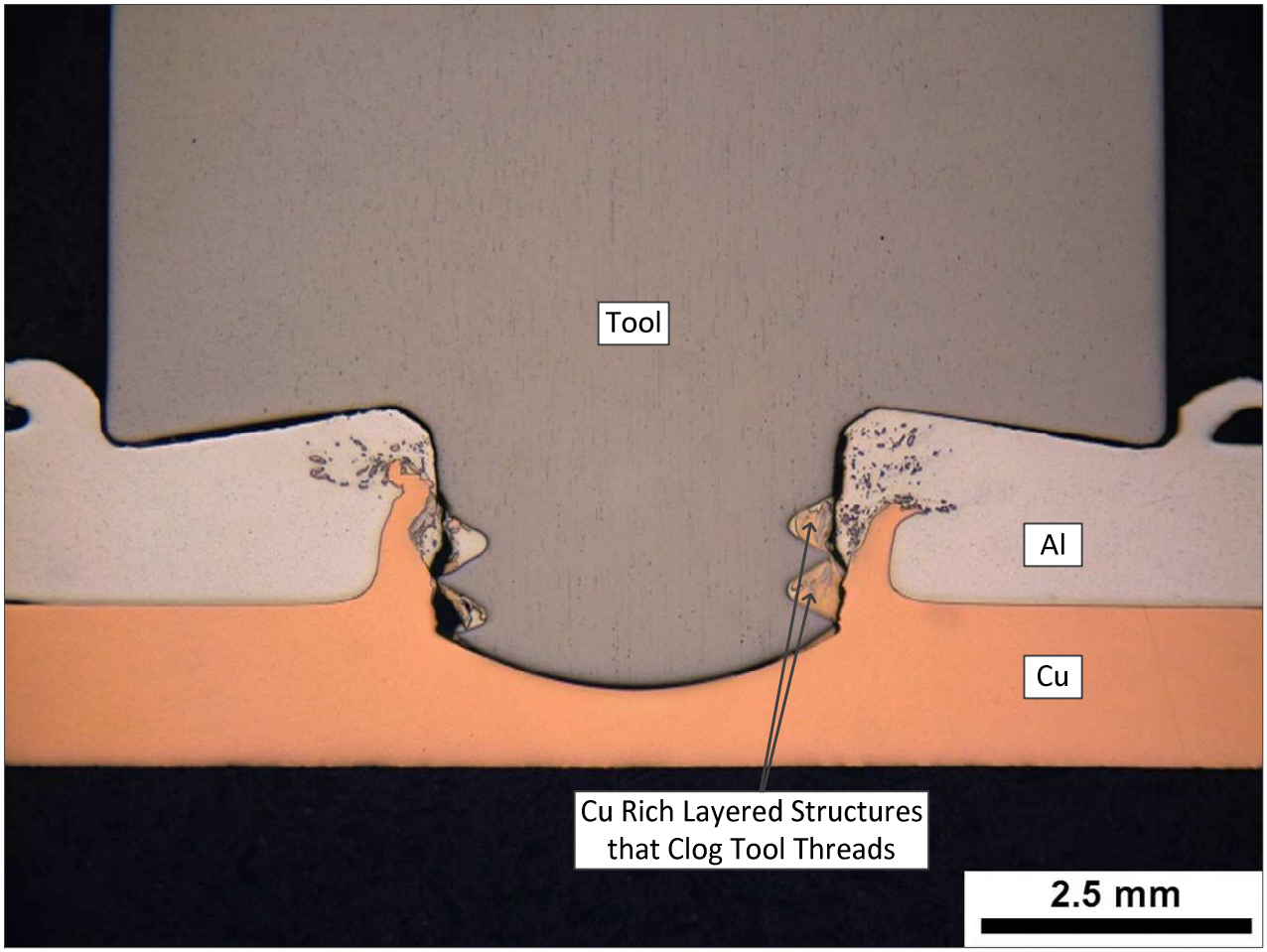

Figure 4-1. A FSSW with the tool remaining in the weld after the dwell time was reached. Welding conditions: 3000rpm, 2.34mm plunge depth, 2.54mm/s plunge rate, 6.0s dwell time. While this weld macrostructure is indicative of a poor quality weld, the same weld parameters have yielded welds of reasonable strength and a macrostructure, less the FSSW tool, similar to Figure 4-2.

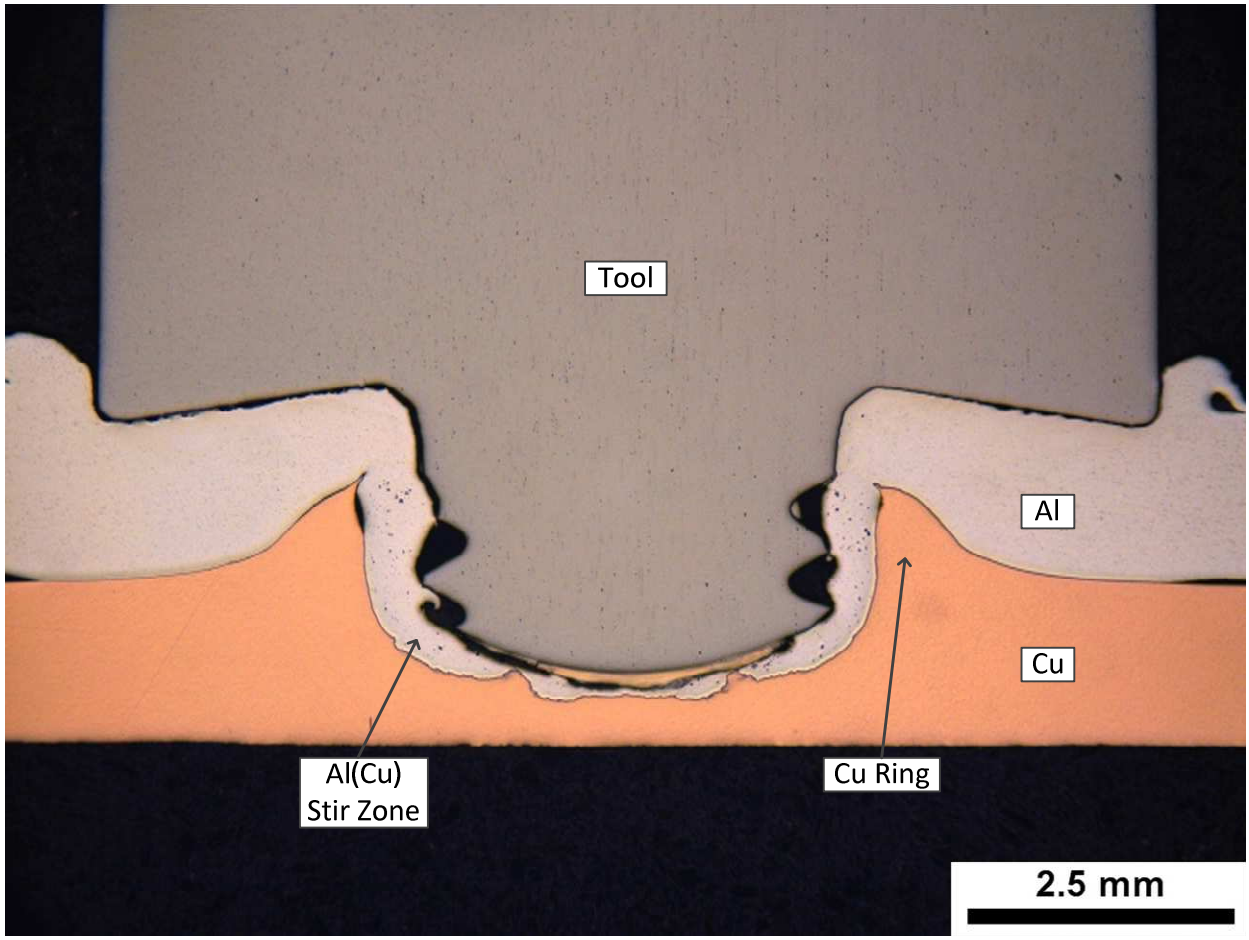

Figure 4-2. A FSSW with the tool remaining in the weld after the dwell time was reached. Welding conditions: 2000rpm, 2.34mm plunge depth. 2.54mm/s plunge rate, 15.0s dwell time.

The source of the particles that could cause tool thread clogging was identified in Chapter 2 during the analysis of material flow. Chapter 2 showed that after the first FSSW is made, a layered structure of material adheres to the tool tip. Figure 4-3 shows how this adhered material changes between two welds. In the case of Figure 4-3, the changes shown are taking place between Weld #5 and Weld #6, but the expectation is that the same changes take place between each weld, after Weld #1 is made (i.e. as soon as material is adhered to the tool tip). This work demonstrates that expectation to be true. Figure 4-3(b) shows how layered material adhered to the tool tip fractures into

numerous large and small particles. The reasonable conclusion is that once this material fractures, the particles are expelled into the stir zone. If these large particles are of sufficient size, they could easily lead to thread plugging.

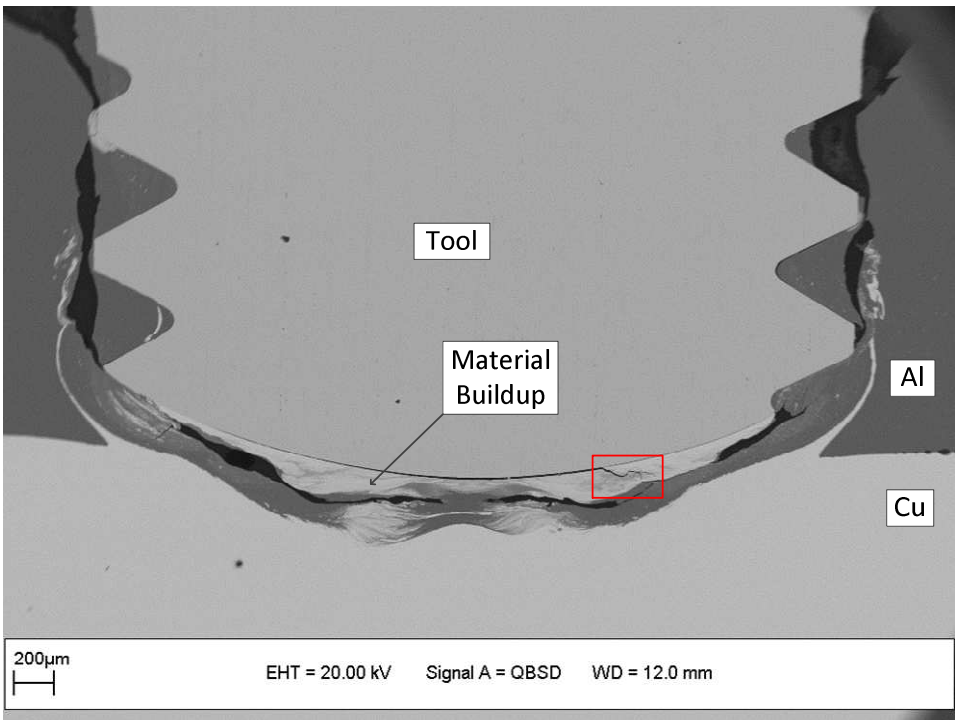

(a)

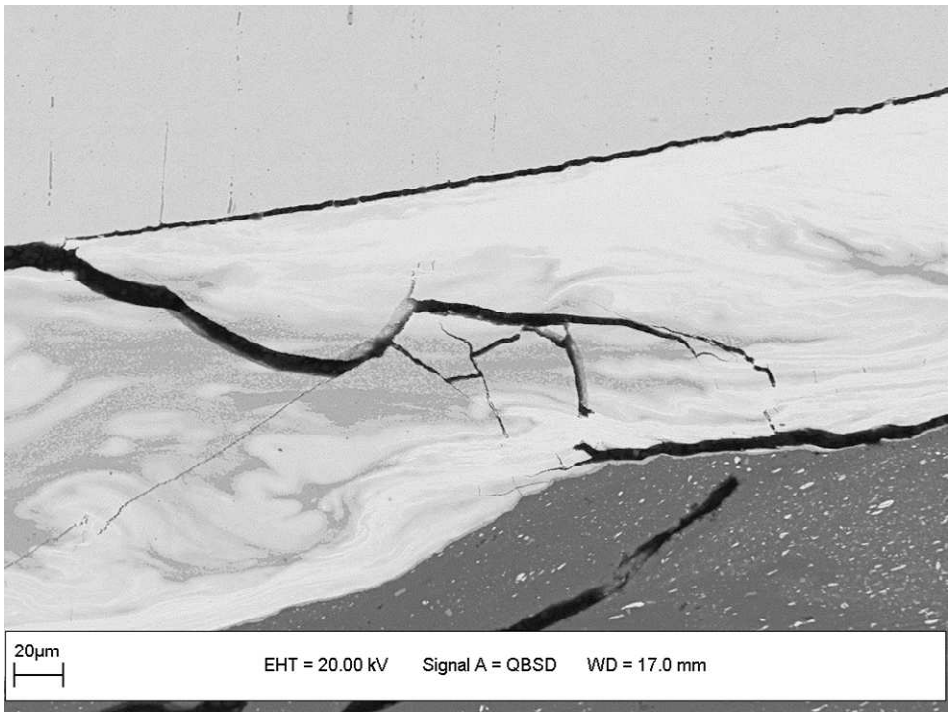

(b)

Figure 4-3. Backscattered electron SEM images of (a) a cross section from the sample made with a 1.82mm plunge depth using a tool that had been used to make five welds previously, and (b) a higher magnification of the red- boxed region in (a). The welding conditions were 2000rpm, 0.21mm/s plunge rate, 1.82mm plunge depth, and a 0.0s dwell time (tool was stopped as soon as it reached the 1.82 plunge depth).

With the likely source of particles identified, the next two steps to improve weld strength consistency are to ensure that the findings in Chapter 2 are valid, and to understand the layered structure that was adhered to the tool tip in metallurgical detail. Using this information, the final step to improving consistency will be explored. This final step involves preventing the layered structure from adhering to the tool (i.e. remove the source for generating large particles) or keeping the layered structures from becoming adhered to the tool thread during the FSSW process.

From personal experiences in metal forming and die casting where material buildup on tools is relatively common, three common techniques for preventing material buildup and adhesion of materials to tools are possible options in FSSW. One option is to redesign the tool or part being made to permit easier flow of material over the tool. A second option is to use materials that improve flow and/or reduce the coefficient of friction between the tool material and the material being moved over the tool (in this case 6061 Al and Cu); these materials can include lubricants or tool coatings. A third option is to use an alternative tool material that improves material flow and/or has a lower coefficient of friction than steel.

Redesigning the tool, as noted in the first option, will not be pursued because this is not particularly practical at this time. The friction stir welding process limits the basic tool design to a cylindrical shape; consequently, dramatic changes that could limit material adhesion could also have other unintended consequences which would require extensive study. Therefore, redesigning the tool was not pursued as part of this research.

Lubricant materials, as suggested in the second option, used to reduce the coefficient of friction in metal forming are not desirable in welding because these typically cause welding defects. However, the use of coatings on the FSSW tool could be a viable option to prevent Cu/Al-Cu intermetallic adhesion, provided the coating is not quickly abraded away. To prevent adhesion of Al and Cu to steel tools in die casting applications, a physical vapor deposited TiCN coating or CrN is typically used [50]. These two materials are suggested as possible options in Al and Cu applications, but unfortunately, the exact coefficient of frictions between 6061 Al, Cu, and Al-Cu intermetallics are unknown. For this work, it will be assumed that both coatings reduce the coefficient of friction as compared to uncoated steel, but the exact amount of this coefficient of friction reduction is unknown. CrN and TiCN coatings are commercially available and were explored as a method to prevent the layered structure from adhering to the tool.

Another method of reducing the coefficient is the use of an alternative material. Instead of the common H13-type tool steel which was used up to this point and works well for Al alloys, a material more suited for FSSW of Cu and its alloys was evaluated. In extrusion and die casting of Cu, tungsten and molybdenum based materials are commonly used [53]. It is difficult to machine a tool from these materials for testing purposes because the materials are very hard. To overcome this issue, these materials are typically pressed, sintered, and ground which for research purposes would be cost prohibitive. To address the cost issue, a machineable tungsten based material with a trade name Densimet 17.7 (93% W with the balance being Ni, Fe, and Mo) was identified. Densimet materials have reportedly been used to make linear Cu FSW

supporting this as an alternative material option [54, 55, 56, 57, 58, 59, and 60]. Additionally, this alloy is intended for use as a replacement for H13 tool steel to minimize aluminum adherence to tools in dieasting applications [69]. The combination of the successful use in FSW of Cu and the alloy having been purposely designed to minimize material adherence makes it a good choice to resolve the material adherence issue observed.

4.2 Experimental Design

The FSSW samples in the experiments presented here consisted of 25mm wide, 50mm long, and 1.5mm thick 6061 Al-T6 (referred to as 6061 Al in this document) with an average hardness of 58HRB and 25mm wide, 50mm long, and 1.5mm thick oxygen-free copper (referred to as Cu in this document) in the H01 condition (i.e. quarter hard) with an average hardness of 73HRF. A lap weld joint with the 6061 Al sheet on top and the Cu sheet at the bottom with a 25mm overlap was used for all welding trials. The compositions, determined by inductively coupled plasma, of the 6061 Al and Cu are shown in Tables 4-1 and 4-2.

Table 4-1. Composition of 6061 Al as determined by ICP and compared to 6061 Al Specification.

	Si	Fe	Cu	Mn	Mg	Cr	Zn	Ti	Al
Sample Comp.	0.69	0.60	0.28	0.006	1.03	0.15	<0.001	0.014	Rem.
Specifi-cation	0.4 - 0.8	0.7 Max	0.15 - 0.40	0.15 Max	0.8 - 1.2	0.04 - .35	0.25 Max	0.15 Max	Rem.

Table 4-2. Composition of oxygen-free copper (weight percent) as determined by ICP and compared to oxygen-free copper specification. Other elements combine to 0.017 weight percent with individual elements all less than or equal to 0.001 weight percent.

	Cu	Ag	As	Sb	S	P	Fe	Ni	Mn	Sn	Other*
Sample Comp.	99.95	0.001	0.002	0.006	0.002	0.001	0.005	0.002	0.001	0.013	0.017
Specification	99.95	----	----	----	----	----	----	----	----	----	

FSSWs were made using a 1991 Hurco BMC 40 CNC milling machine (15 horsepower with a maximum spindle speed of 4000rpm) shown Figure 4-4. The tool design for all welds was a standard threaded pin design using a pre-hardened H13 tool steel (42-46HRC) with a trade name of Viscount 44. The shoulder diameter, pin diameter, thread pitch, and pin length were held constant at 10.00mm, 4.00mm, 0.70mm and 2.34mm, respectively. The shoulder geometry was concave-shaped and the pin tip shape was convex in shape with a 3.96mm radius.

Figure 4-4. 15hp Hurco BMC 40 CNC machining center used for this experiment

As already reported in Chapter 3, the strongest welds were made using a rotation speed of 2000rpm, 0.21mm/s plunge rate, 6.0s dwell time, and 2.59mm plunge depth, and these parameters were held constant for all experiments in this chapter. The dwell time is defined as the time the tool was held at the desired plunge depth. The plunge depth is defined as the total distance that the welding tool tip is plunged into the sample. A 2.59mm plunge depth implies the shoulder of the tool is 0.25mm into the original top surface plane of the 6061 Al sheet since the pin length was 2.34. After welding, each sample was lap shear tensile tested, with a 1.5mm thick spacer added to each end of the sample to minimize bending (see Figure 4-5) using an Instron tension test instrument with a cross-head speed of 2.11mm/s. The maximum load measured at failure for each sample was recorded; this maximum load will be referred to as the weld strength.

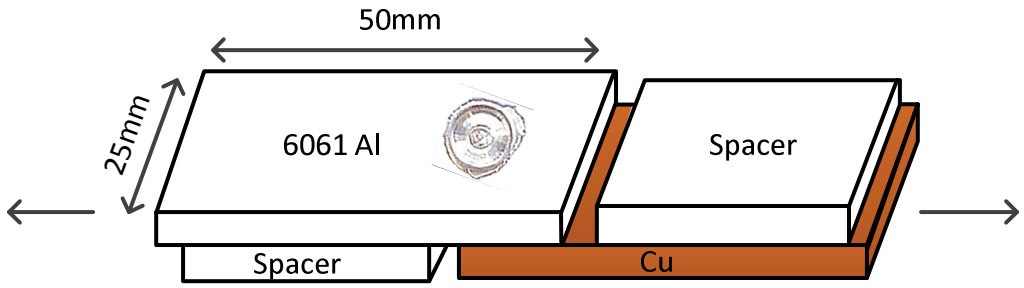

Figure 4-5. Shear sample used to measure FSSW joint strength (note that spacers were added to the sample during testing to minimize sample bending).

To substantiate the earlier findings that weld strength inconsistencies arise from the buildup of a layered Al-Cu intermetallic structure that then sheds during subsequent FSSWs, three experiments were conducted. First, a twenty consecutive weld trial was conducted. The weld strength, as already discussed, was measured for each weld and the tool (one tool was used for this trial) was inspected between each weld. The tool inspection procedure consisted of taking a photomicrography image of the tool tip using a stereomicroscope with the welding tool lying flat on the stereomicroscope's stage. The image was saved as a JPG file and imported into AutoCAD 2008. The visible tool tip was then traced in AutoCAD using a polyline line function. By overlaying the tool tip image of the new, unused tool tip with the tool tip after each weld, the area between the two tool tip lines can be automatically calculated using AutoCAD. Subsequently, this area can be used as an indication of the amount of buildup material adhered to the tool (see Figure 4-6). Since this calculation was done on a magnified image, the area calculated in AutoCAD was divided by 2.475 to account for the magnification of the image. The buildup on the tool is three-dimensional so the actual amount of material is a unit volume, but this would be a very difficult measure. Furthermore, as can be seen in Figure 4-3(a) and in samples where the tool remained in the sample after welding, as shown in Chapter 2, the buildup on the tool is not symmetric on any axis. The

asymmetric nature of the buildup implies that there would be accounted for error the buildup measurement, and therefore, the area measurement described above should be used for qualitative comparison purposes only and not as a definitive value of material buildup. If the area between the two lines is relatively large, there is a substantial of amount material adhering to the tool tip. Conversely, if the area between two lines is relatively small, then the amount of tool tip buildup is small. The measured area is only on the tool tip and does not account for any material in the tool threads. Only the tip material (shown in blue in Figure 4-6) was measured because the hypothesis is that the material that leads to thread clogging is from Cu/Cu-Al intermetallics adhered to the tool tip. Also, as shown in Figure 4-2, in good welds the material in the tool threads were primarily an Al(Cu) solid solution containing small Al-Cu intermetallics particles. The sizes of the intermetallic particles were not large enough to cause any thread clogging that would lead to a poor quality weld.

To gain a better metallurgical understanding of the layered structure, the tool was left in the last sample welded and the dwell time on this last weld was set to 0.0s (the same as the dwell time used for samples in Chapter 2). The produced sample was similar to those produced to understand material flow in Chapter 2, except in this case the tool made twenty welds prior to making the sample for analysis. The sample with the tool remaining was cross-sectioned and metallographically prepared. Metallographic preparation used standard techniques with a final polishing step consisting of 0.04 μm SiC suspension in 100ml water, 100ml ethanol, and 10g iron III nitrate added suspension solution to help remove copper scratches. The sample was then analyzed using a SEM with EDS capabilities.

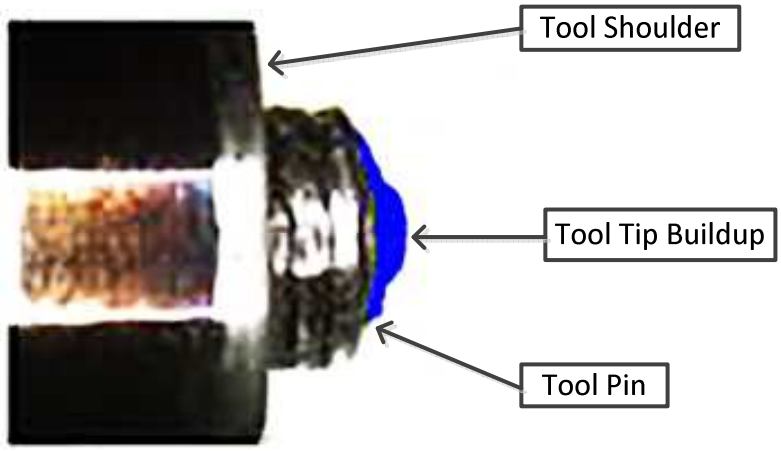

Figure 4-6. Shaded blue area of tool tip shows how the amount of material (as a cross-sectional area) was calculated using AutoCAD.

The second experiment consisted of another twenty consecutive weld trial. This trial was identical to the first trial except for one step. After each weld and before another weld was made, the tool was etched with a NaOH for 600s in an ultrasonic cleaner and then inspected in the same manner as the first. In addition the strength of each weld produced was measured and recorded.

The third experiment consisted of another twenty consecutive weld trial. This trial was identical to the first baseline trial except for one step. After each weld, the tool tip was machined back to its original surface on a lathe such that the tip was mostly free from any material build up. Machining the tool tip back to its original surface was done using CNC lathe. The original tool tip surface was programmed into the CNC computer and between each weld; the FSSW tool was put into the lathe and then machined back to this original and known surface. Once again, the strength of each weld was measured and recorded.

Following these three experiments, an additional three experiments were conducted to evaluate methods to prevent the buildup of material on the tool tip. Each experiment consisted of a twenty weld trial similar to those described above with the tools inspected after each weld and the strength for each weld was measured and recorded. The difference between these three experiments was in the tool material used. In one experiment, the tool material was a tungsten-based tool material with a trade name of Densimet 17.7 (93% W and the balance being Ni, Fe, and Mo) with a hardness of 30 HRC. Another experiment used a tool that was made of pre-hardened H13 tool steel tool steel (42-46HRC) with a trade name of Viscount 44 and with physical vapor deposited CrN coating that was approximately 4um thick. The third and final experiment used a tool that was made of pre-hardened H13 tool steel (42-46HRC) with a trade name of Viscount 44 and with physical vapor deposited TiCN coating that was approximately 1-3um thick. The welding parameters and tool design were held constant and the same as those described earlier.

4.3 Results and Discussion

4.3.1 Baseline Twenty Weld Trial

The visual comparison of the tool appearance after the baseline (standard tool) twenty consecutive weld trial is shown in Figure 4-7. With a new unused tool, the threads and tool tip are easily visible via the inspection technique, and the new tool produced a weld with a strength of 2662N, which is a strength that would be considered excellent weld quality. The tool's appearance after the first weld is shown to the right of

the “After 1 Weld” label. The tool threads are no longer obvious and the tool tip shape is noticeably different as compared to the unused new tool. This tool then produced Weld #2 with strength of 1920N. This strength is an indication of a good quality weld. Producing a weld of this strength with the given tool appearance suggests that the material that fills tool threads moves normally through the tool threads during the FSSW process. If this were not the case, the tool would behave like a threadless pin and produce a low quality weld (less than 1000N). Additionally, the mere presence of build-up on tool tip does not necessarily yield a poor quality weld. Apparent in Figure 4-7 is that the strongest weld was the first weld made using a new tool; suggesting that a tool with clean threads and a clean tip produced welds of higher strength than the same tool with material adhered to the tip and threads. The second strongest weld, with a strength of 2268N (Weld #12 in Figure 4-7), was produced immediately after a weld that had a strength of 989N (Weld #11 in Figure 4-7), which would be considered poor strength. This suggests, along with the third strongest weld being Weld #19, that when a low strength weld is produced, that all subsequent welds will not necessarily be of low strength. The material that clogged the threads was apparently expelled from the threads during the dwell cycle of the current (poor strength weld) or during the early stages of the subsequent (acceptable strength weld) plunge. Most likely, the expulsion takes place during the subsequent plunge because Figure 4-1 shows clogged tool threads at the end weld dwell period.

The area of the weld tip buildup is plotted on the same graph as weld strength in Figure 4-8. The purpose of Figure 4-8 was to determine if a correlation existed between the amount of the material shed or gained and the weld strength. For example, using

Figure 4-8, was it possible to determine if a low-strength weld was produced when a large amount of material was shed from the tool tip during the making of this low-strength weld? The rationale behind this question was that if a large amount of material was shed during the welding process, there would be a high likelihood that a large particle that could clog tool threads should be present in the stir zone. To understand Figure 4-8, the tool tip buildup on the tool from a previous weld should be compared to the tool tip buildup measured after the current weld was made. For example, the tool starts out with 0.00mm^2 of tool buildup (i.e. new tool) and this tool produced a weld with a strength of 2262N. After this weld, the tool-tip buildup was 2.11mm^2. This tool produced a weld with a strength of 1920N and afterwards had a material buildup of 1.12mm^2. Hence, the tool shed approximately 46.9% of the material adhered to the tool tip during the formation of the second weld. In this case, the material that shed during the plunge was then likely stirred into the stir zone of the second weld.

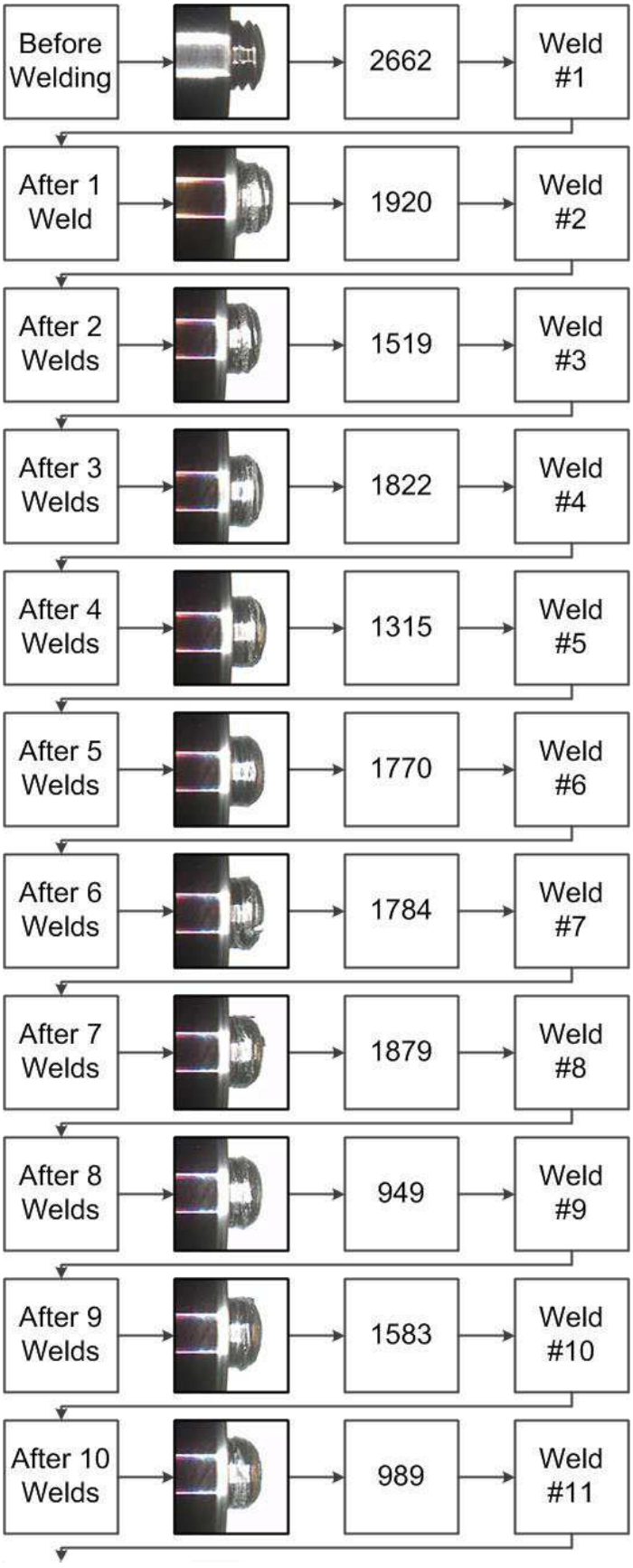
Before Welding
2662
Weld #1
After 1 Weld
1920
Weld #2
After 2 Welds
1519
Weld #3
After 3 Welds
1822
Weld #4
After 4 Welds
1315
Weld #5
After 5 Welds
1770
Weld #6
After 6 Welds
1784
Weld #7
After 7 Welds
1879
Weld #8
After 8 Welds
949
Weld #9
After 9 Welds
1583
Weld #10
After 10 Welds
989
Weld #11

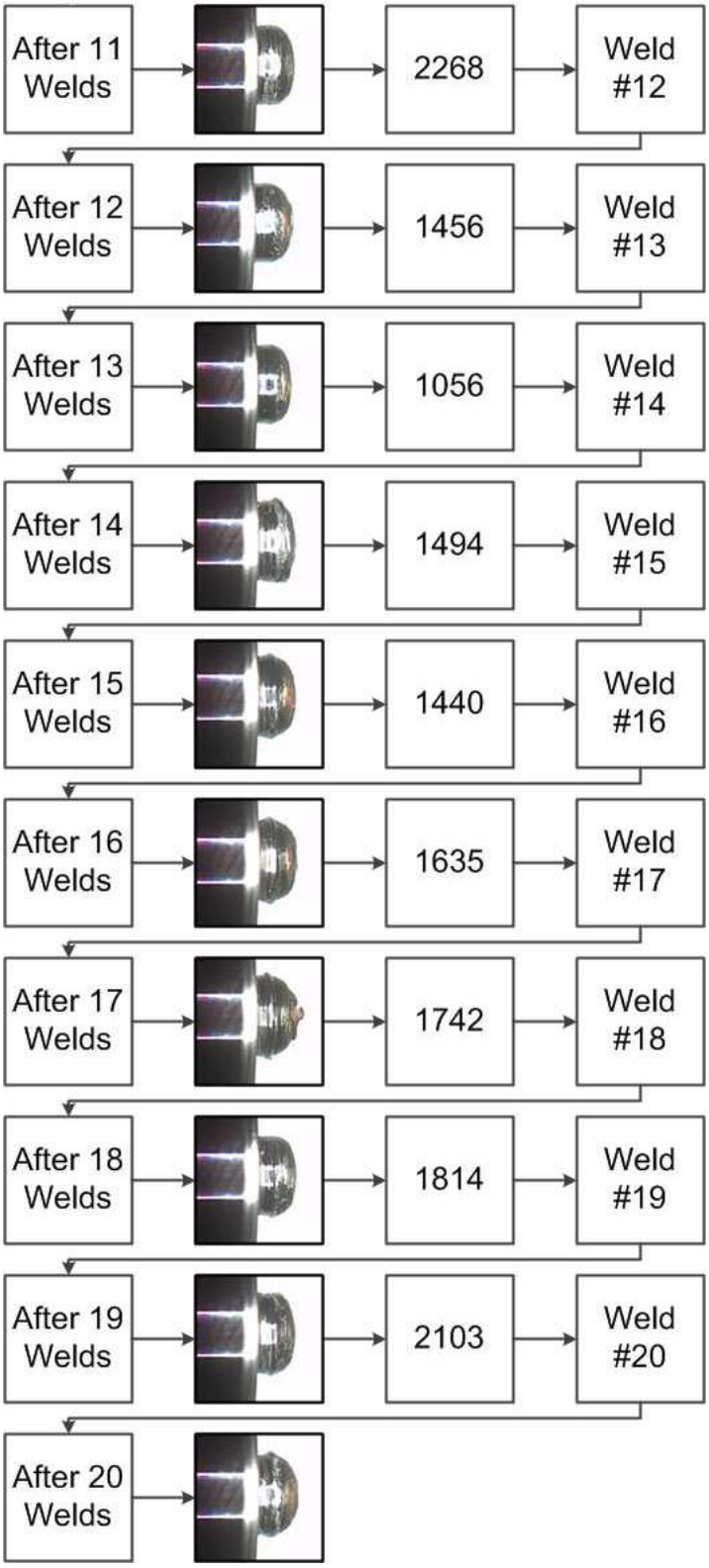

Figure 4-7. Photographs of the FSSW tool and weld strength (in N) produced by the tool for a baseline twenty weld trial using a Viscount 44 (pre-hardened H13) tool steel. The welding parameters used were 2000rpm rotation speed, 2.59mm plunge depth, 0.21mm/s plunge rate, and 6.0s dwell time.

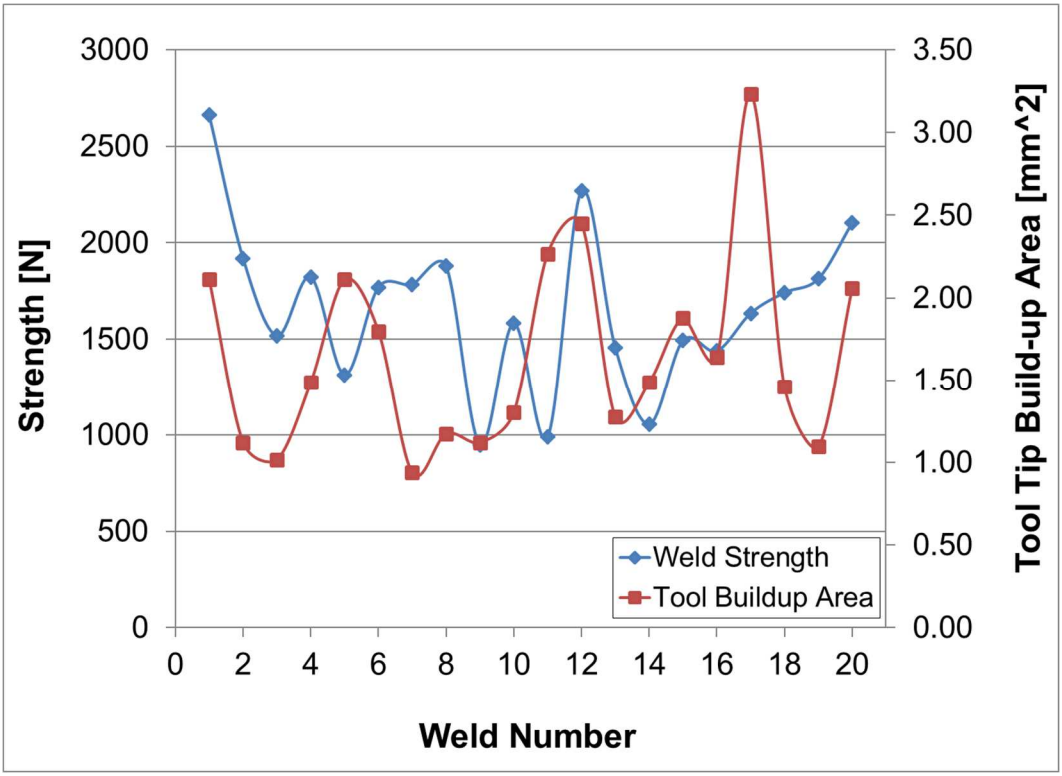

Figure 4-8. Weld Strength and tool build up data are graphically shown for a baseline twenty-weld trial using a Viscount 44 (pre-hardened H13) tool steel. The data presented is from the same trial shown in Figure 4-7. The welding parameters used were 2000rpm rotation speed, 2.59mm plunge depth, 0.21mm/s plunge rate, and 6.0s dwell time.

From Figure 4-8, it is clear that the amount of material shed from the tool tip does not correlate to weld strength. For example, the weld strength dropped from 1920N to 1519N for Welds #2 and #3, yet the amount of material on the tool tip changed very little when Weld #3 was made. If a correlation existed, a substantial drop in material buildup would have been expected. However, this was not the case. Furthermore, the strength dropped from 1583N to 989N for Welds #10 and #11 yet the amount of material on the tool tip increased substantially suggesting that no material was shed during the formation of Weld #11. The increase is opposite what would have been expected if a correlation existed. To make this point final, the weld strength increased from 1742N to

1814N for Welds #17 and #18, yet the amount of material on the tip went down, suggesting material was shed while making Weld #18. For a correlation to exist, the amount of material would have been expected to remain similar or increase slightly (no shedding) during the formation of Weld #18. The lack of a correlation between material buildup and weld strength likely suggests some of the adhered material is shed from the tool when it hits the lower Cu sheet and then rebuilds on the tool during the plunging process. This position can be supported by looking at the sample produced with the tool remaining at the end of this twenty weld trial.

Figure 4-9 shows the sample macrostructure of the weld produced after the twenty weld trial. Based on work already presented, the macrostructure shown in Figure 4-9(a) suggests that this weld would have reasonably high strength and quality (presence of weld-defined stir zone and upward extruded Cu ring). The tool tip material buildup has a layered structure similar to what was shown in Chapter 2. An analysis of the phases present in this buildup will be presented in Sub-section 4.3.2.

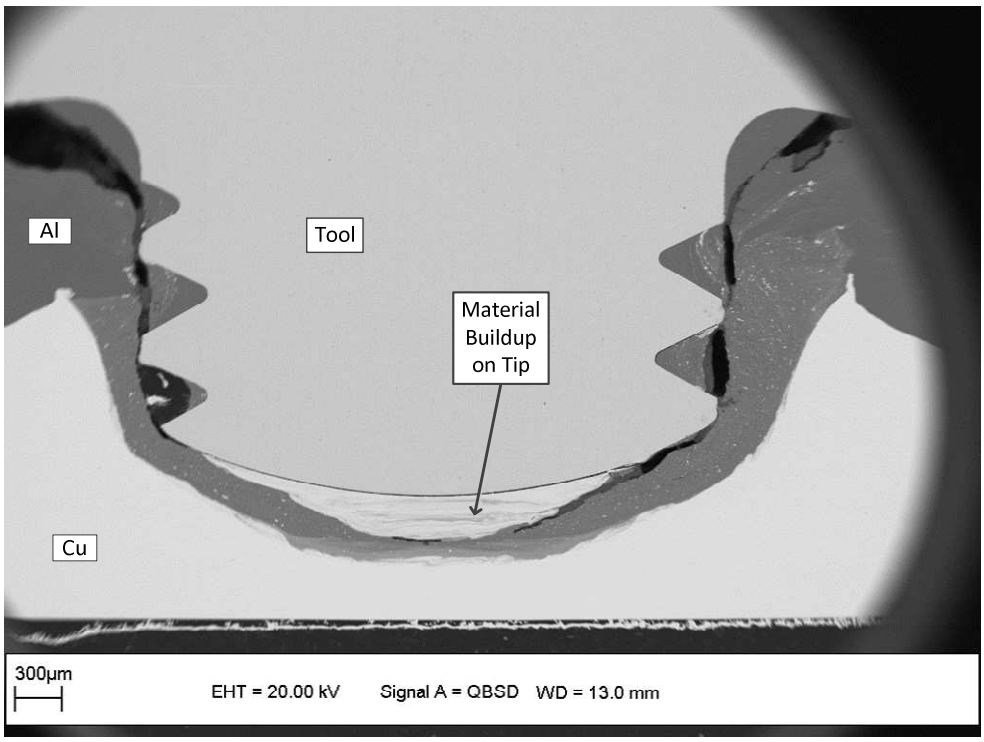

(a)

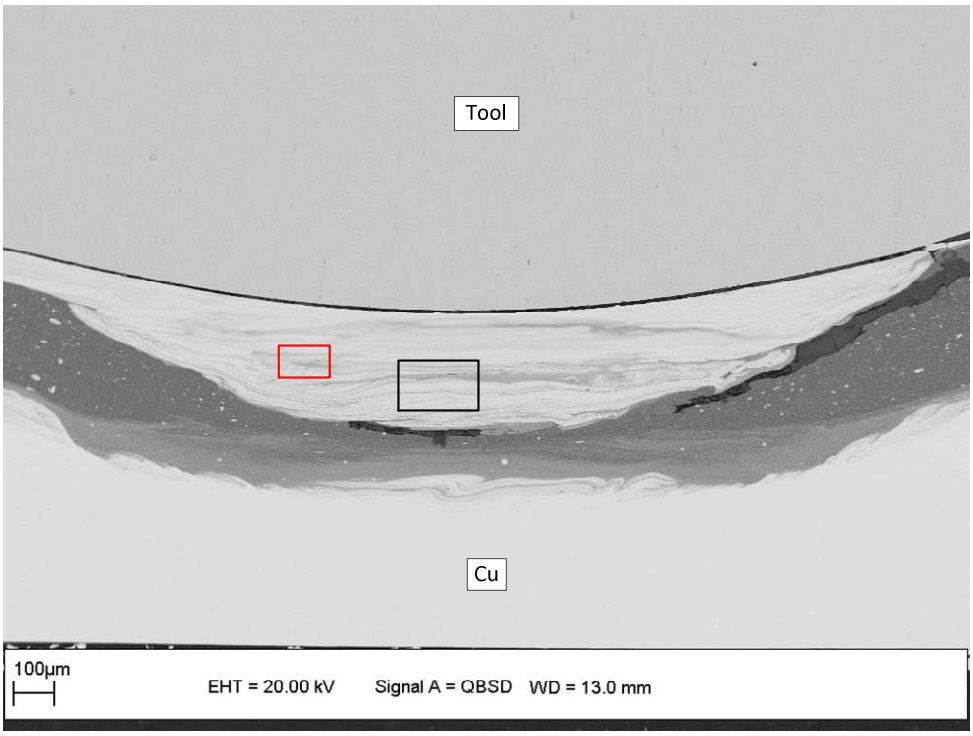

(b)

Figure 4-9. SEM images (a) at low magnification and (b) at a higher magnification of tool tip sample with the tool remaining in it after the twenty welds produced in Figure 4-7. The welding parameters used were 2000rpm rotation speed, 2.59mm plunge depth, 0.21mm/s plunge rate, and 0.0s dwell time.

While analyzing this sample, a complex crack structure was noted in the material build up on the tool tip (See Figure 4-10). Cracks have only been seen in the tools that had made multiple welds prior to cross sectioning a tool for metallurgical evaluation. The crack that appears near the middle of the material build up and would not be expected to spall off when the tool was retracted from the work piece. If material spalled during tool retraction, the appearance of the bottom of the FSSW would appear to be Cu in color, but the bottom of welds are generally white in appearance (aluminum in color). Therefore, more than likely, the buildup remains on the tool and then spalls off during the following weld. The crack does not follow a phase boundary, but transverses multiple phases (i.e. layers in the SEM image) which is not surprising given the brittleness of the Al-Cu intermetallics. The fact that the crack lies in the middle of the material buildup suggests that only a portion would be spalled during subsequent welding. Furthermore, based on the work in Chapter 2, additional tool material buildup would be expected to occur during the plunging process of the next weld. The constant spalling and formation of material continues to support the position that the formation of a poor quality weld is not just the result of material spalling off the tool tip but is also related to the size of the particles that spall (i.e. larger particles are more likely to fill the tool threads and prevent proper macrostructure formation (i.e. well-defined stir zone and upward extruded Cu-ring)). From this work, it appears that one method to ensure weld consistency is to prevent material buildup on the tool tip, thus eliminating the source of large particles that could clog the threads and prevent proper material flow.

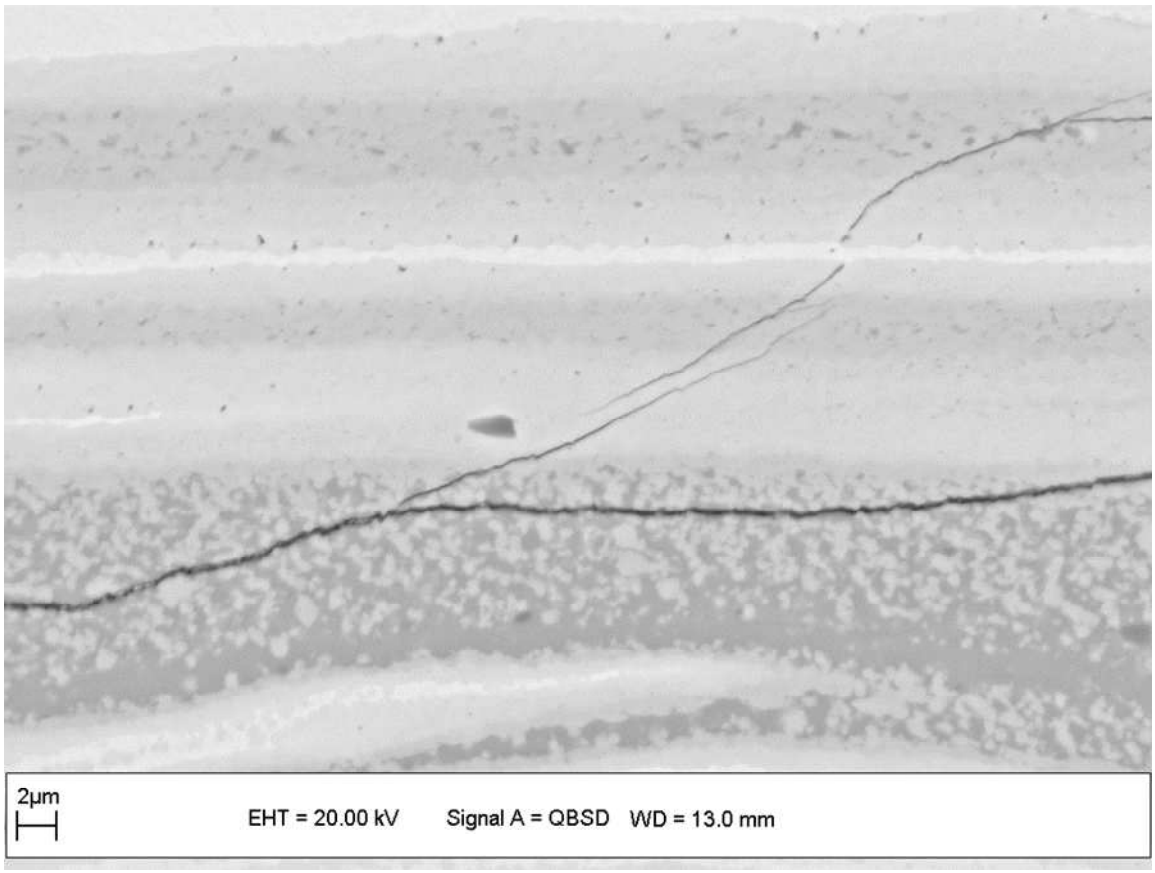

Figure 4-10. Higher magnification of the black-boxed region on Figure 4-9(b) showing the complex crack structure.

4.3.2 Determination of Phases Using X-Ray Diffraction in Tool Tip Buildup Material

SEM-EDS was used begin the determination of the phases present in the material that builds on the FSSW tool tip. The EDS measurements from three spots (see Figure 4-11) of the material buildup are summarized in Table 4-3. The EDS results in Table 4-3 indicate that all of the material on the tool tip is Cu-rich. The three different contrasts in Figure 4-11 suggests that each EDS spectrum was taken on a different Cu-Al phase. The phase present at Spot 1 is a Cu(Al) solid solution. Spot 2 is likely γ_2-Cu_9Al_4 and Spot 3 is likely η_2-CuAl. The Al levels are low for the γ_2 and η_2 phases, but

as noted in the discussion in Chapter 1, these phases are likely and generally present in Al-Cu friction stir welding. Since EDS was inadequate determining the exact phases present, another technique was needed.

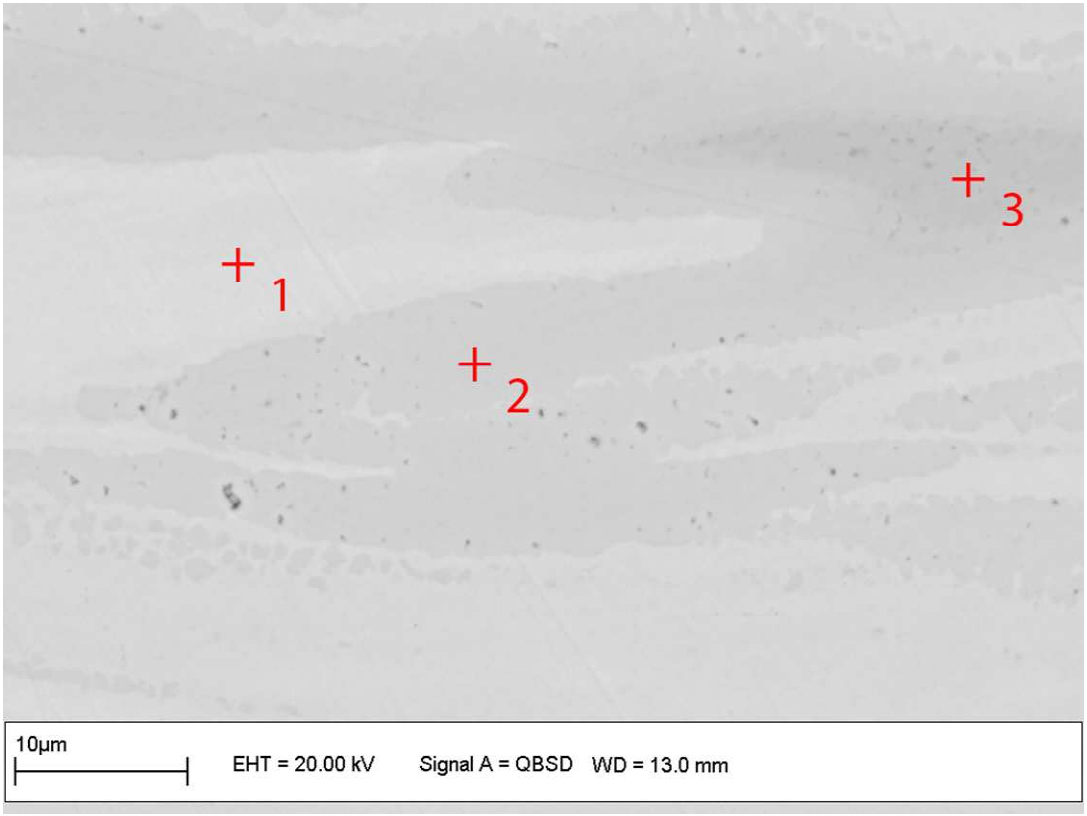

Figure 4-11. SEM Image showing three spots where EDS spectrums were measured in red-boxed region of Figure 4-9(b)

Table 4-3. Semi-quantitative (No standards were used to calculate weight percentages of Cu and Al.) EDS analysis of tool tip material in Figure 4-5.

	Weight % Cu	Weigh % Al
Spot #1	96.2	3.8
Spot #2	86.2	13.8
Spot #3	77.3	22.7

To further explore the phases present in the material that builds up on the tool tip, x-ray diffraction was employed. To use this technique, a Viscount 44 (H13) steel tool

that had made five welds and had visible material on the tip was placed in a lathe, and the material built up on the tool tip was machined off and collected. This material was then placed on the tip of quartz rod and held in place with amorphous grease. The quartz rod and amorphous grease were used as a sample holder ensures that the sample holders did not impact the x-ray diffraction pattern. This sample was then placed in a Ragaku Rapid II X-ray Diffractometer. This instrument used a molybdenum x-ray source with an area detector with a 50kV voltage and 50mA current. The x-ray was collimated to a beam size of 0.10mm. The sample was rotated 360 degrees through the beam with an exposure time of 900s.

The diffraction spectrum for this sample is shown in Figure 4-12. The peaks in Figure 4-12, were indexed using JADE software, and the x-ray diffraction specturm was found to contain two phases: Cu and Cu_9Al_4 (γ_2). The red vertical lines in Figure 4-12 indicate the diffraction peaks associated with Cu and these peaks are all present in this diffraction pattern. The green vertical lines are the expected diffraction peaks for Cu_9Al_4. Only the higher intensity peaks are present and the intensity of these peaks is less than those for Cu. The lower intensities of the Cu_9Al_4 peaks suggest that Cu_9Al_4 was present in lesser amounts than Cu. While a third phase appears to exist in Figure 4-11, no additional phases were detected using this x-ray diffraction technique. Since the amount of this third phase material in Figure 4-11 is relatively small compared to the other two phases, it is suspected that third phase was present in too low of quantities to be detected via this x-ray diffraction technique.

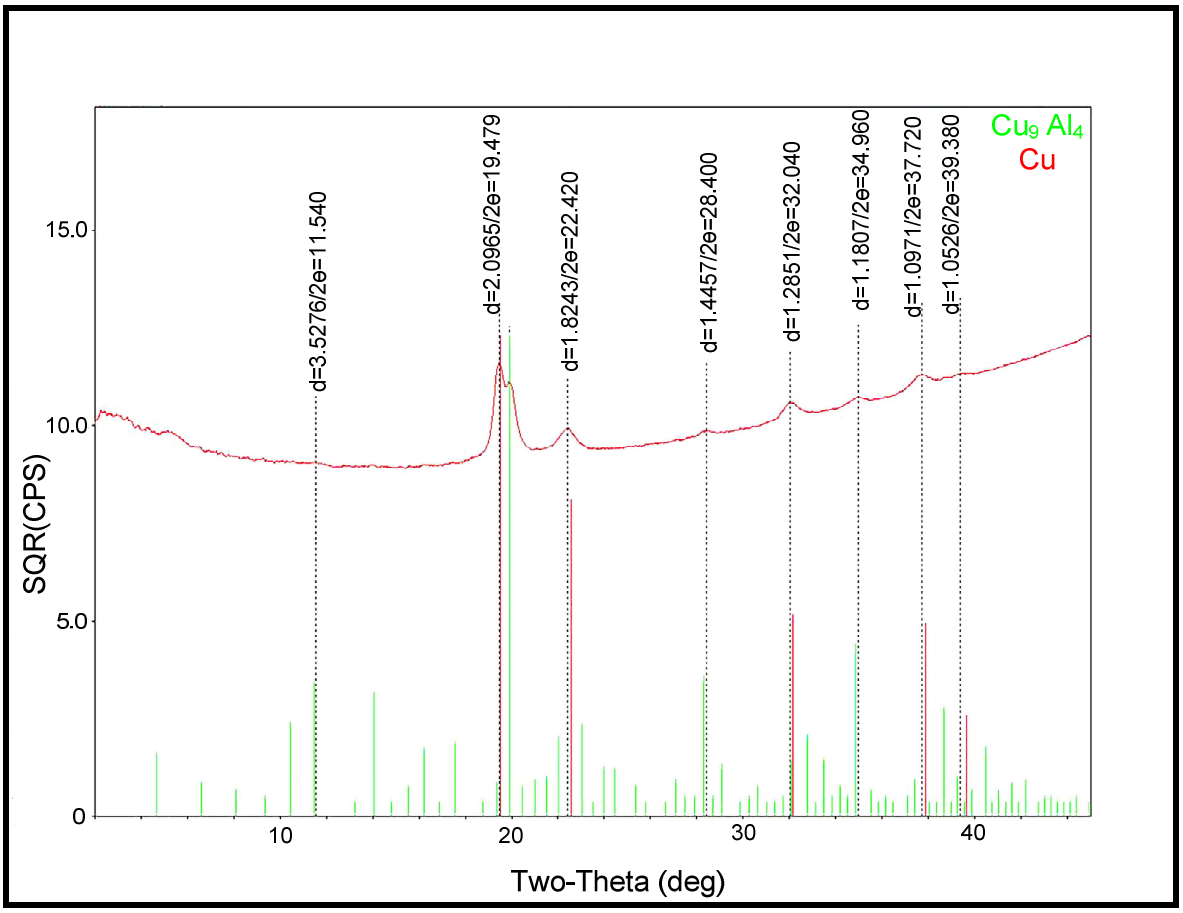

Figure 4-12. X-ray diffraction spectrum of the material built up on a Viscount 44 (H13) steel tool after 5 welds. The welding parameters used were 2000rpm rotation speed, 2.59mm plunge depth, 0.21mm/s plunge rate, and 0.0s dwell time.

The presence of Cu-rich phases in the material that builds up on the tool tip was not surprising. From Chapter 2, when the tool tip touches the lower Cu sheet, the Al from the upper 6061Al sheet is pushed aside and up and only smaller amounts of Al remain on the tool tip; the material touching the tool tip from this point and through the rest of the welding process was shown to be Cu-rich. As shown in the Cu-Al phase diagram in Figure 4-13, Cu is capable of dissolving just under ten weight percent Al from approximately 370˚C to over 550°C which, from Chapter 3, are temperatures that the tool tip could experience during welding. Therefore, much of the Al present on the

tip would likely get dissolved into the Cu and form a Cu(Al) solid solution which is what the EDS analysis indicated. With more Cu present than Al, additional Cu-rich phases (as opposed to Al-rich phases) could also be expected to form. A Cu-rich phase that is commonly observed in welding is Cu_9Al_4 (γ_2) and as would be expected in an Cu-rich region formed on the tool tip. While a third phase is likely apparent in Figure 4-11, it was not detected via x-ray diffraction because it was likely present in too low of quantities. Most material on the tool tip appears to be a Cu(Al) solid solution with some Cu_4Al_9 present.

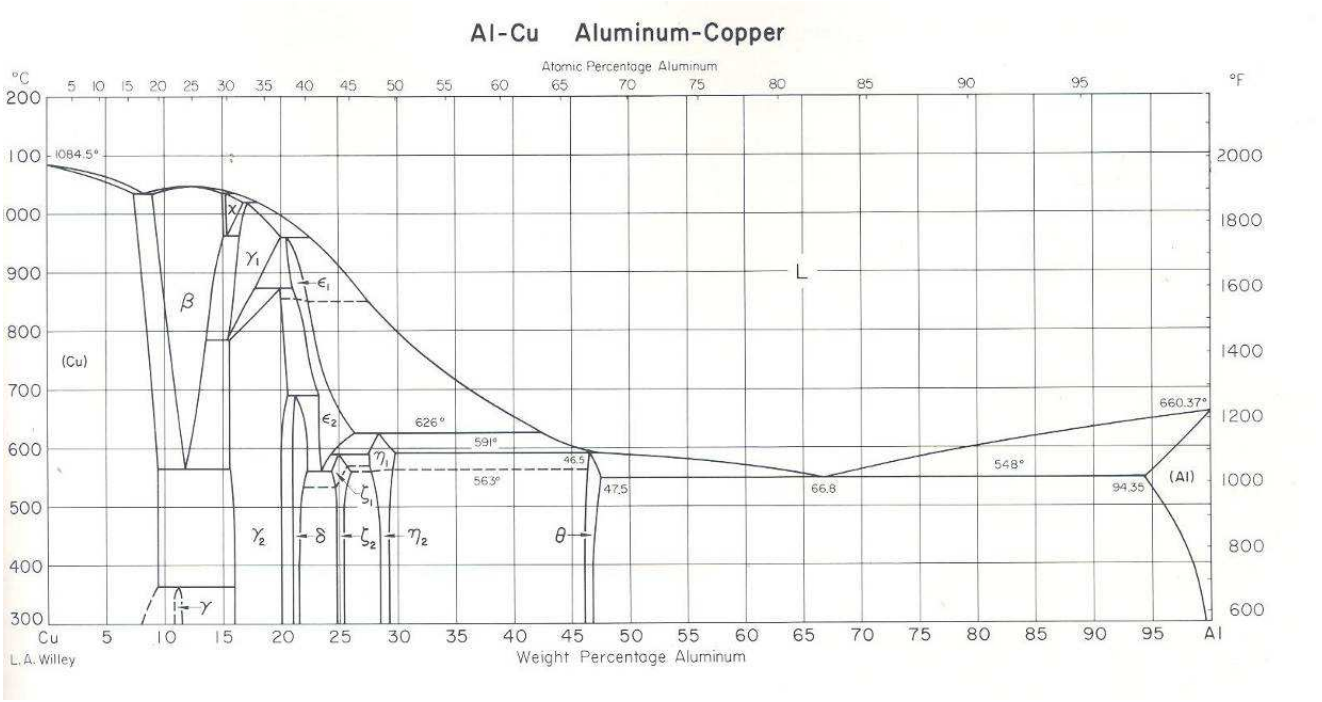

Figure 4-13. Copper-Aluminum Equilibrium Phase Diagram [38]

4.3.3 Twenty Weld Trial using NaOH Cleaned Tool

To investigate the hypothesis that weld strength consistency can be improved by removing the tool tip material buildup between each weld, a twenty weld trial was conducted in which the FSSW tool was etched in NAOH for 600s between each weld.

The purpose of this etching was to remove tool material build up. The tool inspection (before and after etching with NaOH) from this trial, along with the weld strength produced with the etched tool, is shown in Figure 4-14. From Figure 4-14, the NaOH etching process appears to have removed some, but not all, of the material buildup from the tool threads and tip. The graphical representation of the weld strengths, along with the measurement of the tool tip buildup before and after etching, is shown in Figure 4-15. By comparing the weld strength curves in Figures 4-8 and 4-15, the weld consistency was improved and no welds with strengths less 1400N were produced using an etched tool. By comparison, the tool that was not cleaned between each step yielded six of twenty welds with strengths less than 1000N (see Figure 4-8).

The incomplete removal of the tool buildup via the NaOH etching is not completely surprising since the NaOH would not etch the Al-Cu intermetallic compounds on the tool tip. This is graphically shown when the two tool buildup lines in Figure 4-15 lie on top of each other as is the case for Welds 3, 7, 8, 9, 11, 12, 15, 16, 17, 18, and 19. However, if these intermetallic compounds on the tool tip had cracks as shown in Figure 4-10 and the cracking was extensive enough, a portion of the tool tip buildup could break free and fall from the tool due to the use of ultrasonic cleaning to ensure agitation of NaOH solution. It is plausible, but not easily prove-able, that removing the loosely attached, cracked Al-Cu intermetallic tool tip buildup improved weld consistency. Furthermore, an argument could be made that the improved cleanliness of the threads was responsible for the improved weld consistency. Clean threads are not surprising since this material in the threads, as shown in in Chapter 2 and Figure 4-9(a), is an

Al(Cu) solid solution which is etched with NaOH. While cleaning the tool improved consistency additional work is needed to determine why this was the case.

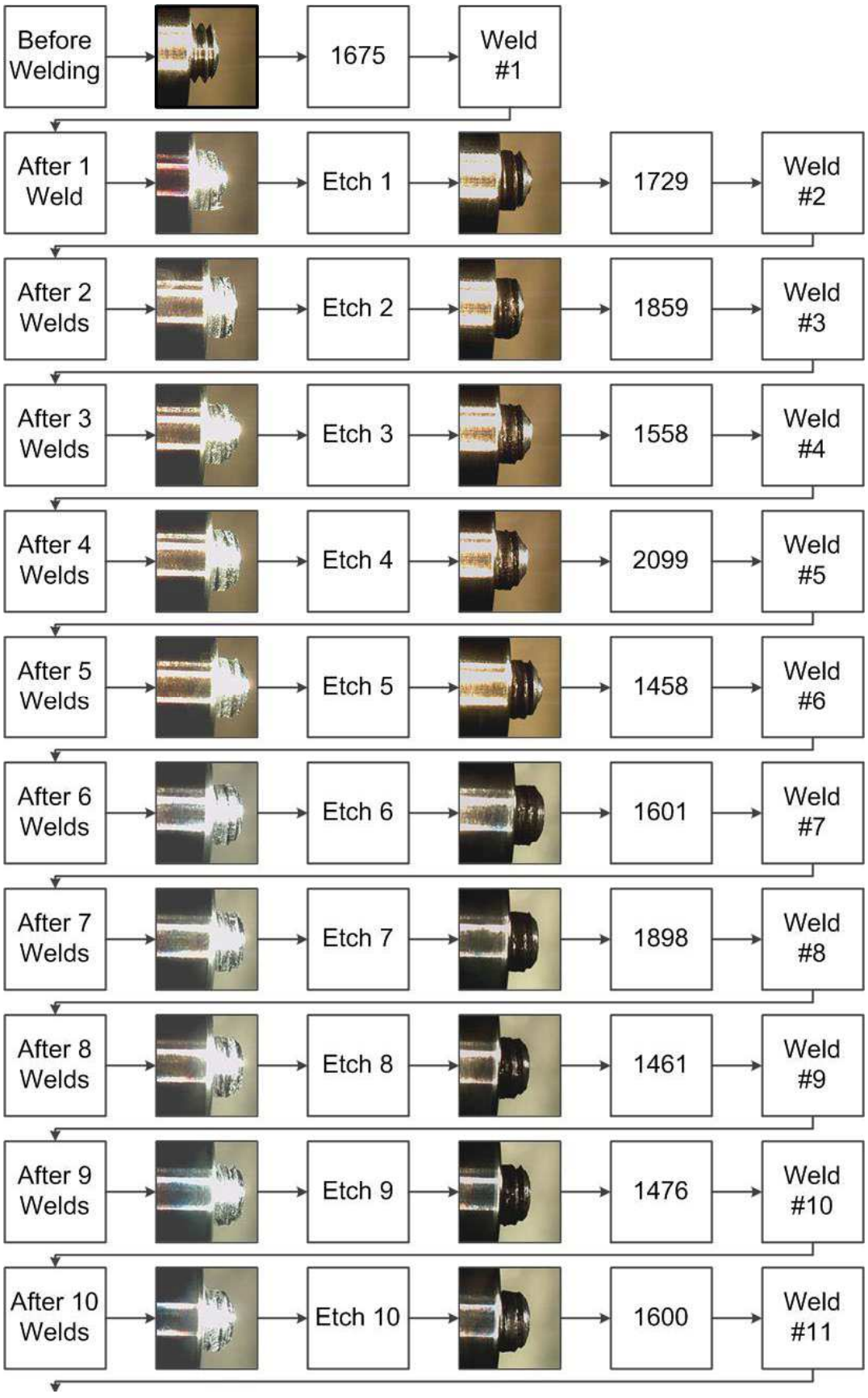
Before Welding
1675
Weld #1
After 1 Weld
Etch 1
1729
Weld #2
After 2 Welds
Etch 2
1859
Weld #3
After 3 Welds
Etch 3
1558
Weld #4
After 4 Welds
Etch 4
2099
Weld #5
After 5 Welds
Etch 5
1458
Weld #6
After 6 Welds
Etch 6
1601
Weld #7
After 7 Welds
Etch 7
1898
Weld #8
After 8 Welds
Etch 8
1461
Weld #9
After 9 Welds
Etch 9
1476
Weld #10
After 10 Welds
Etch 10
1600
Weld #11

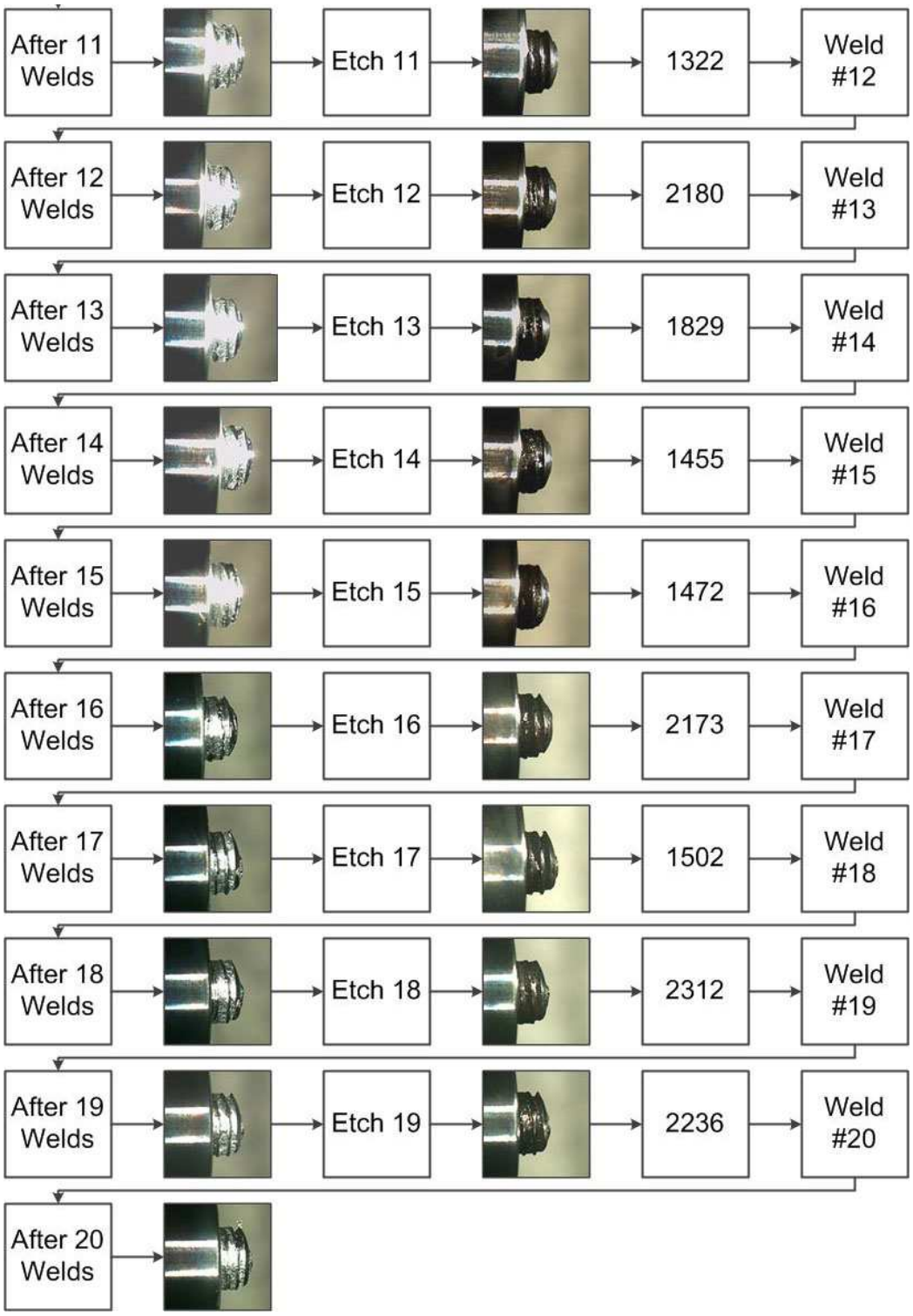

Figure 4-14. Photographs of the FSSW tool after each weld as well as after the Viscount 44 tool was etched clean for 600s using NaOH for a twenty weld trial. The strength produced by each weld (in N) is also shown. The welding parameters used were 2000rpm rotation speed, 2.59mm plunge depth, 0.21mm/s plunge rate, and 6.0s dwell time.

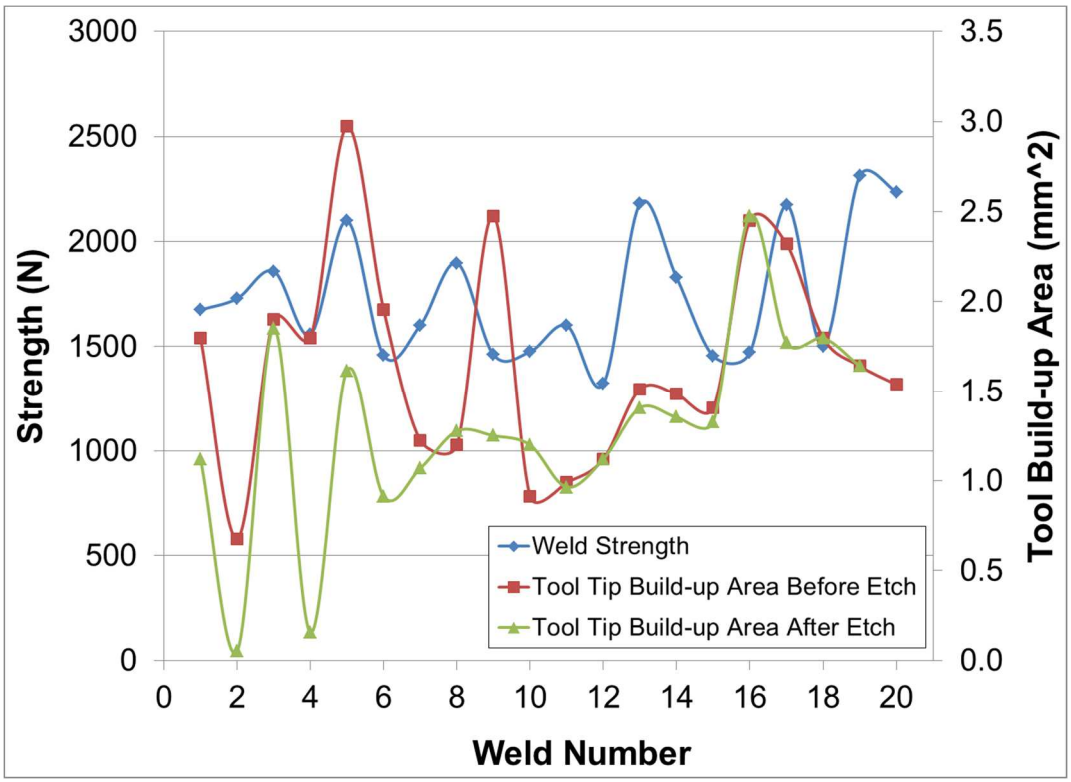

Figure 4-15. Weld Strength and tool build up data graphically shown from a twenty-weld trial using a Viscount 44 tool that was etched clean for 600s using NaOH between each weld. The data presented is from the same trial shown in Figure 4-12. The welding parameters used were 2000rpm rotation speed, 2.59mm plunge depth, 0.21mm/s plunge rate, and 6.0s dwell time.

4.3.4 Twenty Weld Trial Machined-Clean Tool Tip

To remove only the material from the tool tip and leave the materials in the threads, the tool tip for the next twenty consecutive weld trial was machined back to the original steel surface (via the use of a CNC lathe) thus ensuring the tool tip was free from intermetallic buildup. Figures 4-16 show the tools and weld strengths when the tool tip was machined back to the tips original surface between each weld. However, the photographs of the tools in Figure 4-16 show the tool condition immediately after welding and before it was machined clean. A comparison for the new tool used for this trial and the machined clean tool are shown in Figure 4-17. As can be seen, the tool tip

after machining is nearly identical to when it was in the new and unused condition. However, the material in the threads remained unchanged since no machining was done in the thread region. The tool's tip would have looked nearly identical to the lower picture in Figure 4-17 prior to each weld in this twenty weld trial.

The amount of tool buildup after each weld in Figure 4-16 appears less than in Figure 4-7 where no cleaning technique was employed. This supports an earlier claim that only some, not all, of the tool tip material buildup spalls off during plunging of the tool, and as the process progresses, additional material buildup takes place. A graphical presentation of the strengths achieved by machining the tip clean and the amount of tip buildup are shown in Figure 4-18. By ensuring the tool tip is free of any Al-Cu buildup, the weld strength consistency improved over the tool tip that was not cleaned in any manner (Figure 4-8). The weld strengths, when the tool tip was machined clean, were all of reasonable quality and above 1500N. This discovery supported the earlier finding with respect to the tool that was etched using NaOH clean; removing material from the tool tip prior to welding improves weld strength consistency and eliminates low strength welds. The graph in Figure 4-18 supports the observation in Figure 4-17 that the buildup was less when the tip was machined clean, further supporting the likelihood that only some of the tip buildup spalls and rebuilds as the process continues. The partial spalling followed by a rebuild would explain the increased buildup in the initial twenty weld trial where no type of cleaning was used between each weld. While machining appears to be viable option, a better option in a manufacturing environment would be to eliminate the need for any secondary cleaning operation. With this goal two possible options (tool coatings and an alternative material) were explored.

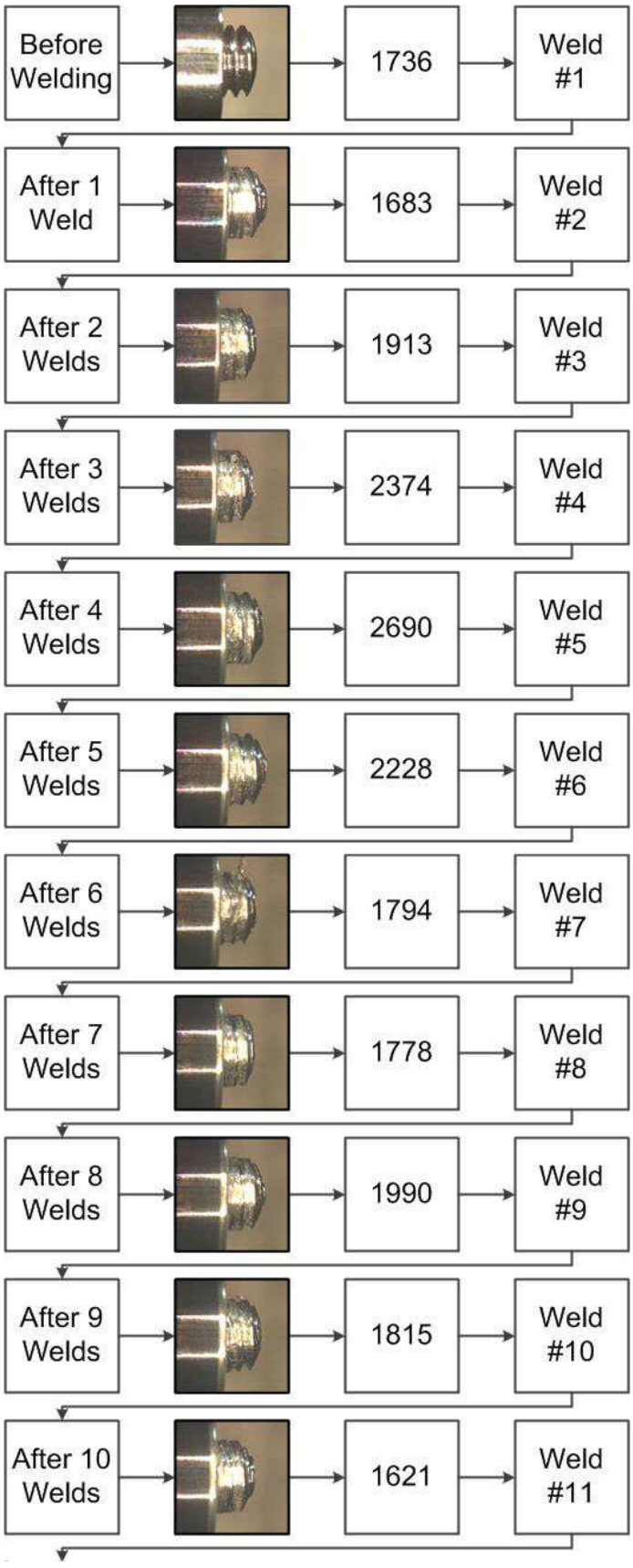
Before Welding
1736
Weld #1
After 1 Weld
1683
Weld #2
After 2 Welds
1913
Weld #3
After 3 Welds
2374
Weld #4
After 4 Welds
2690
Weld #5
After 5 Welds
2228
Weld #6
After 6 Welds
1794
Weld #7
After 7 Welds
1778
Weld #8
After 8 Welds
1990
Weld #9
After 9 Welds
1815
Weld #10
After 10 Welds
1621
Weld #11

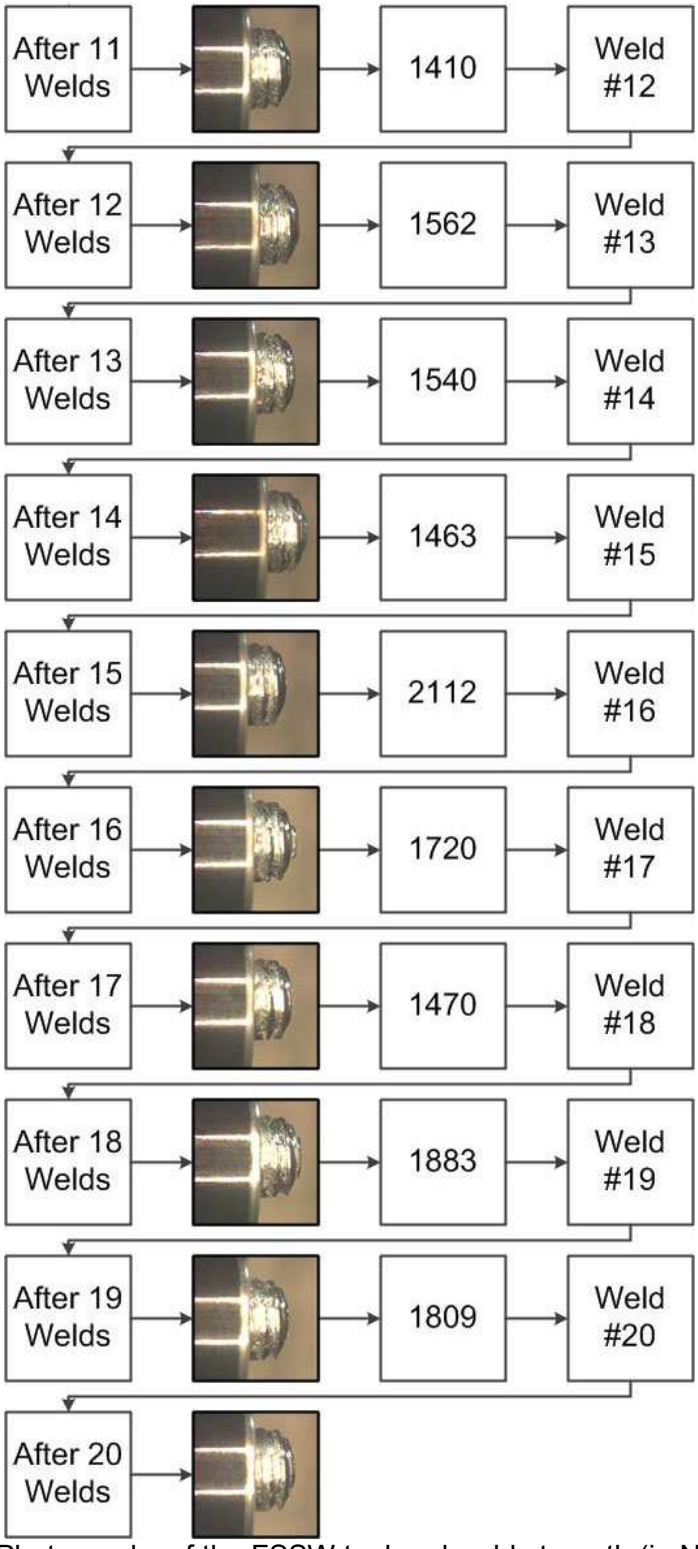

Figure 4-16. Photographs of the FSSW tool and weld strength (in N) produced for a twenty-weld trial where the Viscount 44 tool's tip was machined free of tool buildup prior to each weld. The photographs were taken immediately after welding, before the tip was machined clean. The welding parameters used were 2000rpm rotation speed, 2.59mm plunge depth, 0.21mm/s plunge rate, and 6.0s dwell time.

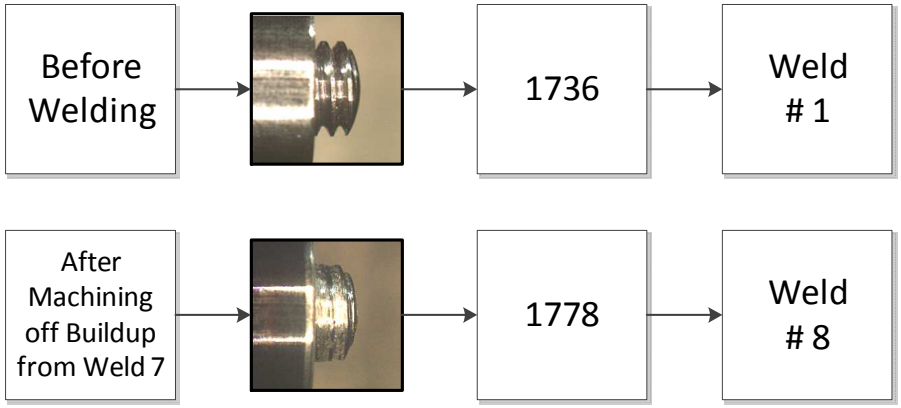

Figure 4-17. A comparison between the new tool prior to making Weld #1 (top photograph) and a tool tip (bottom photograph) after being machined back to its original surface (i.e. tool tip buildup removed). The machined-clean tool (bottom photograph) is after Weld #7; however, the tool tip looked identical to this photo prior to making Welds #2 through #20, which as shown is the same as a new tool tip.

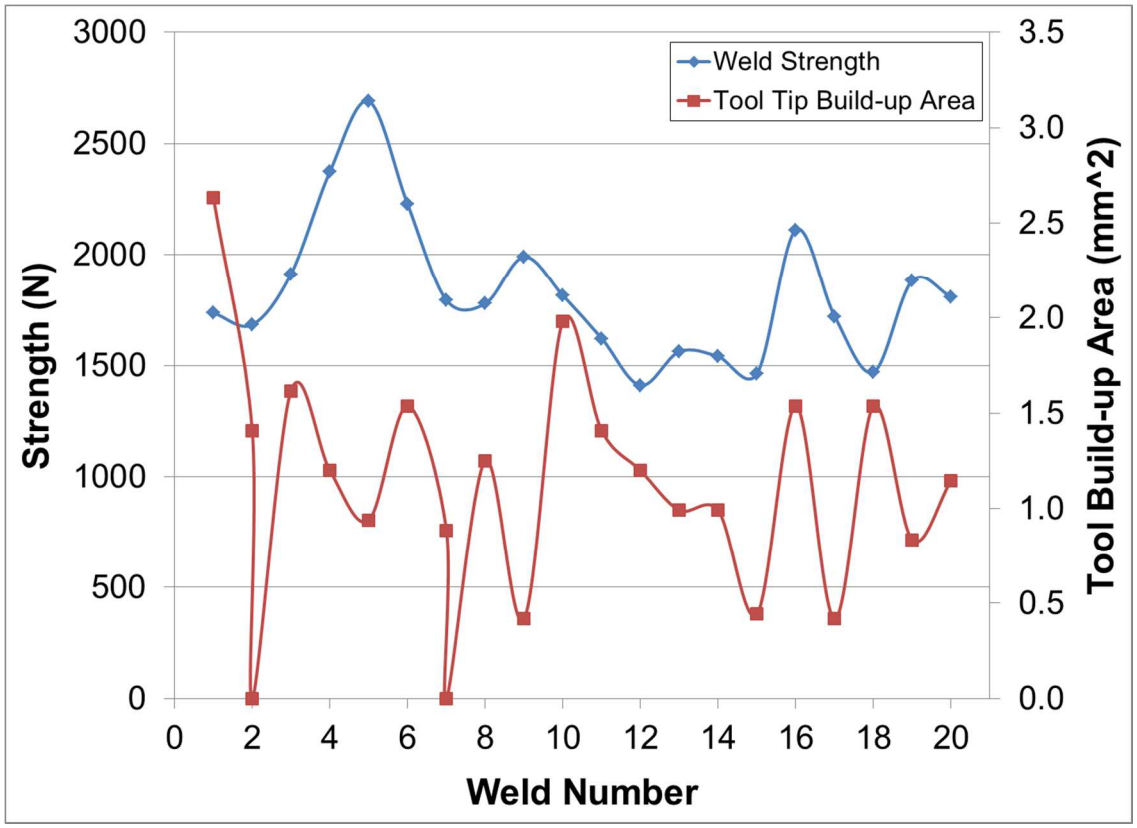

Figure 4-18. Weld Strength and tool material buildup data graphically shown from a twenty-weld trial using a Viscount 44 tool where the tool tip was machined clean of buildup prior to make each weld. The data presented is from the same trial shown in Figure 4-14. The welding parameters used were 2000rpm rotation speed, 2.59mm plunge depth, 0.21mm/s plunge rate, and 6.0s dwell time.

4.3.5 Twenty Weld Trials using TiCN and CrN Coated Tools

The images of the coated tool between each weld and the weld strengths for the TiCN and CrN coated tools are shown in Figures 4-19 and 4-20 respectively. In addition, a graphical representation of the weld strengths and tool material buildup are shown in Figure 4-21. Figure 4-19 shows that when a TiCN coated tool was used, that the tool threads contained less material than in the baseline experiment in Figure 4-7. Additionally, the photographs appear to show less material buildup on the tool tip. This observation is supported by comparing the material buildup curves in Figures 4-8 and 4-21(a). The material buildup curves in Figure 4-21(a) generally show lower buildup numbers than those in Figure 4-8. The weld strengths for the TiCN tool appear similar to those for tools that had been cleaned, with most strengths in the 1500N to 2000N range and some greater than 2000N (see Figure 4-21(a)). Additionally, no strengths less than 1000N were observed. While the tool coating appears to eliminate low-strength welds, it did not eliminate material tip buildup. The tool tip material buildup, as was the case with uncoated tools, changed with each weld, as shown in Figure 4-21(a). However, the level of material buildup appeared to be less than what was observed in the baseline experiment. Two possible explanations for the improved consistency for the TiCN coated tool are: (1) the improvements were the results of less buildup on the tool and (2) the coating has a lower coefficient of friction which permits the larger particles that spall from the tool tip to flow through the tool threads more readily than if the tool was uncoated steel, which is the purpose of the coating. The first possible explanation will be explored in more detail later. The exact value for the coefficient of friction is between TiCN and the numerous materials (Al, Cu, and Al-Cu intermetallics) present in the stir

zone is not known. However, a reasonable assumption is that the coefficient of friction is lower for TiCN as compared to an uncoated H13 steel tool.

Before doing additional work to understand the mechanism(s) responsible for the observed improvement in weld consistency, the robustness of the coating (i.e. whether the coating will last sufficiently long or will quickly wear off the tool) in a 6061 Al to Cu FSSW environment needed to be assessed. To evaluate whether the coating was present at the end of the trial, the tool was cross-sectioned and metallographically prepared. SEM images of the cross-sectioned tool are shown in Figure 4-22. At low magnification (Figure 4-22(a)), the tool threads appear filled with an Al–rich material shown by the darker contrast material within the threads. Also present in the threads are two regions of Cu-rich material (similar to what would be on the tool tip) which are the brighter contrast materials (the region on the Cu-rich region on the right side of the tool image is boxed). The Cu-rich materials are sizable, but in neither case as large as those observed in the thread-clogged sample in Figure 4-1. Two higher magnification images of the tool are shown in Figure 4-22(b) and (c). Figure 4-22(b) is an image of the upper portion of the thread and shows a layer immediately adjacent to the tool surface that would appear to be the tool coating. An EDS line scan (See Figure 4-23) confirmed that this was the tool coating as evident by the Ti peak in the middle of the scan. To the right of the Ti peak was mostly Fe indicating this was the steel tool, and to the left of the peak was Al and Cu lines of nearly equal intensity (the Al and Cu lines lie right on top of each other so the Al line is not easily discernable in the Figure 4-23) which is indicative of the stir zone of the region boxed in Figure 4-22(a) and magnified in Figure 4-22(b). Figure 4-22(c) is of the lower tool thread region and no identifiable tool coating layer was

observed on the lower tool thread surface. EDS analysis confirmed that Ti, which would be indicative the tool coating, was not present. The lack of tool coating on the lower thread demonstrates that the material flow, as discussed in Chapter 2, is in the downward direction along the threads. The downward flow of material along the tool threads would cause the stirred material to impinge more on the lower thread than the upper thread, and thus remove the coating on the lower thread surface. While the tool coating showed improved weld consistency, the lack of robustness, as demonstrated by the coating being worn off the lower thread surface in less than twenty welds, suggests that the TiCN is not a viable long tern solution to the weld strength inconsistency issue.

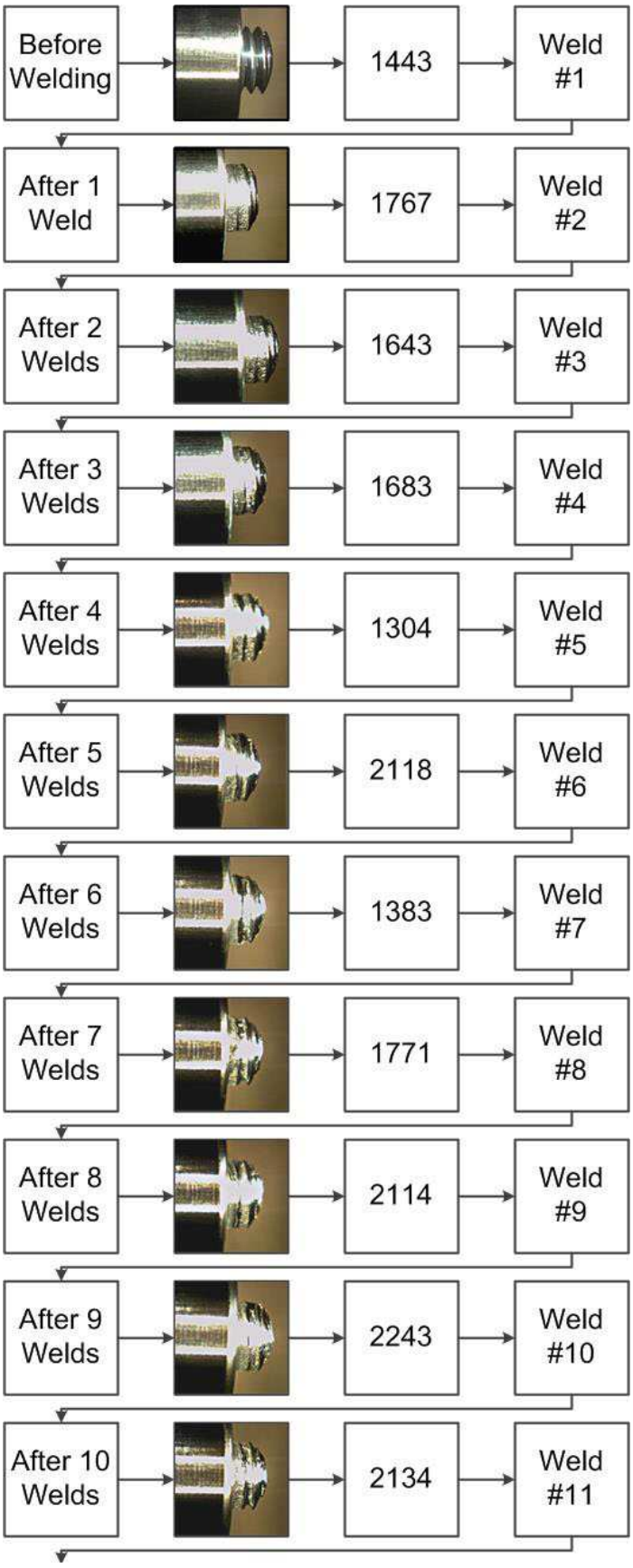
Before Welding
1443
Weld #1
After 1 Weld
1767
Weld #2
After 2 Welds
1643
Weld #3
After 3 Welds
1683
Weld #4
After 4 Welds
1304
Weld #5
After 5 Welds
2118
Weld #6
After 6 Welds
1383
Weld #7
After 7 Welds
1771
Weld #8
After 8 Welds
2114
Weld #9
After 9 Welds
2243
Weld #10
After 10 Welds
2134
Weld #11

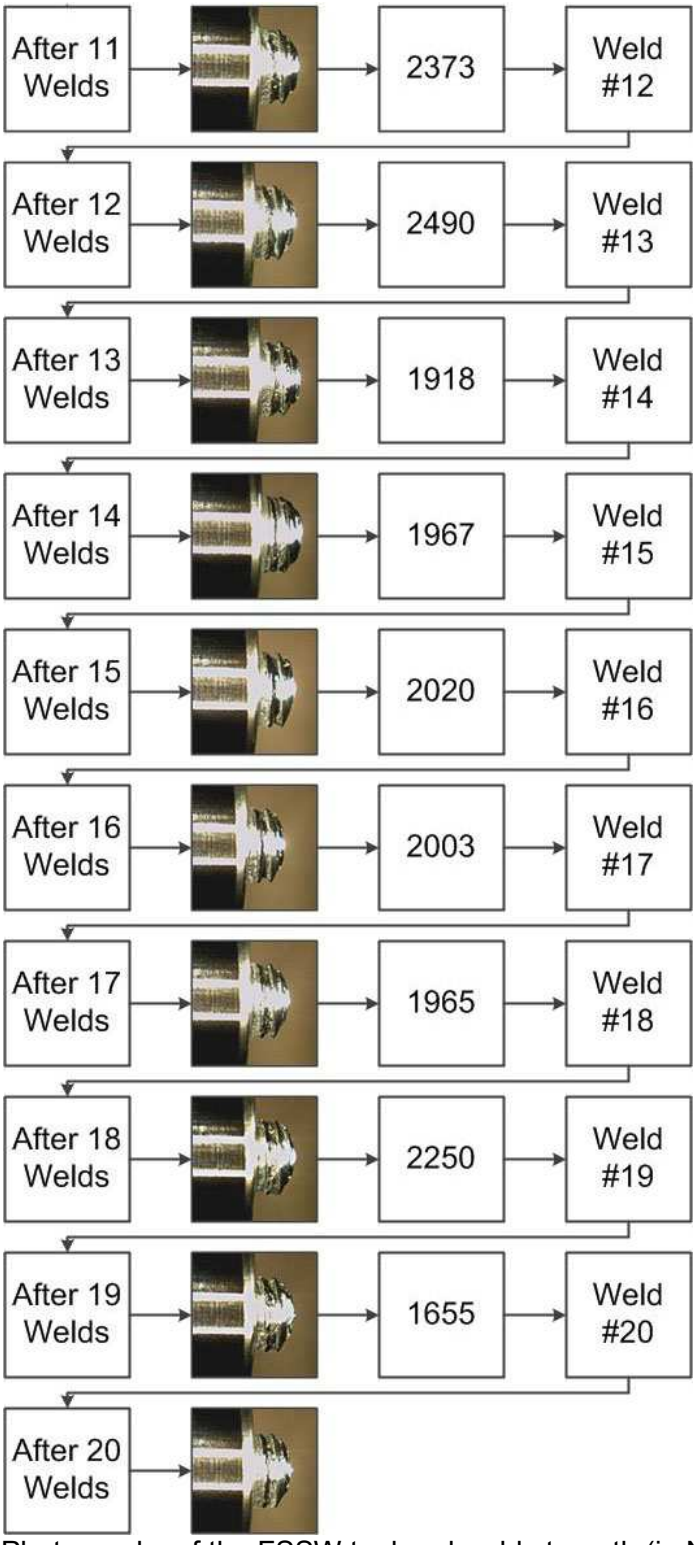

Figure 4-19. Photographs of the FSSW tool and weld strength (in N) produced for a twenty-weld trial using a Viscount 44 with a 1-4um PVD TiCN coating on the tool. The welding parameters used were 2000rpm rotation speed, 2.59mm plunge depth, 0.21mm/s plunge rate, and 6.0s dwell time.

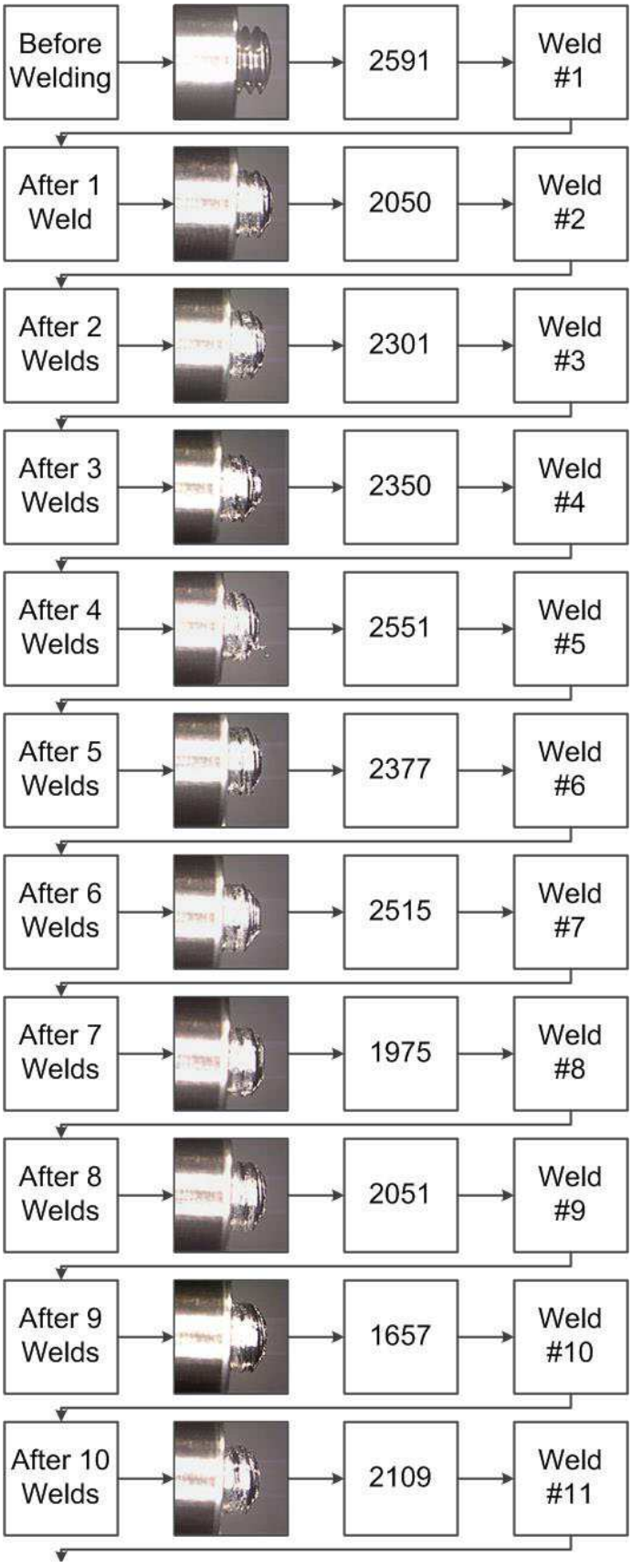
Before Welding
2591
Weld #1
After 1 Weld
2050
Weld #2
After 2 Welds
2301
Weld #3
After 3 Welds
2350
Weld #4
After 4 Welds
2551
Weld #5
After 5 Welds
2377
Weld #6
After 6 Welds
2515
Weld #7
After 7 Welds
1975
Weld #8
After 8 Welds
2051
Weld #9
After 9 Welds
1657
Weld #10
After 10 Welds
2109
Weld #11

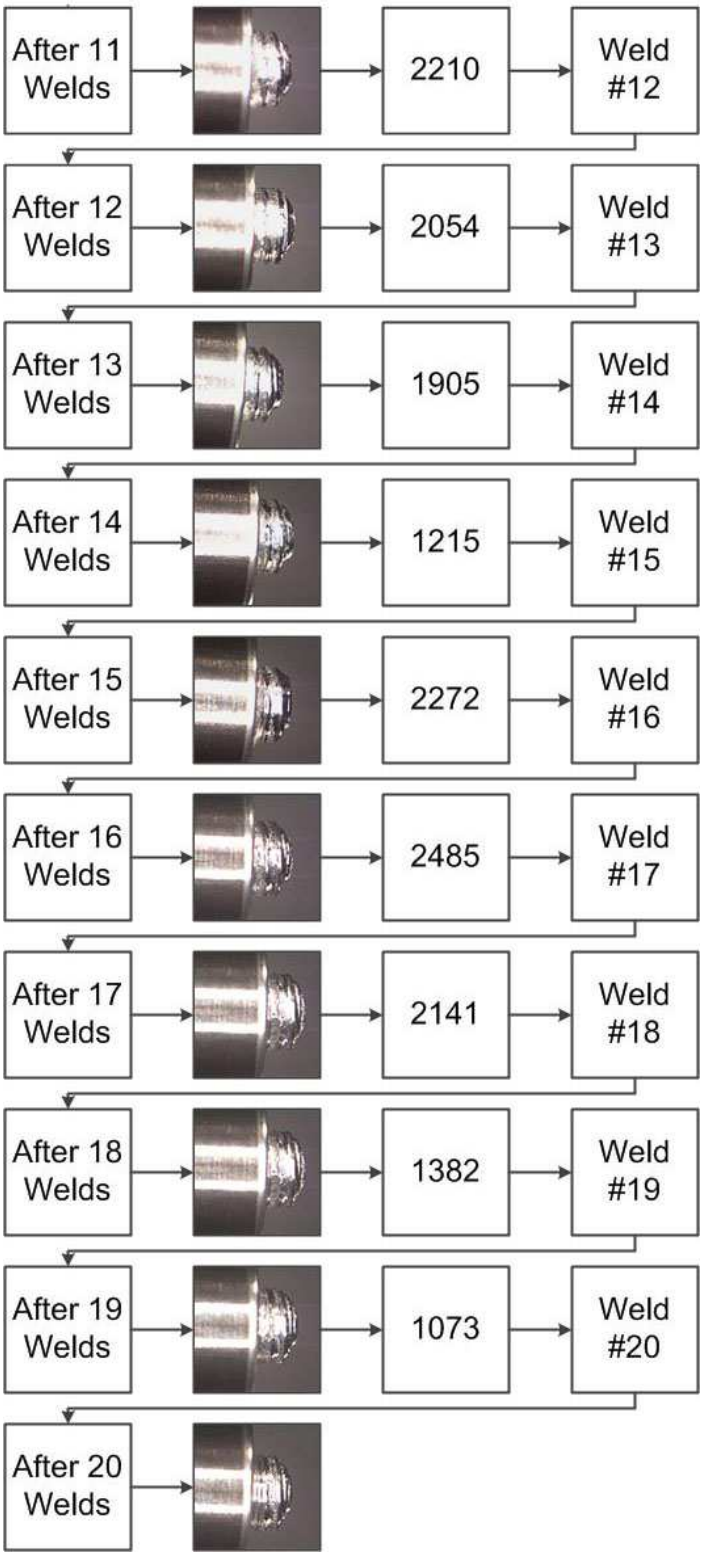

Figure 4-20. Photographs of the FSSW tool and weld strength (in N) produced for a twenty weld trial using a Viscount 44 tool with a 1-4um PVD CrN coating on the tool. The welding parameters used were 2000rpm rotation speed, 2.59mm plunge depth, 0.21mm/s plunge rate, and 6.0s dwell time.

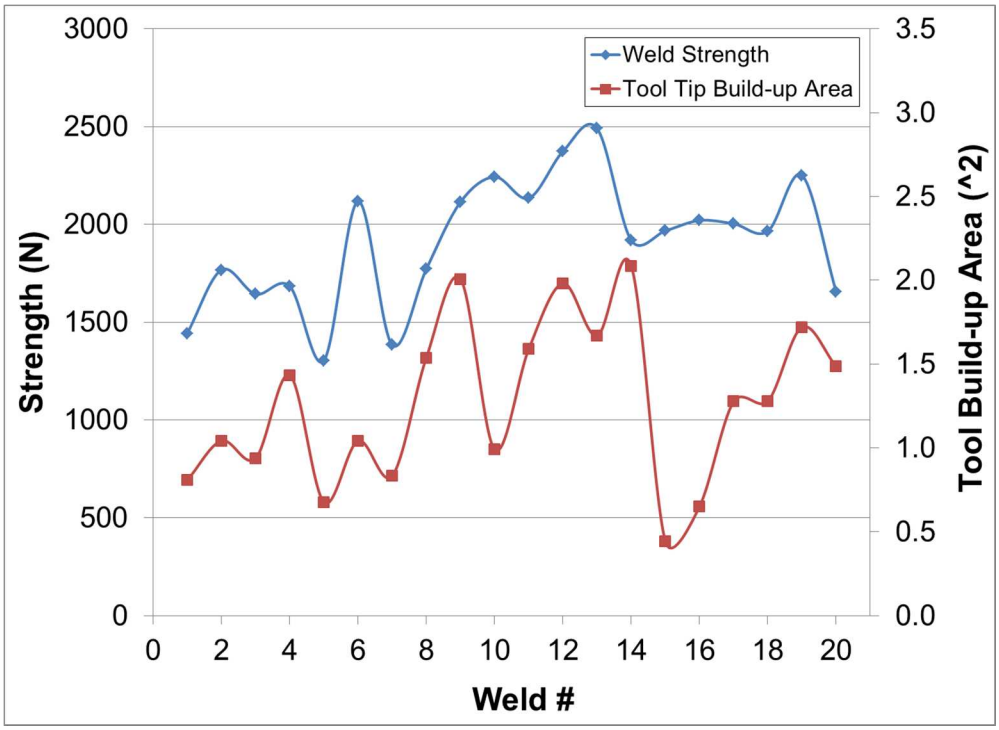

(a)

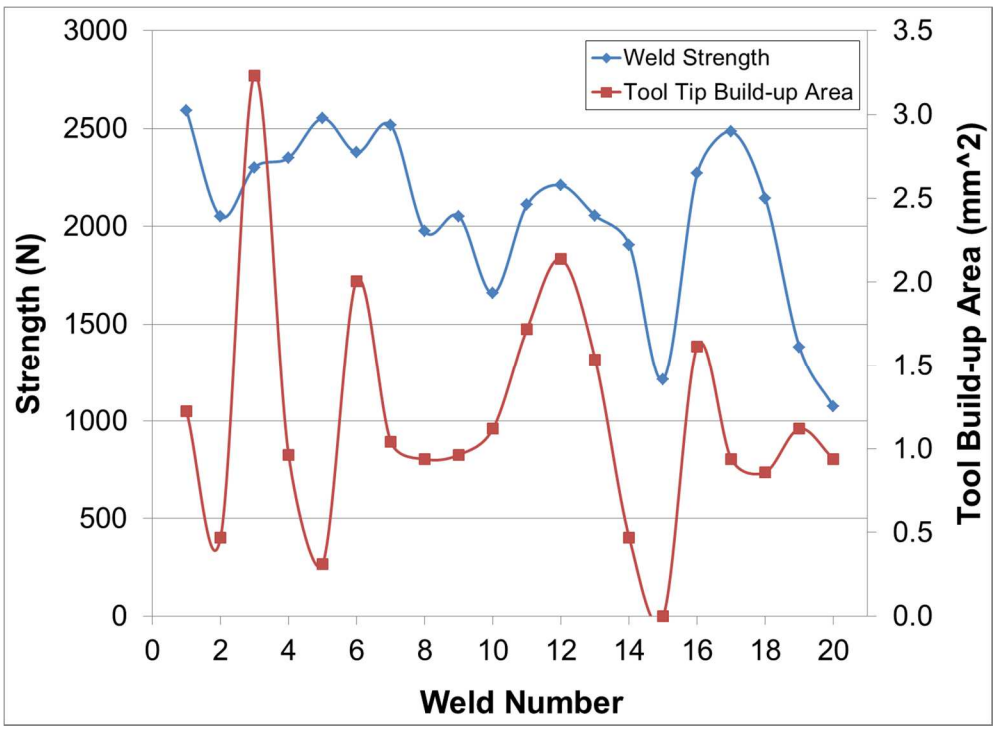

(b)

Figure 4-21. Weld Strength and tool material build up data graphically shown from a twenty weld test of (a) Figure 4-17 where a TiCN coated Viscount 44 tool was used and (b) Figure 4-18 where a Viscount 44 CrN coated tool was used. The welding parameters used were 2000rpm rotation speed, 2.59mm plunge depth, 0.21mm/s plunge rate, and 6.0s dwell time.

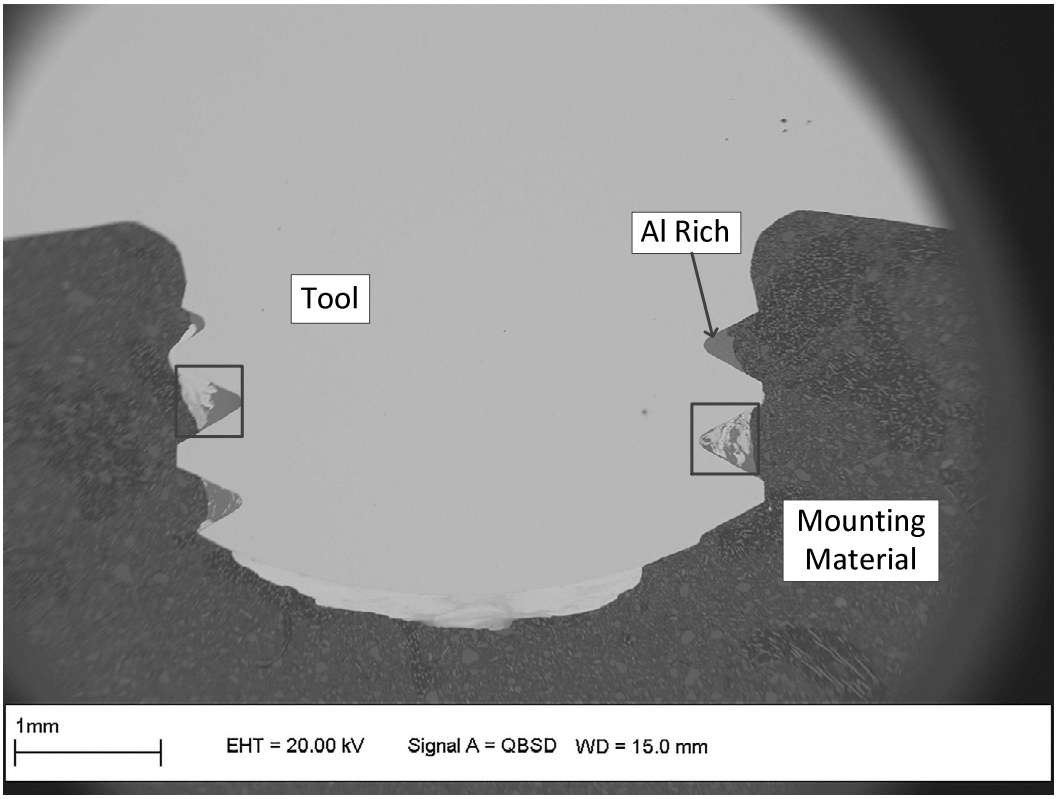
Al Rich
Tool
Mounting Material
1mm
EHT = 20.00 kV
Signal A = QBSD
WD = 15.0 mm

(a)

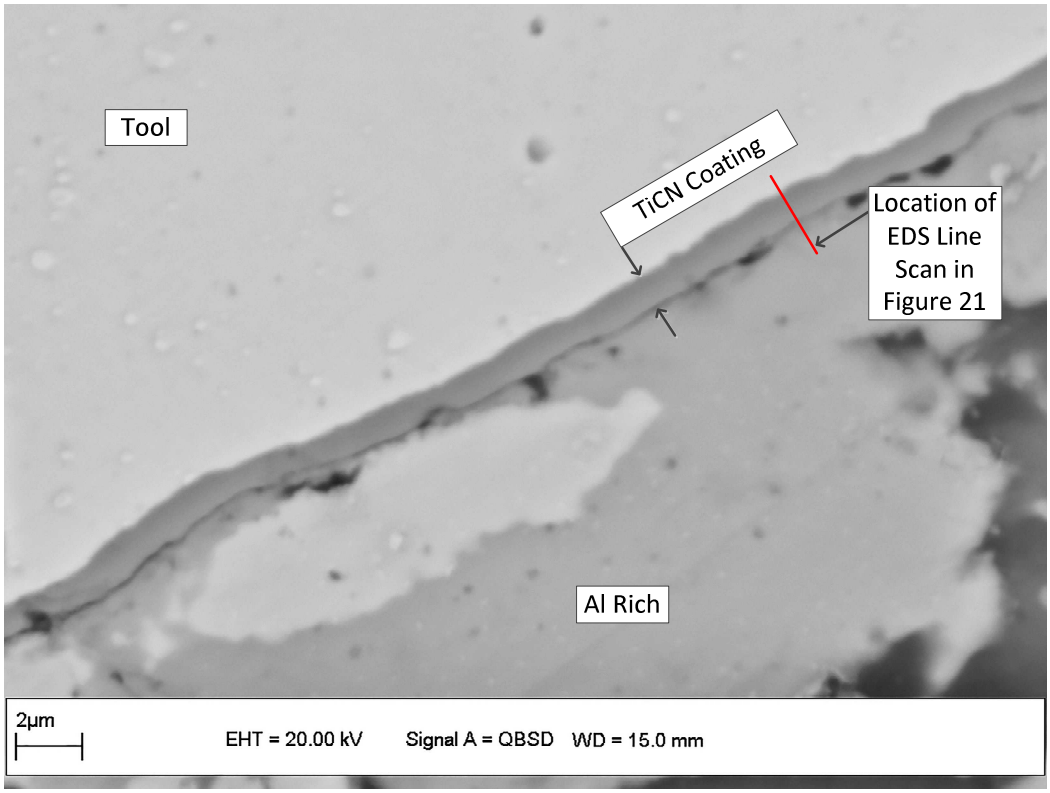
Tool
TiCN Coating
Location of EDS Line Scan in Figure 21
Al Rich
2µm
EHT = 20.00 kV
Signal A = QBSD
WD = 15.0 mm

(b)

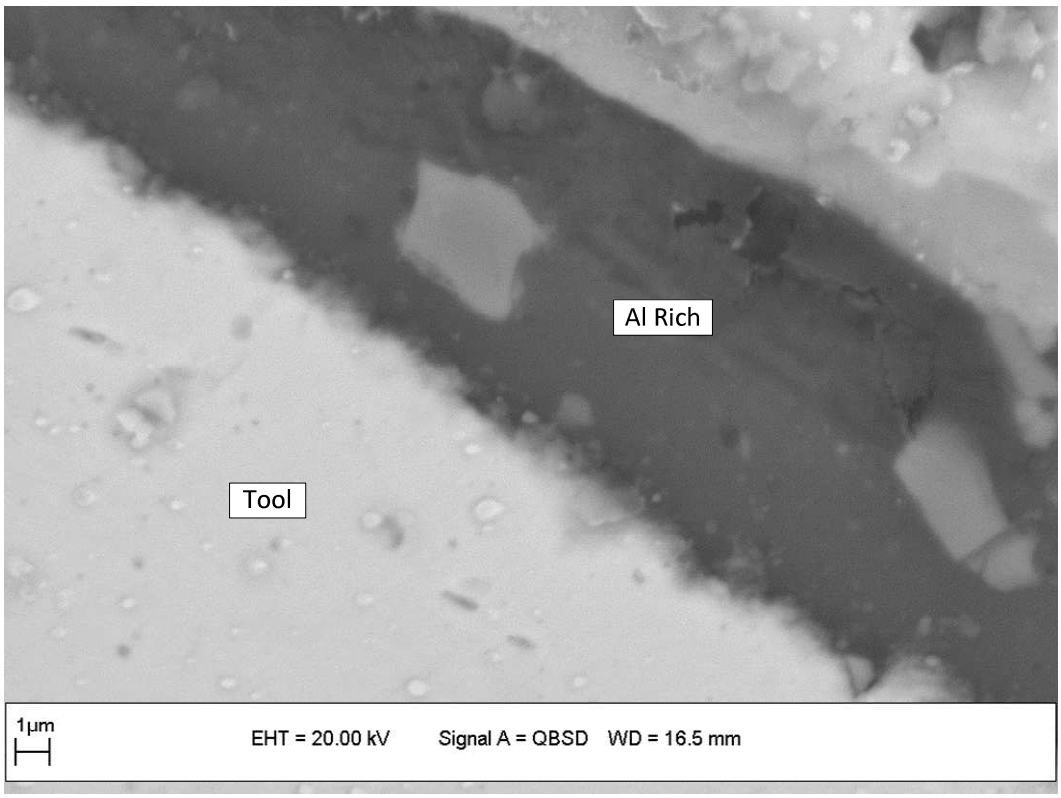

(c)

Figure 4-22. SEM images in Backscattered electron mode of a Viscount 44 tool coated with a PVD TiCN coating with: Figure (a) being a low magnification overview of the tool after a twenty weld trial and Figures (b) and (c) are higher magnification images of (a) along the tool-thread /stir zone interfaces. Figure (b) the upper-side of the tool thread region in the right-side box of (a) shows the presence of the PVD TiCN coating in this area. Figure (c) illustrates the lower-side of the thread region in the right box region of (a) shows the PVD TiCN was no longer present in this region after less than twenty welds. The welding parameters used were 2000rpm rotation speed, 2.59mm plunge depth, 0.21mm/s plunge rate, and 6.0s dwell time.

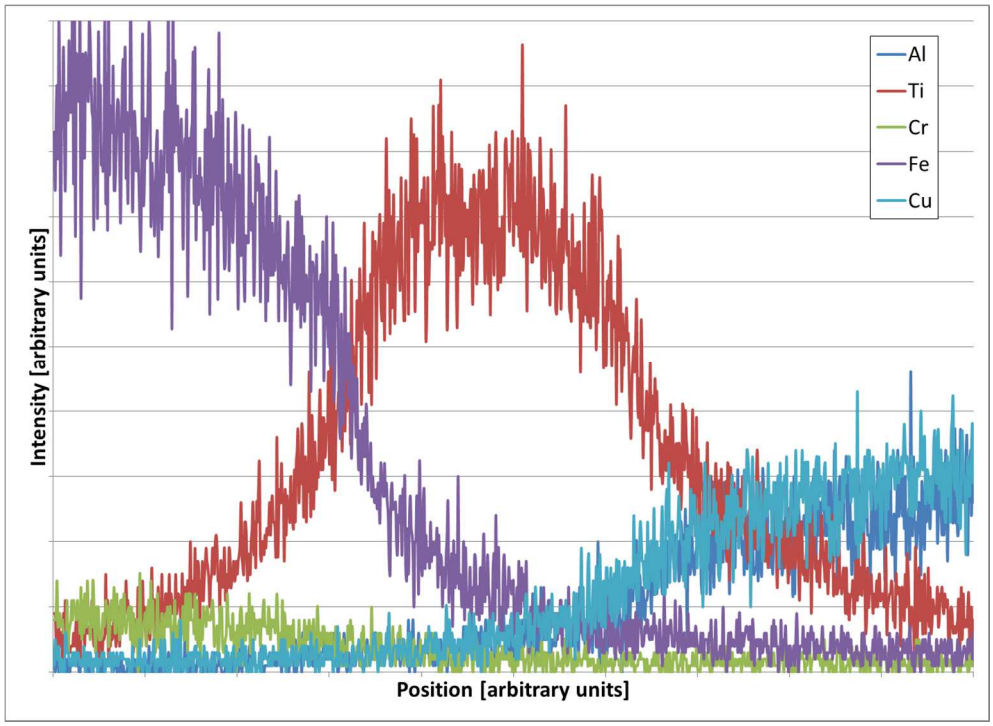

Figure 4-23. EDS line scan data for the red line shown in Figure 4-20(b). The line scan is on a tool thread for a Viscount 44 tool with a PVD TiCN coating and after the tool was used for the twenty weld trial presented in Figure 4-17 and confirms the presence of the TiCN coating on the upper region of tool thread.

The images of the tool after each weld using a CrN coated tool (see Figure 4-20) showed some differences in amount of material buildup on the tool tip as compared to the TiCN coated tool. This difference is particularly evident after Weld #3, which shows significantly more buildup on tool tip that was CrN coated than any images associated with the TiCN coated tool. This significant buildup was then shed during the process of making Weld #4. This is visually apparent in Figure 4-20 and supported by the measurement in Figure 4-21(b). Furthermore, as was the case with the uncoated tool, the strength was not impacted by this large shedding of material, indicated by the large drop in the buildup area curve on Figure 4-21(b) between Welds #3 and #4, while the strength from Weld #3 to Weld #4 increased slightly. The CrN coated tool did produce noticeably stronger welds than the TiCN coated tool and the uncoated tool. 70% of CrN

produced welds had strengths greater than 2000N. However, after Weld #14, the strengths became less consistent with the final strength being of low quality, only 1073N. The likely reason for the noticeable inconsistency late in the trial was that the CrN coating was no longer present. SEM analyses of the cross-sectioned tool confirmed this hypothesis. A low magnification image of the tool is shown in Figure 4-24(a). This image shows that there was a large layered structure in the middle thread along the left side of the image (circled in Figure 24(a)), along with an Al-rich material of darker contrast in the tool threads. It is unclear if the large particle would have actually resulted in a low-quality weld. However, since the layered particle does not completely fill the thread as shown in Figure 4-1, it is unlikely that this tool would have produced a low quality weld. Higher magnification images of the thread regions are shown in Figures 4-24(b) and 4-24(c). In Figure 4-24(b), the CrN tool coating is visible and appears as a contiguous layer along the upper tool thread surface. The presence of the CrN coating layer on the upper thread surface was confirmed via a SEM line scan shown in Figure 4-25 which shows Cr peak in the middle of the scan. In comparison, on the lower thread, as shown in Figure 4-24(c), the CrN coating is a noncontiguous layer, is broken in particles resting on the tool thread surface, and is actually removed from the tool threads on the lower right-side of the image in Figure 4-24(c). EDS analysis confirmed that the block-like structure on the left side of the thread image is primarily Cr which is indicative the CrN coating. This would support the hypothesis after just twenty welds; the tool coating wore off the tool, which could explain the inconsistency in strengths towards the end of the twenty weld trial. The lack of a tool coating on the lower tool thread surface, along with this same issue being observed on a TiCN coated tool,

suggests that tool coatings are not a viable path to improve weld strength in a manufacturing environment where a non-consumable tool is expected to make hundreds, and even thousands, of welds before being replaced.

It is important to note that early in the CrN coated tool trial, high strengths welds were achieved (three of the first seven welds have strengths greater than 2500N and all seven were above 2000N). Even though the tool was building up tool material on its tip and then shedding it in subsequent welds, the strengths remained high during the early welds. Once the tool coating began to wear off the tool, the strengths were closer to those observed for the uncoated tool. As mentioned previously, tool coatings are designed to have lower coefficients of friction compared to uncoated steel. A plausible explanation for the improved strength is that the lower coefficient of friction improved material flow and prevented large particles that spall from the tool tip from clogging the threads. Instead, these large layered particles moved more easily through the thread as a result of the lower coefficient of friction associated with the coated tool surface. This reasoning explains why the welds were more consistent early in the trial, but it does not explain why the strengths were consistently higher than an uncoated steel tool during the same time period.

The likely explanation for consistent increase in weld strength early in the twenty weld trial is that the lower coefficient of friction of the CrN improves the flow of material in the stir zone and thus produces a wider stir zone between the tip of the Cu ring and the weld keyhole. In Chapter 1, a reasonable linear regression equation was established between the width of the stir zone (t in mm) and strength (s in kN):

$$\boldsymbol{s = 2833t + 333} \qquad \textbf{(4-1)}$$

From personal experience in metal stamping applications, tool coatings are used to promote improved flow in difficult-to-form parts. Tool coatings suppliers claim that tool coatings dramatically reduce the coefficient friction between the tool, usually steel, and the material being formed (in many cases steel) producing improved flow. In these challenging forming applications, promoting improved material flow helps the part being formed retain most of the original sheet thickness. In contrast, with uncoated tool in the same application, the material thins to the point of cracking prior to finishing the forming process. Using a low-coefficient friction tool coating could also enhance the flow of material in FSSW. A tool with a lower coefficient of friction surface could facilitate the moving of material down along the tool threads at a higher velocity while at the same time, the surface velocity along the Cu side of the stir zone would likely remain mostly unchanged. The higher velocity of material coming down along the tool could then push more material in the stir zone region between the forming of the Cu ring and the welding tool. Since more material is present in this region, the stir zone would naturally get wider, and a stronger weld would form. This explanation can be supported further by looking at the twenty trial results using the Densimet 17.7 tool.

To support the lower coefficient of friction explanation, it would be desirable to obtain comparative coefficients of friction between the CrN coating and 6061 Al, Cu, and Al-Cu intermetallics. However, these values cannot be found in the open literature, nor are these available from the coating provider [50]. The ASM Metals Handbook [68] has a compilation of coefficients for friction of numerous materials, but only two are relevant to this study. Using a spherically ended pin (made for steel) on a flat piece of Cu, the kinetic coefficient of friction was measured to be 0.82. This same reference lists

a coefficient friction value of 0.25 for a flat steel surfaces sliding on a flat surface of 6061 Al. While these coefficients are relevant to this study, they only provided information for an uncoated tool. For these values to be useful, coefficients of friction between the CrN and 6061 Al and CrN and Cu are needed. The coating supplier publishes a coefficient of friction of 0.80 for steel-on-steel and 0.3 for CrN-on-steel [50]. While exact values are not available for CrN on 6061 Al and Cu, Bartos [50] expects a significant reduction in this coefficient using CrN on 6061 Al and Cu applications. This expectation is supported by improvements observed in tool life using a CrN coating in 6061 Al and Cu applications [50].

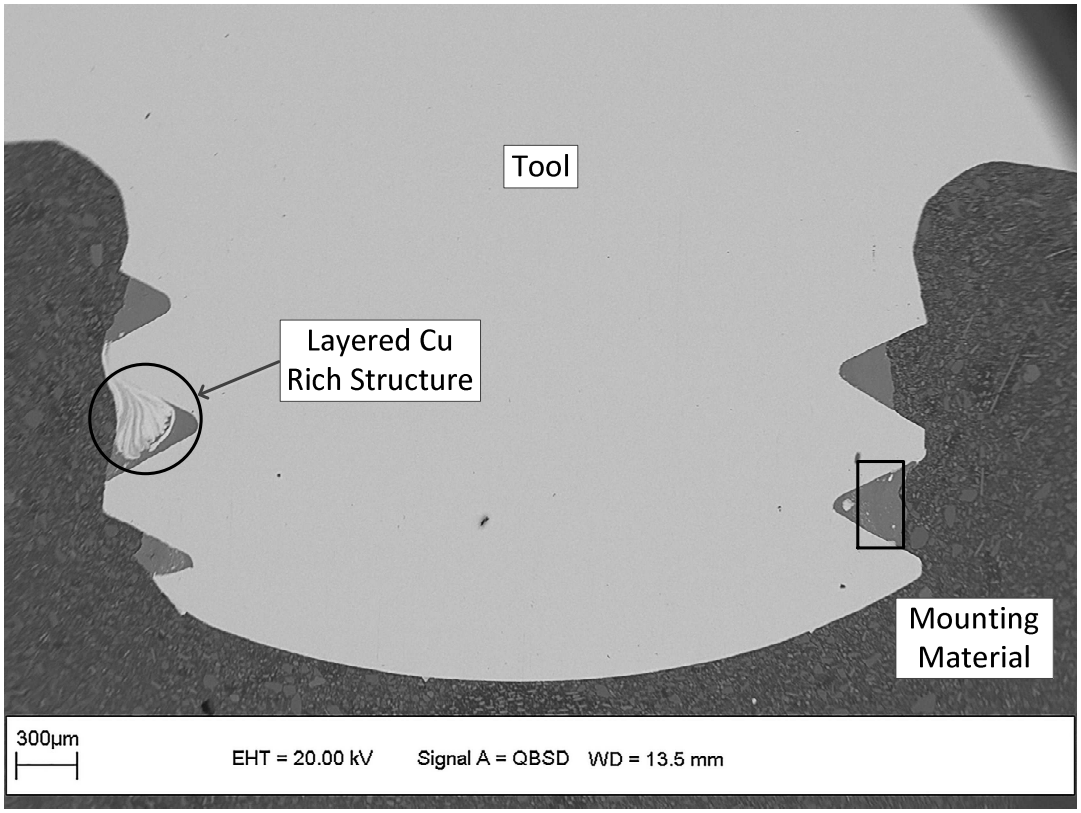
Tool
Layered Cu
Rich Structure
Mounting
Material
300µm
EHT = 20.00 kV
Signal A = QBSD
WD = 13.5 mm

(a)

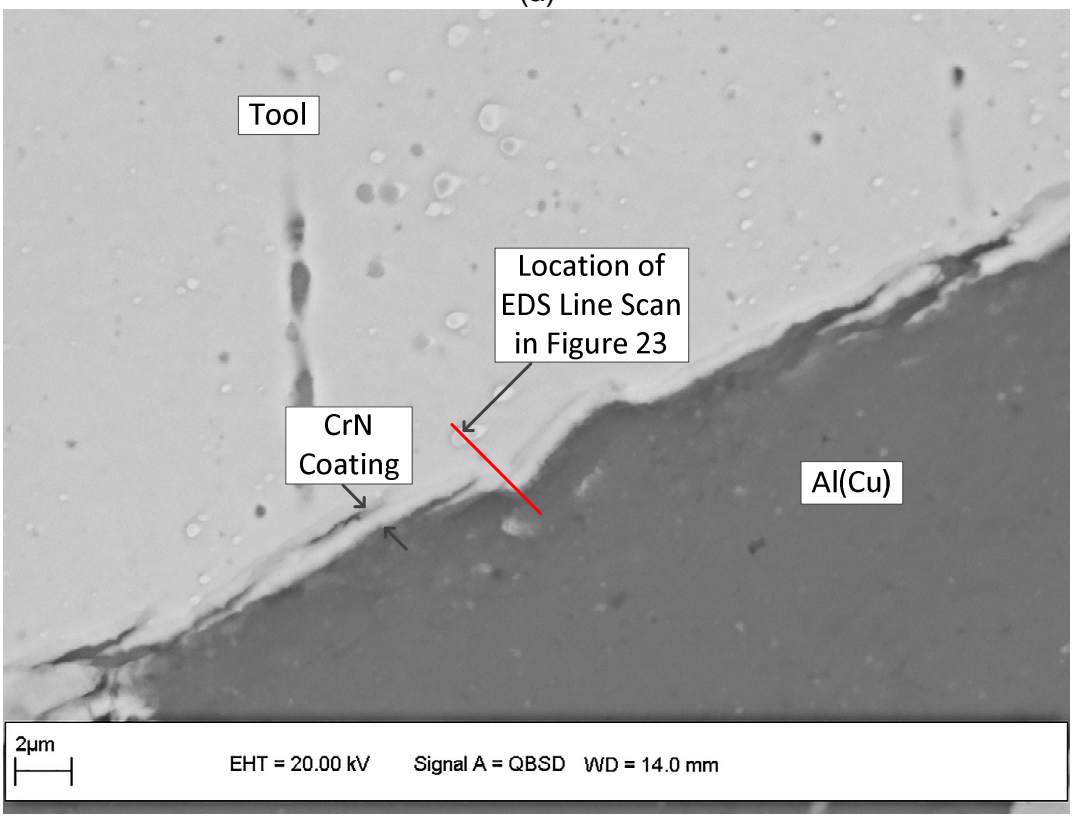
Tool
Location of
EDS Line Scan
in Figure 23
CrN
Coating
Al(Cu)
2µm
EHT = 20.00 kV
Signal A = QBSD
WD = 14.0 mm

(b)

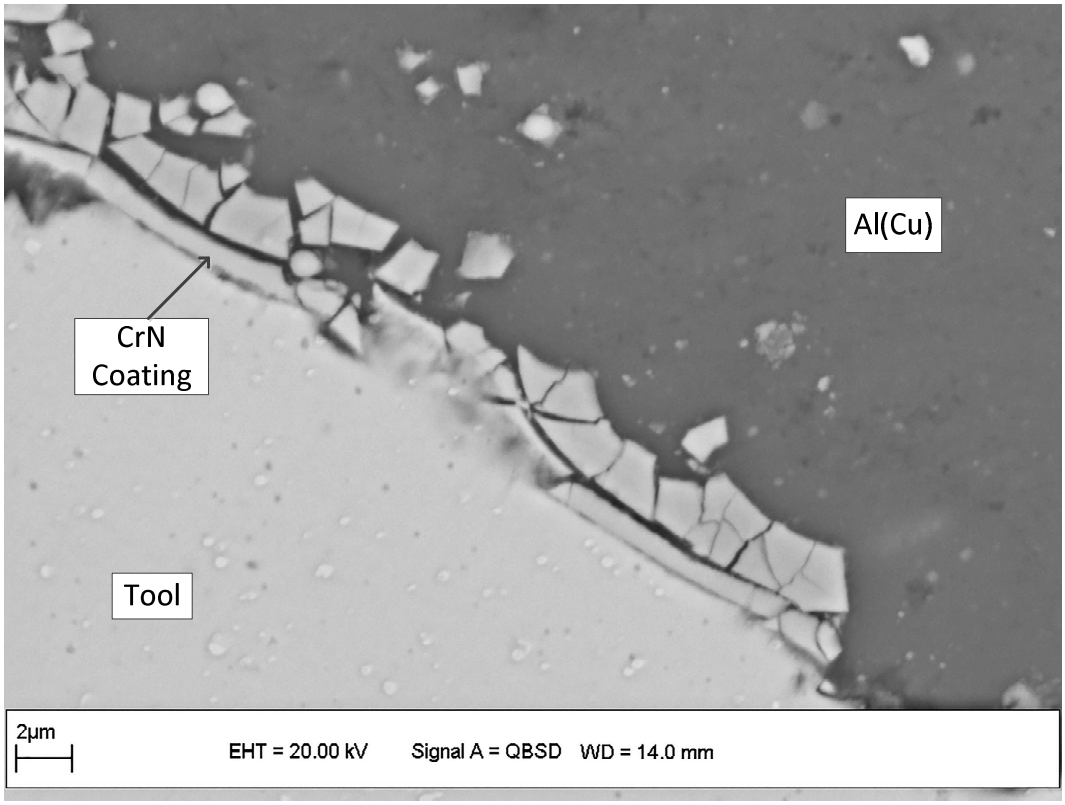

(c)

Figure 4-24. SEM images in a backscattered electron mode of a Viscount 44 tool coated with a PVD CrN coating after a twentyweld trial. Figure (a) shows a low magnification overview of the tool. Figures (b) and (c) are higher magnification images along the tool/stir zone interface in the boxed region of image (a). Figure (b) is the upper-side of the thread region and shows the CrN coating was still present. Figure (c) is the lower-side of the thread region in the circled region of image (a) and shows that the CrN coating was breaking up and being removed from the lower thread region after less than twenty welds. The welding parameters used were 2000rpm rotation speed, 2.59mm plunge depth, 0.21mm/s plunge rate, and 6.0s dwell time.

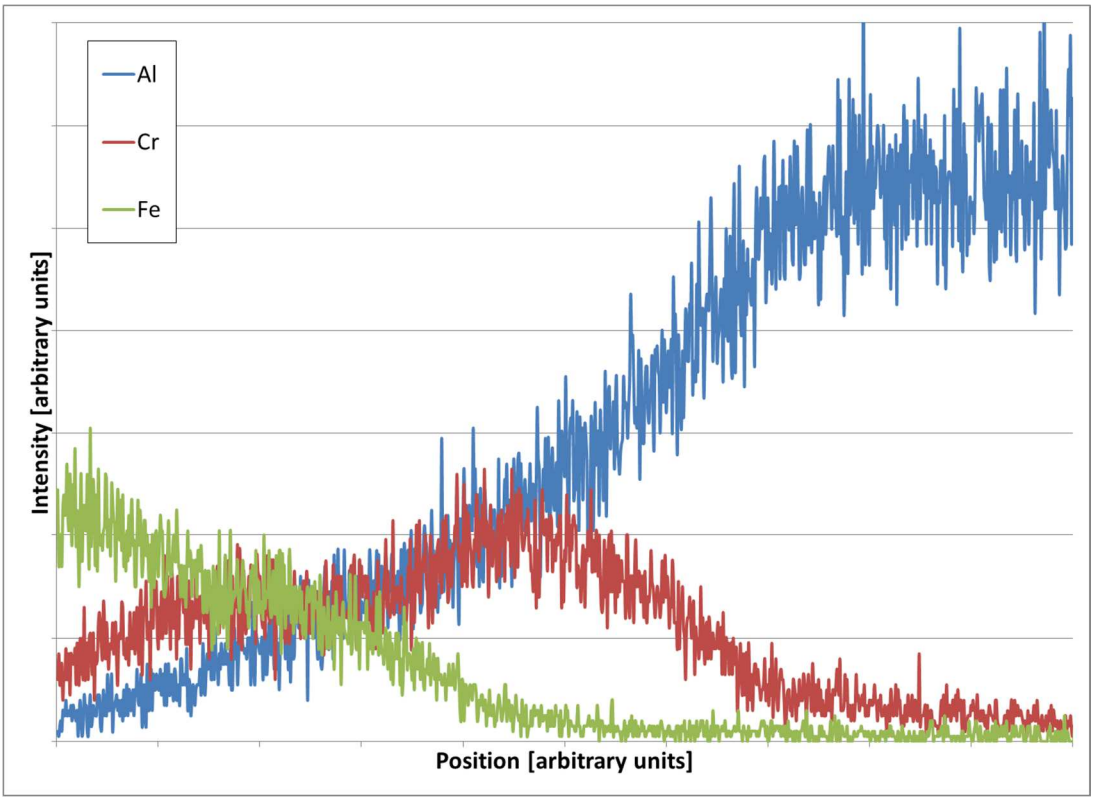

Figure 4-25. Twenty-weld trial using tool fabricated from a tungsten based alloy with a trade name of Densimet 17.7. The welding parameters used were 2000rpm rotation speed, 2.59mm plunge depth, 0.21mm/s plunge rate, and 6.0s dwell time.

4.3.6 Twenty Weld Trial using Densimet 17.7 Tool

The images of the tool and the corresponding weld strengths during the twenty weld trial using the Densimet 17.7 tool are shown in Figure 4-26. In Figure 4-26, the outer diameter of the tool threads are typically visible after each weld, and in some cases, like Welds #6, #7, and #10, the threads are nearly free of any buildup. In comparison, in the baseline trial in Figure 4-7, the tool is aluminum-colored in appearance and the threads are not visible. Having the thread visible on the Densimet 17.7 tool suggests that the Al-rich stir zone material did not as readily adhere to the outer diameter of the tool pin, and supports the Densimet 17.7 manufacturer claim that this material minimizes material adhesion.

While the Densimet 17.7 minimized adherence of aluminum to the tool threads, it did not eliminate nor necessarily even minimize the tool tip buildup as shown in Figures 4-26, and further highlighted in Figure 4-27 where the measured values of the tool tip buildup and corresponding weld strengths are shown. As shown in Figure 4-27, the measured tool tip buildup varies substantially between each weld, and there is no correlation between the amount of buildup or the amount of material shed or gained during the weld, and the weld strength. Figure 4-28(a) shows that the tool tip buildup on Densimet 17.7 is similar in appearance to the material buildup adhered to a H13 (Trade name Viscount 44) steel tool (see Figure 4-9). An EDS line scan, as shown in Figure 4-29, indicates the buildup on the Densimet 17.7 tool tip is a Cu-rich layer structure consisting of Cu(Al) and Al-Cu intermetallics. The EDS line scan (top to bottom in Figure 4-28(b) corresponds to left to right in Figure 4-29) begins on the left side of Figure 4-29 showing the Densimet 17.7 tool material with a high intensity tungsten peak. The Cu intensity increased dramatically when the tungsten peak declined to zero. As the scan continued, still moving from left to right in Figure 4-29, the Cu intensity declined twice while the Al intensity increased, which were indications that Al-Cu intermetallics were present in the layered structure similar to what was observed on the H13 steel tool.

To identify the phases present in the material on the Densimet 17.7 FSSW tool tip, x-ray diffraction was again employed. As was done in Sub-section 4.3.2, material was removed using a machining process, but this time the tool material was Densimet 17.7. This Densimet 17.7 FSSW tool had made five welds. The removed material was placed on the tip of quartz rod and held in place with amorphous grease. The quartz rod containing the tool tip material was then placed in a Ragaku Rapid II X-ray

Diffractometer. This instrument used a molybdenum x-ray source with an area detector with a 50kV voltage and 50mA current. The x-ray beam was collimated to beam size the 0.10mm. The sample was rotated 360 through the beam with an exposure time of 900s. The resulting x-ray diffraction spectrum is shown in Figure 4-30. This diffraction spectrum is similar to the one for a Viscount 44 (H13) steel tool in Figure 4-12. As was the case with the steel tool, only two phases were present: Cu and Cu_9Al_4, and these were the same two phases detected on the tip of the steel tool. Having the same two phases suggests that the type tool material used does not impact the phases that form on the tool tip.

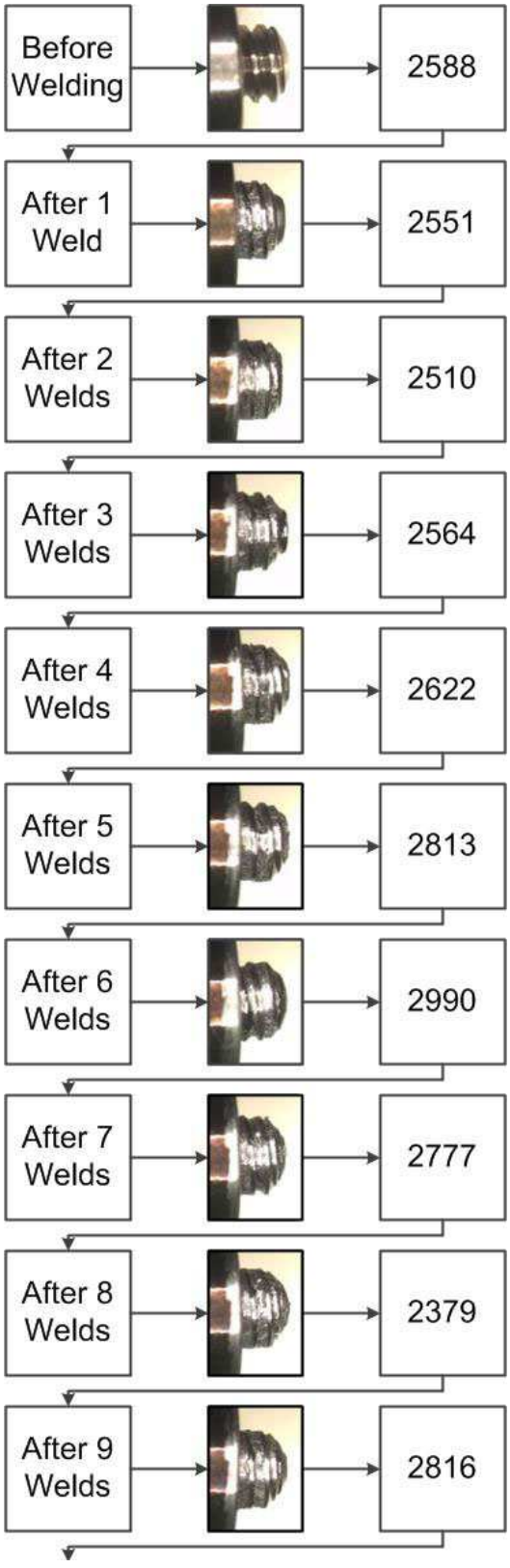
Before Welding
2588
After 1 Weld
2551
After 2 Welds
2510
After 3 Welds
2564
After 4 Welds
2622
After 5 Welds
2813
After 6 Welds
2990
After 7 Welds
2777
After 8 Welds
2379
After 9 Welds
2816

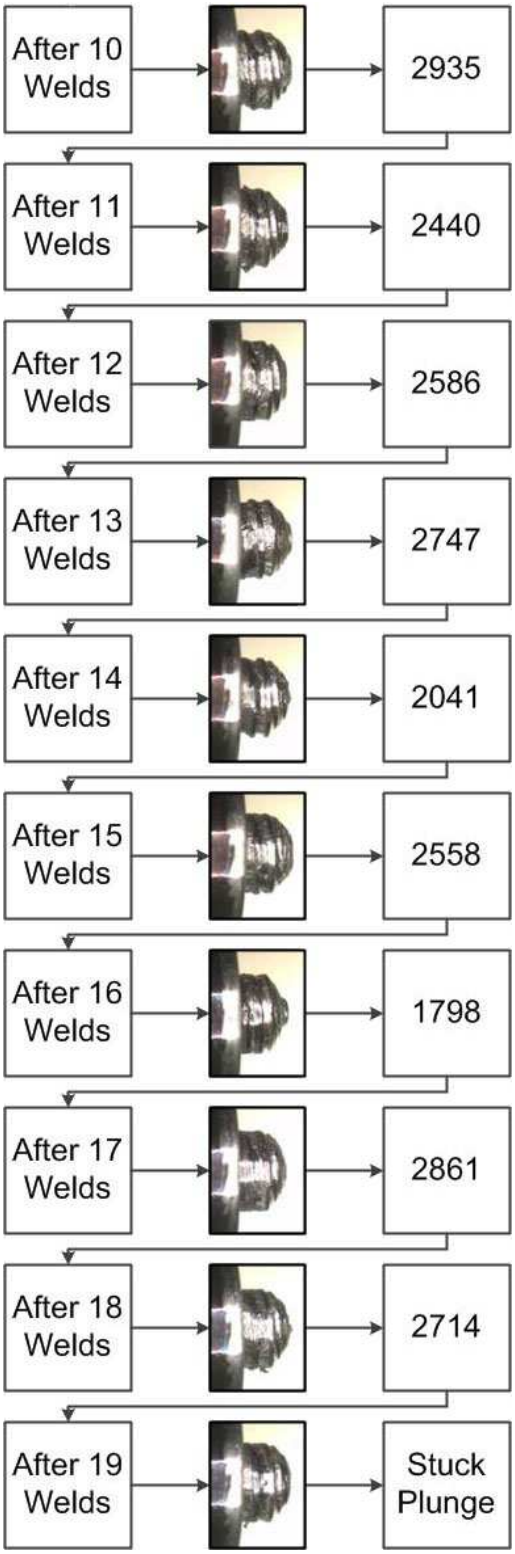

Figure 4-26. Photographs of the FSSW tool and weld strength (in N) produced during a twenty weld trial using tool fabricated from a tungsten-based alloy with a trade name of Densimet 17.7. The welding parameters used were 2000rpm rotation speed, 2.59mm plunge depth, 0.21mm/s plunge rate, and 6.0s dwell time**.**

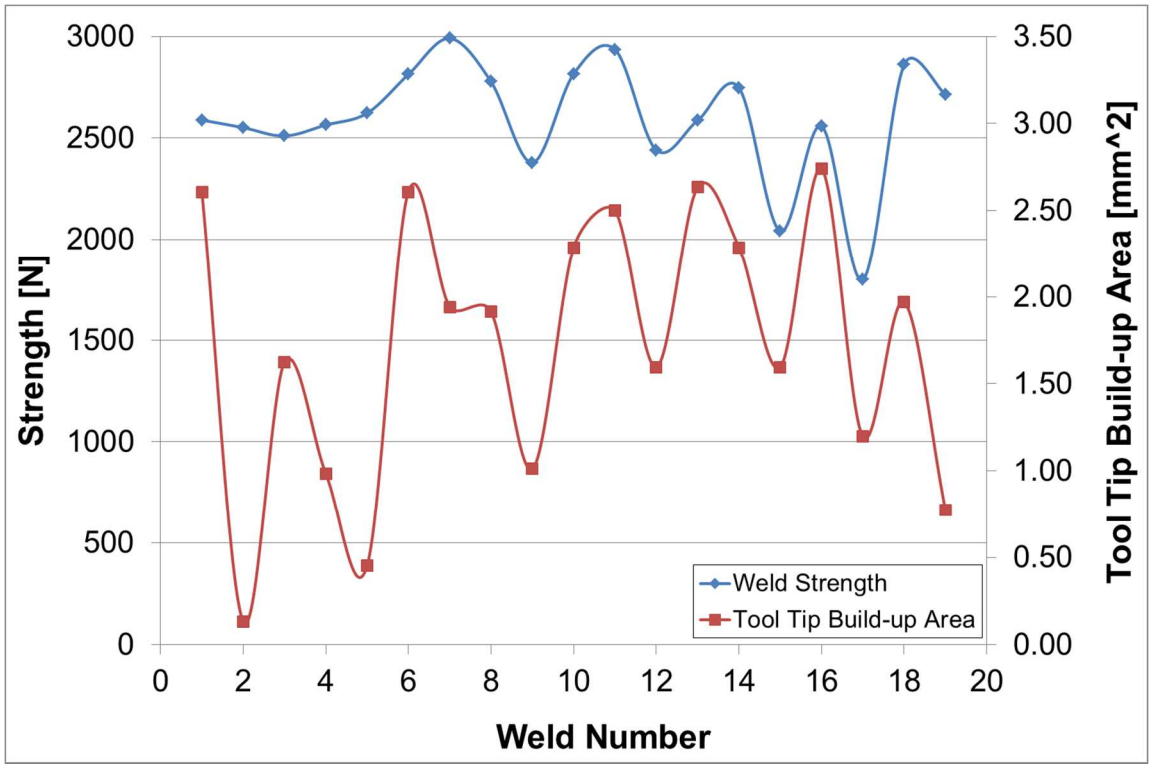

Figure 4-27. Weld Strength and tool build up data graphically shown from a twenty weld trial using a tool fabricated from a tungsten-based alloy with a trade name of Densimet 17.7 shown in Figure 4-24. The welding parameters used were 2000rpm rotation speed, 2.59mm plunge depth, 0.21mm/s plunge rate, and 6.0s dwell time.

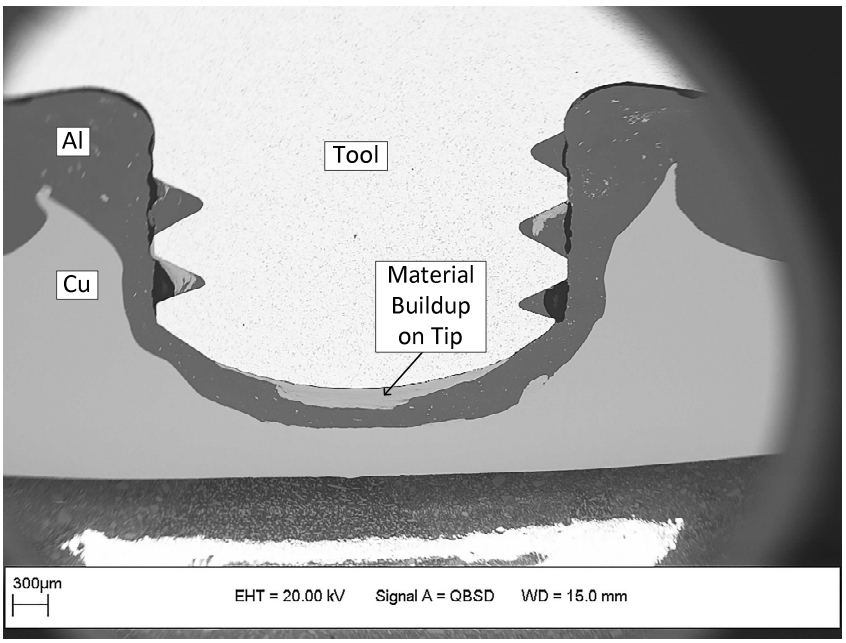

(a)

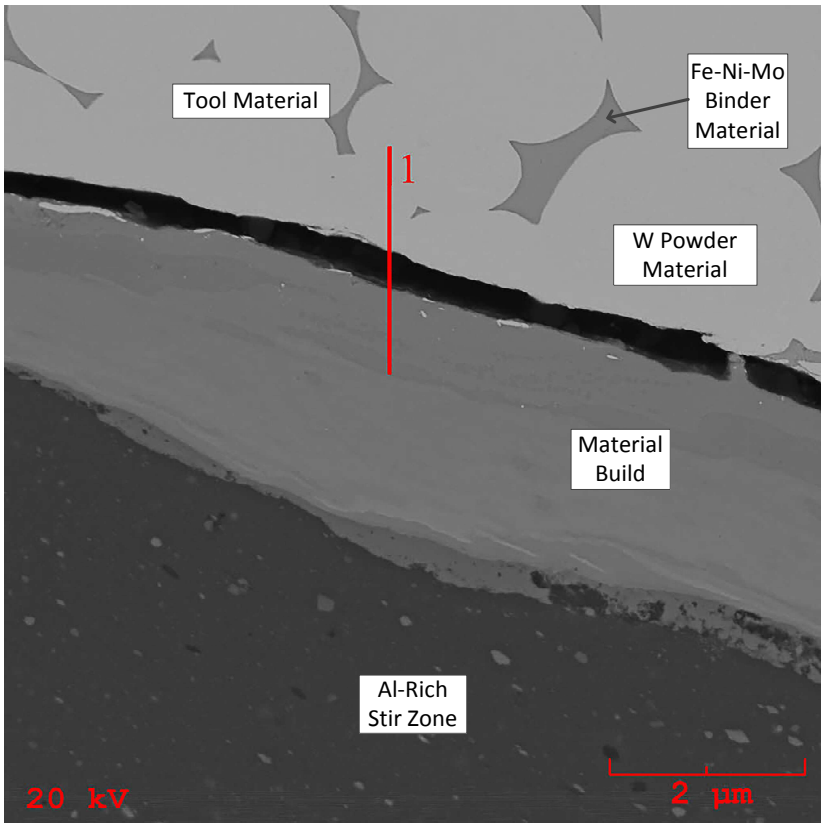

(b)

Figure 4-28. SEM images in the backscattered electron mode of Weld #21 that was made immediately after the twenty weld trial using the Densimet17.7 tool (a) at low magnification and (b) of the boxed region at higher magnification showing the line for the EDS scan in Figure 4-27. The welding parameters used were 2000rpm rotation speed, 2.59mm plunge depth, 0.21mm/s plunge rate, and 6.0s dwell time.

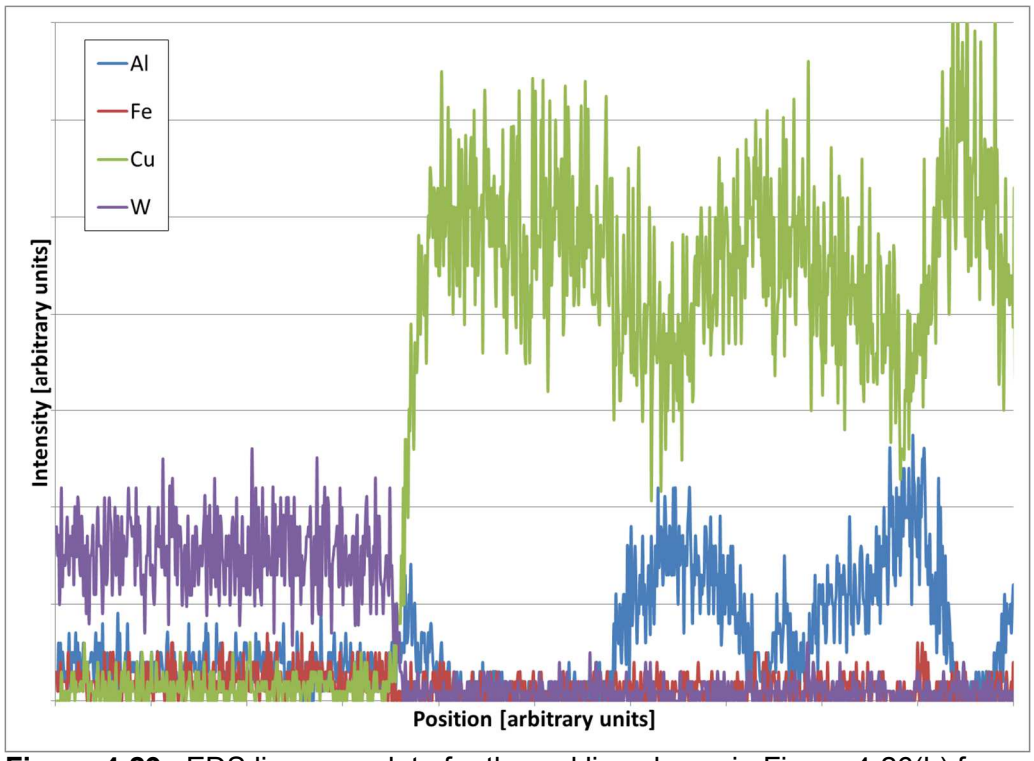

Figure 4-29. EDS line scan data for the red line shown in Figure 4-26(b) from a twenty weld trial using tool fabricated from a tungsten based alloy with a trade name of Densimet 17.7. The welding parameters used were 2000rpm rotation speed, 2.59mm plunge depth, 0.21mm/s plunge rate, and 6.0s dwell time.

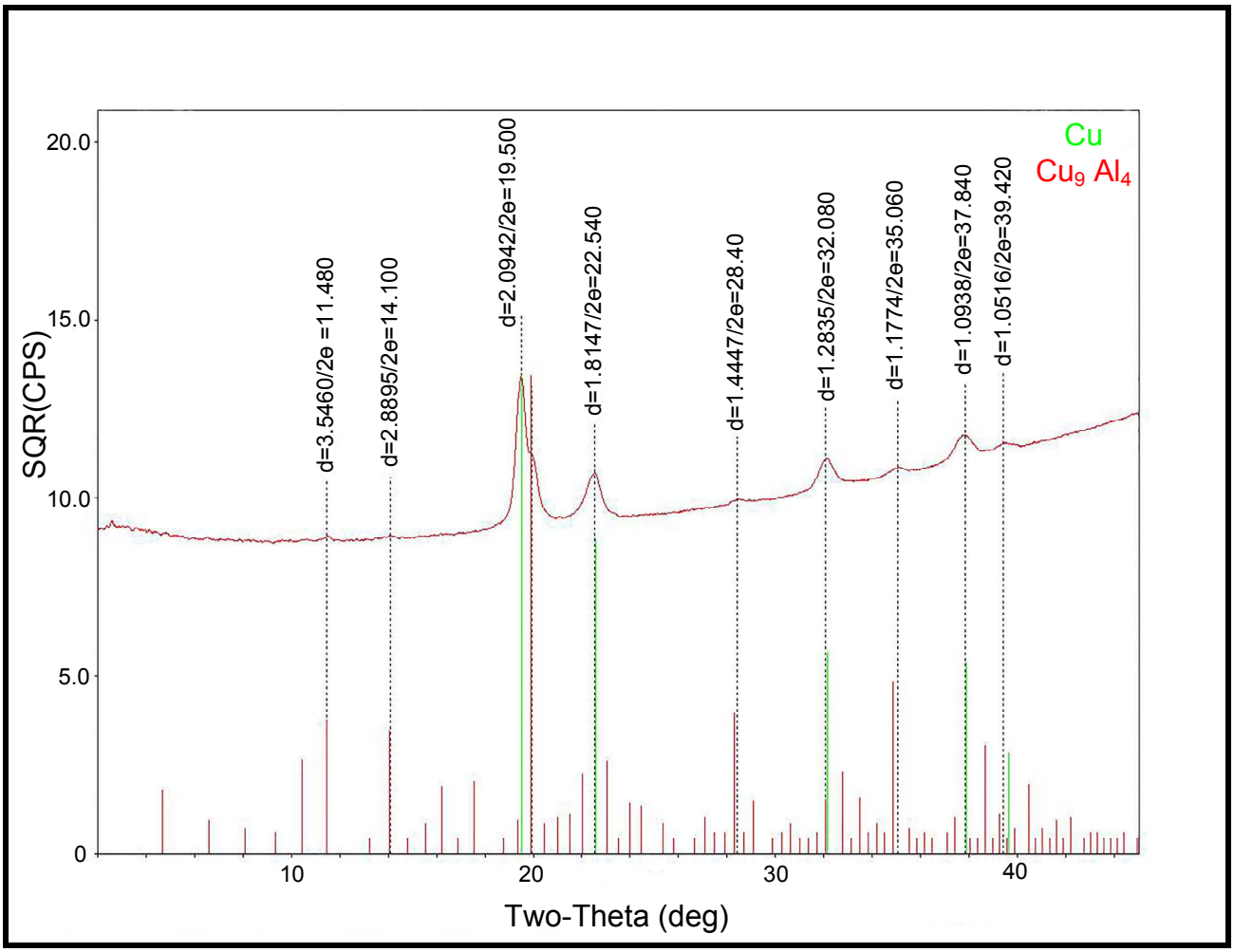

Figure 4-30. X-ray diffraction spectrum of the material built up on a Densimet tool after 5 welds. The welding parameters used were 2000rpm rotation speed, 2.59mm plunge depth, 0.21mm/s plu nge rate, and 0.0s dwell time.

Despite the presence of significant material buildup on the Densimet 17.7 tool tip, the weld strengths appeared noticeably higher than those in the baseline trial using an uncoated H13 steel tool. Furthermore, unlike the CrN coated tool, the high strengths were maintained during the entire welding trial with all but one value greater than 2000N. The one value less than 2000N was 1798N, which was the minimum strength for the twenty weld trial. Because material buildup on the tool tip still occurred, Densimet 17.7 still appeared susceptible to the generation of large layered Al-Cu particles in the

stir zone as evident in the boxed region of Figure 4-28. However, unlike an uncoated steel tool, these large particles apparently move through tool threads and stir zone easily and do not detrimentally affect weld strength.

The reason for the increased weld strength when a Densimet 17.7 tool is used is evident in the last weld made (Weld #20) where the tool was left in the sample (see Figure 4-28). The width of the stir zone, as indicated by the red horizontal line in Figure 4-28, is approximately 0.85mm. Based on Equation (4-1), the predicted weld strength for this weld would be 2741N, which seems reasonable based on other weld strengths in this trial. From Figure 4-28, the width of the stir zone increased because the Cu ring was pushed outward towards the tip. The outward push of the Cu ring increased the stir zone width, and thus, higher weld strengths were achieved. As discussed earlier with the CrN coated tool, improved flow of aluminum in the thread region may have increased material velocity along the threads while the material velocity near the Cu ring surface remained mostly unchanged. If the material velocity along the Densimet 17.7 tool surface increased as compared to a steel surface, more material will accumulate in the stir zone. Since the Cu below the Cu ring is reasonably rigid in the horizontal direction due to the large cross-sectional area which is further restrained by the welding fixture, this material does not substantially deform. However, the tip of the Cu ring, with a much reduced cross-section, and backed by more formable 6061 Al, deformed outward as a result of the additional material that filled the stir zone which produced a wider stir zone and stronger weld.

The reasons for the improved flow associated with the Densimet 17.7 tool as compared to the H13 steel tool could include surface roughness differences and/or

coefficient of friction differences. Measuring surface roughness on an irregular shaped tool is challenging, but the effect of surface roughness was investigated by comparing the weld strength produced with a standard H13 tool steel and another H13 tool steel that was polished using diamond buffing compounds. The polished tool had a mirror like finish when fully polished. A 10 weld trial was completed using both tools with standard weld conditions: 2000rpm, 021mm/s plunge rate, 2.59mm plunge depth, and 6s dwell time. The standard H13 steel tool produced an average weld strength of 1812N compared to the polished H13 steel tool that produced an average strength of 2282N. The improved surface finish improved flow and yielded a 25.9% average strength increase, but still did not achieve the weld strength produced using a Densimet 17.7 tool. The average weld strength using a Densimet 17.7 tool was 2594N, for those welds shown in Figure 4-26, and is 13% stronger than the polished tool. Consequently, not all of the strength increases associated with Densimet can likely be attributed to simply improving the surface finish. Furthermore, the surface roughness of an unpolished tool and the Densimet 17.7 tool was evaluated qualitatively via SEM imaging.

As shown in Figure 4-31, the surface finish of much of the thread surfaces for a new Densimet 17.7 and new unpolished H13 tool steel are very similar with two exceptions. First, the top thread crest of the Densimet tool, as indicated by the arrows in Figure 4-31(a) experienced some edge chipping. The chipping is not particularly surprising given the brittleness of the Densimet 17.7 tool. The bottom thread of the unpolished H13 steel tool exhibited a slightly rougher surface, as shown by arrows in Figure 4-31(b). This slight increase in surface roughness likely stems from some galling of the cutting tool while cutting the thread. Both of these increases in surface roughness

(one for the Densimet 17.7 tool and one for the H13 steel tool) could have led to poor flow. However, since most of the thread surfaces appear similar in roughness, it is unlikely, that much of the 43% weld strength increase can be attributed to a surface roughness difference. This would suggest that coefficient of friction may be a more important factor.

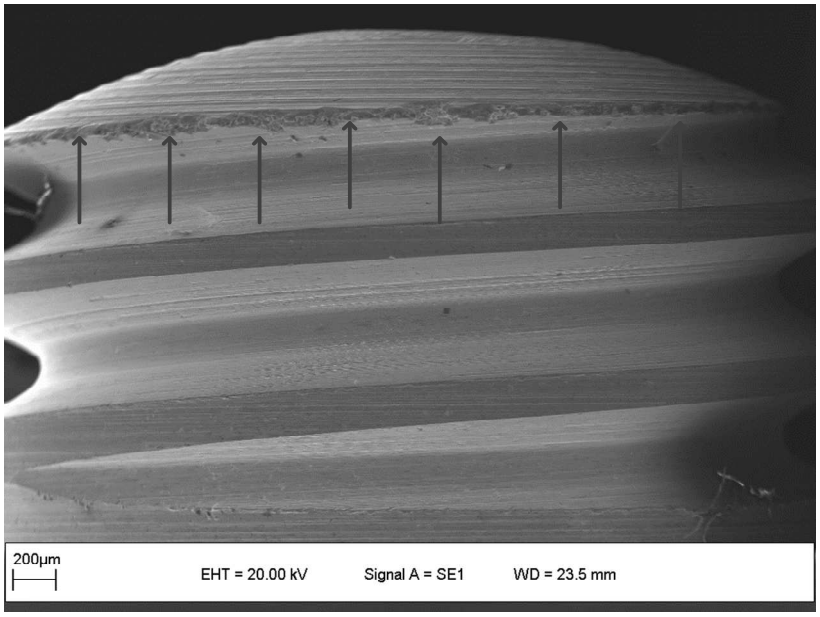

(a)

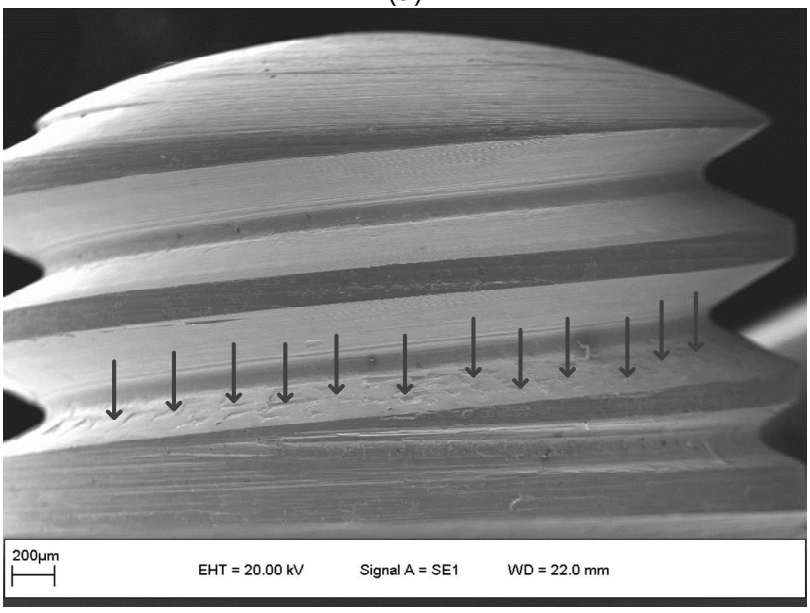

(b)

Figure 4-31. SEM images showing the surface roughness of new/unused tools made of (a) Densimet 17.7 and (b) H13 tool steel. The arrows in each image identify the

differences in surface roughness between the two tools. Aside from the arrowed regions, the surface roughness between the two tools appears similar.

While the coefficient of friction is a measureable parameter, none can be found in the literature or was available from the manufacturer [69]. In an attempt to understand if there is a coefficient of friction difference between H13 steel and Densimet 17.7 two experiments were conducted. First, the shoulder temperature was measured for Densimet 17.7 tool in the same manner as reported in Chapter 3. A comparison between temperature profiles for FSSW 6061 Al to Cu for the Densimet 17.7 tool and the standard H13 steel tool are shown in Figure 4-32. If the coefficient of friction was lower for the Densimet 17.7, the expectation was that the temperature would have been lower as well. Figure 4-32 shows the temperature for Densimet 17.7 tool was about 20°C lower than the H13 tool steel at the end of the plunge. However, given the repeatability of the temperature measurements, as discussed in Chapter 3, concluding if the temperature of the Densimet 17.7 tool was truly lower is difficult. More interesting in the Densimet temperature curve (Figure 4-32) was the slope change, indicating a slower heating rate, and noisier data that can be seen between the two arrows. This change occurs right towards the end of the plunge portion of the weld when the upward extruded Cu ring, necessary for quality weld, forms. Data like this was not seen in any other temperature measurements so the assumption is that the reduced heating rate is a real phenomenon. The reduced heating rate, coupled with the noisier data, could suggest that there was some level of material slip taking place with the Densimet 17.7 tool, which made it easier for material to flow along the thread surfaces during this short portion of the weld when, as shown in Chapter 2, the macrostruture needed for quality weld formation forms. The improved/easier flow could then likely lead to an increased material velocity which could then produce a stronger weld.

A comparison between the torque produced using a Densimet 17.7 and a H13 steel tool is shown in Figure 4-33. The torque curves are nearly identical except for the slightly higher torque levels at the end of the plunge which could provide some support for the lower heating rate, and lower temperatures observed toward the end of the plunge measured with the Densimet 17.7 tool. Lower temperatures would mean the viscosity of aluminum is lower and hence more torque is needed to stir the material. The assumption was that if material was flowing more easily along the Densimet tool, the torque could be lower, but the torque measurement is more of the bulk measurement of the process and may not have been sensitive enough for material flow differences right at the surface of the tool. By comparison the temperature measurement is a measurement that took place at the tool/stir zone interface and would be more likely to measure subtle differences.

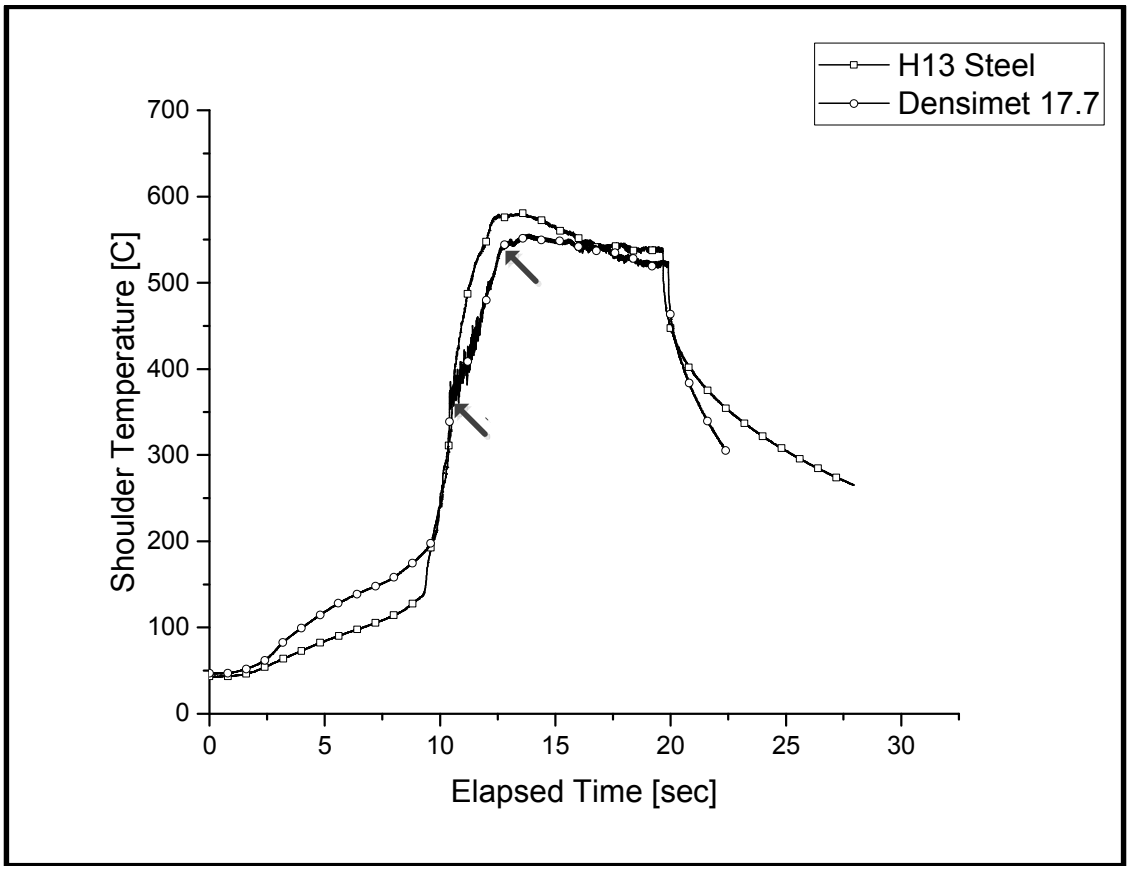

Figure 4-32. Shoulder temperature profiles for a Densimet 17.7 tool and a H13 tool steel using the following welding parameters: 2000rpm rotation speed, 2.59mm plunge depth, 0.21mm/s plunge rate, and 6s weld dwell time.

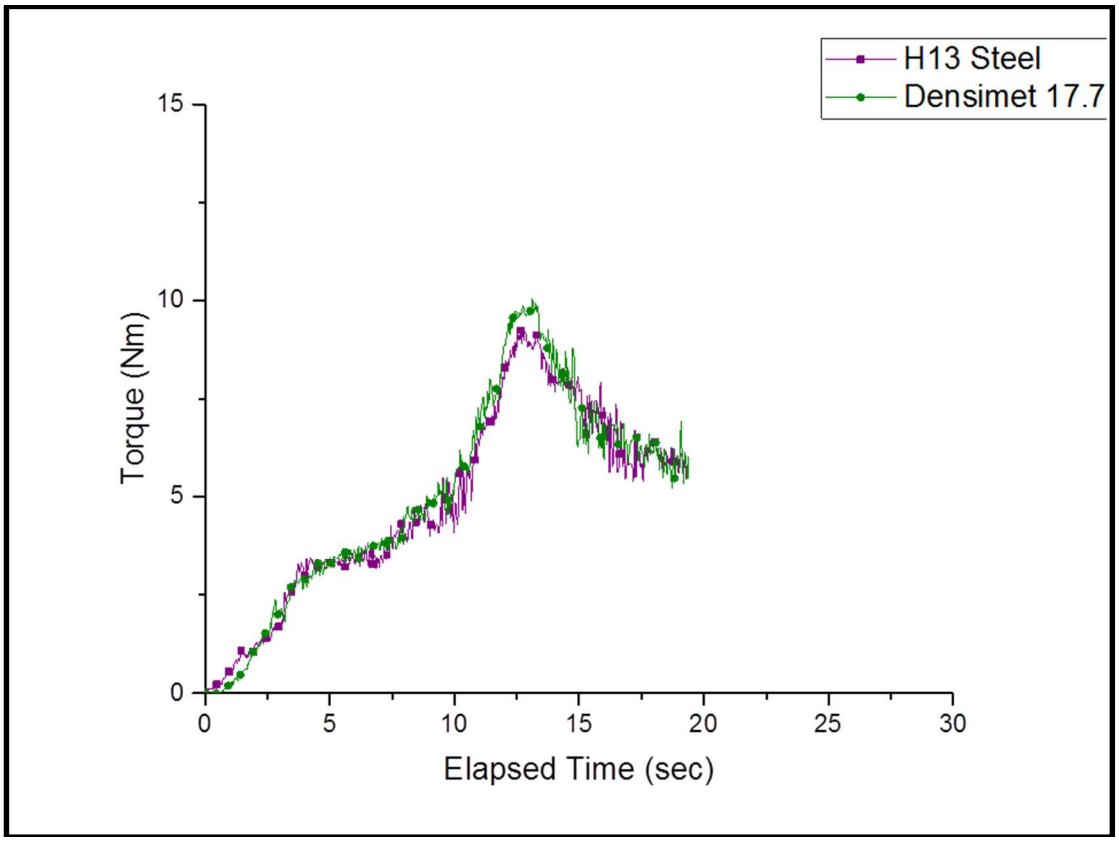

Figure 4-33. Measured torque values for a Densimet 17.7 tool and a H13 tool steel using the following welding parameters: 2000rpm rotation speed, 2.59mm plunge depth, 0.21mm/s plunge rate, and 6s weld dwell time.

Determining the exact cause for the improved flow is difficult and requires substantially more effort and cost due to three confounding factors: (1) surface roughness, (2) coefficient of friction differences, and (3) an approximately 300% difference in thermal conductivity between Densiment 17.7 (73.0W/m-K at 500°C[69]) and H13 (24.7W/m-K at 605°C[73]). Nonetheless, the Densimet 17.7 tool clearly improved weld strength and consistency as compared to the baseline H13 (trade name Viscount 44) steel tool and those tools that were PVD coated with TiCN and CrN (because the coating quickly wore away). However, it did not prevent, as was hoped, a Cu-rich layered structure from building up on the tool tip. Instead, it appears, that the

Densimet 17.7 improved material flow and made it easier for the large layered particles to move along and through the tool thread, which prevented substantial thread clogging and yielded welds of consistently higher strength.

Preventing material buildup using the tool design used in this study appears very difficult. The flow of material caused by tool threads, as discussed in Chapter 2, is down the threads and only extends a short distance under the tool tip. The only time there appears to be significant material flow under the tool tip is from time the shoulder first engages the upper 6061 Al sheet to the end of the plunging process. Even when this material flow takes place the flow is, as shown in Chapter 2, not along the tool surface but splits between the lower Cu sheet and the layered structure that builds up on the tool. The lack of flow beneath the FSSW tool pin was also reported by Su et al. who used a similar tool in FSSW of 5754 Al to 6111 Al [73]. Using Al2O3 tracers, minimal material flow was observed in region under the pin that was 70% of the pin radius. Material that was closer to the peripheral of the tool pin moved downward and outward in the stir zone as was observed for FSSW of 6061 Al to Cu (see Chapter 2). With minimal material flow on the tool tip, material buildup in this region is likely since there is no easy method to “wash” this material away. Therefore, the mostly likely method to prevent tip buildup would be redesigning such that there is substantial material flow on the tip; perhaps a tool that tapers to more of a point than the rounded tip used in this investigation. Alternatively, a tool could be designed to accommodate the buildup such that the buildup is not easily expelled into the stir zone. This design could utilize a concave tip structure as opposed the convex structure used here. Lastly, since the Densimet tool seemed to tolerate the tip buildup, if more robustness is desired, the tip

could be machined back to its original surface on a set schedule. Machining the tip clean would be very similar to the process commonly used in machining resistance spot welding electrodes in a manufacturing environment.

4.4 Conclusions:

1. Cleaning a steel tool via a NaOH etching process improved weld strength consistency, demonstrating that material buildup on a steel tool leads to inconstencies in weld strength.
2. Machining only the tip of steel tool back to its orginial steel surface (removing the layered Cu-rich structure that forms on the tip) improved weld consistency and eliminated low-strength welds. This confirmed that the source of low strength welds was the shedding of layered Cu-rich/Al-Cu intermetallic material on the tool tip. The shedding takes place because the intermetallics are brittle and facture easily into numerous particles of various sizes. Once tip buildup material fractures, particles are are emitted into the stir zone and if these particles are large enough, thread clogging is possbile.
3. A physical vapor deposited CrN tool coating can improve weld strength and consistency as compared to a steel tool. However, the coating was removed from the lower thread surface of the tool within twenty welds. The short life the CrN tool coating and TiCN tool coating indicates that tool coatings are not viable solutions to improving weld consistency in high-volume manufacturing, where tool life expectations are much higher (1000s of welds per tool).
4. A tool made from Densimet 17.7 improved weld strength and consistency.

5. The improved strength of the welds from the Densimet 17.7 tool were the result of a wider stir welding zone between the tip of the upward extruded Cu ring and the weld keyhole. The increase in strength was likely the result of an increased material flow along the surface of the Densimet 17.7 tool surface (as compared to a steel surface).
6. The Densimet 17.7 tool material did not prevent a buildup of material on the tool tip.
7. The Densimet 17.7 tool material appeared to permit the large layered structures, (that would have likely clogged a steel tool) to more easily flow over the thread surface and thus not clog the tool theads.
8. Since no material tested prevented a buildup of material on the tool tip of the design used in this investigation, a new design is likely needed to prevent material buildup on the tool tip.

References

[1] W. Thomas, E. Nicholas, J. Needham, M. Murch, P. Temple-Smith, and C. Dawes, 'Friction Welding', United States Patent Number 5,460,317, October 24, 1995.

[2] J. Record, J. Covington, T. Nelson, C. Sorensen, B. Webb, 'A Look at the Statistical Identification of Critical Process Parameters in Friction Stir Welding', Welding Journal, April 2007, p. 97-s - 103-s.

[3] S.W. Kallee, J.M. Kell, W.M. Thomas, and C.S. Wiesner, "Development and Implementation of Innovative Joining Processes in the Automotive Industry," DVS Annual Welding Conference "Grobe Schweibtechnische Tagung," Essen Germany, 12-14 September 2005

[4] S. Kallee, J. Kell, W. Thomas, C. Wiesner, 'Development and Implementation of Innovative Joining Processes in the Automotive Industry', DVS Annual Welding Conference, Germany, September 2005.

[5] W. Arbegast, 'Friction Stir Welding After a Decade of Development', Welding Journal, March 2006, p. 28 - 35.

[6] M. Fukumoto, M. Tsubaki, T. Yasui, Y. Shimoda, 'Joining of ADC12 and SS400 by Means of Friction Stir Welding', Japan Welding Society 2004, 22 (2), p. 309 - 314.

[7] L. Xing, L. Li, and L. Ke, 'Microstructural investigation on friction stir welds of dissimilar metals between mild steel and copper', Transactions of the China Welding Institution, v28, n 2, February, 2007, p 17-20.

[8] A. Gerlich, P. Su, T. North, G. Bendzsak, 'Friction Stir Spot Welding of Aluminum and Magnesium Alloys', Materials Forum, Vol. 29, 2005.

[9] M. Fukumoto, K. Miyagawa, M. Tsubaki, 'Spot Welding Between Aluminum Alloy and Carbon Steel by Friction Stirring', 6th International Friction Stir Welding Symposium, October 2006.

[10] B. Yilbas, A. Sahin, N. Kahraman, A. Al-Garni, 'Friction Welding of St-Al and Al-Cu Materials', Journal of Materials Processing Technology 49 1995, p. 431 - 443.

[11] R. Mishra, M. Mahoney, 'Friction Stir Welding and Processing', ASM International, March 2007.

[12] L. Fratini, G. Buffa, D. Palmeri, J. Hua, R. Shivpuri, 'Material Flow in FSW of AA7075-T6 Butt Joints: Continuous Dynamic Recrystallization Phenomena', Journal of Engineering Materials and Technology, Vol. 128, July 2006, p. 428 - 435.

[13] A. Elrefaey, M. Takahashi, K. Ikeuchi, 'Preliminary Investigation of Friction Stir Welding Aluminum/Copper Lap Joints', Welding in the World, Vol. 49, No. 3/4, 2005, p. 93 - 101.

[14] S. Bozzi, A. Etter, T. Baudin, A. Robineau, J. Goussain, 'Influence of the Dweel Time on Spot Welding Between 6008 Al Alloy and Steel by FSW', Proceedings of the 6th International Friction Stir Welding Symposium, October 2006.

[15] A. Abdollah-zadeh, T. Saeid, B. Sazgari, 'Weldability and Mechanical Properties of Dissimilar Aluminum-Copper Lap Joints Made by Friction Stir Welding', Welding in South-east

[16] J.F. Hinrichs, C.B. Smith, B.F. Orsini, R. J. DeGeorge, B.J. Smale, P.C. Ruehl, Friction Stir Welding for the 21st Century Automotive Industry, Proceedings of the Fifth International Conference on Friction Stir Welding, Sept 14-16, 2004 (Metz, France), TWI, 2004,

[17] A. Gerlich, P. Su, T. North, 'Friction Stir Spot Welding of Mg-Alloys for Automotive Applications', Magnesium Technology 2005, edited by N. R. Neelameggham, H. I. Kaplan, and B. R. Powell, TMS, 2005.

[18] A. Gerlich, G. Avramovic-Cingara, T. H. North, 'Stir Zone Microstructure and Strain Rate During Al 7075-T6 Friction Stir Spot Welding', Metallurgical & Materials Transactions A, Volume 37, Number 9 / September, 2006, pp. 2773-2786.

[19] J. Ouyang, E. Yarrapareddy, R. Kovacevic, 'Microstructural Evolution in the Friction Stir Welded 6061 Aluminum Alloy (T6-Temper Condition) to Copper', Journal of Materials Processing Technology, 172, 2006, p. 110-122.

[20] K. Savolainen, J. Mononen, T. Saukkonen, H. Hannien, 'A Preliminary Study on Friction Stir Welding of Dissimilar Metal Joints of Copper and Aluminum Paper 79', 6th International Friction Stir Welding Symposium, October 2006.

[21] T. Mozhaiskaya, N. Chekanova, 'Structure and Properties of Welded Aluminum-Copper Joints', Proceedings of the 6th International Friction Stir Welding Symposium, October 2006.

[22] Y. Yang, H. Dong, H. Cao, Y. A. Chang and S. Kou, 'Liquation of Mg Alloys in Friction Stir Spot Welding', Welding Journal, July 2008, pp. 167s – 177s.

[23] P. Liu, Q. Shi, W. Wang, X. Wang, Z.Zhang, 'Microstructure and XRD analysis of FSW joints of copper T2/aluminum 5A06 dissimilar materials, Material Letters 62 (2008), 4106-4108.

[24] H. Okamura and K. Aota, 'Joining Dissimilar Materials with Friction Stir Welding,' Welding International, 2004 18 (11) 852-860.

[25] A. Pietras, 'Frictions Stir Welding Aluminum to Copper', Proceedings of the 6th International Friction Stir Welding Symposium, October 2006.

[26] A. Savitskii, G. Romanov, 'Structure Formation during the Sintering of Aluminum-Copper Alloys', Poroshk. Metall., No. 3, 19–23 (1986).

[27] P. Swann, H. Warlimont, 'The Electron-Metallography and Crystallography of Copper-Aluminum Martensites', Acta Metallurgica, vol. 11, pp 511-527, 1963

[28] Minitab Release 14 Statistical Software, Release 14.20, Minitab, Inc., State College, PA, 2005

[29] Tl. Enjo, K. Ikeuchi, N. Akikawa, 'Diffusion Welding of Copper to Aluminum', Transactions of JWRI Vol. 8, No. 1, 1979, p. 77 - 84.

[30] M. Fukumoto, T. Yashi, Y. Shimoda, M. Tsubaki, T. Shinoda, 'Butt Welding Between Dissimilar Metals by Friction Stirring', Proceeding of the 6th International Friction Stir Welding Symposium, October 2006.

[31] Leonard, AJ (2000). "Microstructure and aging behaviour of FSW in Al alloys 2014A-T651 and 7075-T651". 2nd International Symposium on FSW (CD ROM)

[32] A. Gerlich, M. Yauamoto, T. North, 'Local Melting and Tool Slippage during Friction Stir Spot Welding of Al-Alloys', Journal of Materials Science, Volume 43, Number 1 / January, 2008, pp. 2-11.

[33] H. Ochi, K. Ogawa, Y. Yamamoto, G, Kawai, T. Sawai, 'The Formation of Intermetallic Compounds in Aluminum Alloy to Copper Friction-Welded Joints and Their Effect on Joint Efficiency', Journal of the Japan Welding Society 2003, 21 (3), p. 381 - 388.

[34] Hultgren, Al-Cu (Aluminum-Copper) Landolt-Börnstein - Group IV Physical Chemistry 1615-2018 (Print) 1616-9557 (Online) Volume 5a Ac-Au – Au-Zr Springer-Verlag 10.1007/b20007, 1991, 978-3-540-15516-4, 10.1007/10000866_100, 1-9,

[35] Workman, G. M., and E. D. Nicholas. "Friction Welding Aluminium and its alloys to various metals." Metals and Materials Vol 2 (1986): 138-40.

[36] Fukumoto, Masahiro, Toshiaki Yasui, Masami Tsubaki, and Takeshi Shinoda. "Butt Welding Between Dissimilar Metals By Friction Stirring." Materials Science Forum 449-452 (2004): 433-36.

[37] Nielsen, A., and N. Bay. "Friction Welding Copper to Aluminium." Proceed. Int. Conf. Joining of Metals 2, page 187-193, 1984

[38] Xijing, Wang, Zhang Zhongke, Da Chaobing, and Li Jing. "Microstructures and properties analysis of dissimiliar metal joint in the friction stir welded copper to alumium alloy." Chineese Welding 16 (2007): 57-61.

[39] Tl. Enjo, K. Ikeuchi, N. Akikawa, 'Diffusion Welding of Copper to Aluminum', Transactions of JWRI Vol. 8, No. 1, 1979, p. 77 - 84.

[40] Murr, L. E., G. Sharma, F. Conteras, M. Shiddique, R. D. Flores, D. J. Shindo, K. F. Soto, E. A. Trillo, C. Schmidt, and J. C. McClure. "Joining Dissimliar Aluminium Alloys And Other Metals and Alloys by Friction Stir Welding." Aluminium 2001 Proceedings of the TMS 2001 (Feb. 13th, 2006): 197-211.

[41] Papkala, H., and A. Pietras. "Pressure Welding of Aluminium to Copper." Welding International 20 (2006): 173-82.

[42] H. Chen, S. Heald, 'Reaction and Diffusion at Cu/Al Interfaces Studied Using Glancing-angle Extended X-ray Absorption Fine Structures', The American Physical Society, Physical Review B, Condensed Matter, Third Series, Vol. 42, No. 8, September 15 1990.

[43] G. Preston, 'An X-ray Investigation of Some Copper-Aluminum Alloys', 6th International Friction Stir Welding Symposium, October 2006.

[44] M. Aritoshi, K. Okita, T. Enjo, K. Ikeuchi, F. Matsuda, 'Friction Welding of Copper-Tungsten Sintered Alloy to Pure Aluminum', Japan Welding Society, Vol. 24, No. 1, April 1993, p. 50 - 56.

[45] A. Abdollah-zadeh, T. Saeid, B. Sazgari; Microstructural and mechanical properties of friction stir welded aluminum/copper lap joints*, J. Alloys and Compounds*, 2008, Vol. 460, pp. 535-538.

[46] Jiahu Ouyang, Eswar Yarrapareddy and Radovan Kovacevic, 'Microstructural evolution in the Friction Stir Welded 6061 Aluminum Alloy (T6-temper condition) to Copper' Journal of Materials Processing Technology, Volume 172, Issue 1, 20 February 2006, Pages 110-122

[47] C. Smith, G. Bendzsak, T. North, J. Hinrichs, J. Noruk, R. Heideman, 'Heat and Material Flow Modeling of the Friction Stir-welding Process', Proceeding of the 9th International Conference on Computer Technology in Welding, T. Siewert, C. Pollock (eds.), May 2000

[48] Willey, L. A. "The Al−Cu (Aluminum-Copper) system." Journal of Phase Equilibria 1 (1980). As cited in Metals Handbook

[49] A. Abdollah-zadeh, T. Saeid, B. Sazgari; Weldability and Mechanical Properties of Dissimilar Aluminum-Copper Lap Joints Made by Friction Stir Welding, Journal of Alloys and Compounds, 460-1 (2008),535-538

[50] Personal conversation with Peter Bartos, Owner, Swiss+TeK Coating, Inc., 16616 W. Rogers Drive, New Berlin, WI 53151-2226

[51] P. Su, A. Gerlich, T.H. North, G. J. Bendzak, "Energy Utilisation and Generation during Friction Stir Spot Welding", Science and Technology of Welding and Joining, 2006 Vol. 11, No. 2, Pages 163-169

[52] S. Lathabai, M.J. Painter, G.M.D. Cantin, V.K. Tyagi, “Friction Stir Spot Welding of Automotive Lightweight Alloys”, Proceedings of the 7th International Conference on Trends in Welding Research, May 16-20, 2005.

[53] J.G. Cowie, D.T. Peters, E.F. Brush, Jr., S.P. Midson, “Materials & Modifications to Die Cast the Copper Conductors of the Induction Motor Rotor”, Die Casting Engineer, September 2001, p. 38-46.

[54] M.A. Suotton, A.P. Reynolds, J. Yan, B. Yang, N. Yuan, “Microstructure and Mixed Mode I/II Fracture of AA2524-T351 Base Material and Friction Stir Welds”, Eng. Fract. Mech., Vol 73 (No. 4), 2006, p. 391-407

[55] C.G. Anderson, R.E. Andrews, “Fabrication of Containment Canisters for Nuclear Waste by Friction Stir Welding”, Proceedings of the First International Conference on Friction Stir Welding, June 14-16, 1999 (Thousand Oaks, CA), TWI, paper on CD.

[56] L. Cederqvist, “FSW to Seal 50 mm Thick Copper Canisters – A Weld That Lasts for 100,000 Years”, Proceedings of the Fifth International Conference on Friction Stir Welding, Sept 14-16, 2004 (Metz, France), TWI, paper on CD.

[57] M.W. Mahoney, W.H. Bingle, S.R. Sharma, R.S. Mishra, “Microstructural Modification and Resultant Properties of Friction Stir Processed Cast NiAl Bronze”, Mater. Sci. Forum, Vol. 426-432, 2003, p. 2843-2848.

[58] B. London, J. Fino, A. Pelton, C. Fuller, M. Mahoney, “Friction Stir Processing of Nitinol”, Friction Stir Welding and Processing III, K.V. Jata, W.M. Mahoney, R.S. Mishra, T.J. Lienert, Ed., TMS, 2005, p. 67-74.

[59] L. Christodoulou, W. Palko, C. Fuller, “Equipment and Processing Variables Affecting Friction Stir Processing of NiAl Bronze”, Friction Stir Welding and Processing III, K.V. Jata, M.W. Mahoney, R.S. Mishra, T.J. Lienert, Ed., TMS, 2005, p. 57-66.

[60] K. Savolainen, J. Mononen, T. Saukkonen, H. Hänninen, J. Koivula, “Friction Stir Weldability of Copper Alloys”, Proceedings of the Fifth International Conference on Friction Stir Welding, Sept 14-16, 2004 (Metz, France), TWI, 2004, paper on CD.

[61] R. Heideman, C. Johnson, and S. Kou, 'Metallurgical analysis of Al/Cu friction stir spot welding', Science and Technology of Welding and Joining, 2010, 15(7) pp 597-604.

[62] M. Akbari, P. Bahemmat, M. Haghpanah and M.-K. Besharati Givi, 'Enhancing metallurgical and mechanical properties of friction stir lap welding of Al-Cu using intermediate layer', Science and Technology of Welding and Joining, 2013, 18(6) pp 518-524.

[63] M. Akbari, R. Abdi Behnagh, and A. Dadvand, 'Effect of materials position on friction stir lap welding of Al to Cu', Science and Technology of Welding and Joining, 2012, 17(7) pp 581-588.

[64] P. Xue, B.L. Xiao, D. Wang, and Z.Y. Ma, 'Achieving high property friction stir welded aluminium/copper lap joint at low heat input', Science and Technology of Welding and Joining, 2011, 16(8) pp 657-661.

[65] H.J. Liu, J.J. Shen, L. Zhou, Y.Q. Zhao, C. Liu, and L.Y. Kuang, 'Microstructural characterisation and mechanical properties of friction stir welded joints of aluminium alloy to copper', Science and Technology of Welding and Joining, 2011, 16(1) pp 92-99.

[66] R. Heideman and S. Kou, 'Material Flow in Friction Stir Spot Welds of Aluminum to Copper' Publication in process.

[67] H.J. Liu, J.J. Shen, S.Xie, Y.X. Huang, F. Cui, C. Liu, and L.Y. Kuang, 'Weld appearance and microstructural characteristics of friction stir butt barrier weld joints of aluminum alloy to copper', Science and Technology of Welding and Joining, 2012, 17(2) pp 104-110.

[68] ASM Handbook, Volume 18 10th Edition, Friction, Lubrication, and Wear Technology, ASM International, Materials Park, OH 44073, October 1992.

[69] Deimitech HD17.7 Technical Document, Mi-Tech Metals, Inc. 470101 Massachusetts Ave, Indianapolis, IN 46218.

[70] V. Firouzdor and S. Kou, 'Al-to-Cu Friction Stir Lap Welding', Metallurgical and Material Transactions A, 43A, January 2012, pp 303-315.

[71] A. Fehrenbacher, J.R. Schmale, M.R. Zin and F.E.Pfefferkorn,' Measurement of Tool-Workpiece Interface Temperature Distribution in Friction Stir Welding,'

Journal of Manufacturing Science and Engineering, April 2014, Vol. 136, pp 021009-1-8.

[72] P. Su, A. Gerlich, T.H. North, and G.J. Bendzak, 'Intermixing of Dissimilar Friction Stir Spot Welds,' Metallurgical and Materials Transactions A, March 2007, 38(3), pp 584-595.

[73] MatWeb Material Property Data, www.matweb.com, AISI H13 Hot Work Tool Steel Data Sheet, http://www.matweb.com/search/DataSheet.aspx?MatGUID=e30d1d1038164808a85cf7ba6aa87ef7&ckck=1, 2015.

[74] ASM Metals Handbook, Volume 2 10th Edition, Properties and Selection: Nonferrous Alloys and Special-Purpose Materials, ASM International, Materials Park, OH 44073, October 1990, pp 102-103.

[75] M. Bauser, G. Sauer, and K. Siegert, 'Extrusion 2nd Edition', ASM International, December 2007.